Mechanisms of cancer-induced bone pain in rodent models of disease progression and regression

Valiente Cerro, Diego

Awarding institution:
King's College London

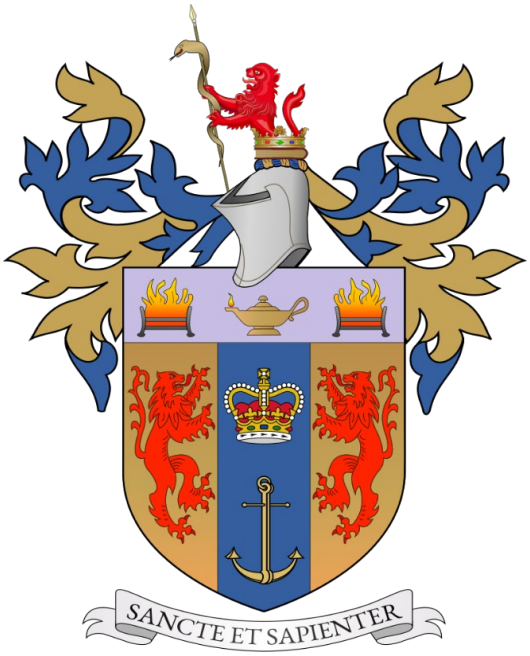

MECHANISMS OF CANCER-INDUCED BONE PAIN IN RODENT MODELS OF DISEASE PROGRESSION AND REGRESSION

Diego Valiente Cerro

A thesis submitted to King's College London for the degree of Doctor of Philosophy

Wolfson Sensory, Pain and Regeneration Centre

Institute of Psychiatry, Psychology & Neuroscience

2024

This project has received funding from the European Union's Horizon 2020 research and innovation programme under the Marie Skłodowska-Curie grant agreement No 814244.

Declaration

I, Diego Valiente Cerro confirm that the work presented in this thesis is my own. Where information has been derived from other sources or when any experimental work has been carried out in conjunction with other researcher/s, I confirm that this has been indicated in the thesis.

February 2024

Abstract

Cancer is inherently linked to pain, making it one of the most common symptoms in cancer patients during the progression, and even remission, of the disease. Specifically, cancer-induced bone pain (CIBP), one of the most frequent forms of cancer pain associated with skeletal metastases, is poorly managed by current analgesic treatments and has become a major area of unmet medical need. To understand the mechanisms underpinning CIBP, the studies presented herein were designed to examine, at both the molecular and circuit level, manifestations of pain in rodent models of CIBP during both disease progression (rat and mouse) and regression (rat).

The results evidence how, following cancer cell tibial implantation, CIBP female rats developed progressive mechanical and thermal heat hypersensitivity in behavioural assays concurrent to progressive trabecular and cortical bone degeneration. While this behavioural phenotype did not correlate with alterations in the electrophysiological properties of spinal deep dorsal horn neurons, diffuse noxious inhibitory controls (DNIC), a unique form of descending modulation, were found to be dysfunctional one week following cancer cell implantation but recovered on posterior weeks. Targeted diphtheria toxin cancer cell ablation on week one led to 1) prolonged DNIC dysregulation, 2) stabilisation of pain-like behaviours, and 3) reversal of bone degeneration. These results were followed by the establishment of a female and male mouse tibial CIBP model, which faithfully recreated the mechanical hypersensitivity and progressive trabecular and cortical bone degeneration observed in the rat CIBP model, with a mirrored impact on DNIC expression. Wishing to tie central nervous system manifestations of pain (dysfunctional DNIC) to activity in the peripheral nervous system, primary afferent activity was measured in naïve mice at the level of the dorsal root ganglion, demonstrating that DNIC evocation had no impact on mass activity. These findings not only expand our understanding of the neural basis of the complex mechanisms driving CIBP, highlighting the dynamic nature of the disease and the need for tailored and mechanistically targeted therapeutical approaches, but also lay the foundation for future studies that will interrogate the synergy between central and peripheral nervous system manifestations of pain.

Covid-19 impact statement

Regrettably, my laboratory experiments were put on hold during the Covid-19 pandemic. My PhD began in September 2019, with my personal animal licence being issued in November 2019. Once I was able to do animal work, finished my training period, and began performing experiments independently, the UK entered the first national lockdown (March to June 2020) restricting my accessing to the facilities. Once back in the laboratory, and as soon as I started obtaining consistent results, the UK entered a second national lockdown (November to December 2020) quickly followed by a third national lockdown (January to March 2021), which restricted my access to research facilities once again. In total, my research activity was impaired over the course of 9 months. This lengthened the time it took for me to obtain both the relevant laboratory technique training and the consistency in independent result collection.

“The brain is a world consisting of a number of unexplored continents and great stretches of unknown territory.”

— Santiago Ramón y Cajal (1852-1934)

A Love Letter to Myself

Acknowledgements

What an odyssey… This thesis was filled with twists and turns, ups and downs, ebbs and flows, highs and lows. Many times, it felt an awful lot like ‘no sleep, bus, club, 'nother club, 'nother club, plane, next place, no sleep, no fear’ (the people who get it, get it). But hey, I made it (I know, shocking). For being there during this adventure, the following people deserve special recognition — I hope I met your expectations, and if not, at least made you laugh.

Kirsty, you have all my gratitude for believing in me and giving me this opportunity. Thank you for always having an open door and motivating me whenever I could not do it myself. Your supervision, guidance, and patience were crucial for this thesis, and I will cherish them forever. Mac, it was an immense privilege getting to learn from you. You always showed interest in my work and challenged me without making me feel small, your legacy will live on forever. We will have a drink whenever we see each other in the next realm.

To all the people in the lab — Anna, Michael, Lucy, Joe (little Joe), Danielle, Zoe, Shreya, Karim; thank you for all your support, you made this an unforgettable experience. Ryan, Mat, and Fran, you are all brilliant and gifted people in your own unique ways. Sorry for my forgetful brain that made you repeat things over and over again. Thank you for teaching me many valuable things, for letting me be my mischievous self, and for listening to my constant moaning. I will miss the moments with you the most.

Joe (big Joe), Viv, Sara, Rayan, and my friends in Spain, thank you for being there and being my rocks. Martyn, thank you for always helping me in the lab with your vast knowledge. Laure, Tatum, and Damini, the original queens in the office, thank you for those early moments that made this experience so special. Ashley, thank you for every single thing you have done, I will never be able to repay you.

And finally, and most importantly, gracias a mi familia, en especial a mi hermana, a mi padre y a mi madre, porque han aguantado años de lloros y ansiedades, porque siempre están ahí cuando los necesito ofreciéndome un hogar al que volver. No podría tener una mejor familia y no podría haberlo hecho sin vosotros, os quiero. Dani, mi marido, el amor de mi vida, qué te voy a decir que no sepas ya… Gracias por tu apoyo, por las risas, por el cariño, por quererme tanto y quererme siempre. Brindo por muchos años de musicales contigo, porque las penas, a tu lado, desaparecen. Esta tesis va por vosotros.

List of contents

List of figures

List of tables

List of abbreviations

5-HT	5-hydroxytryptamine
II_i	Lamina II inner section
II_{id}	Lamina II inner dorsal section
II_{iv}	Lamina II inner ventral section
II_o	Lamina II outer section
AAV	Adeno-associated virus
ACC	Anterior cingulate cortex
ALS	Anterolateral system
AMPA	α-amino-3-hydroxy-5-methyl-4-isoxazole propionic acid
ASIC	Acid-sensing ion channel
ATP	Adenosine 5'-triphosphate
C	Cervical
Ca_v	Voltage-gated sodium channel
CGRP	Calcitonin gene-related peptide
CIBP	Cancer-induced bone pain
CM	Mechanosensitive C-fibre
CM_i	Mechano-insensitive C-fibre
CNS	Central nervous system
Co	Coccygeal
CPM	Conditioned pain modulation
DCML	Dorsal column-medial lemniscus
DCN	Descending control of nociception
DMEM	Dulbecco's modified Eagle medium
DMSO	Dimethyl sulfoxide
DNIC	Diffuse noxious inhibitory controls
DPBS	Dulbecco's phosphate-buffered saline

DPMS	Descending pain modulatory system
DRG	Dorsal root ganglion
DT	Diphtheria toxin
DTR	Diphtheria toxin receptor
EDTA	Ethylenediaminetetraacetic acid
EF	Elongation factor
eGFP	Enhanced green fluorescent protein
F	Fluorescence
FBS	Foetal bovine serum
FIV	Feline immunodeficiency virus
fMRI	Functional magnetic resonance imaging
GABA	Gamma-aminobutyric acid
GC	Genome copies
GCaMP	Green fluorescent protein + calmodulin + peptide M13
GDNF	Glial cell line-derived neurotrophic factor
GFRα	Glial factor receptor α
HB-EGF	Heparin-binding epidermal growth factor
HBSS	Hanks' balanced salt solution
IASP	International Association for the Study of Pain
IB4	Isolectin B4
IC	Insular cortex
ID	Inner diameter
IP	Intraperitoneal
K_{Ca}	Calcium-activated potassium channel
K_{Na}	Sodium-activated potassium channel
K_v	Voltage-gated potassium channel
L	Lumbar
LLC	Lewis lung carcinoma

mGlu	Metabotropic glutamate
MOI	Multiplicity of infection
MRMT-1	Metastatic rat mammary tumour 1
Na_v	Voltage-gated sodium channel
NGF	Nerve growth factor
NMDA	N-methyl-D-aspartate
NN	Non-nociceptive
NS	Nociceptive specific
OD	Outer diameter
P	Post-natal
P2A	Porcine teschovirus-1 2A
PAD	Primary afferent depolarization
PAG	Periaqueductal grey
PFA	Paraformaldehyde
PFC	Prefrontal cortex
PNS	Peripheral nervous system
Puro	Puromycin
RET	Rearranged after transduction
RNA	Ribonucleic acid
ROI	Region of interest
RPMI	Roswell Park Memorial Institute
RVM	Rostral ventromedial medulla
S	Sacral
SI	Primary somatosensory cortex
SII	Secondary somatosensory cortex
SABV	Sex as a biological variable
SC	Subcutaneous
T	Thoracic

T2A	Thosea asigna virus 2A
TG	Trigeminal ganglion
TrKA	Tropomyosin receptor kinase A
TRP	Transient receptor potential
TRPA	Transient receptor potential ankyrin
TRPM	Transient receptor potential melastatin
TRPV	Transient receptor potential vanilloid
TU	Transducing units
WDR	Wide-dynamic range
µCT	Micro-computed tomography
WHO	World Health Organization

CHAPTER

INTRODUCTION

1.1. Overview: pain and cancer

Cancer represents one of the leading causes of death worldwide, accounting for nearly 10 million deaths per year (World Health Organization). Improvements in cancer detection and therapeutic strategies have extended the life expectancy of cancer patients, leading to an increased focus on improving patient quality of life. Sadly, around 50% of cancer patients suffer from moderate to severe pain during the progression, and even remission, of the disease (with numbers reaching nearly 70% in late/terminal stages) (Breivik et al., 2009; Deandrea et al., 2008; van den Beuken-van Everdingen et al., 2016). This, in addition to the inability of cancer pain treatments to target the underlying mechanisms leading any one particular pain state, makes pain one of the most invalidating symptoms in the oncological population.

Cancer-induced pain may be borne from the tumour itself, anticancer treatments (such as chemotherapy, radiotherapy, and/or surgery), and/or pre-existing comorbid diseases (Caraceni and Shkodra, 2019; Cavaletti et al., 2011; Dropcho, 2010; Schreiber et al., 2013; Siembida et al., 2021). Considering that cancer patients present a wide variety of additional symptoms including fatigue, anorexia, cachexia, chronic nausea, dyspnoea, anxiety, and depression, it is easy to understand why the pain experience may escalate to an unbearable level.

Cancers can be broadly divided into primary cancers (original location where the cancer started developing) and secondary cancers (additional locations invaded by metastatic primary cancer cells). Specifically, some of the most common cancers (e.g., breast, prostate, lung) tend to metastasise to skeletal structures, making bones the third most frequent site of metastases (only surpassed by the lungs and the liver) (Ryan et al., 2022). These bone metastases lead to one of the most common types of cancer pain named **cancer-induced bone pain (CIBP)**, with 50% of hospitalised cancer patients suffering from it (Brescia et al., 1992; Grond et al., 1996). Although primary bone cancers (e.g., osteosarcoma, Ewing sarcoma, chondrosarcoma) also produce bone pain, they account for less than 1% of the total diagnosed cancers (Biermann et al., 2013). Secondary bone cancers, on the other hand, are way more frequent, with up to 85% of the patients dying from breast, prostate, or lung cancer showing bone involvement at autopsy (Mercadante, 1997). However, the location and severity of the cancer itself does not always correlate with the severity of the pain. This is best exemplified when considering that, after successful treatment and remission of the disease, around 40% of patients still suffer from chronic

pain (Cox-Martin et al., 2020; Forsythe et al., 2013; Green et al., 2011; Halpern et al., 2022; Jiang et al., 2019; Karlson et al., 2020; Lu et al., 2011; Seretny et al., 2014; van den Beuken-van Everdingen et al., 2007). The mechanisms driving this pain state are poorly understood and, as such, their investigation forms the basis of this thesis. Below, the broader classification and mechanistic underpinning of pain are outlined before a focus on preclinical models, and understanding, of CIBP.

1.2. The burden and classification of pain

Pain has an immense evolutionary importance, serving a vital protective mechanism essential for survival, alerting the body to damage (potential or actual). This permits the organism to take steps to avoid, for example, tissue injury, or to prevent further damage from occurring (Lee and Neumeister, 2020). Without pain, continued exposure of damaged tissue to everyday menial tasks could lead to catastrophic inflammatory cascades and/or painless fractures, that themselves, if untreated, would lead to body deformities, recurrent soft tissue infections, and/or self-mutilating injuries (Nagasako et al., 2003). In short, 'life without pain could really hurt you' (Brand and Yancey, 1993). Short-lived protective pain is referred to as 'acute' pain, one of two broad pain classifications that vary according to their temporal progression:

- **Acute pain:** Its appearance coincides with tissue damage (potential or actual) and resolves once the tissue has healed (Grichnik and Ferrante, 1991). Acute pain is self-limited and, clinically, refers to pain lasting less than 3 months (Michaelides and Zis, 2019).

- **Chronic pain:** This type of pain has no clear biological purpose and arises when pain persists beyond the resolution of the injury or insult (Burma et al., 2017). In the clinical context, chronic pain refers to pain that lasts longer than 3 months (Michaelides and Zis, 2019).

Unfortunately, chronic pain is one of the most common diseases worldwide (Rice et al., 2016), placing a huge burden on the healthcare system and being tightly associated with suffering, social isolation, and disability (Domenichiello and Ramsden, 2019). The prevalence of chronic pain, when reported as a singular condition, is around 30% in the general adult population (Elzahaf et al., 2012; Leadley et al., 2012), suggested to be as high as 75% in some cases in the elderly population (Abdulla et al., 2013), and around 30-40% in the adolescent population (Gobina et al., 2019; King et al., 2011).

Gender (Greenspan et al., 2007), socio-economic background (Janevic et al., 2017), employment and occupational status (Teasell and Bombardier, 2001), lifestyle (to include alcohol consumption and smoking) (Egli et al., 2012; Orhurhu et al., 2015), physical activity (Geneen et al., 2017), nutrition (Brain et al., 2019), and sun exposure (Straube et al., 2009) are all factors known to modulate the prevalence of chronic pain within a population. Clinical components also contribute to the development of chronic pain, including multiple or previous pain conditions (Elliott et al., 2002), multi-morbidities (Dominick et al., 2012), mental health (Lee et al., 2018), surgical and medical interventions (Gan, 2017), weight (Hitt et al., 2007), sleep disorders (Jank et al., 2017), and genetic aspects (Zorina-Lichtenwalter et al., 2016). Finally, attitudes and beliefs towards pain (Blyth et al., 2005), and a history of traumatic events (Nelson et al., 2018) will also impact the propensity of an individual to suffer from chronic pain. Simply put, the experience of pain is a complex personal phenomenon, and one's subjective perception is influenced to varying degrees by biological, psychological, and social factors.

In addition to the pain classification according to its temporal progression (in terms of acute and chronic classifications), pain can also be subdivided according to its mechanistic/etiologic aspects (Kosek et al., 2016; Trouvin and Perrot, 2019):

- **Nociceptive pain:** Encompasses pain that arises from actual or threatened damage to non-neural tissue leading to nociceptor activation.

- **Neuropathic pain:** Comprises any type of pain caused by a lesion or disease of the somatosensory nervous system.

- **Nociplastic pain:** Includes any pain that arises from altered nociception despite no clear evidence of actual or threatened tissue damage causing nociceptor activation nor evidence for disease or lesion of the somatosensory system causing the pain.

Moreover, tissue injury that results in cell damage will likely involve the release of inflammatory mediators which may activate and sensitise nociceptors, leading to **inflammatory pain**. This type of pain typically improves and resolves after the tissue has healed, although a pain component can persist after injury resolution (chronic inflammatory pain) (Kehlet et al., 2006). Thus, every classification of pain can also have an inflammatory component, boosting the complexity of classification of the pain experience.

Cancer pain is a mixed-mechanism pain state exhibiting elements that can be classified as nociceptive, neuropathic, or nociplastic (concurring with inflammatory components in most cases). However, it is also characterised by distinctive modifications to the peripheral nervous system and tissues as well as unique neurochemical changes that cannot be included in any of the categories mentioned (e.g., vascular changes, hypoxic tumorigenic microenvironment, compression/distension/invasion of nerves) (Falk and Dickenson, 2014).

Finally, the verbal descriptive approach also offers a classification of pain according to its characteristics, pain behaviour, and present symptomatology. As a subjective experience, pain is often scored using self-reported pain measures or scales with numerous verbal descriptors (e.g., aching, sharp, tender, throbbing, burning, stabbing, itchy, tiring, exhausting, frightening, annoying, troublesome, miserable) (Wilkie et al., 2001). Nevertheless, verbal descriptors show inconsistent results when used alone to classify pain, and therefore, can offer only marginal utility (Boureau et al., 1990; Putzke et al., 2002). As such, medical diagnoses serve as an additional useful tool when establishing a pain classification, especially regarding chronic pain. In each chronic syndrome, pain is conceived either as a disease itself (chronic primary syndromes) or as a symptom of another health condition (chronic secondary pain syndromes) (Treede et al., 2019).

1.3. Pain vs Nociception

The International Association for the Study of Pain (IASP) describes **pain** as 'an unpleasant sensory and emotional experience associated with, or resembling that associated with, actual or potential tissue damage' (Raja et al., 2020). The pain experience encompasses three dimensions: sensory-discriminative (regarding the location, quality, and severity), affective-motivational (referring to feelings of unpleasantness, distress, and threat), and cognitive-evaluative (reflecting the individual's attitudes and beliefs towards pain) (Melzack, 1999). Nevertheless, some have argued that social factors must be included and that a fourth dimension should be added to the list: the psychosocial dimension (Gustin et al., 2011). Crucially, all the dimensions mentioned may co-exist or exist separately.

Nociception, on the other hand, is defined as 'the neural process of encoding noxious stimuli' (Nitzschke et al., 2022). When discussing nociception, we generally refer to it as one of four main processes of somatosensation. The somatosensory system accounts for processing information

regarding body sensation, including external (environmental) information and the internal body state. Hence, the somatosensitive modalities are responsible of the sensations of touch (mechanoreception), temperature (thermoception), pain (nociception), and body position and movement (proprioception) (Manivannan and Suresh, 2012). It is noteworthy that, even though transmission of nociceptive information results in pain perception under most circumstances, nociception does not always lead to pain, and pain can occur in the absence of measurably noxious stimuli (Garland, 2012).

1.4. Anatomical nociceptive components

1.4.1. Nociceptor functionality

Sensory neurons (also known as primary afferents or first-order neurons) constitute the basic units of the somatosensory system and subserve the peripheral nervous system (PNS) transforming and transmitting external and internal body information to the central nervous system (CNS). The cell bodies of the primary afferents are clustered in the trigeminal ganglia (TG) or the dorsal root ganglia (DRG), depending on whether they innervate, respectively, orofacial areas or the rest of the body. Primary afferents display a pseudounipolar anatomy (see **Figure 1.1**), presenting one single axon that bifurcates generating two branches (or processes), one of which projects to peripheral tissues and the second of which projects to the spinal cord, relaying the information (Dubin and Patapoutain, 2010).

These neuronal processes can be classified according to the electrophysiological and anatomical characteristics of the primary afferent. One of the main characteristics is the presence or absence of a myelin sheath, that increases the efficiency and velocity of the signal transmission and determines the diameter of the fibre (Middleton et al., 2022). Primary afferent fibres may be designated as Aα-, Aβ-, Aδ-, or C-fibre subtypes according to these parameters (or as types I, II, III, and IV, respectively). Aα-fibres are normally related to the transmission of proprioceptive information, Aβ-fibres are mainly responsible for innocuous mechanoreceptive transmission, and Aδ- and C-fibres are generally related to nociception and are responsible for ‘first/sharp’ pain and ‘second/slow’ pain, respectively (see **Table 1.1** for a broad classification of somatosensory fibre types and their characteristics) (Basbaum et al., 2009; Julius and Basbaum, 2001).

Particularly, nociceptors are a subtype of primary afferents characterised by their ‘naked’ (free) nerve endings that preferentially encode and transmit noxious stimuli (defined as high mechanical

pressure, extreme temperatures, and/or exposure to irritant chemicals) (Sneddon, 2018). Thinly myelinated Aδ-fibres and unmyelinated C-fibres that demonstrate exclusive sensitivity to mechanical stimuli are termed 'mechanonociceptors', while those with restricted sensitivities to thermal or chemical stimuli are referred to as 'thermonociceptors' or 'chemonociceptors', respectively. Moreover, fibres can express a combination of these sensitivities, being collectively referred to as 'polymodal' nociceptors (Prato et al., 2017). Broadly, nociceptive Aδ-fibres can be subclassified into type I (characterised by high heat thresholds) and type II (defined by high mechanical thresholds) (Treede et al., 1998; see also Basbaum et al., 2009), whilst nociceptive C-fibres are broadly classified as mechano-sensitive (CM) or mechano-insensitive (CM_i) (Serra et al., 2004; see also Middleton et al., 2021). Interestingly, a unique nociceptor subtype is insensitive to noxious stimulation under normal physiological conditions but becomes mechanically and/or thermally sensitive after the induction of local inflammation, revealing the capacity of nociceptors to become sensitised in disease states. These insensitive nociceptors receive the name of 'silent' or 'sleeping' nociceptors and account for up to 25% of total C-fibres in humans (Schmidt et al., 1995), with lower values in murine species (Kress et al., 1992; Wetzel et al., 2007).

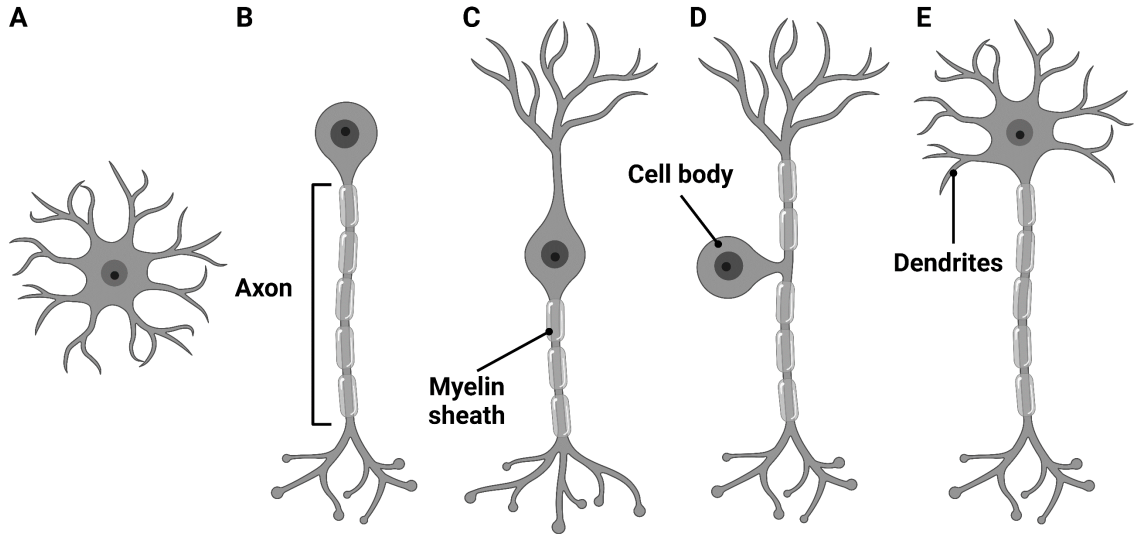

Figure 1.1. Structural classification of neurons. *Neurons can be classified according to the distribution and number of neuronal processes originating from the cell bodies (i.e., axons and dendrites).* ***(A)*** *Anaxonic neuron (e.g., amacrine cells in the retina).* ***(B)*** *Unipolar neuron (e.g., unipolar brush cells in the cerebellum).* ***(C)*** *Bipolar neuron (e.g., olfactory sensory neurons in the nasal epithelium).* ***(D)*** *Pseudounipolar neuron (e.g., sensory neurons or primary afferents).* ***(E)*** *Multipolar neurons (e.g., majority of the neurons in the central nervous system).*

Table 1.1. Classification of peripheral sensory fibres. *Sensory fibres can be divided according to their electrophysiological and anatomical characteristics. Values taken from multiple reference sources (Koga et al., 2005; Sneddon, 2018; West et al., 2015).*

GROUP	FIBRE	DIAMETER	MYELINATION	CONDUCTION	MODALITY	INFORMATION
Type I (Ia & Ib)	Aα	Very large (12-20 µm)	Very thickly myelinated	Super-fast (70-120 m/s)	Proprioception	Body sensation (internal and external)
Type II	Aβ	Large (5-12 µm)	Thickly myelinated	Fast (20-100 m/s)	Proprioception Mechanoreception	Mechanical (light touch and pressure)
Type III	Aδ	Medium (1-6 µm)	Thinly myelinated	Intermediate (5-40 m/s)	Mechanoreception Thermoception Nociception	Mechanical and thermal (innocuous and noxious; fast transmission)
Type IV	C	Small (0.3-2.3 µm)	Unmyelinated	Slow (0.5-2 m/s)	Mechanoreception Thermoception Nociception	Mechanical, thermal, and chemical (innocuous and noxious; slow transmission)

In addition, nociceptors can be classified attending to their genetic and molecular profile. Each new embryonic nociceptor expresses tropomyosin receptor kinase A (TrKA), a transmembrane receptor with high affinity for the nerve growth factor (NGF). These two components (TrKA and NGF) are critical for nociceptor development, with a defect in TrKA leading to congenital insensitivity to pain (Indo et al., 1996). According to the embryonic nociceptive differentiation pathway, nociceptors can be classified into two broad categories (Basbaum et al., 2009):

- **Peptidergic nociceptors:** These nociceptors constitute the largest group and generally maintain TrKA expression, making them NGF-dependant. They are defined by the synthesis and release of sensory neuropeptides such as calcitonin gene-related peptide (CGRP) and/or substance P.

- **Non-peptidergic nociceptors:** These nociceptors usually stop expressing TrKA and, instead, express the transmembrane complex formed by the glial factor receptor α and the 'rearranged after transduction' receptor (GFRα-RET), becoming dependent on the glial cell line-derived neurotrophic factor (GDNF) for survival. They are characterised by the expression of the P2X purinergic ion channel type 3 receptor (P2X3) and/or by isolectin B4 (IB4) binding.

However, even though this historical classification is broadly used, single cell ribonucleic acid (RNA) sequencing studies have proven the existence of numerous additional nociceptive

subpopulations, showing the complexity of primary afferent functional and molecular division (Li et al., 2018; Usoskin et al., 2015; see also Chen et al., 2023). Moreover, several studies have found overlapping markers, features, and functions between species (Price and Flores, 2007; Rostock et al., 2018; Shiers et al., 2021).

The great heterogeneity of nociceptors offers the opportunity to make additional classifications according to the noxious specificity based on the expression of different receptor subtypes. To name a few, nociceptors can express transient receptor potential channels (TRPs), which can be sensitive to heat (e.g., TRPV1), cold (e.g., TRPM8), or chemical irritants (e.g., TRPA1); acid-sensing ion channels (ASICs), sensitive to protons (H^+) and acidic milieu; purinergic P2 receptors, especially sensitive to adenosine 5'-triphosphate (ATP) fluctuations (e.g., P2X3); and/or receptors from the Piezo family, that are mechanosensitive (e.g., Piezo2) (Basbaum et al., 2009; Benarroch, 2015; Della Pietra et al., 2020).

1.4.2. Spinal cord architecture

The spinal cord is a highly organised and complex component of the central nervous system that acts as a modulatory and integrative relay point of peripheral somatosensory input to the brain. The spinal cord also serves as a transmission centre for information originating in higher brain structures associated to peripheral motor control, as well as being accountable for the initiation and coordination of many reflex arcs (Geertsen et al., 2017; Rabchevsky, 2006).

From a structural point of view, the spinal cord is a cylindrical structure of nervous tissue enclosed in the vertebrae bones that can be longitudinally divided into segments determined by the emergence of the spinal nerves. These segments are classified as cervical (C), thoracic (T), lumbar (L), sacral (S), and coccygeal (Co), with the human spinal cord showing a total of 31 segments (C1-C8, T1-T12, L1-L5, S1-S5, and Co1), whilst the murine spinal cord presents 34 (C1-C8, T1-T13, L1-L6, S1-S4, and Co1-Co3) (Molander et al., 1984; Sengul et al., 2012).

The spinal cord shows a clear differentiation between the grey matter and the surrounding white matter (cell bodies and axons, respectively) (see **Figure 1.2**). Specifically, the white matter is grouped in bundles of axons called funiculi that can be classified as dorsal, ventral, and lateral, while the grey matter can be divided into the dorsal and ventral horns (in some segments, a lateral horn can be also present).

The grey matter is arranged in a 'butterfly' or 'H' shape and can be further divided in a series of layers (named the laminae of Rexed) according to their anatomical and electrophysiological characteristics (Rexed, 1954). Ten laminae are recognised (laminae I-X): dorsally located laminae (laminae I-VI) receive and transmit somatosensory information; laminae conforming the ventral horn (laminae VII-IX) receive and transmit motor information; lamina X surrounds the central canal (Dinakar and Stillman, 2016). Moreover, some laminae can be subdivided; the best example being lamina II, that can be divided into an outer (II_o) and an inner (II_i) section. This latter part of lamina II can even be further subdivided into inner dorsal (II_{id}) and inner ventral (II_{iv}) (Alles and Smith, 2018).

In the human spinal cord, the estimated number of cells are in the order of 1.5 billion, with roughly 15% of those cells corresponding to neurons (sensory, motor, and interneurons), 10% to endothelial cells, and 75% to glial cells (Bahney and von Bartheld, 2018). Specifically, sensory neurons in the dorsal horn of the spinal cord can be classified in accordance with their sensitive convergence, which includes the type of information they receive from primary afferents and their respective input sensitivity:

- **Non-nociceptive (NN) neurons:** Responsive only to innocuous mechanical and thermal as well as proprioceptive stimuli. These cells receive peripheral information from Aα-, Aβ-, and Aδ-fibres. They are located predominantly within laminae III and IV but also laminae I and II, to a lesser extent (Almeida et al., 2004; Kibaly et al., 2016).

- **Nociceptive-specific (NS) neurons:** Activated exclusively by strong noxious stimulation and unresponsive to innocuous stimulation. Their activity is mediated by C- and Aδ-fibre input, showing punctiform receptive fields with limited gradual responses to stimulus intensities and fast adaptative firing during prolonged stimulation periods (i.e., the response to the stimulus is transient with a quick decline in firing rate). These cells are vastly located in laminae I and II but can also be present in deeper layers like laminae V, VI, and X (Christensen and Perl, 1970; Coghill et al., 1993).

- **Wide-dynamic range (WDR) neurons:** Reactive to a broad range of input, these neurons are activated by noxious and innocuous stimuli. They manifest considerable convergence from C- and Aδ-fibres as well as Aβ- and Aα-fibres. These cells present gradual responses to the intensity of

the stimulus, variable receptive field sizes, and slow adaptative firing to prolonged stimulation (i.e., minimal firing frequency decline, firing continues for the duration of the stimulus). These neurons are predominantly present in lamina V but can also be found within laminae I, II, IV, VI, and X (Coghill et al., 1993; Dubner et al., 1989).

Of special interest, WDR neuronal properties are conserved across species as they are involved in multiple aspects of nociceptive processing. As previously mentioned, WDRs are defined by fine-tuned intensity coding that correlates to pain thresholds and are generally characterised by prolonged after-firing following noxious stimulation (post-discharge) (O'Neill et al., 2015). Additionally, WDRs encode for **spatial summation**, a multisynaptic physiological phenomenon whereby increasing the area of a stimulus, or concurrent application of noxious stimuli in different areas, have a cumulative effect upon cell activity and nociceptive input (Reid et al., 2015; Sikandar et al., 2013). Spinal WDRs also show temporally driven summation mechanisms known as '**wind-up**' thought to reflect and encode for **temporal summation**, defined as a homosynaptic event where application of a given stimulus in a periodic repeated pattern progressively facilitates neuronal firing rates and nociceptive drive (Staud et al., 2003; Trendafilova et al.,2022).

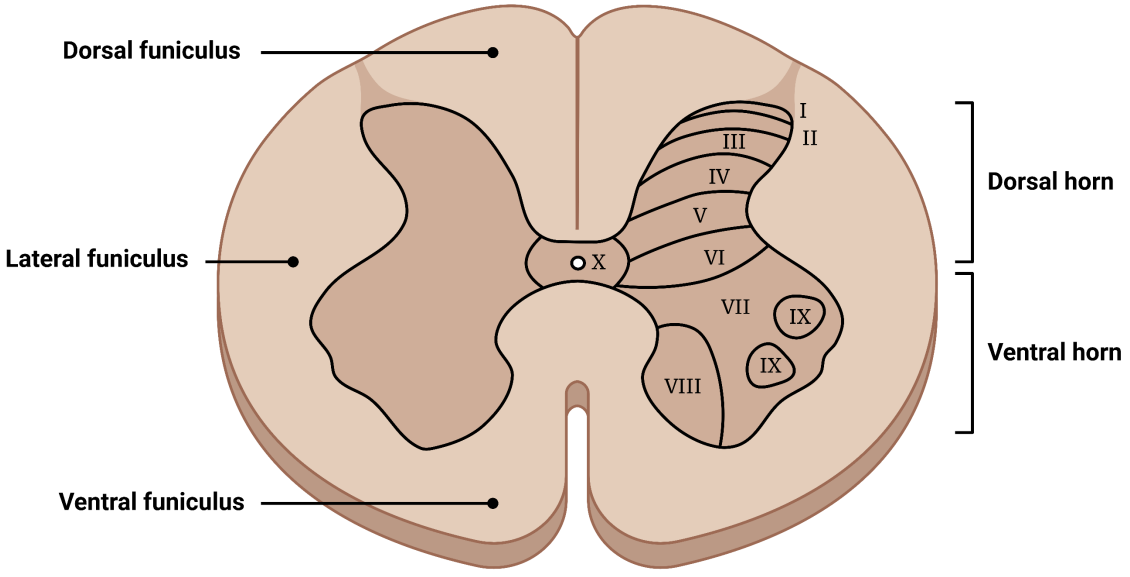

Figure 1.2. Spinal cord functional division. *Transversal section of the spinal cord (lumbar level) representing the inner grey matter (with the characteristic 'butterfly' or 'H' shape) and the surrounding white matter (including funiculi division). The grey matter is divided into dorsal (laminae I-VI) and ventral horns (laminae VII-IX) and is connected to the central canal (lamina X). Lateral horns and laminae subdivisions not pictured.*

1.5. The physiology of nociception

1.5.1. Transducing noxious stimuli

The first step in the nociceptive process is the transformation of a noxious stimulus (internal or external) into an electrochemical signal (action potential) (see **Figure 1.3**). This mechanism (named 'transduction') is performed by the unique and complex mosaic of ion channels present in the primary afferent. Some of the most well characterised channels involved in nociceptive transduction include subtypes of the previously mentioned transient receptor potential channels (TRPs), acid-sensing ion channels (ASICs), purinergic P2 receptors, and receptors from the Piezo family (Benarroch, 2015; Della Pietra et al., 2020).

Typically, neurons present a negative resting membrane potential of -70 mV caused by differences in ionic concentrations against the extracellular environment. The presence of large gradients of ions across the cell and the relative membrane permeability to them are responsible for the maintenance of this value. Thus, when presented with the appropriate stimulus, the corresponding channels undergo conformational changes, leading to complex excitatory and inhibitory ionic fluxes that result in alterations of the membrane potential. If a noxious stimulus is of sufficient intensity and the depolarization surpasses the threshold potential (around -55 mV), the signal is transformed into an **action potential** (around +40 mV) and propagated along the primary afferent (Yam et al., 2018).

The maintenance and propagation of action potentials is caused by the opening of depolarizing voltage-gated sodium (Na_v) and calcium (Ca_v) channels, followed by the repolarizing activity of voltage-gated (K_v), sodium-activated (K_{Na}), and calcium-activated (K_{Ca}) potassium channels. Specific sodium (e.g., $Na_v1.7$, $Na_v1.8$, $Na_v1.9$), calcium (e.g., $Ca_v1.2$, $Ca_v2.2$, $Ca_v3.2$), and potassium channels (e.g., $K_v1.1$, $K_v1.4$, $K_v2.2$, $K_v3.4$, $K_v4.3$, K_v7) are preferentially expressed in nociceptive primary afferents (Benarroch, 2015), where functional abnormalities lead to abnormal nociceptive processing and/or altered pain perception (Bennett et al., 2019; Gribkoff, 2006; Tsantoulas and McMahon, 2014; see also Cregg et al., 2010). Action potentials can initiate in the peripheral terminal of the primary afferent, propagating along the neuron, and terminating in the dorsal horn of the spinal cord. Here, different neurotransmitters are released by the presynaptic terminal into the synaptic cleft (in a calcium dependent manner), resulting in activation of the postsynaptic terminal and the propagation of the signal to the second-order neuron. Virtually all primary afferents use glutamate as their primary neurotransmitter, but additional neurotransmitters

like vasoactive peptide, somatostatin, calcitonin gene-related peptide (CGRP), substance P, and/or ATP may additionally be released depending on the primary afferent fibre (Gold and Gebhart, 2010; Mantyh et al., 1989; Yam et al., 2018). Less frequently, action potentials may also initiate in the central terminal and travel in the 'reverse' direction to the periphery (named dorsal root reflexes) (Willis, 1999).

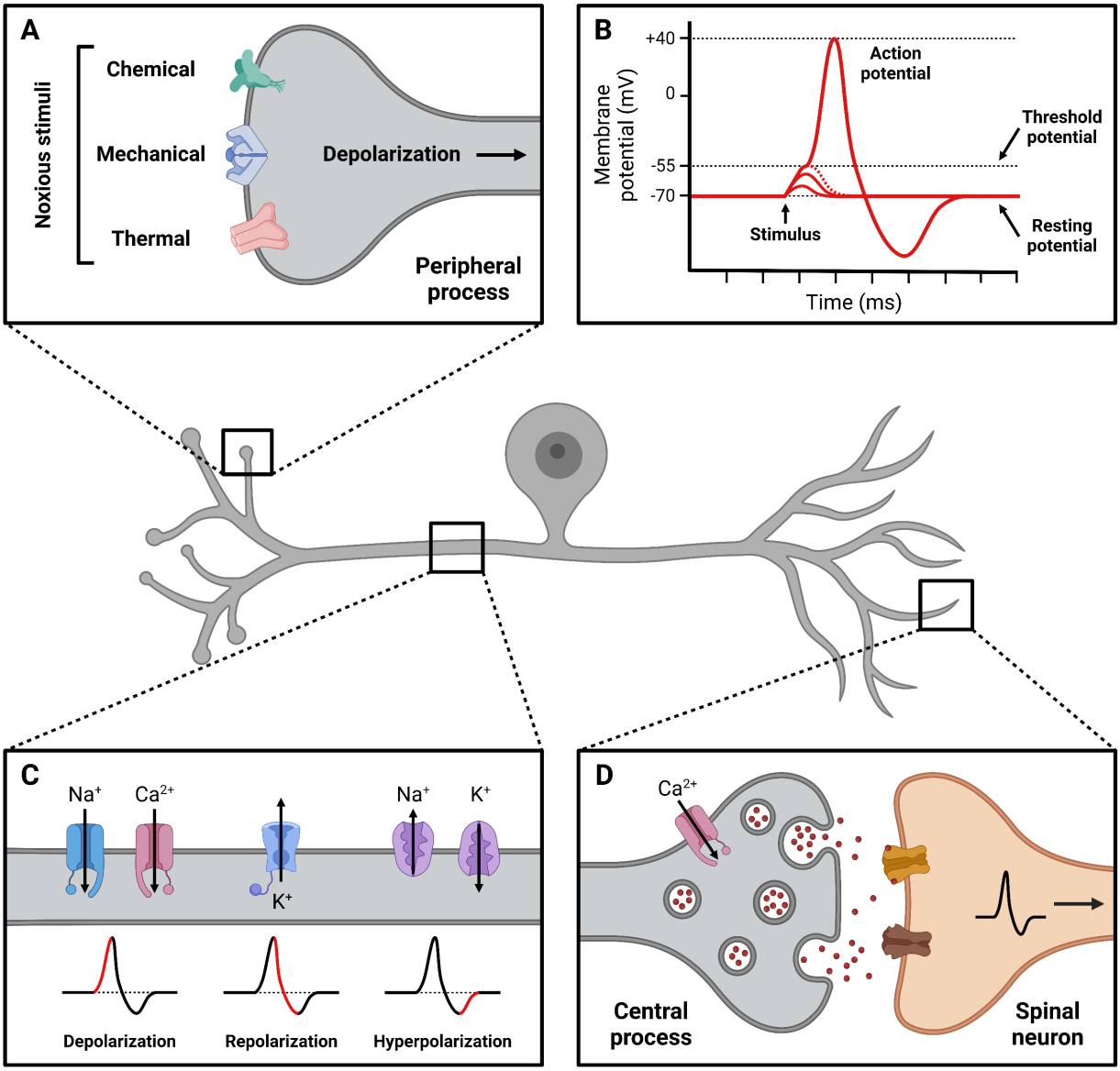

Figure 1.3. Nociceptive transduction in the primary afferent. *Representation of the initiation, propagation, and transmission of the action potential in the nociceptive primary afferent.* ***(A)*** *Natural noxious stimuli (i.e., chemical, mechanical, thermal) activate the corresponding channels in the periphery (e.g., P2X3, Piezo2, TRPV1) and depolarise the primary afferent.* ***(B)*** *If the depolarization reaches the threshold potential (-55 mV), the signal is transformed into an action potential (+40 mV).* ***(C)*** *Action potentials are propagated along the neuron thanks to the depolarizing sodium and calcium channels as well as the hyperpolarizing potassium channels.* ***(D)*** *Once the action potential reaches the central terminal at the spinal cord, neurotransmitter release occurs (e.g., glutamate) in a calcium-dependent manner, and the action potential is transmitted to the second-order neuron.*

1.5.2. Spinal cord nociceptive transmission

After entering the dorsal horn of the spinal cord (via the so-called Lissauer's tract), primary afferent terminals widely arborise and synapse with spinal cord neurons. This allows for signal transmission between primary afferents (first-order neurons) and **projection neurons** (second-order neurons), that will transmit the signal to various supraspinal structures and are concentrated in lamina I (and scattered throughout laminae III–VI) (Wercberger and Basbaum, 2019). However, primary afferents frequently synapse with spinal excitatory or inhibitory interneurons (located predominantly in laminae I, II, and III) that modulate the signal strength and will, ultimately, transmit the information to a projection neuron (Todd, 2010).

Relay of the primary afferent input to the dorsal horn occurs mostly ipsilaterally (same side), however, some input may also be transmitted contralaterally (opposite side). Interestingly, in the dorsal horn, sensory neurons terminate in modality-specific patterns (see **Figure 1.4**). Specifically, Aβ-fibres mainly project to deep laminae (III, IV, and V), Aδ-fibres project primarily to lamina I as well as lamina V, and C-fibres principally project directly to superficial laminae I and II with indirect (polysynaptic) projections to lamina V (Basbaum et al., 2009; D'Mello and Dickenson, 2008).

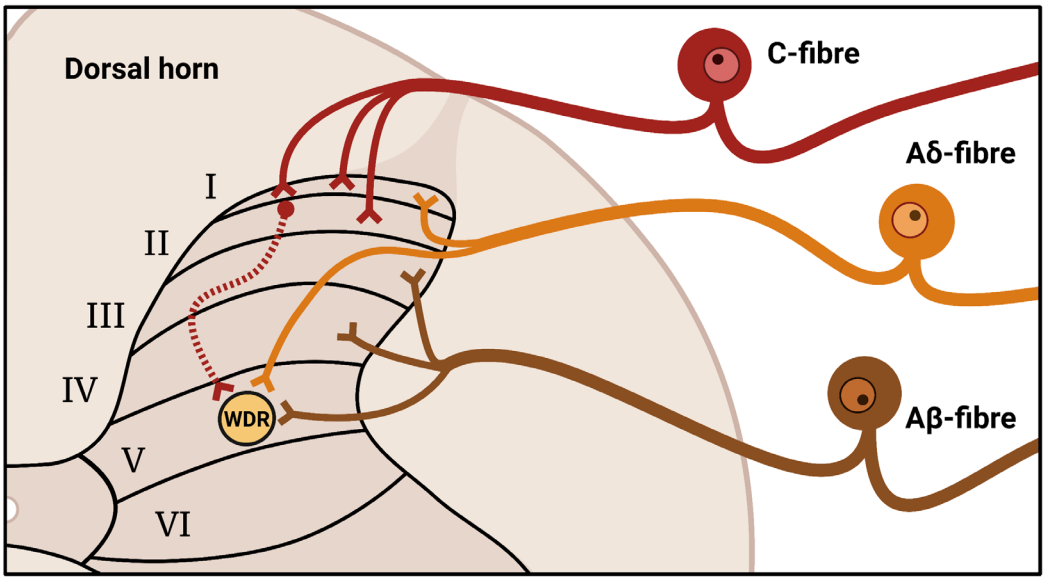

Figure 1.4. Primary afferent laminar projections in the dorsal horn. *Different populations of primary afferents project to different regions of the dorsal horn. Input carried by unmyelinated C-fibres terminates in superficial laminae (laminae I and II) with indirect projections to deeper laminae (lamina V). Aδ-fibres project to both, superficial laminae as well as deeper laminae (laminae I and V, respectively) whilst innocuous information carried by and Aβ-fibres usually ends in deep laminae (laminae III, IV, and V). Laminae subdivisions not pictured. WDR: wide-dynamic range.*

When released at the presynaptic terminal, glutamate can bind to a range of glutamate family receptors present in the membrane of the spinal neurons, including ionotropic AMPA (α-amino-3-hydroxy-5-methyl-4-isoxazole propionic acid), ionotropic NMDA (N-methyl-D-aspartate), and/or metabotropic glutamate (mGlu) receptors (Yam et al., 2018). The activity of these receptors will lead to the creation of an action potential in the spinal neurons (interneurons and/or projection neurons), propagating the signal. Excitatory spinal cord interneurons use glutamate as their major neurotransmitter (glutamatergic), whilst gamma-aminobutyric acid (GABA) and glycine represent the main transmitters of inhibitory spinal cord interneurons (GABAergic and glycinergic, respectively) (Todd, 2010).

1.5.3. Ascending nociceptive pathways

Nociceptive information transmitted to second-order neurons projects (ascends) through the white matter funiculi to supraspinal areas. This occurs in a contralateral manner (vast majority of cases) with projection neurons crossing the midline at different levels, although it can also happen ipsilaterally or bilaterally (Liu et al., 2009; Spike et al., 2003). There are numerous somatosensory ascending pathways originating in the spinal cord (see **Figure 1.5**) that can be anatomically grouped in three main categories (Chandar and Freeman, 2014; Tan et al., 2023):

- **Dorsal column-medial lemniscal (DCML) system:** Relays information primarily related to discriminative (fine) touch, stereognosis, vibratory sense, and conscious proprioception. Includes the fasciculus gracilis and the fasciculus cuneatus, carrying sensory information from the lower and upper body, respectively.

- **Spinocerebellar system:** Largely carries unconscious proprioceptive information to the cerebellum for the coordination of movements and balance. Includes the dorsal (posterior) spinocerebellar tract (or its upper-limb homologue cuneocerebellar tract) and the ventral (anterior) spinocerebellar tract (or its upper-limb homologue rostral spinocerebellar tract).

- **Anterolateral system (ALS):** Predominantly relays pain and temperature sensation, as well as non-discriminative (crude) touch, pressure, and some proprioceptive sensation. Encompasses numerous pathways.

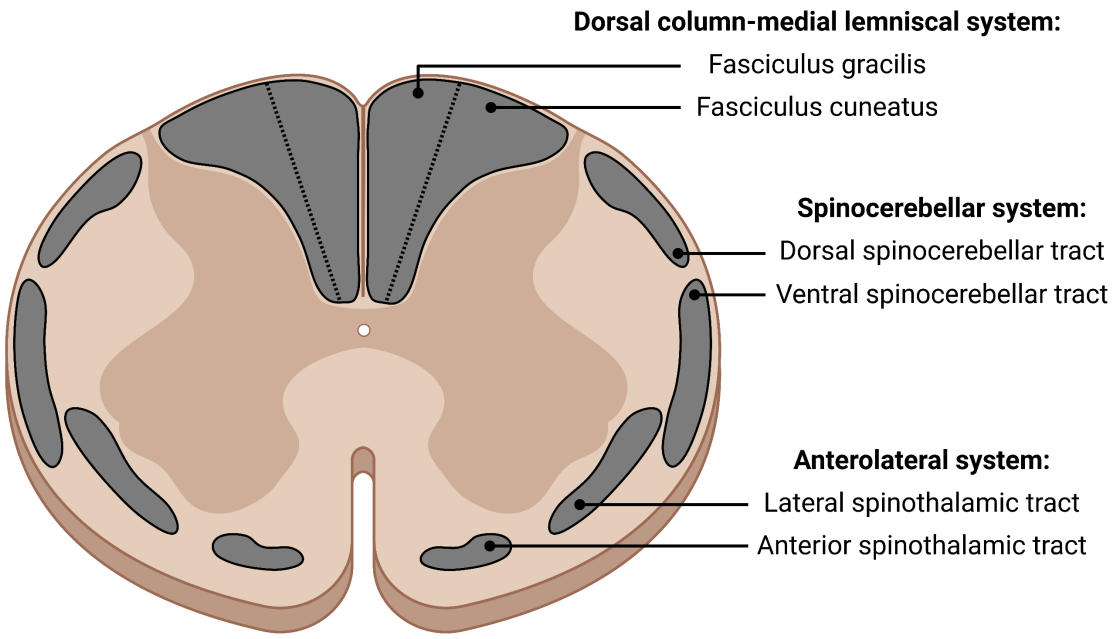

Figure 1.5. Spinal distribution of ascending sensory pathways. *Different ascending pathways projecting to supra-spinal areas show different anatomical distributions in the white matter of the spinal cord. The dorsal-medial lemniscal system, spinocerebellar system, and anterolateral system (with their respective subdivisions) are depicted.*

Of particular interest to the nociceptive process, the anterolateral system (ALS) can be subdivided into different ascending pathways that include different types of projection neurons which themselves can relay (but are not restricted to) nociceptive information (see **Figure 1.6**). These numerous subdivisions, which may present anatomical, functional, and physiological overlaps due to collateral synapses and/or multiple region projections (Al-Khater and Todd, 2009; Spike et al., 2003), include:

- **Spinothalamic tract:** Comprises projections from the spinal cord to the thalamus (e.g., ventral posterolateral nucleus, central lateral nucleus, posterior complex). This tract is formed by the ventral (or anterior) spinothalamic tract, transmitting crude touch and pressure, and the lateral spinothalamic tract, conveying information related to temperature and pain. There is also evidence of a dorsolateral spinothalamic tract that relays nociceptive-specific information (Apkarian and Hodge, 1989; Martin et al., 1990).

- **Spinohypothalamic tract:** Includes ascending projections to the hypothalamus and areas of the brain known to be involved in the production of autonomic, neuroendocrine, and affective-motivational responses to noxious stimuli (Burstein et al., 1990; Burstein et al., 1991).

- **Spinomesencephalic tract:** Encompasses several projection systems that terminate in diverse areas in the midbrain (e.g., periaqueductal grey, superior colliculus/tectum, raphe nuclei). Due to the nature of the different innervated areas, this tract is involved in descending modulation of pain as well as spinovisual reflexes and locomotor responses to pain (Menétrey et al., 1982; Yezierski and Schwartz, 1986).

- **Spinoparabrachial tract:** Projects to the parabrachial regions in the pons with a significant role in the integration of the autonomic, motivational-affective, and endocrinal responses to pain since it relays noxious inputs to other structures (e.g., amygdala, hypothalamus) (Cechetto et al., 1985; Gauriau & Bernard, 2002).

- **Spinoreticular tract:** Terminates in several nuclei of the reticular formation of the brainstem and is involved in the signalling of homeostatic changes, arousal, and affective-motivational responses to pain, as well as activation of endogenous analgesia (Haber et al., 1982; Lima, 1990).

- **Spinocervical tract:** Ascends to the lateral cervical nucleus in the caudal part of the medulla. This tract serves as a relay point to the thalamus receiving mostly tactile and hair movement input, as well as relaying muscular noxious information (Bryan et al., 1974; Cervero et al., 1977).

There are additional ascending antero-lateral pathways like **the spino-olivary tract** (synapses with the olivary nuclei in the medulla, carries proprioceptive information, and is involved in body movement control) (Swenson and Castro, 1983), **the solitary tract** (projects to the solitary nucleus in the medulla, receives mostly noxious visceral information, and it is associated with its modulation) (Traub et al., 1996), **the spinotrigeminal tract** (connects with the spinal trigeminal nucleus in the medulla, relays pain and temperature sensations from the head, and is involved in the integration of head and neck functions) (Phelan and Falls, 1991), and **the spinotelencephalic tract** (relays nociceptive information to different telencephalic structures like the globus pallidus, nucleus accumbens, amygdala, etc., and plays a role in motivational-affective responses to pain) (Burstein et al., 1987).

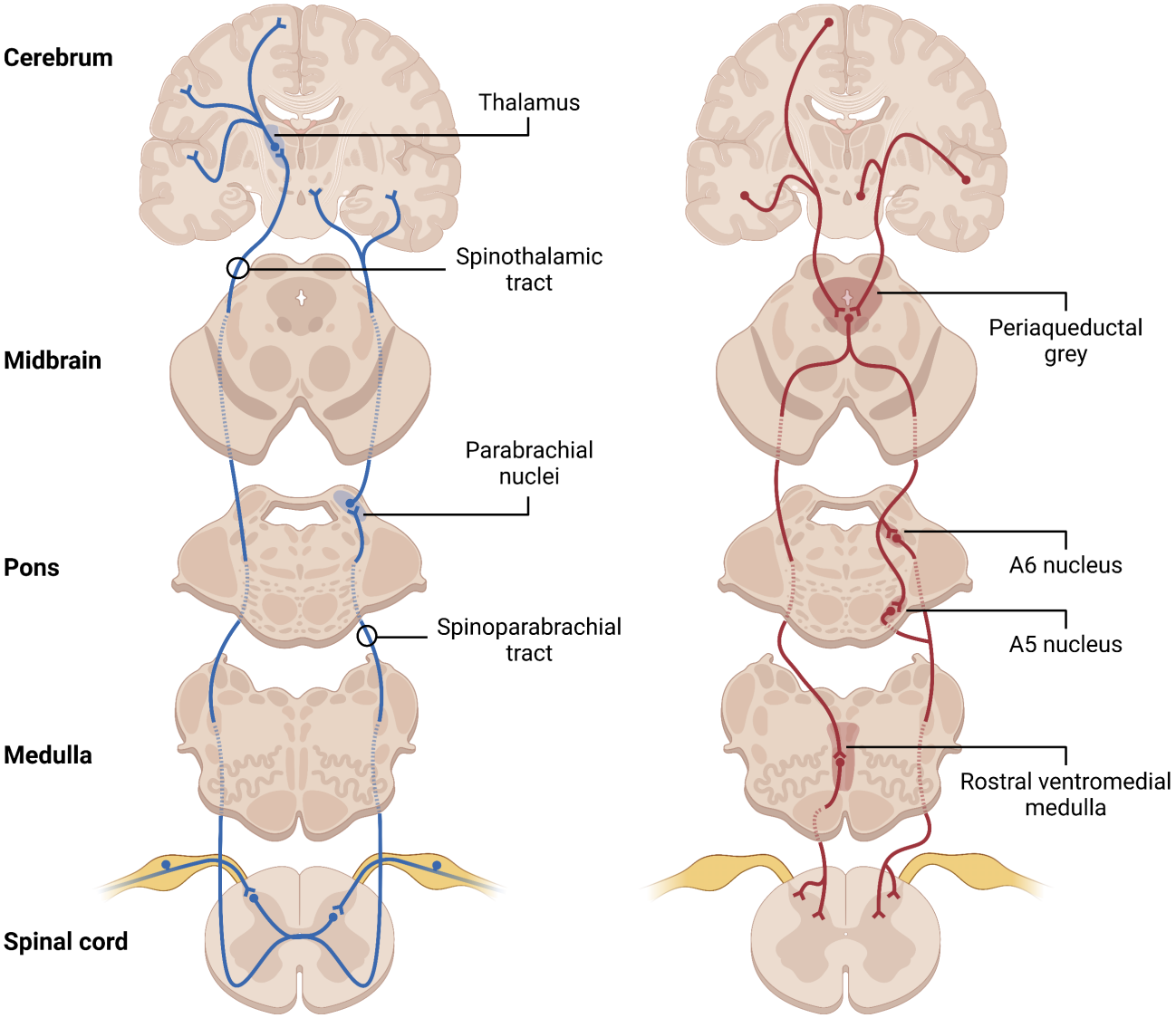

Figure 1.6. Main ascending and descending spinal nociceptive pathways. *Principal ascending nociceptive pathways (i.e., spinothalamic and spinoparabrachial tracts) project to supra-spinal areas (thalamus and parabrachial nuclei, respectively) which connect to regions associated with discriminative and affective components of pain (e.g., insula, somatosensory cortex, anterior cingulate cortex, hypothalamus, amygdala) (left diagram, blue). Descending nociceptive pathways are directed by supraspinal brainstem structures (e.g., periaqueductal grey, rostral ventral medulla, pontine tegmentum nuclei) that are modulated by corticolimbic areas (e.g., amygdala, anterior cingulate cortex, hypothalamus, insula) and project directly to the spinal cord modifying incoming nociceptive information (right diagram, red).*

1.5.4. Descending modulatory nociceptive pathways

Nociceptive information is modulated by descending control pathways that originate in brainstem, midbrain, and higher brain centre structures, highlighting that modulatory controls may be

recruited and further regulated by cognitive and emotional forebrain activity ('top-down' control) from areas involved in memory, attention, mood, etc. (e.g., amygdala, insular cortex, prefrontal cortex) (Bannister, 2019; Chen and Heinricher, 2022; Choi et al., 2018) (see **Figure 1.6**). These discrete modulatory circuits encompass the **descending pain modulatory system (DPMS)** (Granit and Kaada, 1952; Hagbarth and Kerr, 1954; see also Bannister and Hughes, 2023), where the interplay between sensory input and circuits in the DPMS governs pain perception. Despite the immense therapeutic potential, harnessing activity in the DPMS has not yet been realised; the anatomical, pharmacological, and functional nature of the circuits therein needs investigating. Some of the key brainstem areas involved in descending modulation include:

- **Periaqueductal grey (PAG):** The PAG represents a central node in pain modulation where stimulation of this midbrain structure typically inhibits dorsal horn responses to noxious stimuli, eliciting analgesia (Cui et al., 1999; Gerhart et al., 1984; Hosobuchi et al., 1977; Leith et al., 2010; Waters and Lumb, 1997). Direct descending spinal cord projections originating in the PAG are infrequent and mostly to lamina V (Mantyh and Peschanski, 1982; Mouton and Holstege, 1994; Skirboll et al., 1983); rather, PAG-governed descending modulation is largely conveyed through relay areas including the rostral ventromedial medulla and pontine tegmentum nuclei (Bajic and Proudfit, 1999; Lakos and Basbaum, 1988; Odeh and Antal, 2001). The extensive reciprocal connections of the PAG with corticolimbic structures (e.g., hypothalamus, amygdala, parabrachial area, anterior cingulate cortex, prefrontal cortex) (An et al., 1998; Behbehani et al., 1988; Krout et al., 1998; Lee et al., 2022; Rizvi et al., 1991) place it front and centre of circuits that regulate affective and emotional nociceptive integration (Buhle et al., 2013; see also Benarroch, 2012).

- **Rostral ventromedial medulla (RVM):** The RVM is considered a key structure in descending pain modulation that provides bidirectional control over spinal nociceptive processing. Due to the modular organization of the RVM, its stimulation may induce facilitation or inhibition of spinal neuronal activity depending on the intensity of the signal, although some areas show exclusive inhibitory or facilitatory effects. In the biphasic areas, low intensity activation increases spinal neuronal activity, whilst high intensity activation decreases dorsal horn neuronal responses (Urban and Gebhart, 1997; Zhuo and Gebhart, 1990; Zhuo and Gebhart, 1992; Zorman et al., 1981). The neural basis for this bidirectional modulation relies on the engagement and

synchronicity of RVM 'ON-cells', which fire in response to application of a noxious stimulus at the periphery, and 'OFF-cells', which, conversely, stop firing upon application of a noxious stimulus (Fields et al., 1983; Heinricher et al., 1989; Heinricher et al., 1994; Neubert et al., 2004). The RVM exerts its modulatory activity by projecting directly to the dorsal horn (mainly to laminae I, II, and V) (Aicher et al., 2012; Fields et al., 1995; Martin et al., 1985). Although RVM recruitment comes mostly from PAG projections (Aimone and Gebhart, 1986), direct corticolimbic connections (or indirectly via the PAG) can also recruit the RVM (Chen et al., 2017; McGaraughty and Heinricher, 2002; Wagner et al., 2013; see also Chen and Heinricher, 2022).

- **Pontine tegmentum nuclei:** These nuclei provide a putative relay for descending pain modulatory actions. Specifically, activation of the A5, A6, and A7 cell clusters (also known as fifth arcuate, locus coeruleus, and subcoeruleus, respectively) has been historically linked to inhibitory effects and reduction of the nociceptive signal (Burnet and Gebhart, 1991; Margalit and Segal, 1979; Yeomans et al., 1992), but it has been demonstrated that these nuclei can also facilitate nociception, showing a bidirectional nature depending on the cell subpopulation targeted (Hickey et al., 2014; Marques-Lopes et al., 2010; Martin et al., 1999; Nuseir and Proudfit, 2000). All three nuclei have direct projections to the dorsal horn of the spinal cord with descending fibres originating in the A6 presenting the greatest network with projections (most densely) to superficial laminae (I and II), A5 projections to deep laminae (IV, V and VI), and A7 projections predominantly to the ventral horn (with some disperse dorsal horn projections) (Bruinstroop et al., 2012; Clark and Proudfit, 1991; Clark and Proudfit, 1993; Howorth et al., 2009). These nuclei are directly connected to corticolimbic structures (e.g., amygdala, hypothalamus, parabrachial area, prefrontal cortex) (Byrum and Guyenet, 1987; Cedarbaum and Aghajanian; 1978; Chandler et al., 2014) as well as the PAG and RVM (Bajic and Proudfit, 1999; Tanaka et al., 1996; see also Taylor and Westlund, 2017).

Ultimately, descending modulation may proffer tonic or phasic control of spinal neuronal activity, according to the circuit in question (Lapirot et al., 2011; Li et al., 1998; McMahon and Wall, 1988; Sandkühler et al., 1995). Additionally, and contrary to the ascending pathways, descending modulatory pathways show ipsilateral preference (Bruinstroop et al., 2012; Levine et al., 1991) as well as predilection for modulating nociceptive signals over non-nociceptive ones (Mayer et al., 1971; Reynolds, 1969;

Waters and Lumb, 1997). This modulation is exerted at the level of the spinal cord by direct synapses of descending pathway terminals with spinal neurons (projection neurons and/or interneurons) along with indirect volume transmission (non-synaptic diffusion of transmitters in the extracellular matrix allowing for persistent and widespread effects of distant targets) (Marlier et al., 1991; Rajaofetra et al., 1992; Ridet et al., 1993). Despite direct connections between descending projections and primary afferents being sporadic (Hagihira et al., 1990; Light et al., 1983), volume transmission may affect primary afferent activity (Travagli and Williams, 1996).

Broadly, facilitatory descending modulation may be orchestrated by **serotonin** (also known as 5-hydroxytryptamine or 5-HT), while inhibitory descending modulation was traditionally viewed as being underpinned by **noradrenaline** (also called norepinephrine). The predominant source of spinal serotonin arises from the RVM (Bowker et al., 1981; Bowker et al., 1982; Kwiat and Basbaum, 1992), whilst the source of spinal noradrenaline originates in the noradrenergic A5, A6, and A7 nuclei (Kwiat and Basbaum, 1992; Westlund et al., 1983; Westlund et al., 1984). However, individual neurotransmitters may elicit contradictory mechanisms depending on the neuron targeted (e.g., inhibitory interneuron vs excitatory interneuron) and the receptor activated. Serotoninergic receptors can be classified into different families including 5-HT_1 (subdivided into 5-HT_{1A}, 5-HT_{1B}, 5-HT_{1D}, 5-HT_{1E}, and 5-HT_{1F}), 5-HT_2 (involving 5-HT_{2A}, 5-HT_{2B}, and 5-HT_{2C}), 5-HT_3, 5-HT_4, 5-HT_5 (including 5-HT_{5A} and 5-HT_{5B}), 5-HT_6, and 5-HT_7, with their actions being extremely variable (Godínez-Chaparro et al., 2011; Granados-Soto et al., 2010; Kayser et al., 2007; see also Cortes-Altamirano et al., 2018; Eide and Hole, 1993; Millan, 2002). On the other hand, the impact of noradrenaline release in the spinal cord has a more robust consistency with adrenergic receptors being classified as facilitatory α_1- (with α_{1A}, α_{1B}, and α_{1D} subtypes), inhibitory α_2- (subdivided into α_{2A}, α_{2B}, and α_{2C}), or facilitatory β-adrenergic receptors (encompassing β_1, β_2, and β_3 subtypes) (Arora et al., 2021; Asano et al., 2000; Wada et al., 1997; see also Millan, 2002; Pertovaara, 2006).

Of special interest, one of the most widely known noradrenergic descending modulatory mechanisms correspond to **diffuse noxious inhibitory controls (DNIC)**, largely driven by α2-adrenergic receptor responses, although different transmission systems can also modulate their expression (e.g., serotoninergic system, opioidergic system) (Bannister et al., 2015; Bannister et al., 2017; see also Kucharczyk et al., 2021). DNIC describes a circuit that underpins the 'pain inhibits pain' phenomenon

whereby application of a noxious stimulus to one part of the body inhibits pain perception in remote body regions (Le Bars et al., 1979a). This effect is quantified as the inhibitory action of a noxious conditioning stimulus on the firing rates of spinal and trigeminal neurons. For DNIC to be expressed, the conditioning stimulus needs to be noxious, implying Aδ- and/or C-fibre drive (Villanueva and Le Bars, 1995), and the inhibitory actions may present long-lasting effects (even minutes) following its removal if sufficient conditioning intensity is reached (Cadden, 1993). DNIC exclusively act upon convergent wide-dynamic range (WDR) neurons (see **section 1.4.2**), inhibiting their responses to innocuous and noxious stimuli via a hypothesised postsynaptic mechanism (without excluding additional presynaptic mechanisms) (Le Bars et al., 1979a; Le Bars et al., 1979b; Villanueva et al., 1984a; Villanueva et al., 1984b).

While DNIC is a phenomenon restricted to measurement in anesthetised animals, where direct recording of WDR neurons can be made, the descending control of nociception (DCN) reflects a more complex and cognitive-influenced modulatory phenomenon as measured in wakeful animals (Bannister et al., 2021; Nemoto et al., 2023; see also Kucharczyk et al., 2021). A human counterpart may be elicited with a conditioned pain modulation (CPM) paradigm (Harvie et al., 2022; Schliessbach et al., 2019; Yarnitsky et al., 2010). Paradigms used to assess the efficacy and/or expression of DNIC, DCN, or CPM serve as a surrogate measure of activity in the DPMS.

1.5.5. Perception of pain

Pain is a highly subjective, complex, and conscious sensation that often shows a non-linear relationship between nociceptive input and pain perception. In the majority of cases, once the nociceptive signal reaches the cerebrum via subcortical projections, a complex network of cortical structures (including those that originate modulatory controls) will be activated, leading to the perception of pain, 'a subjective awareness of a noxious stimulus'. These cortical areas, widely inter-connected (collectively referred to as the **'pain matrix'**), are mainly involved in the sensory and/or the affective aspects of pain. Although the areas implicated and their level of activation upon perceiving a noxious stimulus differ widely between individuals, brain imaging techniques have demonstrated several standard and frequent cortical structures involved in the perception of pain (Apkarian et al., 2005; Schnitzler and Ploner, 2000):

- **Primary somatosensory cortex (SI):** Suggested to code pain intensity (Timmermann et al., 2001), it is located in the parietal lobe, and receives nociceptive thalamic input (Gingold et al., 1991). Neuronal recordings have shown the SI to respond to noxious stimulation (Kanda et al., 2000; Kenshalo et al., 2000; see also Vierck et al., 2013).

- **Secondary somatosensory cortex (SII):** This parietal-located structure is thought to be involved in the recognition of the noxious nature of a stimulus (Timmermann et al., 2001), receiving nociceptive projections from the thalamus (Stevens et al., 1993). A very small subpopulation of SII neurons have been shown to be responsive to noxious input, with most of them presenting a polymodal phenotype (Dong et al., 1989; Maihöfner et al., 2006; see also Mauguière, 2004).

- **Insular cortex (IC):** Located in the insular lobe, this area is suggested to play a role in autonomic reactions to noxious stimuli as well as pain-related empathy and learning mechanisms (Gu et al., 2012). The nociceptive information received in this area is mostly thalamic (Jasmin et al., 2004) and it has been shown to be activated upon noxious stimulation (Hanamori et al., 1998; Ostrowsky et al., 2002; see also Labrakakis, 2023).

- **Anterior cingulate cortex (ACC):** Located in the frontal lobe, it is hypothesised to be involved in affective pain (i.e., the unpleasantness of pain) as well as pain avoidance behaviours (LaGraize et al., 2004). Receives nociceptive signals from several thalamic nuclei (Xue et al., 2022) and has proved to react to noxious stimuli (Hutchison et al., 1999; Yamamura et al., 1996; see also Fuchs et al., 2014).

- **Prefrontal cortex (PFC):** Comprises a major part of the frontal lobe and is assumed to participate in acute pain processing, pain expectation, aversive learning, and decision making (Zhou et al., 2018), as well as originating endogenous pain modulatory controls due to its connection with the periaqueductal grey (Drake et al., 2021). The PFC receives input from numerous supraspinal structures that may convey nociceptive information (Hoover and Vertes, 2007) and has shown to be activated by noxious stimuli (Condés-Lara et al., 1989; Lorenz et al., 2003; see also Ong et al., 2019).

Additionally, not only a purely somatic phenomenon, pain is also influenced by cognitive aspects. Cognition involves processes like acquisition, processing, storage, and retrieval of information by the brain (Bayne et al., 2019), and is composed of diverse elements (e.g., attention, perception, memory, verbal/language skills, motor skills, executive functioning) that will, ultimately, modify pain perception and bias nociceptive processing in the human brain (Wiech et al., 2008).

1.6. Preclinical models of CIBP

Animal models of cancer-induced bone pain (CIBP) are mainly generated following the injection of various types of cancer cells into the bone marrow of different bones. The mechanistic underpinning of CIBP involves a plethora of interactions between tumour cells, bone cells, immune cells, and bone-innervating neurons that lead to a state of neuronal hyperexcitability in primary sensory neurons (**peripheral sensitization**) as well as hyperexcitability at spinal and supraspinal levels (**central sensitization**) (Zhen et al., 2022) (see **Figure 1.7**).

1.6.1. Peripheral mechanisms of CIBP

Bones constitute a dense sensory-innervated system that can be anatomically divided into cortical (compact outer layer surrounded by the periosteum) and trabecular (spongiform inner layer separated from the cortical layer by the endosteum) tissue. Both cortical and trabecular bone are highly innervated by primary afferents (mainly involving peptidergic Aδ- and C-fibres), meaning that their integrity, if compromised, will contribute to a pain state (Castañeda-Corral et al., 2011; Mach et al., 2002; Steverink et al., 2021).

Bones are in a constant state of remodelling, which is directed by a finely tuned interplay of bone creation (osteoblast-driven) and bone reabsorption (osteoclast-mediated). Cancer cells disrupt this homeostasis by releasing different mediators (e.g., endothelin) that stimulate osteoblast proliferation, leading to the formation of futile bone (Kristianto et al., 2017). These activated osteoblasts then secrete additional ligands (e.g., receptor activator of nuclear factor-kappa B ligand; RANKL) that serve to signal osteoclast proliferation and maturation, triggering excessive bone absorption (Zhang, Li et al., 2022). This creation of new and structurally weak bone together with the weakening of the pre-existing bone, induces painful micro-fractures that not only directly activate nociceptors but can also lead to complete

bone fractures (Oefelein et al., 2002). Thus, bone tumours can be broadly classified into osteosclerotic (e.g., prostate cancer), osteolytic (e.g., breast cancer), or mixed (e.g., bladder cancer), according to whether they preferentially promote bone formation, bone degradation, or show mixed characteristics (Guise et al., 2006).

This abnormal bone remodelling causes acidification of the tumour microenvironment driven by the release of ATP and protons linked to osteoclast activity and bone degradation. Cancer cells have also proven to participate in this acidification by direct release of protons and lactate as they tend to undergo anaerobic respiration even in the abundance of oxygen (Warburg effect), worsened by the fact that bones are a naturally hypoxic environment (Eliasson and Jönsson, 2010). This local acidosis induces direct activation and sensitization of primary nociceptive afferents by stimulation of different channels (e.g., ASIC3, TRPV1, P2X3) (Nagae et al., 2007; Yoneda et al., 2015).

Additionally, and highlighting the importance of the neuro-immune interactions in the development of CIBP, these conditions favour immune cell recruitment in the tumorigenic area, where nociceptors may act as promoters and enhancers of pro-tumoral immune responses (e.g., regulatory T cells, myeloid-derived suppressor cells) while also inhibiting and exhausting anti-tumoral immune responses (e.g., cytotoxic T lymphocytes, natural killer cells) (Balood et al., 2022; Bruno et al., 2021; McIlvried et al., 2022; see also Mardelle et al., 2024). This differentially controlled immune cell recruitment leads to the release of proinflammatory factors and mediators including prostaglandins, cytokines (chemokines, interleukins, and tumour necrosis factor), neurotrophins, bradykinin, and endothelins, known for being powerful nociceptor activators and sensitisers (Eskander et al., 2015; Gokin et al., 2001; Haley et al., 1989; Richter et al., 2010; Taylor-Clark et al., 2008).

Specifically, neurotrophic factors (e.g., NGF) promote tumour cell proliferation increasing intraosseous pressure and activating mechanoreceptive primary afferents (Nencini and Ivanusic, 2017). This, in conjunction with the aforementioned osteoblast/osteoclast imbalance, induces a drastic remodelling of the bone structure leading to direct afferent activation by entrapment, injury, and/or bending of nerves (Park et al., 2018). Moreover, neurotrophic factors initiate the abnormal sprouting and reorganization of bone-innervating primary afferents as well as sympathetic fibres, inducing receptive field size amplification and sensitization (Jimenez-Andrade et al., 2010). This highly

disorganised sprouting causes an intermingling of sensory and sympathetic fibres leading to the creation of neuroma-like connections, allowing sympathetic fibres to potentially trigger nociceptive afferents (Mantyh et al., 2010; Jimenez-Andrade et al., 2011).

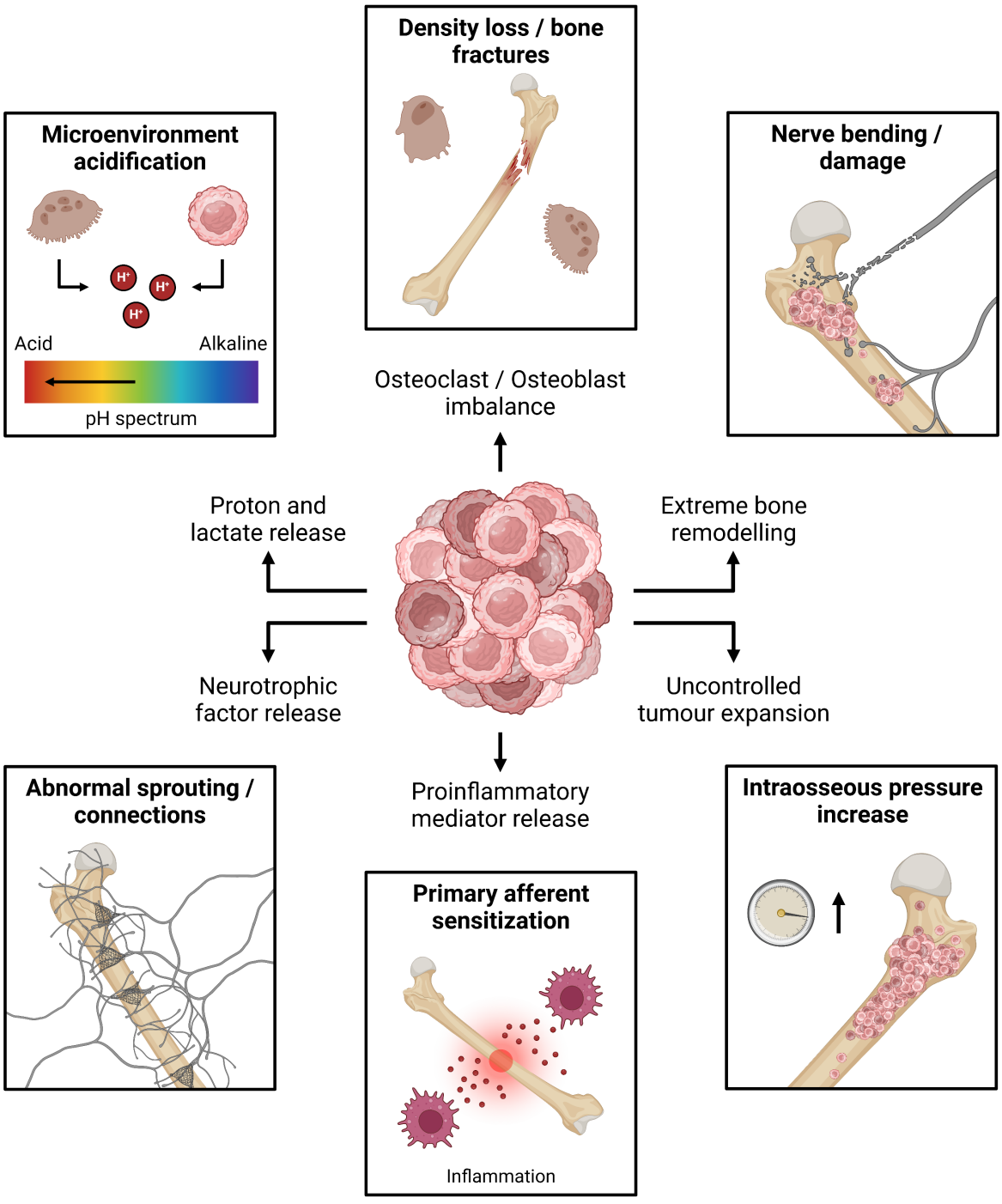

Figure 1.7. Peripheral mechanism driving CIBP. *Tumours weaken the bone structure by creating an osteoclast/osteoblast imbalance. This extreme remodelling entails the release of substances (e.g., protons, lactate) that acidify the microenvironment. Immune cells are additionally recruited in the area and release proinflammatory factors (causing the sensitization of primary afferents) as well as neurotrophic factors (producing abnormal sprouting and neuroma-like connections). Exponentially growing tumours also lead to the entrapment, bending, and damage of nerves as well as an intraosseous pressure increase.*

1.6.2. Central mechanisms of CIBP

Intricated tumour-driven peripheral interactions and the subsequent long-term stimulation of the sensitised primary afferents cause an increase in excitatory glutamate release in the spinal cord, leading to severe immune central responses (e.g., microglia/astrocyte activation, T cell infiltration) (Fu et al., 2016; Huo et al., 2019; Ni et al., 2019; Wu et al., 2022; Yang et al., 2022; Zhang, Liang et al., 2022), which are tightly linked to the release of proinflammatory mediators (known key factors for the initiation and maintenance of central sensitization) (Chen et al., 2018; Hald et al., 2009). This central inflammation has been shown to induce reorganizational changes as well as spinal sensitization by postsynaptic glutamate receptor modifications (e.g., NMDA phosphorylation) (Yanagisawa et al., 2010; Wang et al., 2012; Zhang et al., 2008). This is associated with higher cell metabolism (i.e., c-Fos) and upregulated release of pronociceptive mediators (e.g., dynorphin) (Schwei et al., 1999; Yang et al., 2022). Moreover, alterations in the ratio between nociceptive-specific (NS) and wide-dynamic range (WDR) neurons have been observed in the spinal cord, favouring the latter (Donovan-Rodriguez et al., 2005). This, together with the CIBP-mediated increase in WDR receptive field sizes and WDR neuronal responses to evoked stimuli in superficial layers (with deep layers displaying less pronounced changes), results in an increased probability of responses to low-threshold peripheral inputs with a higher magnitude of response (Donovan-Rodriguez et al., 2005; Urch et al., 2003).

Exacerbated input from sensitised spinal cord neurons may produce frequent and long-lasting stimulation of supraspinal structures which, in turn, impacts descending modulation, promoting inhibitory loss and/or facilitatory gain. Particularly, structures known to be direct participants in descending modulation (e.g., periaqueductal grey, rostral ventromedial medulla) have been shown to exert an enhanced descending serotoninergic facilitation driven by immune activatory actions (Falk, Schwab et al., 2015; Huang et al., 2014; Liu et al., 2012; Ni et al., 2019). Additionally, descending noradrenergic transmission is aberrant during cancer progression (Kucharczyk, Derrien et al., 2020) evidencing that the increased spinal excitability seen in CIBP models is unlikely to be driven simply by peripheral mechanisms, but rather that altered spinal mechanisms and abnormal descending control activity (i.e., centrally mediated mechanisms) contribute also.

1.7. Aims of thesis

Investigating the neurobiology of cancer has emerged as a discipline that tries to unravel tumour-driven modifications in pain processing as well as the interactions and crosstalk between the neurons and the cancer cells in the tumorigenic microenvironment. This thesis aims to elucidate some of the underpinning descending modulatory mechanisms that are involved in the development of chronic pain during cancer progression and following cancer ablation. The understanding of these mechanisms is of utmost importance to develop effective therapeutic interventions and improve patients' quality of life:

- My first aim was to characterise the expression profile of diffuse noxious inhibitory controls (DNIC) in naïve and CIBP female rats, linking results to adrenergic pharmacological manipulation of DNIC expression, behavioural outcomes, and bone microarchitectural analysis (see **Chapter 2** and **Chapter 3**).

- My second aim was to study spinal nociceptive processing following selective cancer cell ablation in CIBP female rats using diphtheria toxin, linking results to DNIC functionality, behavioural outcomes, and bone microarchitecture (see **Chapter 2** and **Chapter 4**).

- My third aim was to develop a tibial CIBP mouse model, linking results to DNIC functionality in naïve and CIBP female and male mice, bone microarchitecture, and behavioural outcomes. Peripheral nerve functionality was additionally assessed in naïve mice before and during application of a conditioning stimulus to assess possible impacts on primary afferent activity (see **Chapter 2** and **Chapter 5**).

CHAPTER

2

MATERIALS AND METHODS

2.1. Animals

Adult female Sprague Dawley rats (Charles River Laboratories or Inotiv, UK) and adult female and male C57BL/6 wild-type mice (Charles River Laboratories, UK) were housed in their respective mixed-sex rooms at the Biological Service Unit (King's College London, UK). Animals were arbitrarily allocated in groups of 3-5 animals per cage on a 12:12 hour light-dark cycle (lights on 7:00 a.m. to 19:00 p.m.). Polysulfone open ventilated cages (conventional EU type IV cage) with raised stainless steel wire bar lids were used for rats (dimensions: 598 × 380 × 200 mm; floor area: 1820 cm^2), whilst polysulfone individually ventilated cages were employed for mice (dimensions: 391 × 199 × 160 mm; floor area: 501 cm^2) (Tecniplast Group, Italy). Chopped aspen wood bedding, recycled paper nesting strands, and enrichment tubes were also provided in every cage (LBS Serving Biotechnology, UK). Highly formulated rodent pellets (LabDiet, USA) and filtered water in clear polycarbonate bottles with stainless steel caps (Tecniplast Group, Italy) were available *ad libitum*. Animal house conditions were strictly controlled, maintaining stable room levels of humidity (55 ± 10%), temperature (22 ± 2°C) and light intensity (350 ± 50 lux).

All procedures described were approved by the UK Home Office and conformed to the Animals (Scientific Procedures) Act 1986 and ARRIVE guidelines (Kilkenny et al., 2010). Every effort was made to limit animal suffering, and the number of animals used is in accordance with IASP ethical guidelines (Zimmermann, 1983).

2.2. Cancer cell lines

Syngeneic metastatic rat mammary tumour cells (**MRMT-1**) isolated from female Sprague Dawley rats (mammary gland adenocarcinoma) were used for the tibial CIBP rat model (Riken BioResource Research Center, Japan). MRMT-1 cells were cultured in T25 flasks (Greiner Bio-One, Austria) using Roswell Park Memorial Institute (RPMI) 1640 medium supplemented with glutamine (L-alanyl-L-glutamine), 10% foetal bovine serum (FBS), and 2% penicillin/streptomycin (Thermo Fisher Scientific, USA). Syngeneic mouse Lewis lung carcinoma cells (**LLC**) isolated from C57BL/6 mice (epidermoid lung carcinoma) were used for the tibial CIBP mouse model (American Type Culture Collection, USA). LLC cells were cultured in T25 flasks with Dulbecco's modified Eagle medium (DMEM) (Merck Group, Germany) supplemented with 10% FBS, and 2% penicillin/streptomycin.

Both MRMT-1 and LLC cell lines were maintained in an incubation chamber (BINDER, Germany) at highly controlled levels of CO_2 (5%), temperature (37°C) and humidity (100%, no condensation). Cell passages were performed every 3-4 days for both cell lines. On the day of the surgery, after medium discard and cell wash with 1X Dulbecco's phosphate-buffered saline (DPBS) (Corning, USA), MRMT-1 or LLC cancer cells (according to whether rat or mouse surgery was to be carried out respectively) were briefly exposed to 0.1% solution of trypsin-ethylenediaminetetraacetic acid (EDTA) for detachment (Thermo Fisher Scientific, USA). Fresh medium was subsequently added, and cells underwent a 5-minute centrifugation cycle at 1000 rpm (Andreas Hettich, Germany). Following supernatant discard, pellet was washed with 1X Hanks' balanced salt solution (HBSS) (Thermo Fisher Scientific, USA) and underwent an additional 5-minute centrifuge cycle at 1000 rpm. The resulting supernatant was again discarded, and cells were re-suspended in HBSS (MRMT-1) or DMEM (LLC). Cell viability was checked using a haemocytometer chamber (also known as Neubauer chamber) (Hausser Scientific, USA) and 0.1% trypan blue staining (Thermo Fisher Scientific, USA) with subsequent dilution to achieve the desired concentration (MRMT-1: 3×10^5 cells/ml; LLC: 4×10^6 cells/ml). Cells were kept on ice until use, and cell viability was checked again after surgery, with no more than 5% of cells found dead.

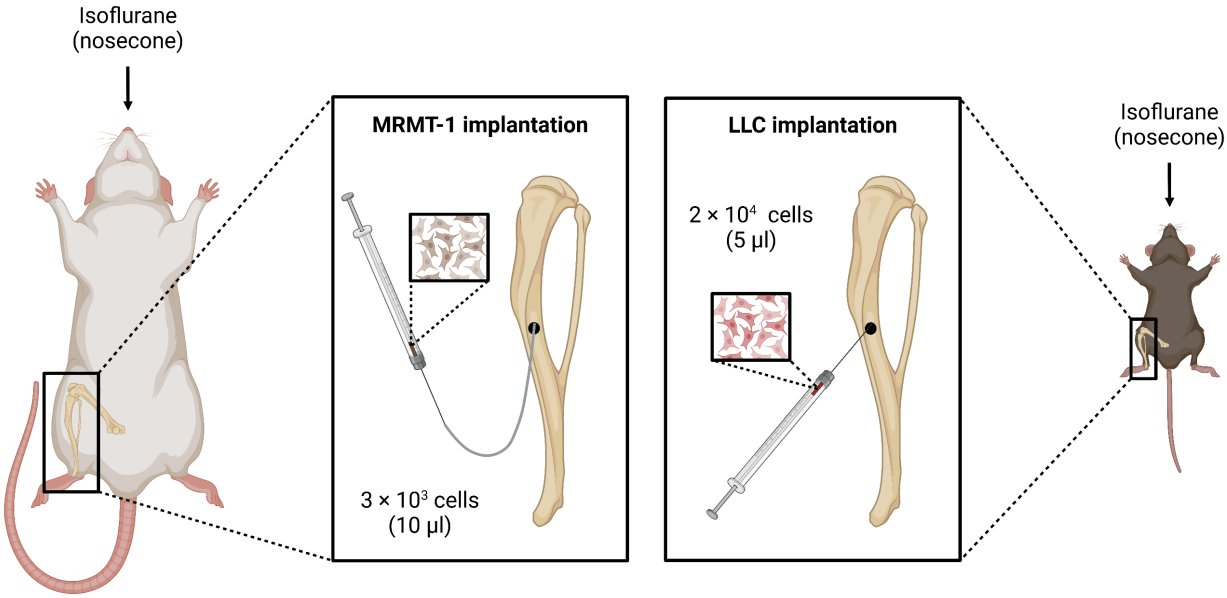

Figure 2.1. Cancer cell implantation surgery. *Following peri-operative analgesia, and under gaseous anaesthesia, the anteromedial surface of the right tibia was carefully exposed. A hole was drilled, and the cancer cells were implanted into the intramedullary cavity using a thin polyethylene tube (rats) or a custom-made needle tip (mice). Rats received 3×10^3 MRMT-1 cancer cells whilst mice received 2×10^4 LLC cells. Bone restorative material was used to plug the hole and wound was skin-sutured.*

2.3. Cancer-induced bone pain models

2.3.1. Rat cancer cell implantation surgery

A validated tibial CIBP rat model was generated as previously described (see **Figure 2.1**) (Kucharczyk, Derrien et al., 2020; Medhurst et al., 2002). Briefly, female rats (160-250 g) were anaesthetised using isoflurane (induction 4% v/v, maintenance 1.5-2% v/v) (Henry Schein, USA) in O_2 (1 l/min). After subcutaneous peri-operative meloxicam injection (50 µl; 2 mg/kg) (Boehringer Ingelheim International, Germany) and carbomer eye protective gel application (Novartis, Switzerland), animals underwent surgical cancer cell implantation into the right tibia. In aseptic conditions, a small incision was made on a shaved and povidone-iodine disinfected area (Vetark Products, UK) of the tibial anteromedial surface. The tibia was carefully exposed with minimal damage to the surrounding tissue. Using a 0.6-mm dental drill (Blackstone Industries, USA), a hole was made in the bone through which a thin polyethylene tube (0.28 mm ID × 0.60 mm OD) (Instech Laboratories, USA) was inserted 1.0-1.5 cm into the intramedullary cavity. With a 50-µl syringe (Hamilton Company, USA) connected to the polyethylene tube, either 3×10^3 MRMT-1 carcinoma cells in 10 µl HBSS or 10 µl HBSS alone (sham) were injected into the cavity. The tubing was removed, and the hole plugged with intermediate bone restorative material (Dentsply Sirona, USA). The wound was irrigated with 0.9% sodium chloride (B. Braun, Germany), skin closed with 4-0 absorbable sutures (Ethicon, USA) following a simple interrupted pattern, and secured with tissue adhesive (3M, USA). Rat breathing rate was visually monitored during the surgery and body core temperature was maintained using a homeothermic blanket (Harvard Apparatus, USA). Animals, placed in a thermo-regulated recovery box until fully awake (ThermoCare, USA), were closely monitored after surgery for any adverse effects, with no post-operative analgesic regime.

2.3.2. Mouse cancer cell implantation surgery

The tibial CIBP mouse model was designed, optimised, and established following a previously described and validated femoral CIBP mouse model for reference (see **Figure 2.1**) (de Clauser et al., 2020; Honore et al., 2000). Female and male mice (18-31 g) were anaesthetised using isoflurane (induction 4% v/v, maintenance 1.5-2% v/v) in O_2 (1 l/min), subcutaneously injected with peri-operative buprenorphine (50 µl; 0.1 mg/kg) (Ceva, France), and eye-protected with carbomer gel. Following disinfection of the shaved area, the tibial anteromedial surface was exposed with minimal damage to

surrounding tissue. Subsequently, a hole was made in the bone using a 0.5-mm dental drill and a custom-made 34-gauge needle (ESSLAB, UK) attached to a 10-µl syringe (Hamilton Company, USA) was inserted in the intramedullary cavity. Bone wax (Ethicon, USA) was used as sealant to avoid any leakage during the implantation. Subsequently, either 2×10^4 LLC cells in 5 µl DMEM or 5 µl DMEM alone (sham) were injected into the cavity. The needle was removed, and the hole was plugged with wax and additional bone restorative material. Saline solution was used to irrigate the wound and 6-0 absorbable sutures (Ethicon, USA) and surgical adhesive glue were employed for wound closure. Breathing and body core temperature were monitored and controlled during the surgical intervention. Animals recovered in a thermo-regulated recovery box until fully awake and were regularly monitored for any adverse effects on the days following surgical intervention with no post-operative analgesic regime.

2.3.3. Diphtheria toxin receptor cancer cell transduction

Modification of MRMT-1 cells was achieved by genomic alteration (lentiviral integrative transduction) to confer diphtheria toxin (DT) sensitivity. Precisely, the lentiviral custom-made construct (pFIV3.2-EF1α-DTR-P2A-eGFP-T2A-puro; 5.1×10^9 TU/ml) (University of Iowa, USA) was cloned into the feline immunodeficiency virus (FIV) and expressed the elongation factor 1α (EF1α, promoter), the DT receptor (simian DTR, gene of interest), the enhanced green fluorescent protein (eGFP, transduction marker), and puromycin resistance (puro, selection marker). Equimolar expression was achieved thanks to the presence of 2A self-cleaving peptides (P2A and T2A). The control construct expressed the exact same elements with the exception of the DTR gene (pFIV3.2-EF1α-eGFP-T2A-puro; 4.4×10^9 TU/ml).

Transduction efficiency was optimised at different multiplicities of infection (MOIs), representing the ratio of infectious virions to cells. MRMT-1 cells were seeded in a 24-well plate (Thermo Fisher Scientific, USA) at a cell density of 1×10^3 cells per well in 500 µl of medium. Following cell attachment (1 hour in the incubation chamber after seeding), cells were exposed to a viral MOI of 1000. After 24h, additional medium (500 µl) was added in each well and cells were left undisturbed for an extra 48h. Cells were then transferred to normal T25 flasks and cultured as previously detailed (see **section 2.2**). Following several cell passages, transduced cells were selected using the aminonucleoside antibiotic puromycin (optimised at 2.5 µg/ml) (Merck Group, Germany). For any cell growth and viability comparisons between cell lines, cells were seeded in normal T25 flasks at a cell density of 5×10^5 cells

per flask and incubated for 3 days. Following incubation, alive, dead, and total cells were counted and compared using a haemocytometer chamber and 0.1% trypan blue staining. This process was repeated in 5 consecutive occasions.

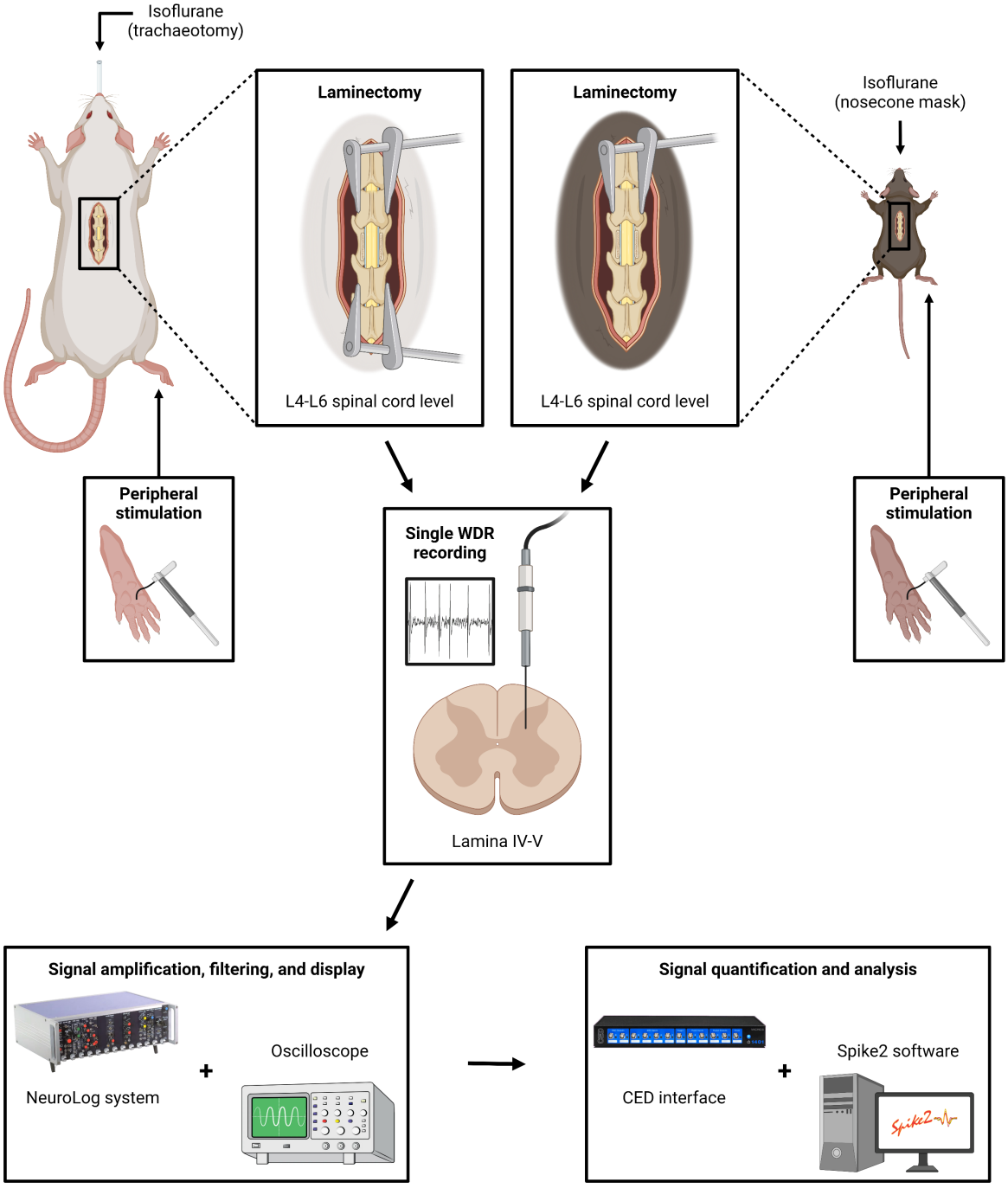

Figure 2.2. Overview of in vivo spinal cord electrophysiological recordings. *Under gaseous anaesthesia, animals were secured and fixed to a stereotaxic frame. A laminectomy was performed to expose the lumbar spinal cord and the electrode was manually lowered through the dorsal horn. Action potentials generated by single WDRs following stimulation of the right hind paw were amplified, filtered, and displayed on an oscilloscope, and subsequently quantified and analysed using Spike2 software. WDR: wide-dynamic range.*

2.3.4. Diphtheria toxin cancer cell ablation

The generation of the MRMT-1_DTR_eGFP (expressing DTR) and the control MRMT-1_eGFP (lacking DTR) cell lines allowed for targeted cancer cell ablation using DT. Diphtheria toxin (Santa Cruz Biotechnology, USA) was diluted in saline solution and stored at -80°C until use. Animals received daily intraperitoneal (IP) DT injections for 4 consecutive days at specific timepoints (starting at post-operative days 3, 7, or 14). This 4-day treatment consisted of one high dose DT injection (300 µl; 0.02 mg/kg) followed by three lower dose DT injections (300 µl; 0.004 mg/kg) using previously optimised DT concentrations (Raoof et al., 2021).

2.4. *In vivo* spinal cord electrophysiology

2.4.1. Rat electrophysiological set-up

In vivo spinal cord electrophysiological recordings in female rats (200-290 g) were performed in surgical animals on post-operative weeks 1, 2, or 3, or on weight-matched naïve rats, as previously described (see **Figure 2.2**) (Kucharczyk, Derrien et al., 2020). Briefly, animals were anesthetised in an induction box delivering 4% v/v isoflurane in a gaseous mix (0.5 l/min) of nitrous oxide (N_2O) and oxygen (O_2) at a 3:2 ratio. Rats were then transferred to a nose cone and, once areflexive, underwent a tracheotomy following blunt dissection of surrounding tracheal muscle and tracheal transverse incision. A polyethylene cannula (1.57 mm ID × 2.08 mm OD) (Scientific Commodities, USA) was inserted and secured with 3-0 silk threads (Corza Medical, USA) and surgical adherent glue. For the remainder of the experiment, the anaesthetic gaseous mix was delivered directly through the cannula. The respiratory rate was visually monitored throughout, and the core body temperature was controlled via rectal probe feedback and maintained at 37°C using a homeothermic blanket.

Rats were subsequently secured to a stereotaxic frame using ear bars (Kopf Instruments, USA), and the vertebral column was exposed under 2.5% v/v isoflurane. The vertebral column was clamped and fixed following paraspinal incisions at the upper spinal cord levels. Muscle and vertebrae were removed (laminectomy) to expose the desired spinal cord segments (L4-L6, receiving peripheral input from the hind paw), with saline solution regularly applied to prevent dehydration. Extra paraspinal incisions were made below the laminectomy level to place an additional clamp for straightness and stabilization purposes. Rats were maintained at 1.5-2% v/v isoflurane levels for the rest of the

experiment. Isoflurane overdose (5% v/v) followed by cervical dislocation were performed at the end of the experiment.

2.4.2. Mouse electrophysiological set-up

In vivo spinal cord electrophysiological recordings in female and male mice (20-33 g) were performed in surgical animals on post-operative weeks 1-2 or 3-4, or on weight-matched naïve mice, as previously described (see **Figure 2.2**) (Trendafilova et al., 2022). Briefly, mice were anesthetised using an induction box at 4% v/v isoflurane in a gaseous mix (0.5 l/min) of nitrous oxide and oxygen at a 3:2 ratio. Once reflex loss occurred, animals were placed on a mouse stereotaxic frame adaptor (World Precision Instruments, USA) and secured with zygomatic bars. For the duration of the experiment, the gaseous mix was delivered through a nosecone mask attached to the adaptor (World Precision Instruments, USA). Core body temperature was maintained at 37°C by the use of a homeothermic blanket, and respiratory rate was visually monitored during the experiment. After a clean skin cut, the vertebral column was exposed under 2.5% v/v isoflurane. Following paraspinal incisions above the area of the recording segments, a single clamp was positioned and stabilised. A laminectomy was performed to expose the L4-L6 segments of the spinal cord (hind paw input), and mineral oil (Merck Group, Germany) was applied regularly to prevent dehydration. Mice were maintained at 2% v/v isoflurane levels at the beginning of the recording with progressive lowering of the isoflurane level according to experiment progression (lower limit at 0.5% v/v). Isoflurane overdose (5% v/v) prior to cervical dislocation was carried out at the end of the experiment.

2.4.3. Wide-dynamic range neuronal recordings

Extracellular recordings were made from deep dorsal horn neurons using parylene-coated tungsten electrodes (diameter: 125 µm; impedance: 2 MΩ) (A-M systems, USA) that were manually inserted into a headstage fixed to a micro-manipulator (Narishige Group, Japan) and connected to an AC NeuroLog recording system (Digitimer, UK). To ground the system, a lead was attached to the stereotaxic frame and a second lead was connected to the animal. Subtraction of the animal signal (“B”) from the electrode signal (“A”) was performed to reduce interference, with the resulting signal being recorded by the NeuroLog system. A hum bug noise eliminator (Digitimer, UK) was also in place for removal of mains or line noise (50-60 Hz). This signal was subsequently amplified (amplification gain

between 5×10^4 - 5×10^5, depending on the cell), filtered (low and high frequency cut off points of 1 kHz and 5 kHz, respectively), and displayed on an oscilloscope (Tektronix, USA) as well as being made audible via the sound system. Data was then captured (20 kHz sampling frequency), quantified, and analysed with a CED 1401 interface coupled to Spike2 software (Cambridge Electronic Design, UK) (see **Figure 2.2**).

Recordings were obtained from single wide-dynamic range (WDR) neurons located in deep dorsal horn laminae (IV-V), characterised according to the neuronal response to both innocuous and noxious stimuli in a graded manner with coding of increasing intensity. Receptive fields were located by periodic light tapping of the glabrous surface of the hind paw and stimulated using an array of natural stimuli, with the number of fired action potentials recorded along this stimulation period. Each trial consisted of consecutive stable baseline responses to the stimulus (<10% variation) followed by responses to concomitant activation of diffuse noxious inhibitory controls (DNIC).

Concisely, receptive fields in the rat recordings were stimulated using dynamic mechanical (squirrel-hair filbert head No2 artist's brush), punctate mechanical (8 g, 26 g, and 60 g von Frey monofilaments) (North Coast Medical, USA), and punctate mechanical stimuli upon DNIC activation (8 g DNIC, 26 g DNIC, and 60 g DNIC). The number of action potentials fired during a 10-second stimulation window was recorded. This set of stimulations was repeated in four occasions (trials) per recording in the described order, with a minimum rest period of 30 seconds between each stimulus and a 5-minute non-stimulation recovery period between each trial to avoid sensitisation (see **Figure 2.3**). The number of action potentials fired during the stimulation period was averaged for every stimulus and used for statistical analysis.

Similarly, mouse receptive fields underwent 10-second dynamic mechanical (brush), punctate mechanical (1 g, 4 g, 8 g, and 15 g), punctate mechanical with DNIC induction (15 g DNIC), and thermal (42°C, 45°C, and 48°C) stimulation. The number of action potentials fired was recorded and a rest period was allowed between each stimulus (minimum of 30 seconds) to avoid sensitization (see **Figure 2.3**). Each stimulus was recorded once in the described order, except 15 g and 15 g DNIC, that had one repetition. Heat stimulation was applied with a constant waterjet onto the centre of the receptive field.

For statistical analysis, the number of action potentials fired was used and/or averaged according to the stimulus.

2.4.4. Electrophysiological DNIC quantification

DNIC were induced using a noxious stimulus on a distant part of the body (conditioning stimulus), while the peripheral receptive field was concurrently stimulated with the stimulus of choice (testing stimulus). A DNIC response was quantified as an inhibitory effect on neuronal firing during the simultaneous application of the test stimulus and the conditioning stimulus, compared to the baseline response during the application of the test stimulus alone.

To induce DNIC in rats, a micro serrefine clamp (pressure force: 125 g; length: 13 mm) (AgnTho's AB, Sweden) was applied to the ipsilateral ear exactly 5 seconds before any peripheral stimulation and left undisturbed for the whole 10-second stimulation period. For DNIC induction in mice, a micro serrefine clamp was applied on the tail of the animal 5 seconds before any stimulation and left in place during the subsequent receptive field stimulation (see **Figure 2.3**).

2.4.5. Rat spinal cord pharmacology

Following baseline and DNIC data collection, female rats underwent pharmacological characterisation of WDR activity (to include a measure of DNIC expression) following topical spinal cord administration (100 µg in 50 µl) of the selective α2-adrenoceptor antagonist atipamezole hydrochloride (Cayman Chemical, USA) using previously optimised concentrations (Bannister et al., 2015). Atipamezole was previously dissolved in a solution mix of 97% normal saline, 2% polyethoxylated castor oil, and 1% dimethyl sulfoxide (DMSO) (Merck Group, Germany). Each drug dose effect was followed for 60 minutes with tests performed at 10, 20, 30, 40, and 60 minutes after drug administration. For each time point, a single trial consisting of punctate mechanical stimuli (8 g, 26 g, and 60 g) and punctate mechanical stimuli upon activation of DNIC (8 g DNIC, 26 g DNIC, and 60 g DNIC) were performed. The number of action potentials fired was recorded during the 10-second stimulation window, with a minimum rest period of 30 seconds between each stimulus. A single neuronal pharmacological recording per rat was performed, comparing post-drug cell-firing rates against pre-drug averaged values for each stimulus.

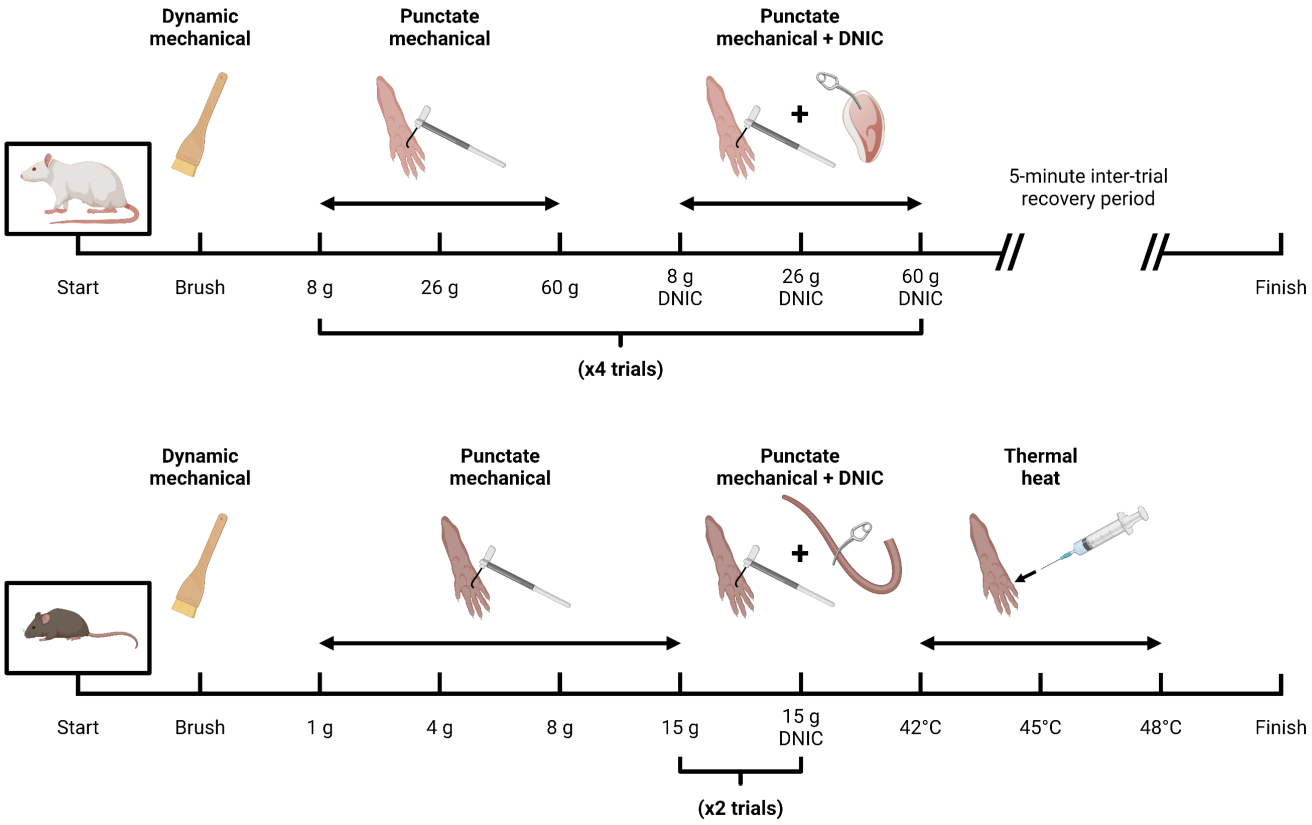

Figure 2.3. Peripheral stimulation protocol during in vivo spinal cord electrophysiology. *The receptive field located in the right hind paw of the animal was stimulated with a battery of different natural stimuli. DNIC were induced by noxious clamp application (125 g) on the ipsilateral ear (rats) or tail (mice). A recovery period (minimum of 30 seconds) was allowed between each stimulation to avoid cell sensitization. DNIC: diffuse noxious inhibitory controls.*

2.5. *Ex vivo* micro-computed tomography

Following *in vivo* spinal cord electrophysiological recordings, isoflurane overdose, and cervical dislocation, tibial samples were collected from rats (post-operative week 1, 2, or 3) and mice (post-operative week 1-2 or 3-4), or weight -matched naïve animals. Tibiae, carefully cleaned from surrounding muscle and tissue, underwent a 2-day paraformaldehyde (PFA) fixation (4%) followed by ethanol preservation (70%) (Merck Group, Germany), and were stored at 4°C until scanning. Tibial samples were scanned using SkyScan 1172F, an *ex vivo* micro-computed tomography (µCT) scanner with embedded software (Bruker Corporation, USA) and incorporated 11 Mp camera (Hamamatsu, Japan).

Tibial samples were placed in the scanner, with a pre-heated X-ray tube operating under strictly set parameters (rat values / mouse values) of source voltage (59 kV / 50 kV), source current (167 µA / 200 µA), rotation (0.60 degrees), frame averaging (2 frames), random movement compensation (20

pixels), exposure (960 ms), filtering (aluminium, 0.5 mm), and voxel sizing (8 µm / 5 µm). Samples were then reconstructed transforming the 2D projection images into 3D volumes using NRecon software (Bruker Corporation, USA), being automatically compensated for any misalignments, and with consistent values for smoothing (Gaussian kernel, 1 pixel-width), ring artifact reduction (10-15 units), beam-hardening correction (40% / 35%), and attenuation coefficient (minimum of 0.00 and maximum of 0.16). Following reconstruction, samples were re-oriented using DataViewer software (Bruker Corporation, USA), so that the long axis of the bone was aligned along the Z axis or perpendicular to the Y axis.

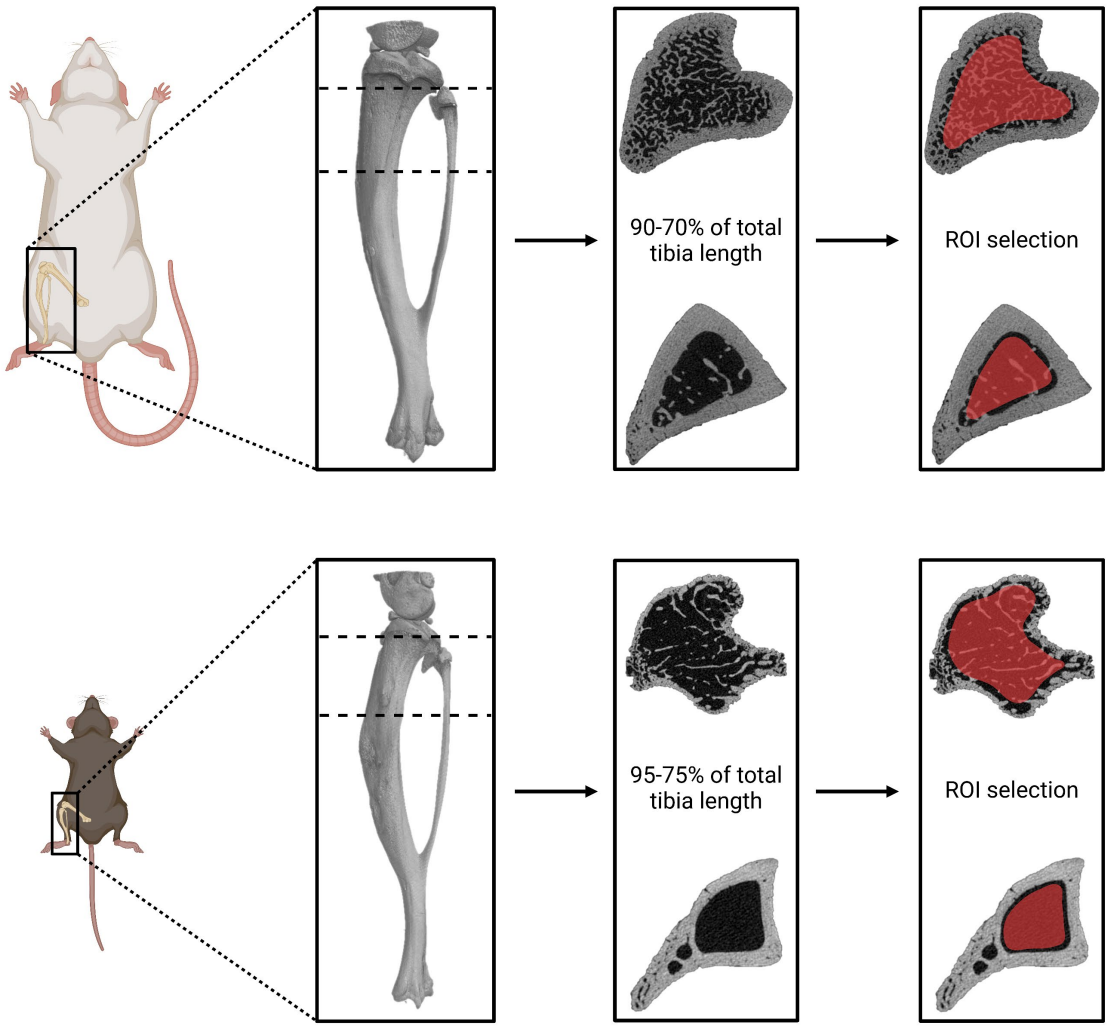

Figure 2.4. Micro-computed tomography analysis. *Following scanning, reconstruction (transformation of 2D projection images to 3D volumes), and reorientation (alignment of the long axis of the bone to the Z axis), samples were segmented. Cortical and trabecular bone were separated by ROI drawing (90-70% of total tibial length in rats; 95-75% of total tibial length in mice). The selected ROIs underwent subsequent 2D/3D analysis. Samples depicted are from sham female animals. ROI: region of interest.*

Finally, 2D/3D analyses were performed using CTAn software (Bruker Corporation, USA). Total tibial length was measured, and regions of interest (ROIs) were chosen based on the tumour growing zone. This area, corresponding to 90-70% of total tibial length in rats and 95-75% of total tibial length in mice, was selected for further analysis. Trabecular ROIs were separated from cortical ROIs by freehand drawing, leaving some free voxels from the endocortical surfaces in order to avoid inclusion of remnants of primary spongiosa associated with cortical bone (see **Figure 2.4**). Morphometric parameters of the ROIs were recorded and analysed using CTAn BatMan plugin software (Bruker Corporation, USA). Additional CTvox software (Bruker Corporation, USA) was used for 3D volume rendering, visualisation, and production of colour-coded images. In order to assess cortical and trabecular tissue/bone mineral density, two calcium hydroxyapatite bone phantoms with known mineral densities (0.25 and 0.75 g/cm^3) were used (Bruker Corporation, USA). Bone phantoms were scanned and reconstructed with the same settings used for rat and mouse tibiae.

2.6. *In vivo* dorsal root ganglion calcium imaging

2.6.1. Calcium indicator injection

Green fluorescent genetically encoded calcium indicators based on calmodulin / M13-peptide (GCaMP) in their slow variant (GCaMP6s) were used to label primary afferents in female and male mice via adeno-associated viral vector serotype 9 (AAV9) delivery. Newborn pups (litters comprising 7-8 mice) from pregnant C57BL/6 wild-type mice (Charles River Laboratories, UK) were briefly separated from their mothers at post-natal days 2-5 (P2-P5) and were returned after receiving a single subcutaneous (SC) injection containing 5 µl of the virus (AAV9.CAG.GCaMP6s.WPRE.SV40; 2.4 × 10^{13} GC/ml) (Addgene, USA). Every injection was delivered at the nape of the neck using a 10-µl disinfected syringe and a 30-gauge needle (Hamilton Company, USA). Mice were sex-divided and separated from their mother after weaning and left undisturbed until the calcium imaging session.

2.6.2. Calcium imaging recording set-up

In vivo calcium imaging recordings were performed on naïve female and male mice (20-33 g) as previously described (Goodwin et al., 2022). Mice were anesthetised using isoflurane (4% v/v) inside an induction box. Once areflexive, animals received a single intraperitoneal (IP) injection of urethane (300 µl; 1.00 g/kg) (Sigma, UK) and were maintained under anaesthesia using low levels of isoflurane during

the surgical procedure (2% v/v) and the rest of the experiment (0.5-1.0% v/v). Core body temperature was maintained at 37°C using a homeothermic heating mat and breathing rate was visually monitored throughout the experiment.

Subsequently, a clean skin cut was made into the shaved back skin to expose the vertebral column. Overlying muscle at the L3, L4, and L5 vertebral segments was removed, and the mouse vertebral column was secured to the custom-made imaging stage using a spinal clamp (Precision Systems and Instrumentation, USA) at the L2 vertebra. Bone surrounding the DRG at the L3 level (leg input) was carefully removed with the exposed DRG being washed and frequently hydrated with saline solution. After complete DRG exposure, a second spinal clamp was secured at the lower dorsal spinous process (L4 level) and the animal was positioned intermediate between prone and lateral recumbent to achieve a horizontal-plane DRG orientation. Finally, the exposed cord and DRG were covered with translucent silicone elastomer (World Precision Instruments, USA) to maintain moisture and a physiological microenvironment during the recordings.

Mice were subsequently placed under the upright confocal/multiphoton microscope Eclipse Ni-E focusing nosepiece type (Nikon, Japan). The microscope stage was diagonally orientated to optimise the DRG focus and the temperature in the full enclosure incubation chamber (Solent Scientific, UK) was kept at 32°C for the duration of the experiment. All images were acquired using the Nikon imaging software-elements advanced research (NIS-Elements AR) (Nikon, Japan) in 1-photon mode using a 10X dry objective and a 488-nm argon ion laser line. GCaMP signal was collected at 500-550 nm and time series recordings were taken with a resolution of 512 × 512 pixels and a partly open pinhole with galvo-resonant scanner for video-rate acquisition. Image acquisition varied between 4-8 Hz depending on the experimental requirements and signal strength (typically at 7.6 Hz). At the end of the experiment, mice were sacrificed by isoflurane overdose (5% v/v), followed by pentobarbital sodium intraperitoneal injection (300 µl; 200 mg/ml) (Animalcare, UK). Several minutes after breathing ceased the DRG was scanned in confocal mode with several z-steps to reconstruct the previously functionally imaged area in higher resolution.

2.6.3. Primary afferent calcium recordings

Animals underwent direct calf stimulation. In order to avoid any random movement, the pre-shaved leg was secured and stabilised. Peripheral stimulation followed a strict timeline (see **Table 2.1**) and comprised a battery of dynamic mechanical (brush), tonic mechanical (100 g, 300 g, 500 g, and 700 g pressures), tonic mechanical upon DNIC activation (300 g DNIC and 700 g DNIC), electrical volley (7.5 mA; 2 ms; 2 Hz), and electrical volley upon DNIC activation stimuli. Each peripheral stimulation had a duration of 10 seconds with a 2-minute non-stimulation period provided between each stimulation to allow cell activity to return to baseline values. Tonic mechanical pressure was applied using a graded custom-made pressure manipulator attached to a rectangular stimulation tip (6 × 4 mm with 24 blunt pins in a 6 × 4 distribution) (Avere Solutions, Germany). This device was electrically controlled and was previously used in calcium imaging recordings (Oehler et al., 2022). An electrical NeuroLog stimulator (Digitimer, UK) was used to deliver the current via two tuberculin needles inserted into the receptive field of the tibial area, followed by a 3-minute recovery period after needle insertion.

2.6.4. Calcium imaging DNIC quantification

DNIC were induced using a noxious stimulus on a distant part of the body (conditioning stimulus), while concurrent to this, the peripheral receptive field was stimulated with the stimulus of choice (testing stimulus). A DNIC response was quantified as an effect on neuronal activity during the simultaneous application of the test stimulus and the conditioning stimulus, compared to the baseline response during the application of the test stimulus alone. During *in vivo* dorsal root ganglion calcium recordings, DNIC were induced by applying a clamp to the ipsilateral ear concurrent to the primary afferent stimulation. The ear clamp was left undisturbed for the whole 10-second stimulation period.

2.6.5. Calcium imaging data analysis

For every recording, the Nikon Elements software (Nikon, Japan) was used to obtain the raw files (ND2 format), which were subsequently processed through Fiji/ImageJ software (National Institutes of Health, USA) and converted into TIFF format files (Schindelin et al., 2012; Schneider et al., 2012). These files were then imported into the image analysis pipeline Suite2P (Howard Hughes Medical Institute, USA) where they underwent motion correction, automatic region of interest (ROI) detection, and signal extraction (Pachitariu et al., 2016). Following ROI detection and signal extraction, three background

regions without any visible neurons were selected using Fiji/ImageJ software. The averaged pixel values obtained from these three background regions were subtracted from every ROI in the corresponding frame to remove excess noise. Fluorescence intensity (F) was then calculated for every ROI using a custom Python script* and underwent stringent selection criteria where a signal reaching baseline fluorescence plus 4 standard deviations qualified as a response. Additionally, to generate normalised data, the calculation $\Delta F/F_0 = (F_t - F_0)/F_0$ was performed, where F_t is the fluorescence at time t and F_0 is the fluorescence average over a baseline period (see **Table 2.1**). To avoid any aberrant amplification due to low F_0 in some neurons (i.e., low basal fluorescence), whenever $F_0 < 1$, the F_0 value in the previous formula was changed to 1 in the denominator (but not in the numerator) (Chisholm et al., 2018; Ingram et al., 2023). Finally, fluorescence intensity was analysed only for responding cells. Non-responding cells (insensitive to the chosen modality or outside the stimulated receptive field) were not analysed as they would artificially introduce biased zero values, diluting any possible differences.

Table 2.1. Peripheral stimulation protocol during in vivo calcium imaging. *The receptive field located in the calf of the animal was stimulated with a battery of different stimuli following the stimulation protocol detailed below. DNIC were induced by noxious clamp application on the ipsilateral ear. A recovery period of 2 minutes was allowed between each stimulation to avoid cell sensitization. DNIC: diffuse noxious inhibitory controls.*

TEST	AREA	STIMULUS	DURATION	STIMULATION	
Test 1	Calf	Mechanical	24 minutes	Baseline Brush 100 g 300 g 500 g 700 g	Ear clamp 300 g 700 g 300 g DNIC 700 g DNIC Ear clamp
Test 2	Calf	Electrical	8 minutes	Baseline Electrical Ear clamp Electrical DNIC	

* *Calcium imaging custom Python script was provided and run by Dr Alina-Cristina Marin.*

2.7. Behavioural testing

2.7.1. Experimental conditions and timeline

Behavioural experiments were performed in designated rat or mouse behaviour rooms with stable light, humidity, and temperature testing conditions. All items and pieces of equipment were consistently placed and positioned the same way throughout the experiments. No different species, strains, or animal sexes were present in the room at any point. Behavioural testing was carried out in a single batch (per species) during late wintertime with every test being performed by the same researcher (Diego Valiente). New laboratory polycotton coats (1st BioTech, UK) were strictly assigned to a specific animal group (female rats, female mice, or male mice) and stored in different rooms for the remainder of the experiments to avoid scent cross-contamination. Nitrile gloves (Ansell, Belgium) were utilised for mouse handling and testing, whereas no gloves were employed for rats. Perfumes and strong deodorants were entirely avoided, and experiments were performed in silence (some ambient background sound present).

All experiments abided by strict timing. Thorough room and equipment disinfection was carried out every morning prior to testing (6:30 to 7:00 a.m.). Rooms were additionally ventilated in order to clear any remaining odours (7:00 to 7:30 a.m.). Animals were allowed to acclimatise in the behaviour room in the absence of the researcher for 30 minutes before testing (7:30 to 8:00 a.m.). Deep hand washing up to the elbow level was performed by the researcher during this time with unscented soap. A further 15-minute acclimatization period was allowed for the animals once the researcher entered the room (8:00 to 8:15 a.m.), with behavioural tests starting at 8:15 a.m. Animal testing order was randomised for each cage in every testing session using a computer-based random order generator, while cage sequential order was consistently maintained. Following every cage, gloves were renewed, and every surface and piece of equipment used were meticulously cleaned.

All animals underwent one handling session to get accustomed to the researcher (10 minutes per individual animal; day 10 prior to surgery) and three habituation sessions to get familiarised with the equipment and experimental protocols (days 8, 6, and 4 prior to cancer cell implantation). No stimulation was applied to the animals during habituation sessions to avoid animal priming. Following baseline measurements (day 2 preceding CIBP surgery), cages were randomly allocated to an experimental group using a computer-based random order generator. All cages had the same number

of animals (5 animals per cage) with every animal in the same cage corresponding to the same experimental group. Cancer cell implantation surgery (day 0) was performed by the same researcher as previously described (see **section 2.3**), with consistent timing for each animal (around 20 minutes per rat and 30 minutes per mouse) and receiving the same number of sutures (3 simple interrupted sutures with surgeon knots per animal). Rat behavioural post-surgical readouts were taken on days 2, 7, 14, 21, 28, and 35, while mouse readouts were taken on post-surgical days 2, 7, 14, 21, and 28. The researcher was blinded following CIBP surgery and remained blinded until data analysis was finalised.

2.7.2. Non-evoked behavioural assessment

After the acclimatization period, animals were taken out of the cage using the cupping method and placed inside the plexiglass enclosure (rat or mouse size) of the **static weight bearing** station (Linton Instrumentation, UK). Hind limbs were positioned on top of the two weighing pads, ensuring that each hind paw was laid on a separate plate and the spine of the animal was straightened and aligned. Forelimbs were rested in the plexiglass designated area, while the tail was positioned outside the loading pads through the assigned orifice and delicately but firmly grasped to avoid the animal from turning. Once the animal acquired a relaxed position, the mass exerted by each hind paw was measured 3 times (expressed in grams), with a resting period between measurements to allow the animal to re-equilibrate or slightly shift weight distribution (around 10-20 seconds). Measurements from each paw were averaged and results were transformed into the percentage of total weight borne on each side (summation of rear legs' bearing was considered 100%).

2.7.3. Evoked behavioural assessment

Following non-evoked paradigms, female rats (but not mice) underwent nociceptive thermal withdrawal threshold assessment using the **plantar test** (also known as Hargreaves test) (Ugo Basile, Italy). Rats were placed in a modular square enclosure (dimensions: 200 × 200 × 250 mm) that allowed for lined-up animal testing (maximum of 4 rats), with 3 or 2 animals being successively tested at any given time. Prior to any stimulation, rats were left undisturbed for 3 minutes in the enclosure. The plantar surface of the hind paw was then stimulated by a constant infrared focused light source applied through a translucent glass pane (170 mW/cm^2) with the test automatically finishing once a paw withdrawal occurred, or as soon as the cut-off limit was reached (25 seconds). Three measurements of

the nociceptive threshold (measured as the withdrawal latency) were recorded and averaged in the ipsilateral rat hind paw with a 2-minute inter-stimulus recovery period between each stimulation. Every surface was thoroughly cleaned after each animal line-up, making sure the glass surface was completely dry during the whole experiment.

Additionally, both rats and mice underwent nociceptive mechanical withdrawal threshold assessment using the **paw pressure test** algesimeter (also known as Randall-Selitto test) (Ugo Basile, Italy). Animals were restrained using the encircling method in rats and the scruffing method in mice. The plantar surface of the hind paw was carefully placed on the designated plinth and increasing mechanical force was applied onto the dorsal surface of the hind paw using either a cone-shaped tip (rats) or a chisel-shaped tip (mice). Steady increasing pressure (rats: 15 g/s; mice: 7.5 g/s) was applied and the test was finished after a withdrawal response or vocalisation occurred, or when the cut-off limit was reached (rats: 200 g; mice: 150 g). Three measurements were recorded and averaged in the ipsilateral rat hind paw whilst one ipsilateral and one contralateral readout were obtained in mice. Every stimulation was followed by a 2-minute inter-stimulus recovery period.

2.8. Experimental design, statistical analysis, and illustrations

Experimental group sizes, selected to provide sufficient statistical power for detection of differences between experimental groups, were determined based on the effect reported in previously published studies using *in vivo* spinal cord electrophysiology (Kucharczyk, Derrien et al., 2020), micro-computed tomography (Kucharczyk, Chisholm et al., 2020), *in vivo* dorsal root ganglion calcium imaging (Kucharczyk, Chisholm et al., 2020), and behavioural testing (Falk, Ipsen, et al., 2015) in the CIBP model. To ensure the integrity of the experimental results, blinding was implemented throughout the *in vivo* calcium imaging and behavioural experiments. Additionally, when experimental work was carried out in conjunction with other researcher/s, the external researcher was always blinded to experimental conditions. Animal subjects comprised the experimental units for *in vivo* electrophysiology, *in vivo* dorsal root ganglion calcium imaging, and behavioural testing (with single spinal WDRs and responsive DRG primary afferent somas considered replicates within the same experimental unit). Individual tibial samples were the experimental units for micro-computed tomography. Each experimental unit was randomly assigned to its respective experimental group to minimize confounding variables.

Data were analysed using SPSS v.28 (IBM, USA) and are expressed as the mean ± SEM. For comparisons between two groups or comparisons within a single group across time, data were assessed for normality (Kolmogorov-Smirnov). If data did not follow a normal distribution, non-parametric tests were performed. For comparisons between three or more groups (or two groups across time), data were tested for normality (Kolmogorov-Smirnov) and variances homogeneity (Levène). Whenever normality was violated but data showed homoscedasticity (variances homogeneity), parametric tests were still used due to the robustness of the test to not normally distributed data (Blanca et al., 2017; Blanca et al., 2023). If homoscedasticity was additionally violated, non-parametric tests were used if possible. Whenever non-parametric tests were not a possibility (e.g., in the case of 2-way repeated measures ANOVAs or 2-way mixed ANOVAs), data were transformed (logarithmic transformation) to achieve homoscedasticity. Whenever data were non-spherical (Mauchly), the Greenhouse-Geisser adjusted F ratios were employed. A significance level of $p < 0.05$ was used to determine statistical significance for all comparisons, with post hoc analyses conducted whenever this threshold p-value was exceeded (except for two-group comparisons, where the p-value obtained directly from the statistical test was used). All figures and graphs were created using GraphPad Prism v.10 (GraphPad Software, USA) or BioRender software (BioRender, Canada).

CHAPTER

3

RESULTS I: DNIC EXPRESSION IS DYNAMIC IN A CIBP FEMALE RAT MODEL OF DISEASE PROGRESSION

3.1. Introduction

Diffuse noxious inhibitory controls (DNIC) describes the phenomenon whereby the application of a noxious stimulus to one part of the body (conditioning stimulus) inhibits pain generated by another noxious stimulus applied to a remote body region (testing stimulus) (see **section 1.5.4**). The inhibitory effect is mediated via a descending circuit, manifests as a reduction in spinal or trigeminal wide-dynamic range (WDR) neuronal activity, and is noradrenergic in nature, subserved by α2-adrenergic receptors (Bannister et al., 2015). Interestingly, DNIC expression is dysfunctional in different animal models of chronic pain (Bannister et al., 2015; Bannister et al., 2017; Boyer et al., 2017; Lockwood and Dickenson, 2019; Lockwood et al., 2019; Patel and Dickenson, 2020; Phelps et al., 2019), correlating with the absence of descending control of nociception (DCN) in wakeful chronic pain animal models (Irvine et al., 2020; Navratilova et al., 2020; Phelps et al., 2019; Yoneda et al., 2020). Clinically, application of a conditioned pain modulation (CPM) paradigm (where CPM is the human DCN counterpart) also displays impairments in patients living with chronic pain (Albu et al., 2015; Cathcart et al., 2010; King et al., 2009; Kosek and Ordeberg, 2000; Normand et al., 2011; see also Lewis et al., 2012).

Importantly, many of these chronic pain conditions have shown sexual dimorphism at multiple levels in preclinical studies, ranging from differential immune responses (Alessio et al., 2021; Lopes et al., 2017), proinflammatory mediators (Chistyakov et al., 2018), gene-expression profiles (Stephens et al., 2019), primary afferent responsiveness (Cabañero et al., 2022), pain-like phenotype progression (Francis-Malavé et al., 2023; Sorge et al., 2011; Vacca et al., 2016), and/or drug treatment responses (Inyang et al., 2019; Sorge et al., 2015), revealing distinctive underlying pain mechanisms. Specifically, one chronic pain condition that can also be affected by sexual dimorphism and circulating hormones is cancer pain, being especially important in prostate (Hsieh et al., 2005) and breast (Yue et al., 2010) cancers.

Numerous cancers may metastasise to the bone, leading to cancer-induced bone pain (CIBP), one of the most common types of chronic cancer pain sharing mixed nociceptive, neuropathic, and/or nociplastic pain components alongside inflammatory elements and distinct cancer-related modifications (see **section 1.6**). Such distinct modifications include dysfunctionality in descending modulatory controls where DNIC expression was previously shown to be dynamic during disease progression in male rats (Kucharczyk, Derrien et al., 2020). Therefore, the possibility of sexually dimorphic traits together with

specific policies mandating the integration of sex as a biological variable (SABV) in preclinical studies means that the investigation of the mechanisms driving CIBP in both male and female animals is necessary to achieve inclusive clinically relevant results.

3.2. Rationale and aims

Despite great advances in preclinical research using animal pain models, a clear gravitation towards the inclusion of only male data is historically undeniable. This situation is reinforced by the expectation that preclinical female data would inherently present higher variability due to cycling gonadal hormones, needing to increase sample sizes. However, these female hormonal effects do not outweigh inter-subject male variability, therefore including female animals in preclinical studies is not equivalent to larger sample sizes (Becker et al., 2016; Itoh and Arnold, 2015; see also Beery, 2018; Mogil, 2020).

In the CIBP rat model, the most commonly used cancer cell line comes from a rat mammary gland adenocarcinoma, making the inclusion of both sexes even more necessary. Specifically, the male CIBP rat model has shown a dynamic DNIC functionality where DNIC expression was absent 1 week after cancer cell implantation surgery but recovered 2 weeks post-surgery (Kucharczyk, Derrien et al., 2020). These cancer progression stages, named 'early' and 'late' stage respectively, refer to the degree of bone destruction: trabecular integrity is predominantly compromised on week 1, whilst trabecular as well as cortical bone lesions dominate by week 2 (Kucharczyk, Chisholm et al., 2020). Thus, with no prior electrophysiological investigation of DNIC expression in naïve female or CIBP female rats, this chapter characterises DNIC expression in both sets of animals. I performed *in vivo* spinal electrophysiological characterisation of deep dorsal horn WDR neurons and DNIC expression alongside spinal pharmacological manipulation of α2-adrenergic receptors and bone morphometric analysis. Additionally, to assess CIBP effects on animal behaviour, rodent pain-like phenotypes were analysed.

3.3. Materials and methods

Naïve, sham, and CIBP female Sprague Dawley rats (see **section 2.1**) underwent *in vivo* spinal cord electrophysiology for single-unit WDR characterisation under isoflurane anaesthesia where CIBP and sham rats underwent tibial cancer cell implantation surgery (or sham surgery) 1, 2, or 3 weeks prior to

the spinal cord recordings according to the timeline of the experiment (see **section 2.2** and **section 2.3**). Evoked WDR firing rates to natural stimuli (dynamic mechanical brush and punctate mechanical von Frey) were recorded before and during simultaneous ipsilateral application of a noxious conditioning stimulus (ear clamp, 125 g) to evoke DNIC (see **section 2.4**). Recordings were followed by spinal cord pharmacology (see **section 2.4**) before euthanasia and bone collection for analysis (see **section 2.5**). Evoked and non-evoked behavioural testing was also carried out in naïve, sham, and CIBP female rats (see **section 2.7**). For the statistical analysis, a value of $p < 0.05$ was considered significant for all comparisons (see **section 2.8**).

3.4. Results

3.4.1. CIBP female rats present with mechanical and thermal hyperalgesia

Pain-like behaviours were studied in naïve (n = 10), sham (n = 10), and CIBP (n = 10) female Sprague Dawley rats on pre-surgical day 2 (baseline) and post-operative days 2, 7, 14, 21, 28, and 35 (with CIBP rats only reaching day 21 for ethical reasons). Following baseline data collection, CIBP and sham rats underwent surgical tibial cancer cell implantation (or sham surgery) (day 0). Animal weight prior to behavioural testing (baseline weight) showed no differences between any of the groups (1-way ANOVA: $F_{(2, 27)} = 0.944$, $p > 0.05$). Analysis of animal weight over time between groups (2-way mixed ANOVA) revealed weight gain across time ($F_{(1.935, 52.246)} = 197.207$, $p < 0.001$; Bonferroni post hoc), with this weight gain being consistent across all groups ($F_{(3.870, 52.246)} = 0.653$, $p > 0.05$) (see **Figure 3.1A**).

Static weight-bearing: The non-evoked paradigm revealed significant differences in the rear-leg body weight distribution between groups across time (2-way mixed ANOVA: $F_{(8, 108)} = 14.279$, $p < 0.001$). When compared to naïve rats, sham rats showed no differences in weight distribution at any given timepoint (Bonferroni post hoc: $p > 0.05$ for all tests). In contrast, CIBP rats showed gradual impairment of weight distribution on the ipsilateral (cancer-bearing) leg from day 7 onwards (Bonferroni post hoc: $p < 0.05$) but not before (Bonferroni post hoc: $p > 0.05$) (see **Figure 3.1B**). Sham rats did not show any differences on day 28 (Independent Samples Test: $t_{(18)} = -0.905$, $p > 0.05$) nor on day 35 (Independent Samples Test: $t_{(18)} = 0.519$, $p > 0.05$) when compared to naïve rats.

Plantar test: Thermal ipsilateral paw stimulation revealed significant differences between groups across time (2-way mixed ANOVA: $F_{(8, 108)} = 2.917$, $p < 0.01$). When compared to naïve rats, sham rats

showed no differences at any given timepoint (Bonferroni post hoc: $p > 0.05$ for all tests). In contrast, CIBP rats showed thermal hypersensitivity on the ipsilateral (cancer-bearing) leg on day 21 (Bonferroni post hoc: $p < 0.01$) but not before (Bonferroni post hoc: $p > 0.05$) (see **Figure 3.1C**). Sham rats did not show any differences on day 28 (Independent Samples Test: $t_{(18)} = 0.126$, $p > 0.05$) nor on day 35 (Independent Samples Test: $t_{(18)} = 0.258$, $p > 0.05$) when compared to naïve rats.

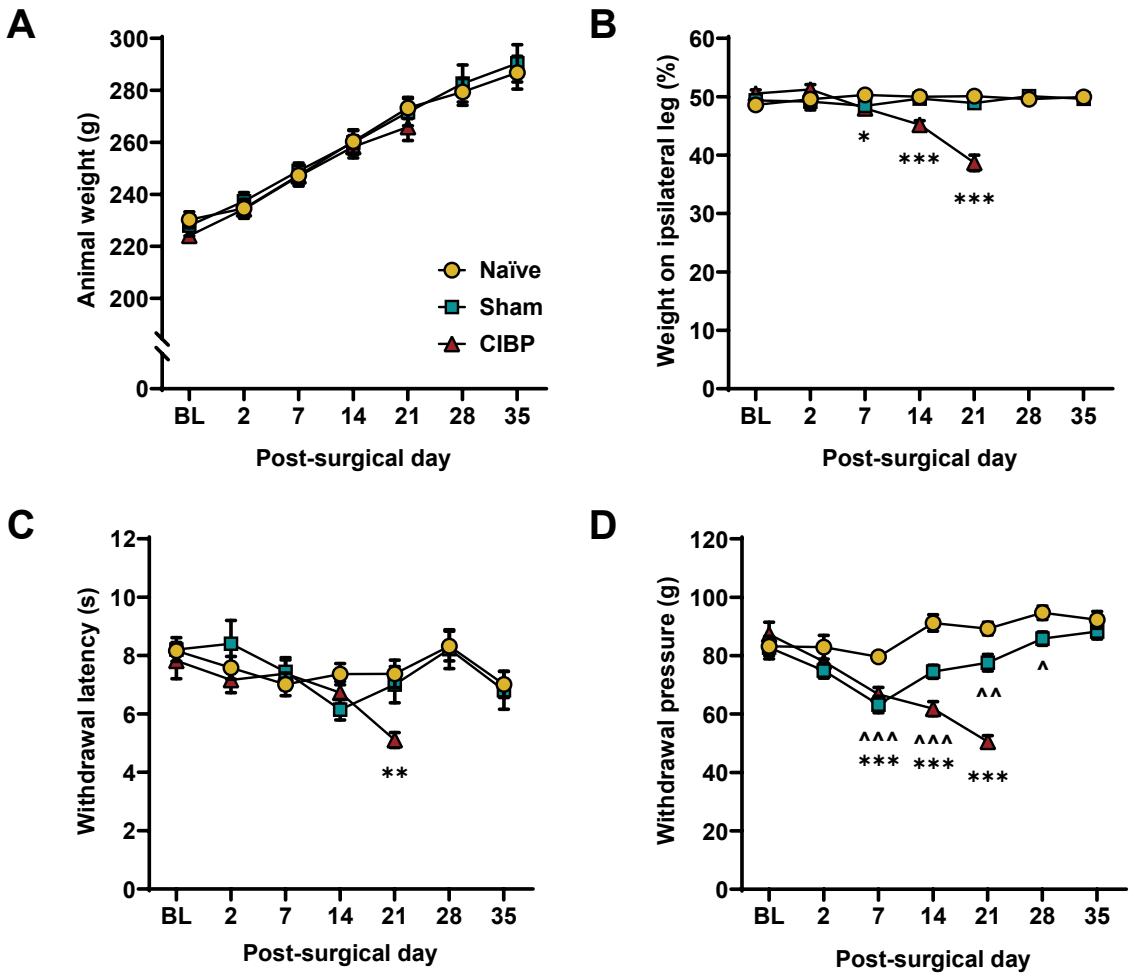

Figure 3.1. Cancer progression leads to mechanical and thermal hypersensitivity in CIBP female rats. (A) *Animal weight gain following surgery.* ***(B)*** *Weight percentage born on the ipsilateral leg (expressed as % of total rear-bearing weight) (static weight-bearing test).* ***(C)*** *Paw withdrawal latency in response to ipsilateral heat stimulation (plantar test).* ***(D)*** *Paw withdrawal threshold in response to gradual mechanical ipsilateral pressure (paw pressure test). Differences between control sham and naïve rats (^) and between CIBP and naïve rats (*) are included. *P < 0.05; **P < 0.01; ***P < 0.001. Data represent mean ± SEM. Each line represents the same group of naïve (n = 10), sham (n = 10), or CIBP (n = 10) female rats across time. The figure key presented in (A) is valid for the entire figure. CIBP: cancer-induced bone pain.*

Paw pressure test: Mechanical ipsilateral paw stimulation revealed significant differences between groups across time (2-way mixed ANOVA: $F_{(5.699, 76.930)} = 13.286$, $p < 0.01$). When compared to naïve rats, both sham and CIBP rats showed mechanical hypersensitivity on the ipsilateral (cancer-bearing) leg from day 7 onwards (Bonferroni post hoc: $p < 0.01$) but not before (Bonferroni post hoc: $p > 0.05$) (see **Figure 3.1D**). The differences between sham and naïve rats were also present on day 28 (Independent Samples Test: $t_{(18)} = 2.727$, $p < 0.05$) but disappeared by day 35 (Independent Samples Test: $t_{(18)} = 1.042$, $p > 0.05$).

Summarising, the behavioural data clearly demonstrate that tumour growth in CIBP female rats produces ipsilateral thermal and mechanical hypersensitivity, leading to changes in body weight distribution with rats favouring the non-tumour bearing side.

3.4.2. CIBP female rats show compromised bone macro and microstructure

Evaluation of bone integrity in naïve, sham, and CIBP female Sprague Dawley rats was carried out using high-resolution micro-computed tomography (μCT) following collection of tibiae (with the corresponding fibula and patella) from sham week 1 (n = 5), sham week 2 (n = 5), sham week 3 (n = 5), CIBP week 1 (n = 5), CIBP week 2 (n = 5), and CIBP week 3 (n = 5) rats, where a naïve group provided the reference control for all comparisons (n = 5).

Sham groups (week 1, week 2, and week 3): Total tibial length showed no differences between any of the groups (1-way ANOVA: $F_{(3, 16)} = 2.338$, $p > 0.05$) nor signs of macroscopic bone damage (see **Figure 3.2A**). When compared to naïve rats, trabecular bone properties were stable with no notable significant differences (see **Table 3.1** for a result overview). Of special interest, the trabecular tissue mineral density (degree of mineralization within the bone volume of interest) remained stable (Kruskal-Wallis test: $H_{(3)} = 6.269$, $p > 0.05$) (see **Figure 3.2B**). Cortical bone morphometric characteristics followed a similar pattern (see **Table 3.1** for a result overview), with cortical tissue mineral density showing no differences at any given timepoint (1-way ANOVA: $F_{(3, 16)} = 3.747$, $p < 0.05$; Bonferroni post hoc: $p > 0.05$ for all comparisons against naïve rats) (see **Figure 3.2B**).

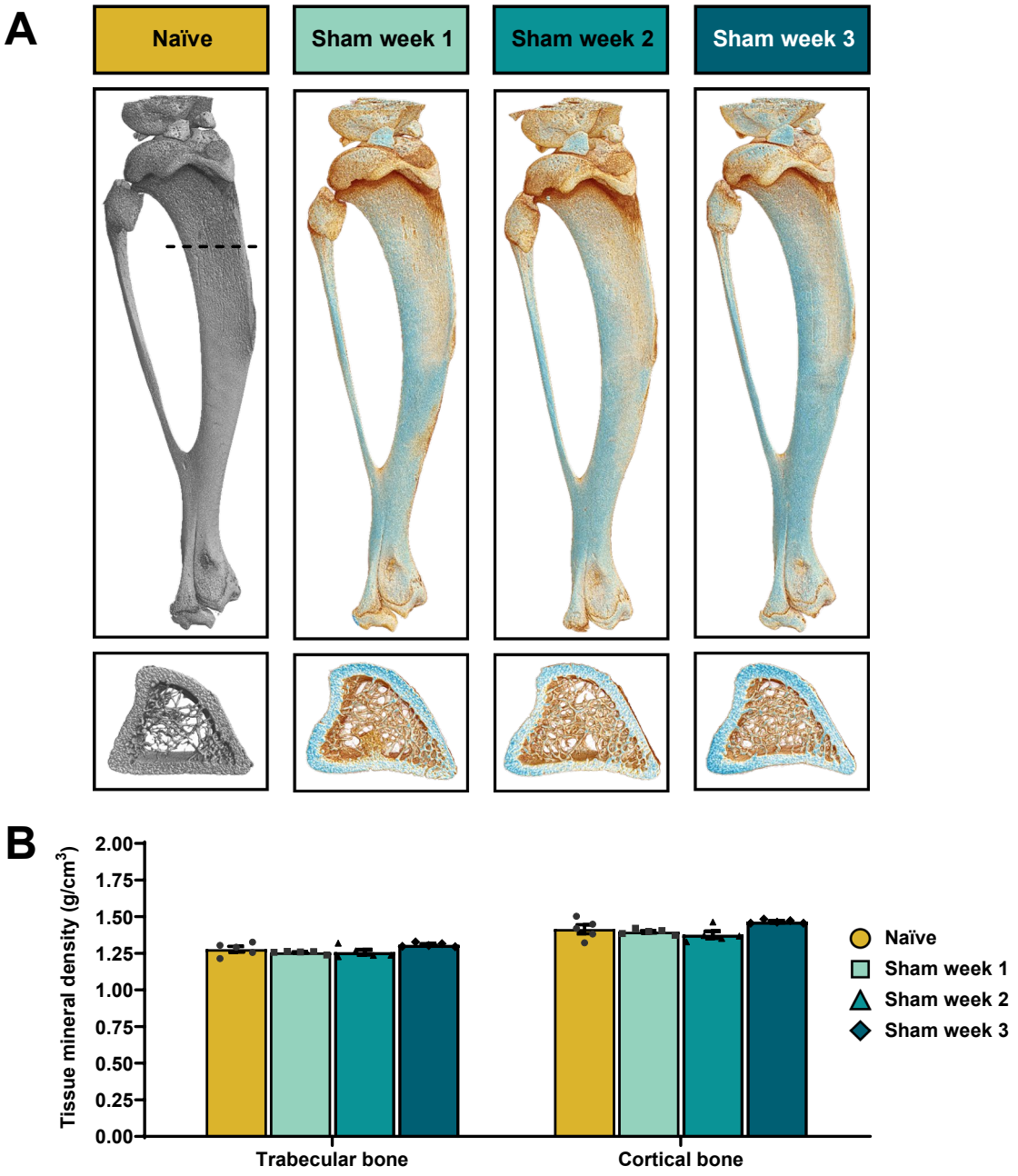

Figure 3.2. Bone macro and microarchitecture remain stable in sham female rats. (A) *Representative scanned tibial samples (micro-computed tomography) showcasing the lack of macroscopic changes following sham surgery.* ***(B)*** *Trabecular and cortical tissue mineral density (degree of mineralization within the bone volume of interest) comparisons. Data represent mean ± SEM. Each dot corresponds to individual tibial samples from naïve (n = 5), sham week 1 (n = 5), sham week 2 (n = 5), or sham week 3 (n = 5) female rats.*

Table 3.1. Impact of sham surgery on rat bone microarchitecture. *Summary of representative parameters obtained from the trabecular and cortical micro-computed tomography tibial analysis. Data represent the mean ± SEM from naïve (n = 5), sham week 1 (n = 5), sham week 2 (n = 5), and sham week 3 (n = 5) female rats. One-way ANOVA with Bonferroni post-hoc test: *p < 0.05, **p < 0.01 (comparisons against naïve rats). Whenever homoscedasticity was not met, Welch's one-way ANOVA with Games-Howell post-hoc test was performed (or Kruskal-Wallis test with Dunn-Bonferroni post hoc test if data were additionally not normally distributed).*

		Naïve	Sham week 1	Sham week 2	Sham week 3
Trabecular total surface	mm^2	79.20 ± 3.54	87.32 ± 2.35	**92.00 ± 2.84***	81.74 ± 2.52
Trabecular bone surface	mm^2	212.95 ± 42.69	269.21 ± 29.06	315.76 ± 37.40	220.25 ± 18.69
Trabecular bone surface fraction	%	70.92 ± 3.36	74.88 ± 1.97	76.60 ± 2.23	72.45 ± 2.22
Trabecular total volume	mm^3	28.61 ± 2.98	33.74 ± 1.98	36.97 ± 2.14	29.58 ± 1.91
Trabecular bone volume	mm^3	4.42 ± 0.98	5.03 ± 0.69	6.36 ± 0.76	4.53 ± 0.45
Trabecular bone volume fraction	%	15.16 ± 2.54	14.78 ± 1.55	16.94 ± 1.29	15.93 ± 2.13
Trabecular number	mm^{-1}	2.01 ± 0.30	2.20 ± 0.20	2.34 ± 0.21	2.13 ± 0.27
Trabecular pattern factor	mm^{-1}	14.07 ± 1.22	15.17 ± 1.78	13.50 ± 0.74	13.67 ± 0.93
Trabecular separation	mm	0.42 ± 0.10	0.30 ± 0.02	0.30 ± 0.03	0.39 ± 0.08
Trabecular thickness ($x10^{-2}$)	mm	7.44 ± 0.16	6.68 ± 0.19	7.29 ± 0.20	7.43 ± 0.18
Trabecular tissue mineral density	g/cm^3	1.28 ± 0.02	1.26 ± 0.01	1.26 ± 0.02	1.31 ± 0.01
Connectivity density ($x10^{-5}$)	mm^{-3}	3.86 ± 0.71	5.01 ± 0.80	4.95 ± 0.77	4.27 ± 0.77
Degree of anisotropy	N/A	0.66 ± 0.01	0.65 ± 0.01	0.65 ± 0.01	0.63 ± 0.01
Fractal dimension	N/A	2.40 ± 0.04	2.44 ± 0.03	2.47 ± 0.03	2.42 ± 0.03

		Naïve	Sham week 1	Sham week 2	Sham week 3
Cortical total area (mean)	mm^2	9.04 ± 0.51	9.95 ± 0.35	10.52 ± 0.31	9.53 ± 0.30
Cortical bone area (mean)	mm^2	4.33 ± 0.16	4.25 ± 0.09	4.47 ± 0.06	4.67 ± 0.10
Cortical bone area fraction	%	48.23 ± 2.14	42.88 ± 1.17	42.64 ± 1.38	49.07 ± 1.35
Cortical total surface (mean)	mm^2	134.92 ± 4.04	142.49 ± 2.45	148.47 ± 3.18	142.87 ± 2.65
Cortical bone surface (mean)	mm^2	326.30 ± 21.92	390.73 ± 19.21	400.40 ± 18.92	333.85 ± 7.32
Cortical bone surface fraction	%	70.56 ± 0.87	73.18 ± 0.63	72.86 ± 0.58	70.02 ± 0.35
Cortical thickness	mm	0.25 ± 0.01	**0.20 ± 0.01****	0.21 ± 0.01	0.27 ± 0.01
Cortical tissue mineral density	g/cm^3	1.41 ± 0.03	1.40 ± 0.01	1.38 ± 0.02	1.47 ± 0.01
Cortical porosity	%	51.86 ± 2.14	57.23 ± 1.17	57.47 ± 1.38	51.03 ± 1.35
Connectivity density ($x10^{-5}$)	mm^{-3}	1.00 ± 0.00	1.60 ± 0.25	1.20 ± 0.20	1.20 ± 0.00
Eccentricity	N/A	0.61 ± 0.03	0.61 ± 0.01	0.58 ± 0.03	0.61 ± 0.02

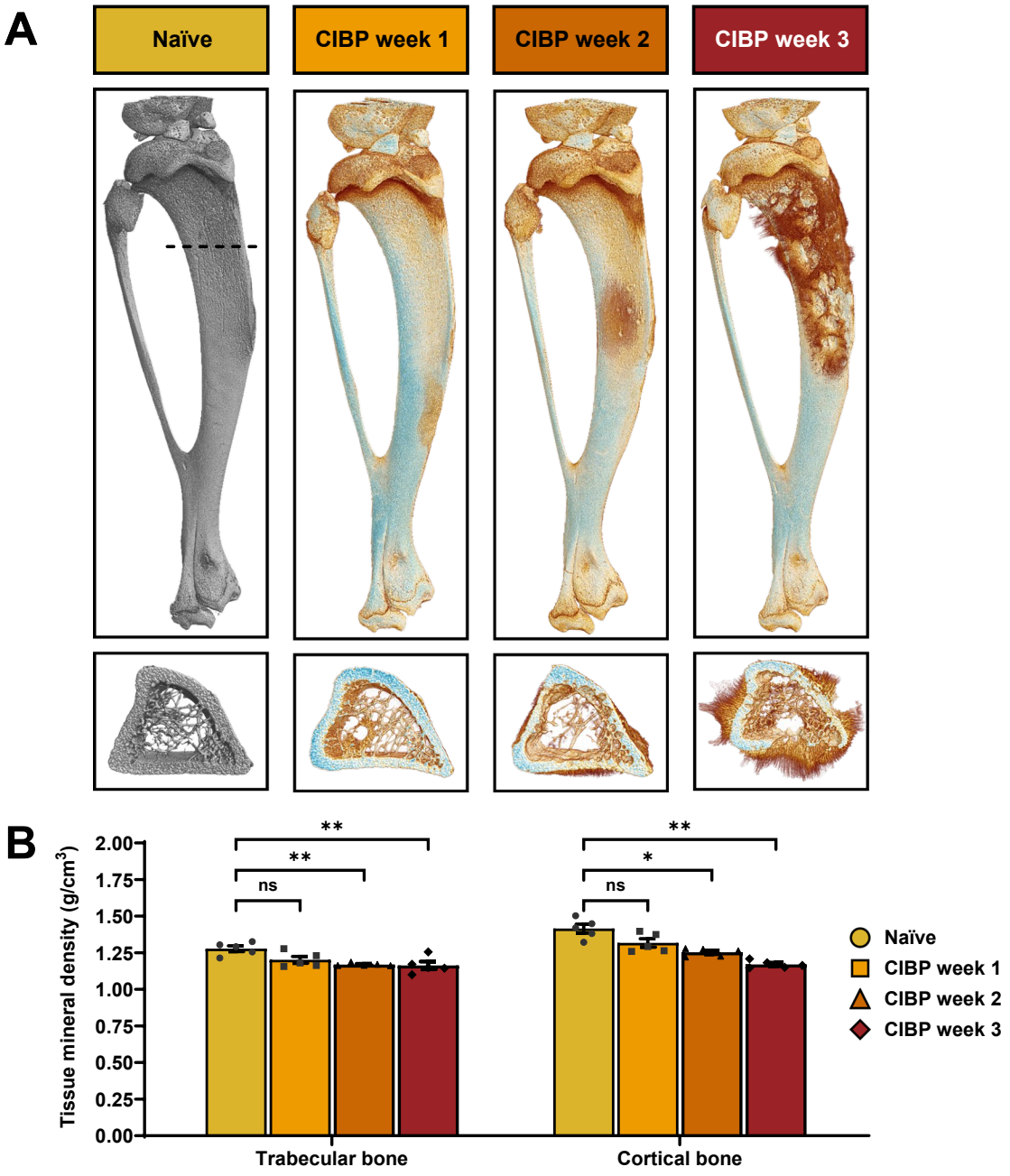

Figure 3.3. Bone macro and microarchitecture progressively degenerate in CIBP female rats. (A) *Representative scanned tibial samples (micro-computed tomography) showcasing the macroscopic changes following CIBP surgery.* ***(B)*** *Trabecular and cortical tissue mineral density (degree of mineralization within the bone volume of interest) comparisons. *P < 0.05; **P < 0.01. Data represent mean ± SEM. Each dot corresponds to individual tibial samples from naïve (n = 5), CIBP week 1 (n = 5), CIBP week 2 (n = 5), or CIBP week 3 (n = 5) female rats. CIBP: cancer-induced bone pain.*

Table 3.2. Impact of cancer cell implantation on rat bone microarchitecture. *Summary of representative parameters obtained from the trabecular and cortical micro-computed tomography tibial analysis. Data represent the mean ± SEM from naïve (n = 5), CIBP week 1 (n = 5), CIBP week 2 (n = 5), and CIBP week 3 (n = 5) female rats. One-way ANOVA with Bonferroni post-hoc test: *p < 0.05, **p < 0.01, ***p < 0.001 (comparisons against naïve rats). Whenever homoscedasticity was not met, Welch's one-way ANOVA with Games-Howell post-hoc test was performed (or Kruskal-Wallis test with Dunn-Bonferroni post hoc test if data were additionally not normally distributed). CIBP: cancer-induced bone pain.*

		Naïve	CIBP week 1	CIBP week 2	CIBP week 3
Trabecular total surface	mm^2	79.20 ± 3.54	83.58 ± 2.83	85.32 ± 1.95	88.07 ± 3.25
Trabecular bone surface	mm^2	212.95 ± 42.05	262.15 ± 21.04	228.51 ± 41.53	125.16 ± 14.44
Trabecular bone surface fraction	%	70.92 ± 3.36	75.55 ± 1.24	71.02 ± 3.64	58.08 ± 2.46
Trabecular total volume	mm^3	28.61 ± 2.98	31.76 ± 2.04	32.68 ± 1.77	35.06 ± 2.43
Trabecular bone volume	mm^3	4.42 ± 0.98	4.87 ± 0.51	4.06 ± 0.82	1.99 ± 0.27
Trabecular bone volume fraction	%	15.16 ± 2.54	15.34 ± 1.29	12.55 ± 2.40	5.77 ± 0.83
Trabecular number	mm^{-1}	2.01 ± 0.30	2.31 ± 0.16	1.96 ± 0.37	**0.92 ± 0.11***
Trabecular pattern factor	mm^{-1}	14.07 ± 1.22	14.43 ± 0.65	16.40 ± 2.03	**23.33 ± 1.13****
Trabecular separation	mm	0.42 ± 0.10	0.31 ± 0.03	0.37 ± 0.05	0.55 ± 0.05
Trabecular thickness ($x10^{-2}$)	mm	7.44 ± 0.16	**6.60 ± 0.15***	**6.40 ± 0.03***	**6.20 ± 0.22***
Trabecular tissue mineral density	g/cm^3	1.28 ± 0.02	1.20 ± 0.02	**1.17 ± 0.01****	**1.16 ± 0.03****
Connectivity density ($x10^{-5}$)	mm^{-3}	3.86 ± 0.71	5.19 ± 0.31	4.01 ± 1.01	1.29 ± 0.21
Degree of anisotropy	N/A	0.66 ± 0.01	0.66 ± 0.01	0.64 ± 0.02	0.57 ± 0.03
Fractal dimension	N/A	2.40 ± 0.04	2.45 ± 0.02	2.38 ± 0.05	**2.35 ± 0.03***

		Naïve	CIBP week 1	CIBP week 2	CIBP week 3
Cortical total area (mean)	mm^2	9.04 ± 0.51	9.50 ± 0.41	10.11 ± 0.27	**14.52 ± 2.06***
Cortical bone area (mean)	mm^2	4.33 ± 0.16	4.05 ± 0.13	4.10 ± 0.12	4.12 ± 0.53
Cortical bone area fraction	%	48.23 ± 2.14	42.75 ± 0.93	40.68 ± 1.85	**29.04 ± 2.58****
Cortical total surface (mean)	mm^2	134.92 ± 4.04	137.00 ± 3.92	156.78 ± 7.40	**293.24 ± 32.55***
Cortical bone surface (mean)	mm^2	326.30 ± 21.93	380.44 ± 18.81	429.71 ± 23.48	**1013.32 ± 332.21****
Cortical bone surface fraction	%	70.56 ± 0.87	73.43 ± 0.70	73.13 ± 1.48	73.81 ± 3.98
Cortical thickness	mm	0.25 ± 0.01	**0.20 ± 0.01***	**0.18 ± 0.01***	**0.10 ± 0.02*****
Cortical tissue mineral density	g/cm^3	1.41 ± 0.03	1.32 ± 0.03	**1.25 ± 0.01***	**1.17 ± 0.01****
Cortical porosity	%	51.86 ± 2.14	57.37 ± 0.93	59.45 ± 1.85	**71.19 ± 2.60****
Connectivity density ($x10^{-5}$)	mm^{-3}	1.00 ± 0.00	1.60 ± 0.25	2.20 ± 0.20	**11.20 ± 4.26****
Eccentricity	N/A	0.61 ± 0.03	0.62 ± 0.01	0.59 ± 0.02	0.55 ± 0.02

CIBP groups (week 1, week 2, and week 3): Total tibial length showed no differences between any of the groups (1-way ANOVA: $F_{(3, 16)} = 1.738$, $p > 0.05$) despite clear progressive macroscopic bone damage (see **Figure 3.3A**). When compared to naïve rats, trabecular bone properties showed progressive degradation (see **Table 3.2** for a result overview). Of special interest, trabecular tissue mineral density (degree of mineralization within the bone volume of interest) showed differences on week 2 and week 3 (1-way ANOVA: $F_{(3, 16)} = 6.913$, $p < 0.01$; Bonferroni post hoc: $p < 0.01$), but not before (Bonferroni post hoc: $p > 0.05$) (see **Figure 3.3B**). Cortical bone morphometric characteristics followed a similar degradation pattern (see **Table 3.2** for a result overview), with cortical tissue mineral density showing differences from week 2 onwards (Welch's 1-way ANOVA: $F_{(3, 8.381)} = 22.233$, $p < 0.001$; Games-Howell post hoc: $p < 0.05$), but not before (Games-Howell post hoc: $p > 0.05$) (see **Figure 3.3B**).

These results showcase how disease progression affects trabecular and cortical bone properties in CIBP rats, with trabecular bone being compromised from week 1, while cortical bone was additionally impaired from week 2 onwards. Reduction in tissue mineral density tightly reflects visually evident bone lesions.

3.4.3. DNIC are expressed in naïve female rats

Spinal WDR responses to natural stimuli as well as DNIC expression were studied in naïve female Sprague Dawley rats under isoflurane anaesthesia in a gaseous N_2O/O_2 mix (see **Figure 3.4A**). A minimum of one and maximum of two neurons were recorded per rat ($n = 30$; $N = 26$). Each WDR neuron responded to dynamic brush and punctate von Frey stimulation with intensity coding to 8 g, 26 g, and 60 g bending forces (1-way RM-ANOVA: $F_{(1.388, 40.240)} = 294.859$, $p < 0.001$; Bonferroni post hoc: $p < 0.001$ for all tests) (see **Figure 3.4B**). Upon application of a noxious ear clamp (conditioning stimulus), WDR baseline neuronal activity was significantly reduced for all von Frey filaments tested (2-way RM-ANOVA: $F_{(2, 58)} = 7.479$, $p < 0.01$; Bonferroni post hoc: $p < 0.001$ for all tests) (see **Figure 3.4C** and **Figure 3.4D**). The inhibitory effect of DNIC (% reduction of cell activity with respect to baseline upon ear clamp application) was differentially affected according to the von Frey bending force (Friedman test: $\chi^2_{(2)} = 13.400$, $p < 0.01$; Dunn-Bonferroni post hoc) (see **Figure 3.4E**). These results clearly evidence a functional DNIC system expressed upon noxious conditioning stimulation in naïve female Sprague Dawley rats.

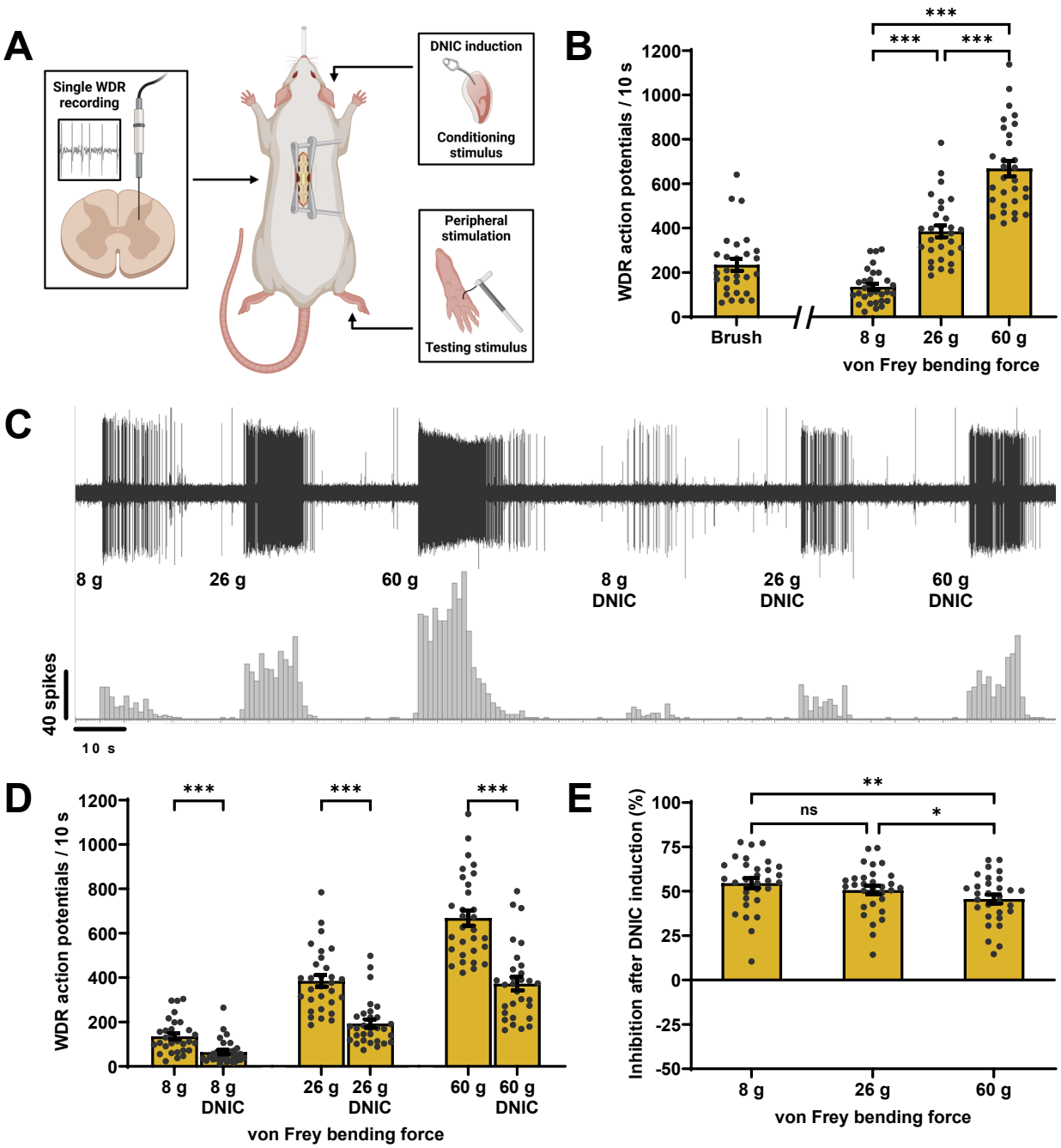

Figure 3.4. DNIC are expressed in naïve female rats. (A) *Schematic representation of the experimental paradigm.* ***(B)*** *WDR neuronal responses to dynamic mechanical stimulation (brush) and increasing punctate mechanical forces (von Frey).* ***(C)*** *Representative example of spinal WDR neuronal traces and action potential quantification before and upon simultaneous noxious ear clamp application (DNIC).* ***(D)*** *DNIC effects on WDR baseline activity.* ***(E)*** *Inhibitory DNIC effect comparison (% reduction in cell activity with respect to baseline) attending to different von Frey bending forces. *P < 0.05; **P < 0.01; ***P < 0.001. Data represent mean ± SEM. Each dot corresponds to an individual cell from naïve female rats (n = 30, N = 26). WDR: wide-dynamic range; DNIC: diffuse noxious inhibitory controls.*

3.4.4. DNIC are not affected by the oestrous cycle in naïve female rats

Every naïve electrophysiological readout was classified as proestrus (n = 8; N = 8), estrus (n = 6; N = 6), metestrus (n = 9; N = 6), or diestrus (n = 7; N = 7) according to the stage of the oestrous cycle determined following fresh vaginal sample collection and analysis*. Neuronal WDR responses to dynamic brush (1-way ANOVA: $F_{(3, 24)} = 0.705$, $p > 0.05$) and punctate von Frey stimulation (2-way mixed ANOVA: $F_{(4.135, 35.840)} = 0.172$, $p > 0.05$) showed no significant differences between any of the groups (see **Figure 3.5A** and **Figure 3.5B**, respectively). Upon application of a noxious ear clamp (conditioning stimulus), WDR baseline neuronal activity was significantly reduced for all von Frey filaments tested in proestrus (2-way RM-ANOVA: $F_{(2, 14)} = 47.843$, $p < 0.001$; Bonferroni post hoc: $p < 0.01$ for all tests), estrus (2-way RM-ANOVA: $F_{(2, 10)} = 157.303$, $p < 0.001$; Bonferroni post hoc: $p < 0.05$ for all tests), metestrus (2-way RM-ANOVA: $F_{(2, 16)} = 28.881$, $p < 0.001$; Bonferroni post hoc: $p < 0.01$ for all tests), and diestrus (2-way RM-ANOVA: $F_{(2, 12)} = 21.276$, $p < 0.001$; Bonferroni post hoc: $p < 0.001$ for all tests) (see **Figure 3.5C** for 60 g von Frey). The inhibitory effect of DNIC (% reduction of cell activity with respect to baseline upon ear clamp application) was comparable throughout groups for 8 g von Frey (Kruskal-Wallis test: $H_{(3)} = 4.149$, $p > 0.05$), 26 g von Frey (Kruskal-Wallis test: $H_{(3)} = 1.200$, $p > 0.05$), and 60 g von Frey (Kruskal-Wallis test: $H_{(3)} = 3.059$, $p > 0.05$) bending forces (see **Figure 3.5D**). These results demonstrate that WDR neuronal responses to mechanical stimuli as well as DNIC expression and inhibitory intensity are not affected by the oestrous cycle in naïve female Sprague Dawley rats.

3.4.5. Spinal α2-adrenoceptors mediate DNIC in naïve female rats

Following spinal WDR and DNIC characterisation, an investigation of the pharmacological control of DNIC was carried out in naïve female Sprague Dawley rats. Following topical spinal cord atipamezole (a selective α2-adrenoceptor antagonist), WDR activity and DNIC expression were recorded at 10-, 20-, 30-, 40-, and 60-minutes post-drug application. One neuron was recorded per naïve rat (n = 7; N = 7).

Topical spinal atipamezole application showed no effect on evoked WDR neuronal activity across time (2-way RM-ANOVA: $F_{(2.071, 12.426)} = 2.316$, $p > 0.05$) (see **Figure 3.6A** for 60 g von Frey), and it was not differentially affected according to the von Frey bending force (2-way RM-ANOVA: $F_{(10, 60)} = 0.653$, $p > 0.05$). Upon application of a noxious ear clamp (conditioning stimulus), atipamezole abolished DNIC

* *Electrophysiological rat recordings were classified by Dr Caitlin McIntyre according to their stage in the oestrous cycle.*

expression for every von Frey filament tested (3-way RM-ANOVA: $F_{(10, 60)} = 5.344$, $p < 0.001$; Bonferroni post hoc: $p > 0.05$ up to 60 minutes) (see **Figure 3.6C** and **Figure 3.6D** for 60 g von Frey) (see **Figure 3.7** for individual von Frey forces). The inhibitory effect of DNIC (% reduction of cell activity with respect to baseline upon ear clamp application) showed significant differences along time for 8 g von Frey (Kruskal-Wallis test: $H_{(5)} = 15.172$, $p < 0.01$; Dunn-Bonferroni post hoc), 26 g von Frey (Kruskal-Wallis test: $H_{(5)} = 18.959$, $p < 0.01$; Dunn-Bonferroni post hoc), and 60 g von Frey (Kruskal-Wallis test: $H_{(5)} = 24.571$, $p < 0.001$; Dunn-Bonferroni post hoc) bending forces (see **Figure 3.6B** for 60 g von Frey). These results confirm that DNIC are subserved by noradrenergic transmission via α2-adrenoceptors in naïve female Sprague Dawley rats.

3.4.6. DNIC expression is dynamic in the CIBP female rat model

CIBP and sham Sprague Dawley female rats underwent surgical tibial cancer cell implantation (or sham surgery) 1, 2, or 3 weeks prior to the electrophysiological recordings. A minimum of one and maximum of two neurons were recorded per sham week 1 (n = 15, N = 14), sham week 2 (n = 15, N = 15), sham week 3 (n = 15, N = 12), CIBP week 1 (n = 15, N = 14), CIBP week 2 (n = 15, N = 14), and CIBP week 3 (n = 15, N = 12) rat under isoflurane anaesthesia in a gaseous N_2O/O_2 mix, where a naïve group provided the reference control for all comparisons (n = 15; N = 13).

Sham groups (week 1, week 2, and week 3): Neuronal WDR responses to dynamic brush (1-way ANOVA: $F_{(3, 52)} = 0.456$, $p > 0.05$) and punctate von Frey stimulation (2-way mixed ANOVA: $F_{(3.883, 72.476)} = 0.646$, $p > 0.05$) showed no significant differences between any of the groups (see **Figure 3.8A** and **Figure 3.8B**, respectively). Upon application of a noxious ear clamp (conditioning stimulus), WDR baseline neuronal activity was significantly reduced for all von Frey filaments tested in sham week 1 (2-way RM-ANOVA: $F_{(2, 28)} = 20.361$, $p < 0.001$; Bonferroni post hoc: $p < 0.001$ for all tests), sham week 2 (2-way RM-ANOVA: $F_{(1.247, 17.453)} = 45.733$, $p < 0.001$; Bonferroni post hoc: $p < 0.001$ for all tests), and sham week 3 rats (2-way RM-ANOVA: $F_{(2, 28)} = 86.749$, $p < 0.001$; Bonferroni post hoc: $p < 0.001$ for all tests) (see **Figure 3.8C** for 60 g von Frey). The inhibitory effect of DNIC (% reduction of cell activity with respect to baseline upon ear clamp application) was comparable throughout groups for 8 g von Frey (Kruskal-Wallis test: $H_{(3)} = 3.919$, $p > 0.05$), 26 g von Frey (Kruskal-Wallis test: $H_{(3)} = 5.852$, $p > 0.05$), and 60 g von Frey (Kruskal-Wallis test: $H_{(3)} = 4.305$, $p > 0.05$) bending forces (see **Figure 3.8D**).

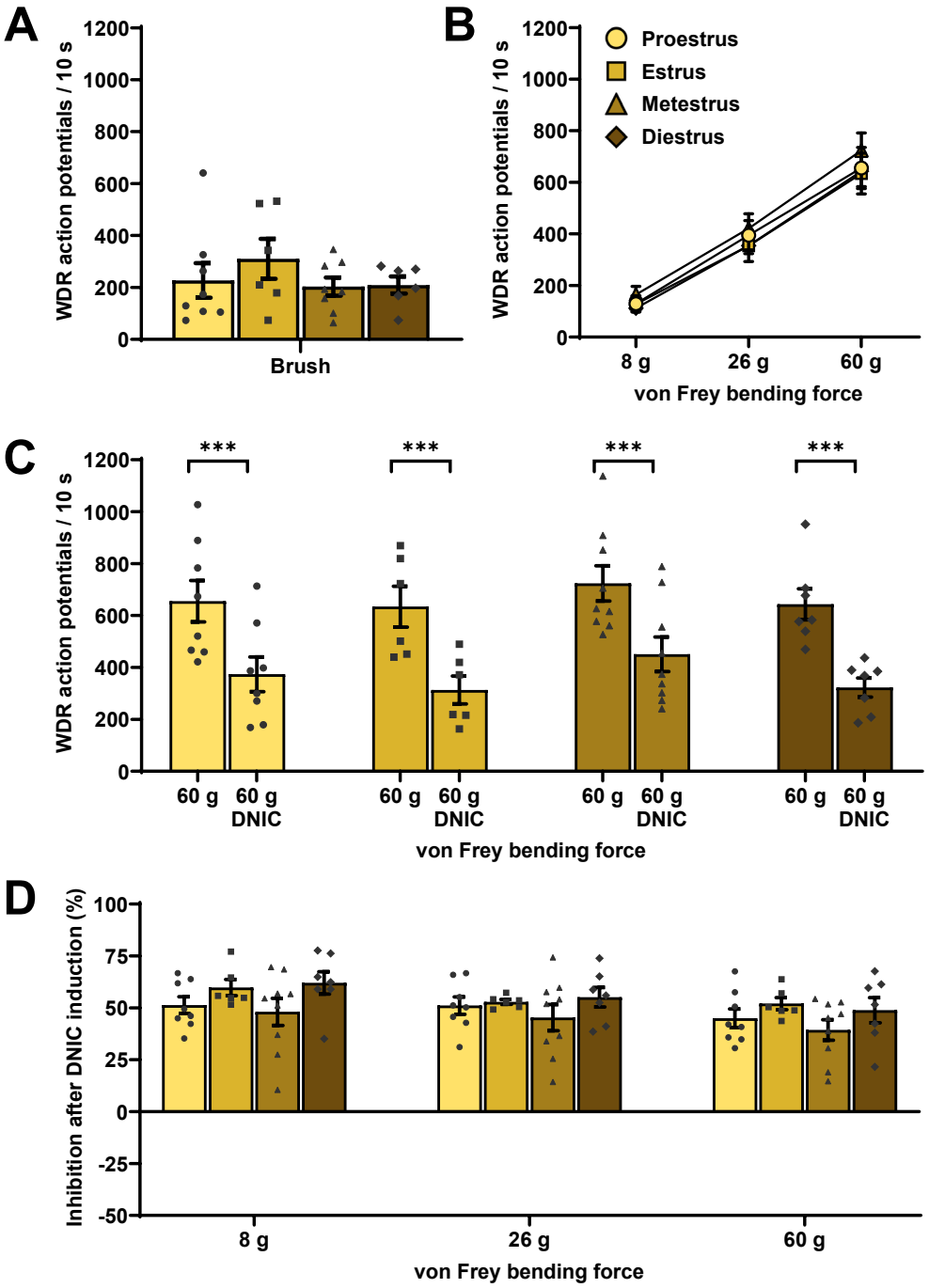

Figure 3.5. DNIC are not affected by the oestrous cycle in naïve female rats. (A) *WDR neuronal responses to dynamic mechanical stimulation (brush).* ***(B)*** *WDR neuronal responses to increasing punctate mechanical forces (von Frey).* ***(C)*** *DNIC effect on WDR baseline activity upon simultaneous noxious ear clamp application (60 g von Frey).* ***(E)*** *DNIC effect comparison (% reduction in cell activity with respect to baseline) attending to different von Frey bending forces. ***P < 0.001. Data represent mean ± SEM. Each dot corresponds to an individual cell from naïve female rats in proestrus (n = 8; N = 8), estrus (n = 6; N = 6), metestrus (n = 9; N = 6), or diestrus (n = 7; N = 7). The figure key presented in (B) is valid for the entire figure. WDR: wide-dynamic range; DNIC: diffuse noxious inhibitory controls.*

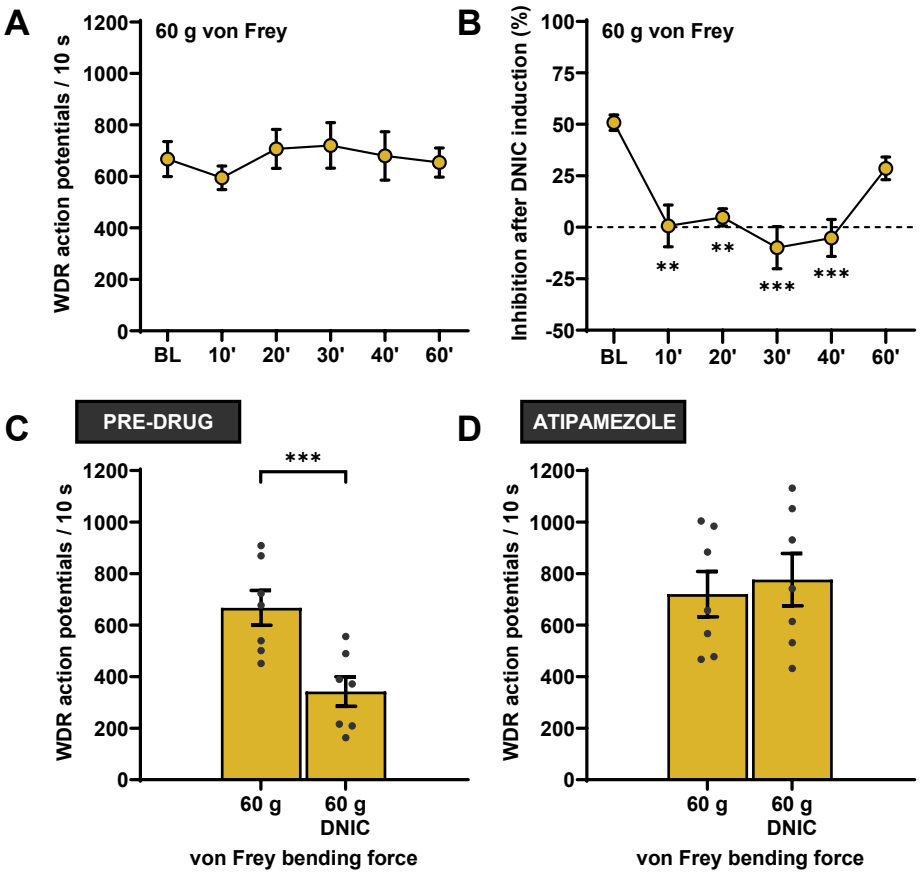

Figure 3.6. Spinal α2-adrenergic receptors mediate DNIC in naïve female rats. (A) *Atipamezole effect on evoked WDR neuronal responses (60 g von Frey).* ***(B)*** *Atipamezole effect on DNIC (% reduction in cell activity with respect to baseline) (60 g von Frey).* ***(C)*** *and* ***(D)*** *DNIC effect on WDR baseline activity upon simultaneous noxious ear clamp before (pre-drug) and 30 minutes after atipamezole application, respectively (60 g von Frey). **P < 0.01; ***P < 0.001. Data represent mean ± SEM. Each line represents the same group of cells across time and each dot corresponds to an individual cell from naïve female rats (n = 7, N = 7). WDR: wide-dynamic range; DNIC: diffuse noxious inhibitory controls.*

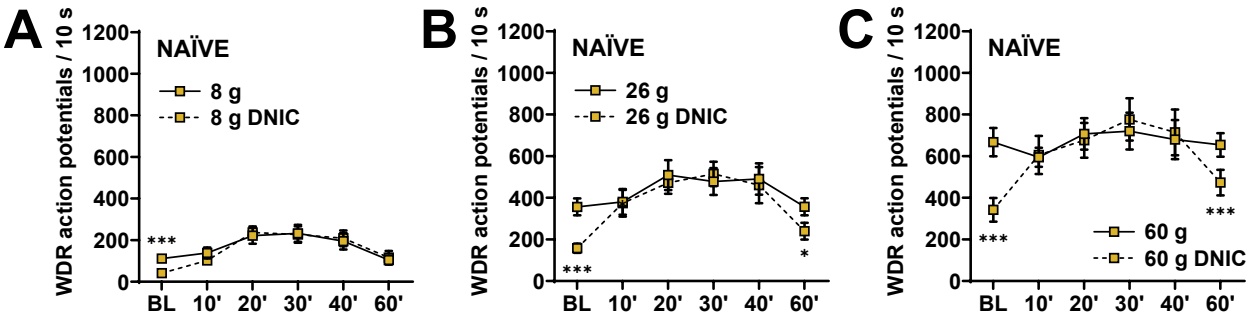

Figure 3.7. Spinal α2-adrenergic receptors mediate DNIC in naïve female rats (continued). *Atipamezole effect on evoked WDR neuronal responses to* ***(A)*** *8 g,* ***(B)*** *26 g, or* ***(C)*** *60 g von Frey stimulation alone or upon simultaneous ear clamp application (DNIC). *P < 0.05; ***P < 0.001. Data represent mean ± SEM. Each line represents the same group of cells across time from naïve female rats (n = 7, N = 7). WDR: wide-dynamic range; DNIC: diffuse noxious inhibitory controls.*

CIBP groups (week 1, week 2, and week 3): Neuronal WDR responses to dynamic brush (1-way ANOVA: $F_{(3, 52)} = 1.653$, $p > 0.05$) and punctate von Frey stimulation (2-way mixed ANOVA: $F_{(4.380, 81.761)} = 1.009$, $p > 0.05$) showed no significant differences between any of the groups (see **Figure 3.9A** and **Figure 3.9B**, respectively). Upon application of a noxious ear clamp (conditioning stimulus), WDR baseline neuronal activity was significantly reduced for all von Frey filaments tested in CIBP week 2 (2-way RM-ANOVA: $F_{(1.247, 17.453)} = 45.733$, $p < 0.001$; Bonferroni post hoc: $p < 0.001$ for all tests) and CIBP week 3 rats (2-way RM-ANOVA: $F_{(2, 28)} = 92.127$, $p < 0.001$; Bonferroni post hoc: $p < 0.001$ for all tests), but not in CIBP week 1 rats (2-way RM-ANOVA: $F_{(2, 28)} = 0.082$, $p > 0.05$) (see **Figure 3.9C** for 60 g von Frey). Thus, the inhibitory effect of DNIC (% reduction of cell activity with respect to baseline upon ear clamp application) showed significant differences between groups for 8 g von Frey (Kruskal-Wallis test: $H_{(3)} = 33.772$, $p < 0.001$), 26 g von Frey (Kruskal-Wallis test: $H_{(3)} = 33.791$, $p < 0.001$), and 60 g von Frey (Kruskal-Wallis test: $H_{(3)} = 33.753$, $p < 0.001$) bending forces. These differences were observed in CIBP week 1 rats for all von Frey forces (Dunn-Bonferroni post hoc: $p < 0.001$ for all tests), but not in CIBP week 2 nor week 3 rats when compared to naïve rats (Dunn-Bonferroni post hoc: $p > 0.05$ for all tests) (see **Figure 3.9D**).

These results showcase that cancer progression does not affect WDR neuronal responses to mechanical stimulation in CIBP female rats. However, similar to that shown in CIBP male rat data, disease progression correlates with dynamic DNIC expression in CIBP female rats, whereby DNIC is abolished on post-surgical week 1, but once again recovered on post-surgical weeks 2 and 3 (see **Figure 3.10** and **Figure 3.11**).

3.4.7. Spinal α2-adrenoceptors mediate DNIC in CIBP female rats

Following spinal WDR and DNIC characterisation, an investigation of the pharmacological control of DNIC was carried out in sham and CIBP female Sprague Dawley rats 1, 2, or 3 weeks post-cancer cell implantation (or sham surgery). Following topical spinal cord atipamezole (a selective α2-adrenoceptor antagonist), WDR activity and DNIC expression were recorded at 10-, 20-, 30-, 40-, and 60-minutes post-drug application. One neuron was recorded per sham week 1 ($n = 6$; $N = 6$), sham week 2 ($n = 7$; $N = 7$), sham week 3 ($n = 7$; $N = 7$), CIBP week 1 ($n = 7$; $N = 7$), CIBP week 2 ($n = 7$; $N = 7$), and CIBP week 3 rat ($n = 6$; $N = 6$), where a naïve group provided the reference control for all comparisons ($n = 7$; $N = 7$).

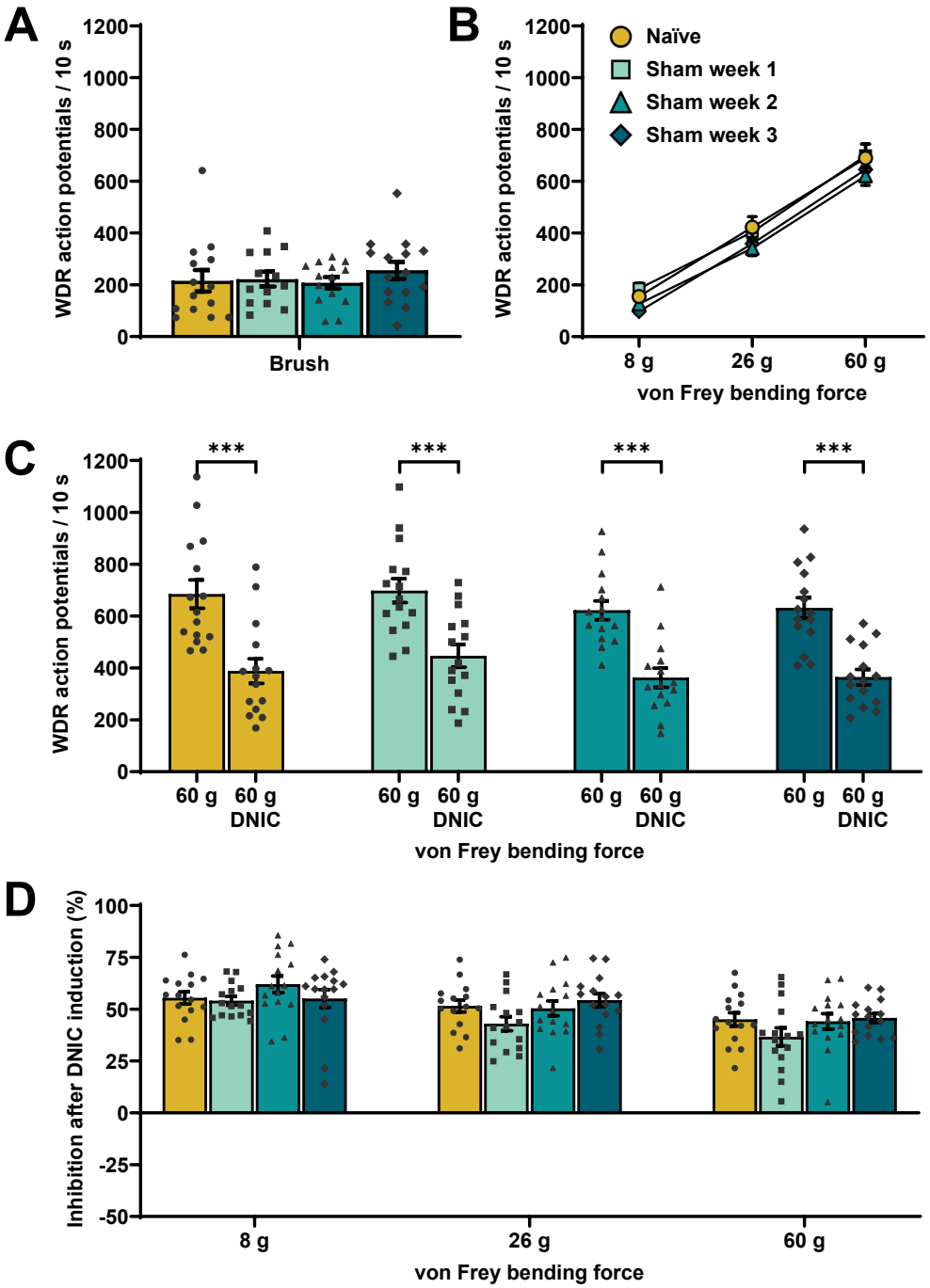

Figure 3.8. DNIC are expressed in sham female rats. (A) *WDR neuronal responses to dynamic mechanical stimulation (brush).* ***(B)*** *WDR neuronal responses to increasing punctate mechanical forces (von Frey).* ***(C)*** *DNIC effects on WDR baseline activity upon simultaneous noxious ear clamp (60 g von Frey).* ***(D)*** *DNIC effect comparison (% reduction in cell activity with respect to baseline) attending to different von Frey bending forces. ***P < 0.001. Data represent mean ± SEM. Each dot corresponds to an individual cell from naïve (n = 15; N = 13), sham week 1 (n = 15, N = 14), sham week 2 (n = 15, N = 15), or sham week 3 (n = 15, N = 12) female rats. The figure key presented in (B) is valid for the entire figure. WDR: wide-dynamic range; DNIC: diffuse noxious inhibitory controls.*

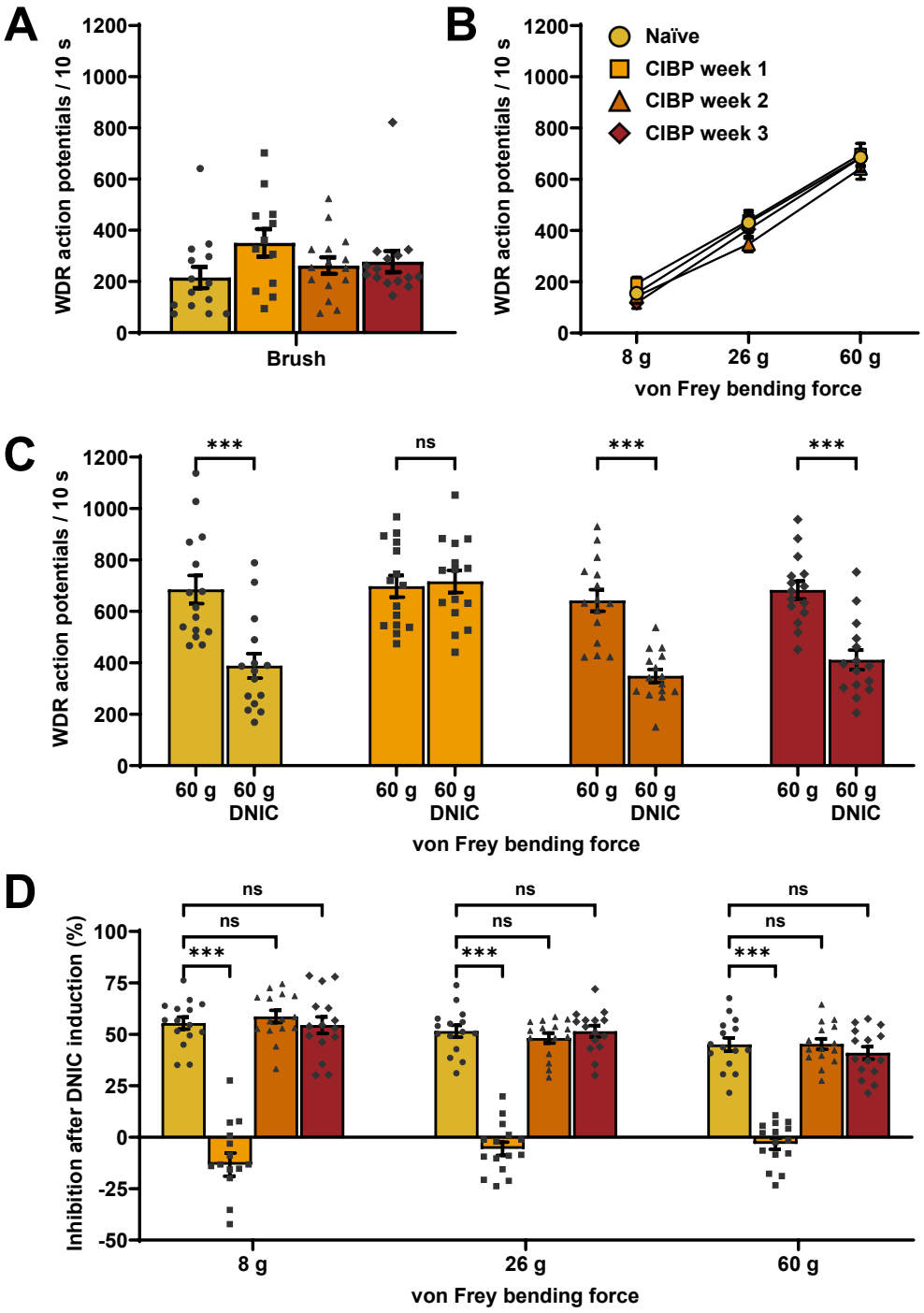

Figure 3.9. DNIC are dynamically expressed in CIBP female rats. (A) *WDR neuronal responses to dynamic mechanical stimulation (brush).* ***(B)*** *WDR neuronal responses to increasing punctate mechanical forces (von Frey).* ***(C)*** *DNIC effects on WDR baseline activity upon simultaneous noxious ear clamp (60 g von Frey).* ***(D)*** *DNIC effect comparison (% reduction in cell activity with respect to baseline) attending to different von Frey bending forces. ***P < 0.001. Data represent mean ± SEM. Each dot corresponds to an individual cell from naïve (n = 15; N = 13), CIBP week 1 (n = 15, N = 14), CIBP week 2 (n = 15, N = 14), or CIBP week 3 (n = 15, N = 12) female rats. The figure key presented in (B) is valid for the entire figure. WDR: wide-dynamic range; CIBP: cancer-induced bone pain; DNIC: diffuse noxious inhibitory controls.*

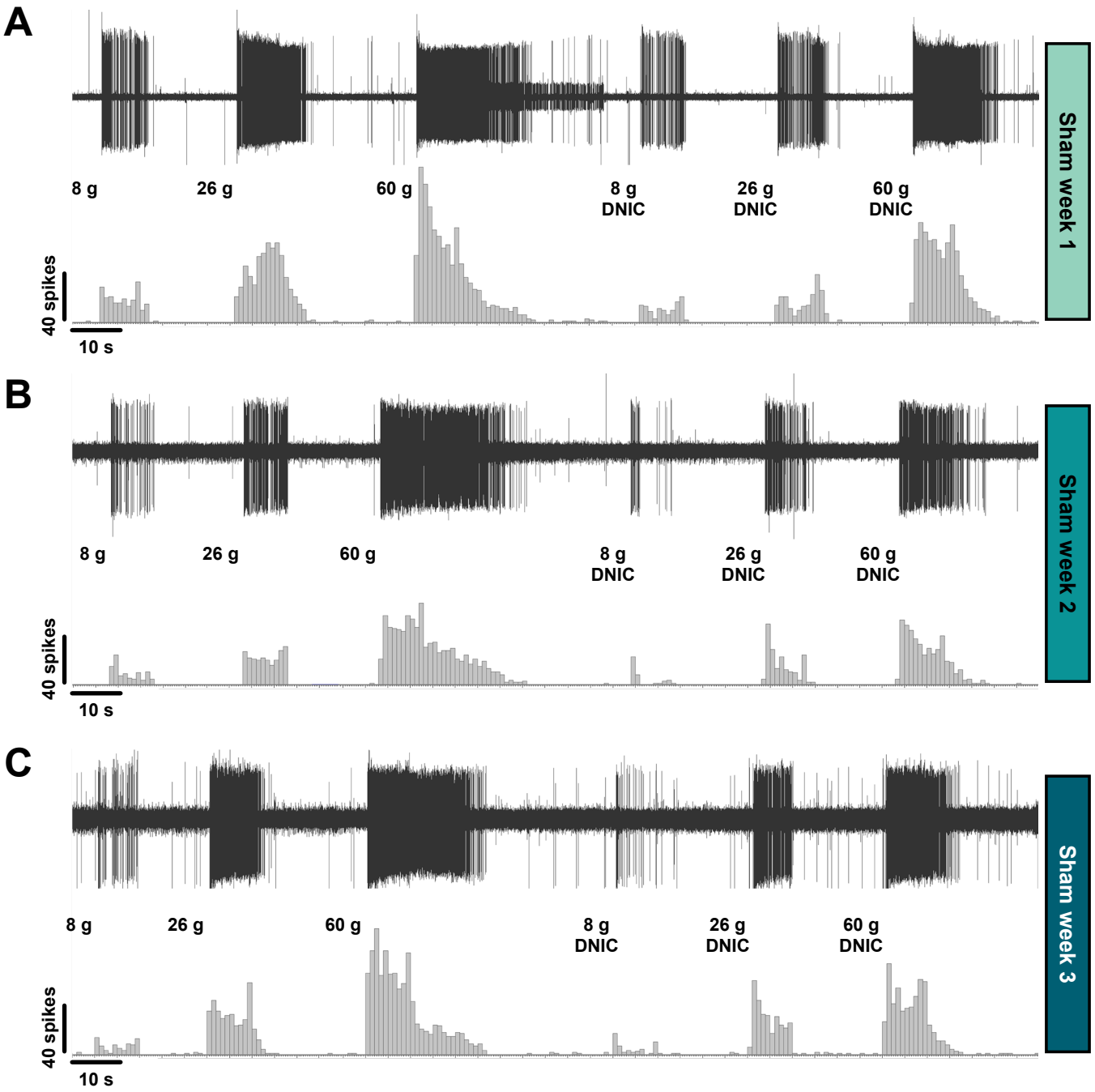

Figure 3.10. DNIC are expressed in sham female rats (neuronal traces). *Representative examples of spinal WDR neuronal traces and action potential quantification in* ***(A)*** *sham week 1,* ***(B)*** *sham week 2, and* ***(C)*** *sham week 3 female rats before and upon simultaneous noxious ear clamp application (DNIC). Each example corresponds to the same cell during the same stimulation trial. Some non-stimulation periods (resting time between each stimulus) may have been cropped out for illustrative purposes. DNIC: diffuse noxious inhibitory controls.*

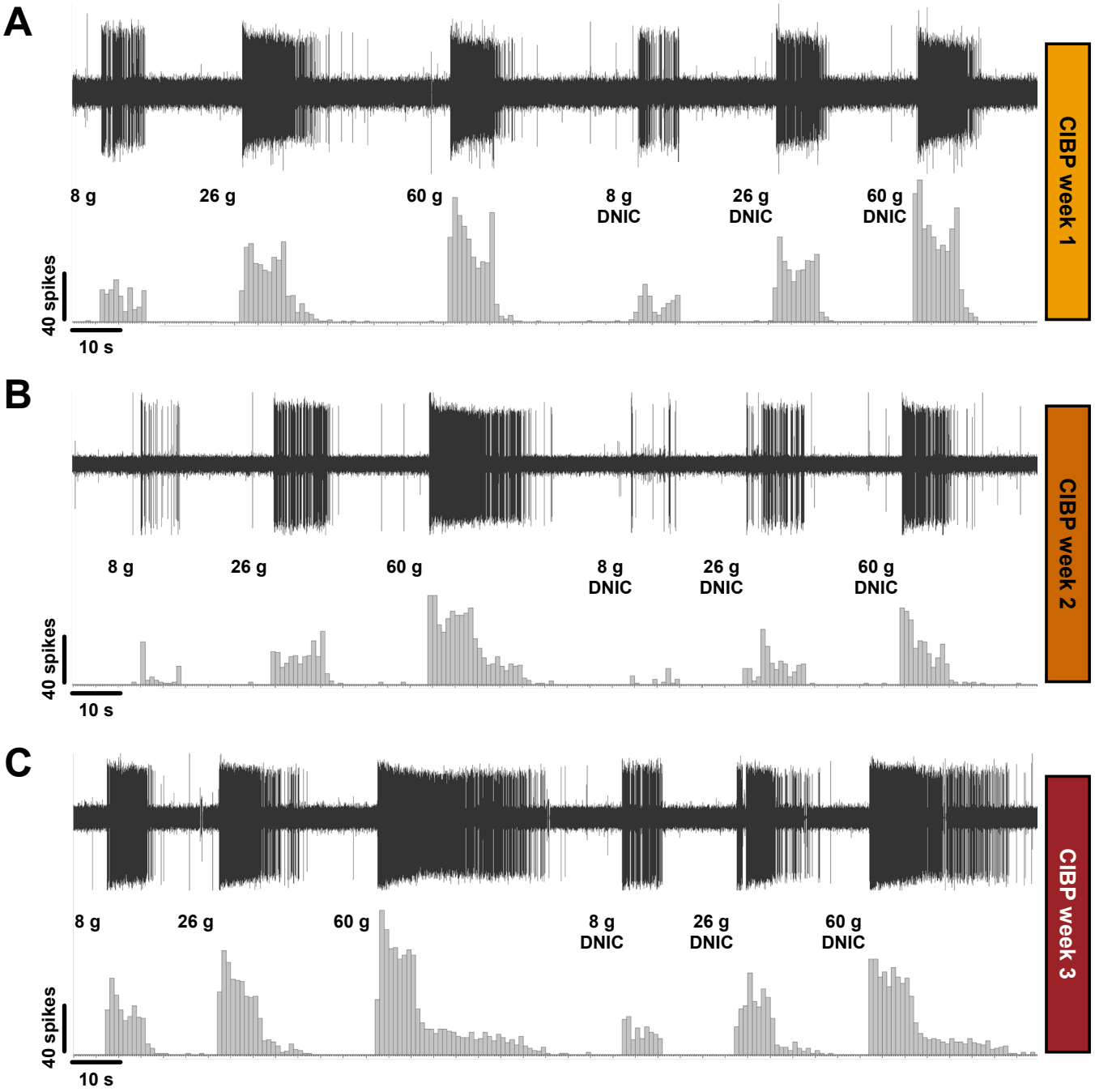

Figure 3.11. DNIC are dynamically expressed in CIBP female rats (neuronal traces). *Representative examples of spinal WDR neuronal traces and action potential quantification in* ***(A)*** *CIBP week 1,* ***(B)*** *CIBP week 2, and* ***(C)*** *CIBP week 3 female rats before and upon simultaneous noxious ear clamp application (DNIC). Each example corresponds to the same cell during the same stimulation trial. Some non-stimulation periods (resting time between each stimulus) may have been cropped out for illustrative purposes. CIBP: cancer-induced bone pain; DNIC: diffuse noxious inhibitory controls.*

Sham groups (week 1, week 2, and week 3): Topical spinal atipamezole application showed a facilitatory effect on evoked WDR neuronal activity in sham week 1 (2-way RM-ANOVA: $F_{(5, 25)} = 3.161$, $p < 0.05$; Bonferroni post hoc), sham week 2 (2-way RM-ANOVA: $F_{(5, 30)} = 3.838$, $p < 0.01$; Bonferroni post hoc), and sham week 3 rats (2-way RM-ANOVA: $F_{(5, 30)} = 5.841$, $p < 0.001$; Bonferroni post hoc), with this increase being consistent across different von Frey forces ($F_{(10, 50)} = 1.031$, $p > 0.05$; $F_{(10, 60)} = 1.003$, $p > 0.05$; and ($F_{(10, 60)} = 1.696$, $p > 0.05$; respectively) (see **Figure 3.12A**). Upon application of a noxious ear clamp (conditioning stimulus), atipamezole abolished DNIC expression for every von Frey filament tested in sham week 1 (3-way RM-ANOVA: $F_{(10, 50)} = 2.259$, $p < 0.05$; Bonferroni post hoc: $p > 0.05$ up to 60 minutes), sham week 2 (3-way RM-ANOVA: $F_{(10, 60)} = 4.511$, $p < 0.001$; Bonferroni post hoc: $p > 0.05$ up to 60 minutes), and sham week 3 rats (3-way RM-ANOVA: $F_{(10, 60)} = 3.258$, $p < 0.01$; Bonferroni post hoc: $p > 0.05$ up to 60 minutes) (see **Figure 3.12C**, **Figure 3.12D**) (see **Figure 3.13** for individual von Frey forces). The inhibitory effect of DNIC (% reduction of cell activity with respect to baseline upon ear clamp application) for 8 g von Frey (2-way mixed ANOVA: $F_{(15, 115)} = 0.641$, $p > 0.05$), 26 g von Frey (2-way mixed ANOVA: $F_{(15, 115)} = 0.679$, $p > 0.05$), and 60 g von Frey (2-way mixed ANOVA: $F_{(10.121, 77.598)} = 1.033$, $p > 0.05$) bending forces showed no differences when compared to naïve rats (see **Figure 3.12B**).

CIBP groups (week 1, week 2, and week 3): Topical spinal atipamezole application showed a facilitatory effect on evoked WDR neuronal activity in CIBP week 1 (2-way RM-ANOVA: $F_{(5, 30)} = 4.321$, $p < 0.01$; Bonferroni post hoc) and CIBP week 3 rats (2-way RM-ANOVA: $F_{(5, 25)} = 4.468$, $p < 0.001$; Bonferroni post hoc), with this increase being consistent across different von Frey forces ($F_{(10, 60)} = 0.964$, $p > 0.05$; and $F_{(10, 50)} = 1.156$, $p > 0.05$; respectively). Atipamezole showed no effect in evoked WDR neuronal activity in CIBP week 2 rats (2-way RM-ANOVA: $F_{(5, 30)} = 1.364$, $p > 0.05$), being differentially affected according to the von Frey bending force ($F_{(10, 60)} = 2.972$, $p < 0.01$; Bonferroni post hoc) (see **Figure 3.14A**). Upon application of a noxious ear clamp (conditioning stimulus), atipamezole abolished DNIC expression for every von Frey filament tested in CIBP week 2 (3-way RM-ANOVA: $F_{(10, 60)} = 6.660$, $p < 0.001$; Bonferroni post hoc: $p > 0.05$ up to 60 minutes) and week 3 rats (3-way RM-ANOVA: $F_{(10, 50)} = 4.817$, $p < 0.01$; Bonferroni post hoc: $p > 0.05$ up to 60 minutes), but did not impact DNIC expression in CIBP week 1 rats (3-way RM-ANOVA: $F_{(10, 60)} = 1.239$, $p > 0.05$) (see **Figure 3.14C**, **Figure 3.14D**) (see **Figure 3.15** for individual von Frey forces). The inhibitory effect of DNIC (% reduction of cell activity with respect to baseline upon ear clamp application) for 8 g von Frey (2-way mixed ANOVA: $F_{(10.516, 2.270)} =$

2.270, $p < 0.05$), 26 g von Frey (2-way mixed ANOVA: $F_{(8.452, 64.796)} = 2.708$, $p < 0.05$), and 60 g von Frey (2-way mixed ANOVA: $F_{(9.932, 72.838)} = 2.717$, $p < 0.01$) bending forces showed differences between groups. These differences were shown exclusively at baseline by CIBP week 1 rats when compared to naïve rats (Bonferroni post hoc: $p < 0.001$), but not for any other timepoint (Bonferroni post hoc: $p > 0.05$ for all tests) nor any other CIBP group (week 2 and week 3) (Bonferroni post hoc: $p > 0.05$ for all tests) (see **Figure 3.14B**).

These results confirm that, in line with those results observed in CIBP male and naïve female rats, there is a fully functional noradrenergic system sub-serving DNIC expression in sham and CIBP female rats. Thus, DNIC inhibition is blocked by selective α2-adrenoceptor antagonists (i.e., atipamezole) at any post-surgical week, except on CIBP week 1 rats, where DNIC expression is absent.

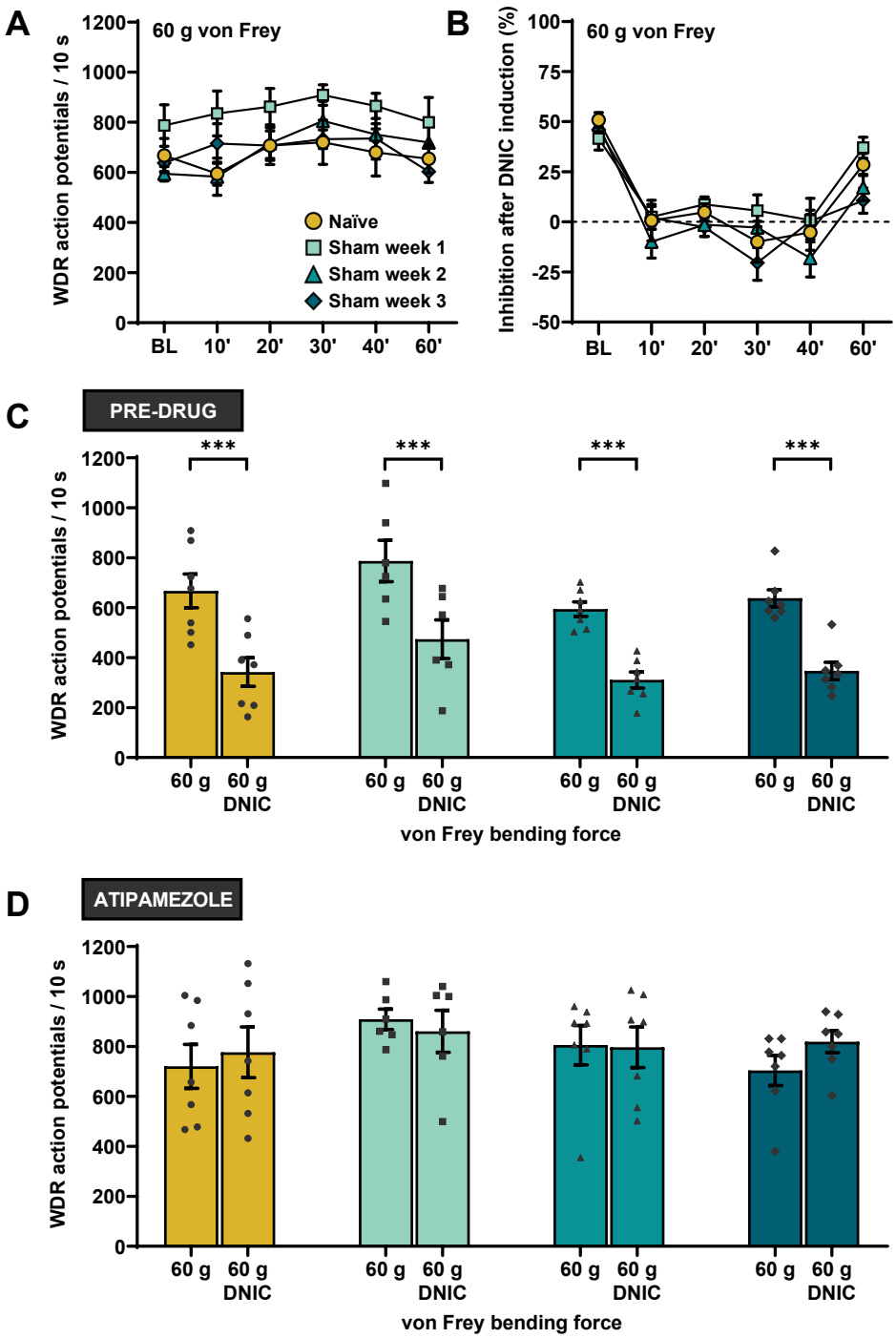

Figure 3.12. Spinal α2-adrenergic receptors mediate DNIC in sham female rats. (A) *Atipamezole effect on evoked WDR neuronal responses (60 g von Frey). Comparisons against their respective baselines.* ***(B)*** *Atipamezole effect on DNIC (% reduction in cell activity with respect to baseline) (60 g von Frey). Comparisons against naïve values.* ***(C)*** *and* ***(D)*** *DNIC effect on WDR baseline activity upon simultaneous noxious ear clamp before (pre-drug) and 30 minutes after atipamezole application, respectively (60 g von Frey). ***P < 0.001. Data represent mean ± SEM. Each line represents the same group of cells across time and each dot corresponds to an individual cell from naïve (n = 7, N = 7), sham week 1 (n = 6; N = 6), sham week 2 (n = 7; N = 7), or sham week 3 (n = 7; N = 7) female rats. The figure key presented in (A) is valid for the entire figure. WDR: wide-dynamic range; DNIC: diffuse noxious inhibitory controls.*

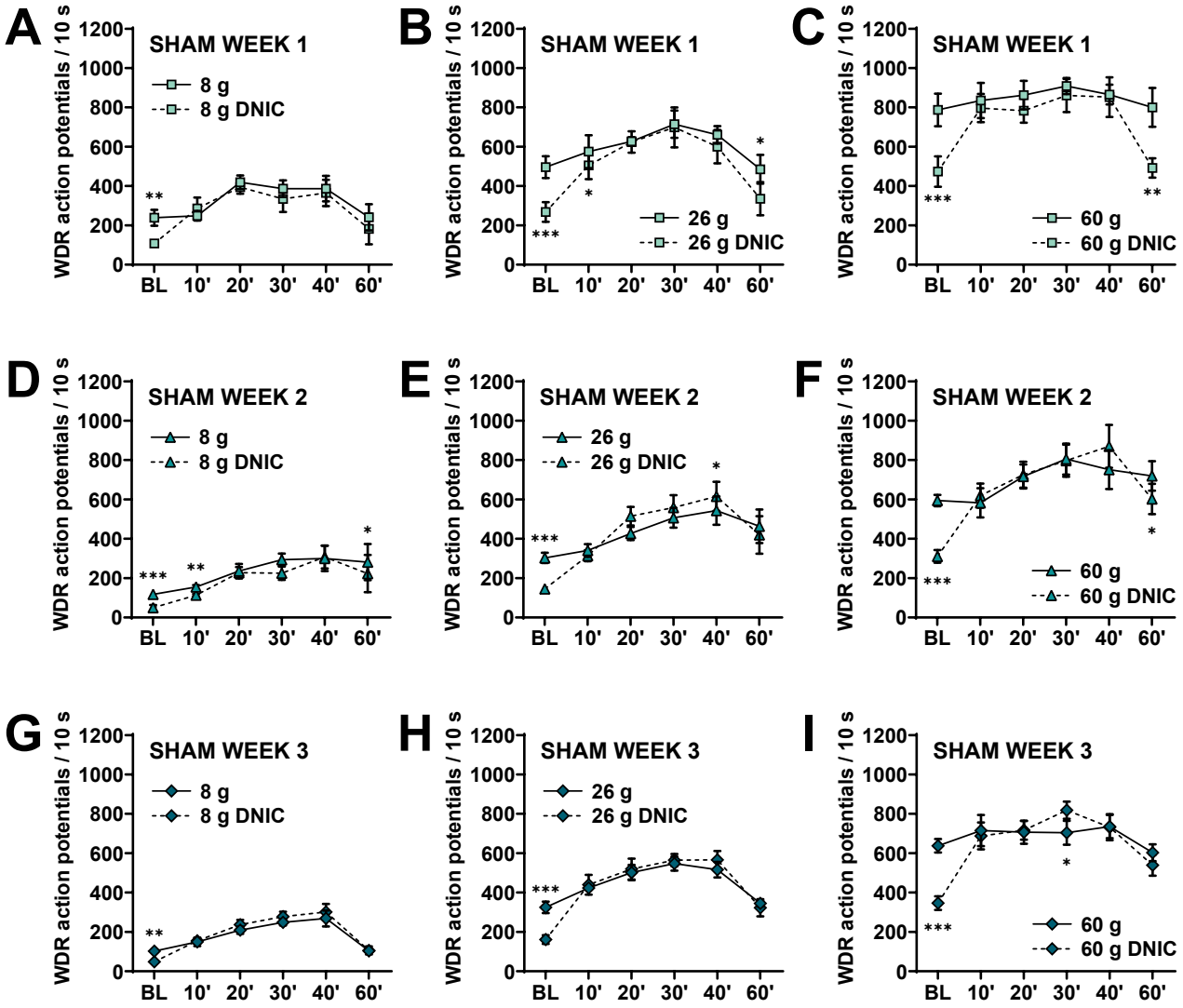

Figure 3.13. Spinal α2-adrenergic receptors mediate DNIC in sham female rats (continued). *Atipamezole effect on evoked WDR neuronal responses to 8 g, 26 g, or 60 g von Frey stimulation alone or upon simultaneous ear clamp application (DNIC) in* ***(A) (B) (C)*** *sham week 1,* ***(D) (E) (F)*** *sham week 2, and* ***(G) (H) (I)*** *sham week 3 rats, respectively. *P < 0.05; **P < 0.01; ***P < 0.001. Data represent mean ± SEM. Each line represents the same group of cells across time from sham week 1 (n = 6; N = 6), sham week 2 (n = 7; N = 7), or sham week 3 (n = 7; N = 7) female rats. WDR: wide-dynamic range; DNIC: diffuse noxious inhibitory controls.*

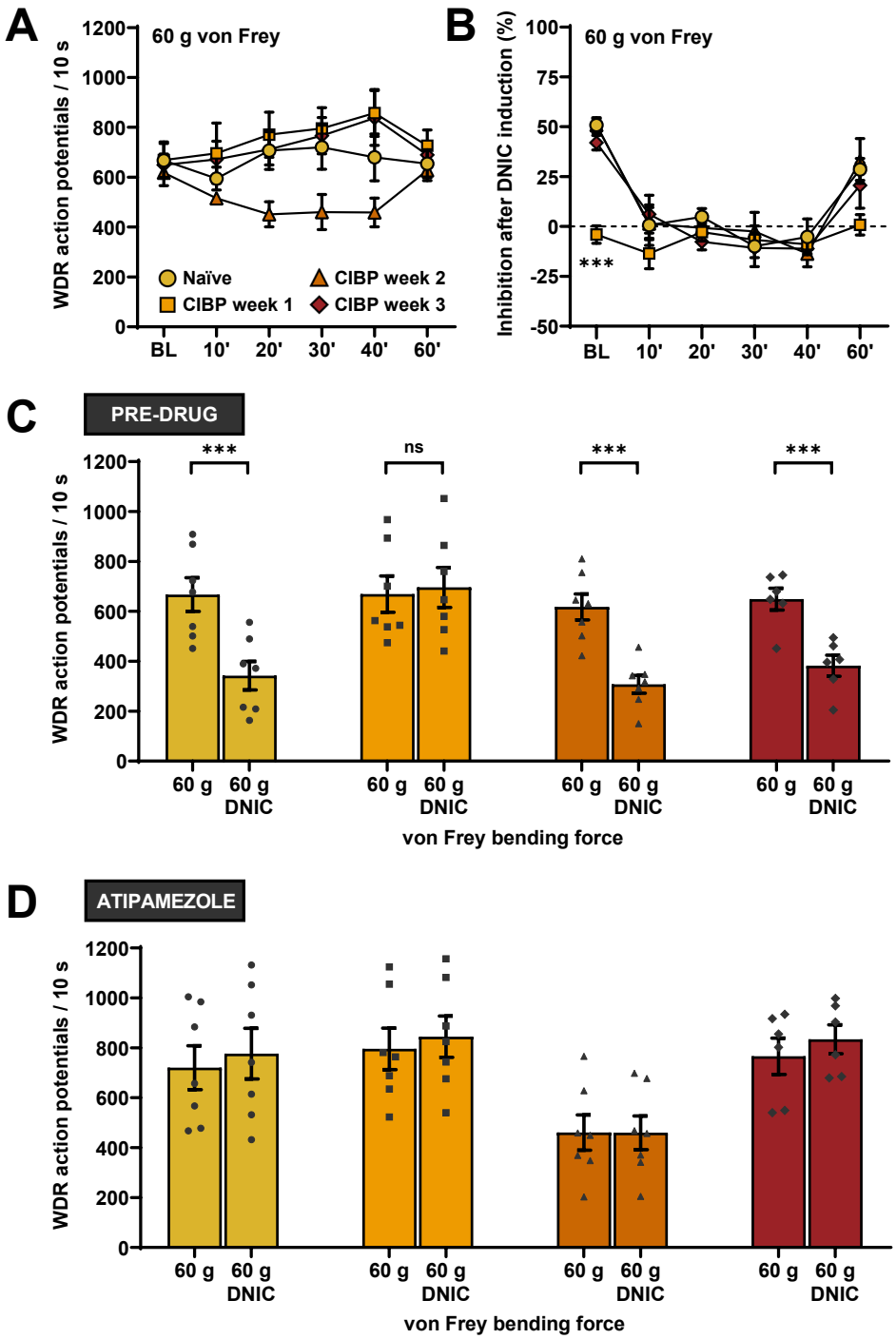

Figure 3.14. Spinal α2-adrenergic receptors mediate DNIC in CIBP female rats. (A) *Atipamezole effect on evoked WDR neuronal responses (60 g von Frey). Comparisons against their respective baselines.* ***(B)*** *Atipamezole effect on DNIC (% reduction in cell activity with respect to baseline) (60 g von Frey). Comparisons against naïve values.* ***(C)*** *and* ***(D)*** *DNIC effect on WDR baseline activity upon simultaneous noxious ear clamp before (pre-drug) and 30 minutes after atipamezole application, respectively (60 g von Frey). ***P < 0.001. Data represent mean ± SEM. Each line represents the same group of cells across time and each dot corresponds to an individual cell from naïve (n = 7, N = 7), CIBP week 1 (n = 7, N = 7), CIBP week 2 (n = 7, N = 7), or CIBP week 3 (n = 6, N = 6) female rats. The figure key presented in (A) is valid for the entire figure. WDR: wide-dynamic range; CIBP: cancer-induced bone pain; DNIC: diffuse noxious inhibitory controls.*

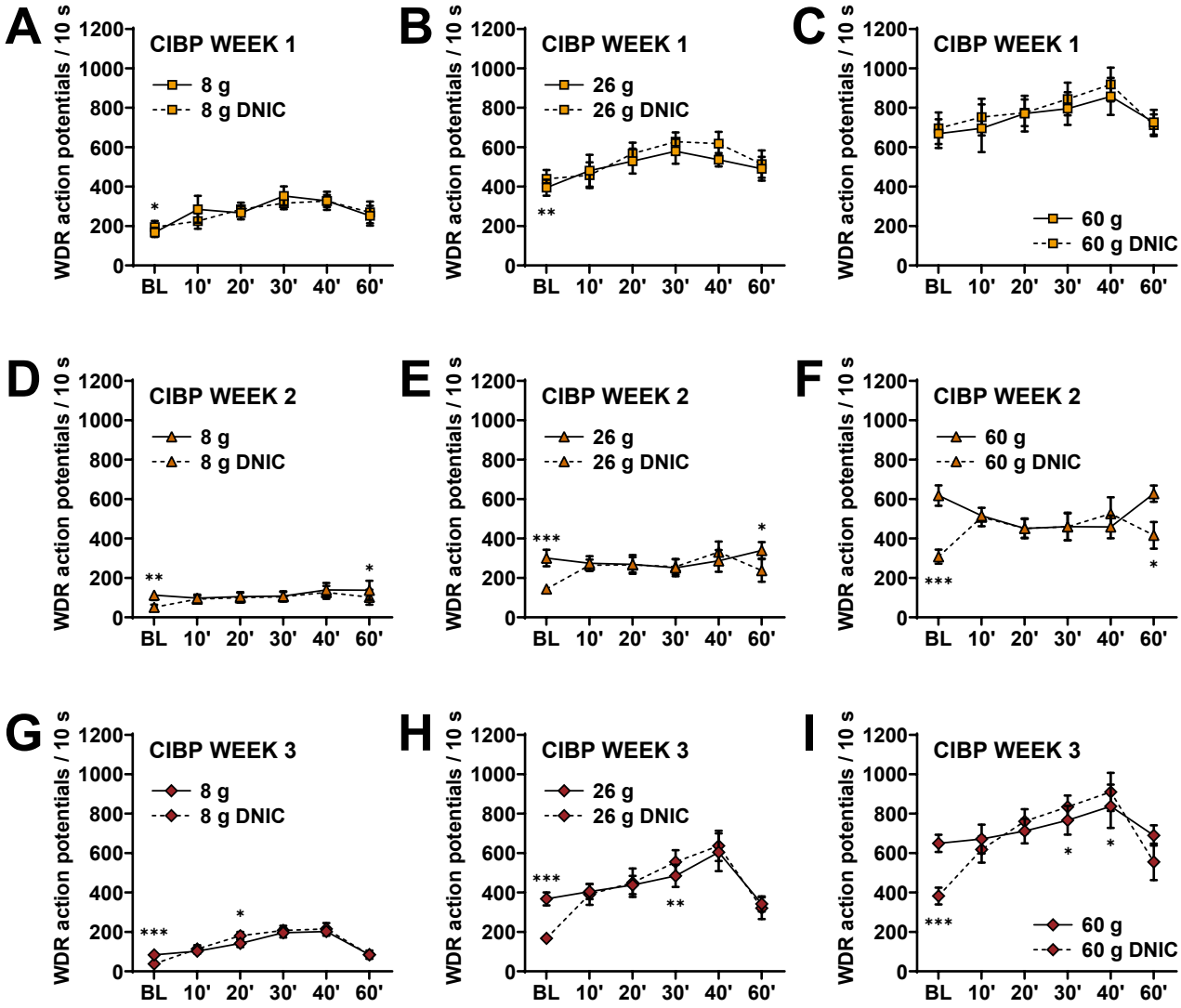

Figure 3.15. Spinal α2-adrenergic receptors mediate DNIC in CIBP female rats (continued). *Atipamezole effect on evoked WDR neuronal responses to 8 g, 26 g, or 60 g von Frey stimulation alone or upon simultaneous ear clamp application (DNIC) in* ***(A) (B) (C)*** *CIBP week 1,* ***(D) (E) (F)*** *CIBP week 2, and* ***(G) (H) (I)*** *CIBP week 3 rats, respectively. *P < 0.05; **P < 0.01; ***P < 0.001. Data represent mean ± SEM. Each line represents the same group of cells across time from CIBP week 1 (n = 7, N = 7), CIBP week 2 (n = 7, N = 7), or CIBP week 3 (n = 6, N = 6) female rats. WDR: wide-dynamic range; CIBP: cancer-induced bone pain; DNIC: diffuse noxious inhibitory controls.*

3.5. Discussion

3.5.1. Tumour progression in CIBP female rats

Both mechanical and thermal detection anomalies are a common symptom in cancer patients suffering from pain (Dams et al., 2021; Lipton et al., 1991; Scott et al., 2012) and are deeply affected by the type of anticancer treatment (Martland et al., 2020). Here I provide evidence of how localised tibial MRMT-1 cancer cell injection results in the progressive development of mechanical ipsilateral hypersensitivity in a CIBP rat model. These characteristic mechanical hypersensitivity, motor impairments, and pain-related loading elements have been recapitulated in previous studies using the MRMT-1 cell line under different behavioural paradigms showing the reproducibility of the model (Doré-Savard et al., 2010; Falk, Ipsen, et al., 2015; Kucharczyk, Derrien et al., 2020; Medhurst et al., 2002; Tétreault et al., 2011). Additionally, my results demonstrate that CIBP female rats present with thermal heat hypersensitivity, a phenomenon also evidenced in previous studies using different CIBP rodent models (Liu et al., 2021; Menéndez et al., 2003; Xu et al., 2013; Yang et al., 2017).

As expected, these gradual pain-related behaviours correlate with progressive trabecular and cortical bone destruction. The high-resolution morphometric analysis presented here reveals clear signs of small radiolucent tibial trabecular lesions on week 1, loss of trabecular bone and erosion of the cortical bone by week 2, and full thickness cortical bone loss and severely compromised bone integrity by week 3 (evidenced by tissue mineral density and thickness reduction in CIBP rats) following cancer cell implantation surgery. Osteolytic lesions (i.e., creation of cavities, holes, and weakened bone areas) appearing by week 3 are accompanied by marked signs of potential fracture and match previously described timeframes in CIBP female rats (Salamanna et al., 2013). Interestingly, and in contrast to female rats, osteolytic macroscopic lesions appear on CIBP male rats on week 2, as previously described (Kucharczyk, Chisholm et al., 2020). These results suggest a slower tumour growth rate in female rats, something that could be inferred from previous behavioural outcomes (Ungard et al., 2020; Zhu et al., 2017) and could also be linked to previous studies showing how female rats present a higher chance of recovery following cancer cell implantation (Falk, Al-Dihaissy, et al., 2015).

The mechanisms driving this differential sex-dependent tumour growth are not simple to elucidate as MRMT-1 cancer cells express α-oestrogen receptors (Barrière et al., 2019; Doré-Savard et al., 2010), which stimulate cell proliferation, initiate mutations, and promote breast carcinogenesis in

both humans and animals (Turan et al., 2004; Yue et al., 2010; see also Yager and Davidson, 2006). Thus, CIBP female rats should present a higher cancer division rate. However, and adding another layer of complexity, androgens (e.g., testosterone) can be transformed into oestrogens (e.g., oestradiol) by aromatase actions (Roncati et al., 2016). Interestingly, cancerous breast metastatic cells present increased aromatase expression, making androgens a key factor in cancer cell malignancy and survivability in oestrogen-deprived conditions, which could explain the higher growth rate seen in male rats (Mukhopadhyay et al., 2015; Sikora et al., 2009; Sonne-Hansen and Lykkesfeldt, 2005; see also Hankinson and Eliassen, 2007). These intricate and multilayered hormonal interactions in the CIBP model remain elusive and require extensive future study.

3.5.2. WDR activity and DNIC expression in naïve female rats

There are a disproportionate number of females living with chronic pain compared to males (Zimmer et al., 2022). This imbalance is driven by numerous factors including a higher susceptibility to develop pain-associated chronic conditions, greater willingness to seek medical help, higher pain sensitivity, and greater reporting of pain (all of which are proposed affected by female-linked gendered and cultural norms) (Kröner-Herwig et al., 2012; Neziri et al., 2011; Riley et al., 1998; Samulowitz et al., 2018; see also Mogil, 2012; Mogil, 2020). In accordance, preclinical studies have also demonstrated that female animals characteristically exhibit lower thresholds to noxious stimuli and exaggerated pain responses to prolonged pain (Barrett et al., 2002; Gaumond et al., 2002; Nicotra et al., 2014; Terner, Barrett et al., 2003; Terner, Lomas et al., 2003), although the animal strain tested can have a drastic impact in these results (DeLeo and Rutkowski, 2000; Vendruscolo et al., 2004). All these factors highlight that including female animals in preclinical studies is of utmost importance.

In the present body of work, I evidenced DNIC expression in naïve female rats and comparable evoked WDR neuronal responses to those previously reported in male rat studies. I also observed similar WDR activity inhibition following the concomitant application of a noxious conditioning stimulus (ear clamp) (consistently reaching 40-60% inhibition) (Bannister et al., 2015; Cummins et al., 2020; Kucharczyk, Derrien et al., 2020; Kucharczyk et al., 2023; Patel and Dickenson, 2020). The data also support that sex hormonal fluctuations during the oestrous cycle do not impact electrophysiological readouts (including WDR evoked activity and DNIC inhibitory effects), showcasing that the inclusion of

female animals in WDR and DNIC *in vivo* electrophysiological studies is not equivalent to larger sample sizes.

Additionally in this chapter, and following its male counterpart, I evidenced DNIC expression in naïve female rats as governed by noradrenaline, revealed by abolished DNIC upon spinal application of atipamezole (a selective α2-adrenoceptor antagonist). These results highlight a fully functional phasic noradrenergic system subserving DNIC in naïve female rats, something already well established in male rats (Bannister et al., 2015; Bannister et al., 2017; see also Kucharczyk et al., 2021). Moreover, despite spinal atipamezole not demonstrating a significant effect on baseline WDR activity in naïve female rats, the presence of a tonic noradrenergic input has been evidenced in previous electrophysiological male rat studies, where atipamezole showed a facilitatory effect in WDR baseline activity (Bannister et al., 2015; Green et al., 1998; Lockwood et al., 2019; Patel et al., 2018).

It is worth noting that sex-driven differences when comparing WDR baseline activity and/or the inhibitory effect of DNIC (marked by the phasic noradrenergic drive during the application of a noxious conditioning stimulus) may still exist. Previous data have demonstrated that primary afferents in female rats are more likely to respond to mechanical stimulation (Ross et al., 2018) and there is also evidence that the descending control of nociception (DCN) in wakeful animals is weaker in females compared to males (Da Silva et al., 2018; Da Silva et al., 2020). Thus, modest sex differences remain to be explored.

3.5.3. WDR activity in CIBP female rats

The characteristic 'pain' phenotype expressed by CIBP rats has been previously linked to an increased peripheral input, driven by augmented primary afferent sensitivity (Zhu et al., 2016) and/or increased number of recruited primary afferents (threefold increase in CIBP rats) (Kucharczyk, Chisholm et al., 2020). These recruited afferents were hypothesised to be 'silent' nociceptors that had been 'un-silenced' by the inflammatory mediators and neurotrophic factors present in the tumoral microenvironment (Kucharczyk, Chisholm et al., 2020; Prato et al., 2017). An enhanced nociceptive peripheral input would suggest hyperexcitability in the spinal cord of the model described herein, causing increased WDR activity. Hyperexcitability in superficial dorsal horn WDR neurons (laminae I and II) in response to natural and electrical stimuli has been electrophysiologically reported in CIBP male rats (Donovan-Rodriguez et al., 2004; Donovan-Rodriguez et al., 2005). Interestingly, here I provide evidence

of a lack of hyperexcitability in deep dorsal horn WDR neurons of CIBP female rats, in line with previous studies using the exact same model in male rats (Falk, Schwab et al., 2015; Kucharczyk, Derrien et al., 2020). However, it is worth mentioning that some studies have reported extremely marginal higher deep dorsal horn WDR neuronal responses in CIBP rats in response to electrical and/or thermal, but not mechanical, stimuli (Donovan-Rodriguez et al., 2006; Urch et al., 2003).

This divergence in responsiveness between superficial and deep dorsal horn WDR neurons in the CIBP rat model could be partly explained based on the projection site of primary afferents. Superficial laminae receive direct inputs from Aδ- and C-fibres as well as silent nociceptors (Prato et al., 2017), whilst deep laminae receive direct inputs from large Aβ- and small Aδ- fibres as well as indirect polysynaptic connexions from superficial C-fibres (Basbaum et al., 2009). This differential input, in addition to the extreme plasticity and heterogeneity of spinal networks, may lead to changes in transmission circuits that promote inhibitory mechanisms in deeper laminae to compensate for a gain of peripheral input. The reverse has been shown in models of neuropathy where the experimental model induces substantial denervation (e.g., spinal nerve ligation), but deep dorsal horn WDR baseline activity remains unchanged, suggesting an increase in neuronal excitability to compensate for a loss of peripheral input (Brignell et al., 2008; Patel et al., 2014).

3.5.4. DNIC expression in CIBP female rats

As previously mentioned, descending inhibitory controls have been shown to be impacted in different animal pain models. Under anaesthesia, electrophysiological DNIC expression on WDR neurons has shown to be absent in animal pain models (Bannister et al., 2015; Bannister et al., 2017; Lockwood and Dickenson, 2019; Lockwood et al., 2019; Patel and Dickenson, 2020; Phelps et al., 2019). Interestingly, cancer pain male animal models have shown a dynamic DNIC effect, where DNIC expression is lost (week 1) and then recovered further in the course of the disease (week 2) (Kucharczyk, Derrien et al., 2020). This dynamism has not been seen in any previous animal pain models, highlighting the intricacy of the mechanisms subserving this disease. In this chapter, I have provided clear evidence of dynamic DNIC expression in female rats, replicating the same timeframe seen in male rats with DNIC expression being abolished on week 1 and recovered by weeks 2 and 3 following cancer cell implantation. The replication of the same DNIC expression pattern despite slower tumour growth in

female rats evidences a clear dynamic reorganization of spinal descending modulatory actions that are more tightly linked to peripheral plasticity and input barrage rather than tumour size. However, this dynamic reorganization is not limited to inhibitory descending controls, as facilitatory descending spinal mechanisms are also altered in CIBP rats (Donovan-Rodriguez et al., 2006).

Additionally, and similarly to naïve rats, I have demonstrated that DNIC are subserved by noradrenaline in both sham and CIBP female rats. Spinal atipamezole application (a selective α2-adrenoceptor antagonist) inhibited DNIC expression in all sham and CIBP groups, except for week 1 CIBP rats (where DNIC were not expressed in the first instance). The source of spinal noradrenaline is exclusively supraspinal and limited to the A5, A6 (locus coeruleus), and A7 pontine nuclei (Howorth et al., 2009; Westlund et al., 1983). The results provided in this chapter could be explained by recent studies showing how restricted activation of direct spinally-projecting noradrenergic neurons located in the ventral locus coeruleus abolished DNIC expression, while the dorsal locus coeruleus had either no effect or facilitated DNIC functionality (Kucharczyk et al., 2022). Thus, one could speculate that cancer progression in the CIBP model originates plastic descending modulatory changes, leading to a maladaptive communication between the locus coeruleus and DNIC circuits (e.g., A5 nucleus), driving the loss of DNIC expression on week 1. On posterior weeks, where DNIC expression is recovered, this coerulean maladaptive communication could be reverted, or plastic changes could occur to compensate for it, restoring DNIC expression.

Moreover, in this chapter, atipamezole also showed a facilitatory effect on baseline WDR activity in sham rats (weeks 1, 2, and 3) as well as CIBP rats (weeks 1 and 3), revealing a tonic inhibitory noradrenergic drive. In line with these results, both inhibition and lesion of the major descending pathway for noradrenergic fibres (i.e., dorsolateral funiculus) have proved to increase WDR baseline activity, indicative of tonic inhibitory noradrenergic actions (Kucharczyk et al., 2023; Villanueva et al., 1986). However, individualised inhibition of the providers of spinal noradrenaline (A5, A6, and A7 nuclei) has no effect on WDR baseline activity (Kucharczyk et al., 2023). This situation may be indicative of an underlying interplay between these nuclei and their spinal output that cannot be reached by their individual manipulation.

3.6. Summary

In conclusion, these data evidence the expression of a functional noradrenergic DNIC system in female rats. The integrity of this descending pain modulatory pathway is compromised by disease progression in the animal CIBP model, leading to a transient DNIC expression loss. Mechanisms underpinning these deep and complex plastic changes are crucial for understanding sensorimotor modulation in health and disease to reach tailored and effective patient therapeutical approaches.

CHAPTER

RESULTS II: DNIC EXPRESSION REMAINS ALTERED IN A CIBP FEMALE RAT MODEL OF DISEASE REGRESSION

4.1. Introduction

Diphtheria toxin (DT), produced by *Corynebacterium diphtheriae*, is a potent bacterial toxin that leads to eukaryotic cell death by binding to the ubiquitously expressed heparin-binding epidermal growth factor-like growth factor (HB-EGF) receptor, inactivating elongation factor 2 (EF2), and inhibiting protein synthesis (Bennett and Eisenberg, 1994; Gill, 1982). Importantly, rodents are mainly insensitive to its toxic effects due to amino acid receptor changes that impede the toxin from binding and entering rodent specific cells (Mitamura et al., 1995; Cha et al., 1999). This impervious nature has been exploited by the research community for targeted and conditional cell ablation, allowing for the functional characterisation of specific cell lineages (Buch et al., 2005; Saito et al., 2001). Specifically, in rodent pain studies, different subsets of sensory neurons (Abrahamsen et al., 2008; Pogorzala et al., 2013; Santana-Varela et al., 2021), immune cells (Liu, Liu et al., 2022; Lopes et al., 2017; Raoof et al., 2021), neural stem cells (Li et al., 2023), and spinal neurons (Albisetti et al., 2023; Cheng et al., 2017; Frezel et al., 2023) have been targeted in this manner.

As previously mentioned, pain is one of the most invalidating symptoms in the oncological population, where cancer-induced bone pain (CIBP) is frequently present in metastatic cases (Brescia et al., 1992; Grond et al., 1996). Whilst preclinical oncological studies have previously employed DT targeted ablation with a focus on cancer immunosurveillance and immunotherapy (Dupont and Vosshenrich, 2019; Oraki Kohshour et al., 2014; Teijeira et al., 2022; Zhang, Dong et al., 2023), pain studies have focused on unveiling the mechanisms driving CIBP using animal models of disease progression that successfully recreate this clinical phenomenon (Ji et al., 2022; Kucharczyk, Derrien et al., 2020; Medhurst et al., 2002; Schwei et al., 1999) (see **section 1.6**). However, the fact that patients experience pain during both the active and remission stage of the disease (Haenen et al., 2022; Jensen et al., 2010; van den Beuken-van Everdingen et al., 2007; van den Beuken-van Everdingen et al., 2016), where CIBP is an especially frequent symptom in cases where survival is prolonged (Brown and Farquhar-Smith, 2017), highlights the importance of investigating the mechanisms that underpin CIBP in the remission state.

With the progressively higher survival rates and the increasing proportion of patients achieving successful curative treatment, improving quality of life and maximising symptom relief during the remission phase of the disease have become a priority in the preclinical research community. To achieve

pain symptom relief, it is necessary to deeply investigate the mechanisms that underpin CIBP in this remission state such that mechanistically targeted analgesics may be revealed.

4.2. Rationale and aims

Despite numerous advances using animal models that recreate the progressive pathophysiology of CIBP, an animal model that allows for mechanisms underpinning pain after cancer remission/ablation to be studied is not widely described. For this part of the thesis, I established a model that would allow me to ablate a bone dwelling tumour for subsequent analysis of pain-like phenotypes. Specifically, I used a modified cancer cell line expressing the simian diphtheria toxin receptor (DTR) to confer DT sensitivity.

In the previous chapter, I demonstrated that the expression of diffuse noxious inhibitory controls (DNIC), a naturally occurring pain inhibitory pathway (see **section 1.5.4**), is dynamic in CIBP female rats, being absent 1 week after cancer cell implantation, and recovered by post-surgical weeks 2 and 3. In the study described herein I investigated the effect of cancer ablation on DNIC expression at key timepoints in the CIBP female rat model by performing *in vivo* spinal electrophysiological characterisation of deep dorsal horn wide-dynamic range (WDR) neurons and DNIC expression alongside spinal pharmacological manipulation of α2-adrenergic receptors and bone morphometric analysis. Additionally, to assess cancer regression effects on animal behaviour, rodent pain-like phenotypes were analysed.

4.3. Materials and methods

CIBP female Sprague Dawley rats (see **section 2.1**) underwent *in vivo* spinal cord electrophysiology for single-unit WDR characterisation under isoflurane anaesthesia where rats underwent tibial cancer cell implantation surgery 1, 2, or 3 weeks prior to spinal cord recordings according to the timeline of the experiment (see **section 2.2** and **section 2.3**). All experiments included in this chapter incorporated the use of the transduced MRMT-1 cell lines expressing the simian DTR (CIBP_DTR_eGFP) (i.e., sensitive to the toxin) or the control group equivalent (CIBP_eGFP) (i.e., insensitive to the toxin). Daily DT injections were performed for 4 consecutive days at different key timepoints (injections starting on day 3, day 7, or day 14) (see **section 2.3**). Evoked WDR firing rates to natural stimuli (dynamic mechanical brush and punctate mechanical von Frey) were recorded before and during simultaneous ipsilateral application of a noxious conditioning stimulus (ear clamp, 125 g) to

evoke DNIC (see **section 2.4**). Recordings were followed by spinal cord pharmacology (see **section 2.4**) before euthanasia and bone collection for analysis (see **section 2.5**). Evoked and non-evoked behavioural testing was also carried out in naïve, CIBP_eGFP, and CIBP_DTR_eGFP female rats (see **section 2.7**). For the statistical analysis, a value of $p < 0.05$ was considered significant for all comparisons (see **section 2.8**).

4.4. Results

4.4.1. Cancer cell transduction does not affect *in vitro* cell growth nor viability

In vitro cell line growth and viability were assessed following transduction and puromycin selection in transduced MRMT-1_eGFP (n = 5) and MRMT-1_DTR_eGFP (n = 5) cells, as well as unmodified MRMT-1 cells (n = 5). Cell growth, quantified as number of alive cells/ml, showed no differences between cell lines (1-way ANOVA: $F_{(2, 14)} = 0.797$, $p > 0.05$) (see **Figure 4.1A**)*. Cell viability, measured as the percentage of alive cells in the total cell count, also showed no differences between cell lines (Kruskal-Wallis test: $H_{(2)} = 3.120$, $p > 0.05$) (see **Figure 4.1B**). Additionally, both MRMT-1_eGFP and MRMT-1_DTR_eGFP cells showed construct stability evidenced by the expression of green fluorescence after 20 cell passages (see **Figure 4.1C**).

4.4.2. Cancer ablation on week one does not resolve mechanical hypersensitivity in CIBP female rats

Pain-like behaviours were studied in naïve (n = 10), CIBP_eGFP (n = 10), and CIBP_DTR_eGFP (n = 10) female Sprague Dawley rats on pre-surgical day 2 (baseline) and post-operative days 2, 7, 14, 21, 28, and 35 (with CIBP_eGFP rats only reaching day 21 for ethical reasons). Following baseline data collection, CIBP_eGFP and CIBP_DTR_eGFP rats underwent surgical tibial cancer cell implantation (day 0) with subsequent daily DT injections performed on post-surgical days 7-10 (+ DTd7). Animal weight prior to behavioural testing (baseline weight) showed no differences between any of the groups (1-way ANOVA: $F_{(2, 27)} = 2.063$, $p > 0.05$). Analysis of animal weight over time between groups (2-way mixed ANOVA) revealed weight gain across time ($F_{(2.153, 58.137)} = 339.452$, $p < 0.001$; Bonferroni post hoc), with this weight gain being consistent across all groups ($F_{(4.306, 58.137)} = 1.789$, $p > 0.05$) (see **Figure 4.2A**).

* *Cell counting and seeding were performed by Mr Benjamin Wan in consecutive timely-separated batches.*

Static weight-bearing: The non-evoked paradigm revealed significant differences in the rear-leg body weight distribution between groups across time (2-way mixed ANOVA: $F_{(5.656,\ 76.359)} = 10.101$, $p < 0.001$). When compared to naïve rats, both CIBP_eGFP (+ DTd7) and CIBP_DTR_eGFP (+ DTd7) rats showed gradual impairment of weight distribution on the ipsilateral (cancer-bearing) leg from day 7 onwards (Bonferroni post hoc: $p < 0.01$ for all tests), but not before (Bonferroni post hoc: $p > 0.05$) (see **Figure 4.2B**). The differences between CIBP_DTR_eGFP (+ DTd7) and naïve rats were also present on day 28 (Independent Samples Test: $t_{(18)} = 5.169$, $p < 0.001$) and day 35 (Independent Samples Test: $t_{(18)} = 4.489$, $p < 0.001$).

Plantar test: Thermal ipsilateral paw stimulation revealed no significant differences between groups across time (2-way mixed ANOVA: $F_{(5.870,\ 79.248)} = 1.168$, $p > 0.05$) (see **Figure 4.2C**). CIBP_DTR_eGFP (+ DTd7) rats did not show any differences on day 28 (Independent Samples Test: $t_{(18)} = 0.505$, $p > 0.05$) nor on day 35 (Independent Samples Test: $t_{(18)} = 1.059$, $p > 0.05$) when compared to naïve rats.

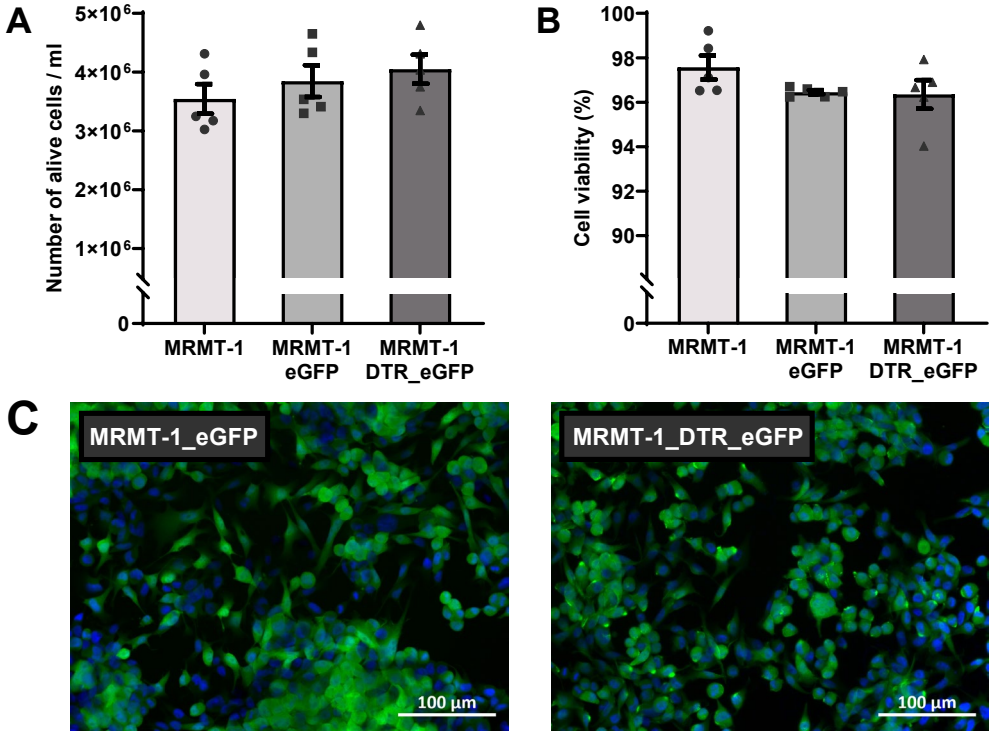

Figure 4.1. Cancer cell transduction does not affect in vitro cell dynamics. (A) *Cell growth comparisons between unmodified (MRMT-1) and transduced cell lines.* ***(B)*** *Cell viability comparison (% of alive cells in the total cell count) between cell lines.* ***(C)*** *Representative images of both transduced cell lines 20 cell passages after cell transduction and puromycin selection. Data represent mean ± SEM. Each dot corresponds to different cell counts (performed in consecutive timely-separated batches) from MRMT-1 (n = 5), MRMT-1_eGFP (n = 5), or MRMT-1_DTR_eGFP (n = 5) cells. DTR: diphtheria toxin receptor.*

Paw pressure test: Mechanical ipsilateral paw stimulation revealed significant differences between groups across time (2-way mixed ANOVA: $F_{(5.749, 77.616)} = 9.638$, $p < 0.001$). When compared to naïve rats, both CIBP_eGFP (+ DTd7) and CIBP_DTR_eGFP (+ DTd7) rats showed mechanical hypersensitivity on the ipsilateral (cancer-bearing) leg from day 7 onwards (Bonferroni post hoc: $p < 0.01$) but not before (Bonferroni post hoc: $p > 0.05$) (see **Figure 4.2D**). The differences between CIBP_DTR_eGFP (+ DTd7) and naïve rats were also present on day 28 (Independent Samples Test: $t_{(18)} = 6.502$, $p < 0.001$) and day 35 (Independent Samples Test: $t_{(18)} = 4.632$, $p < 0.001$).

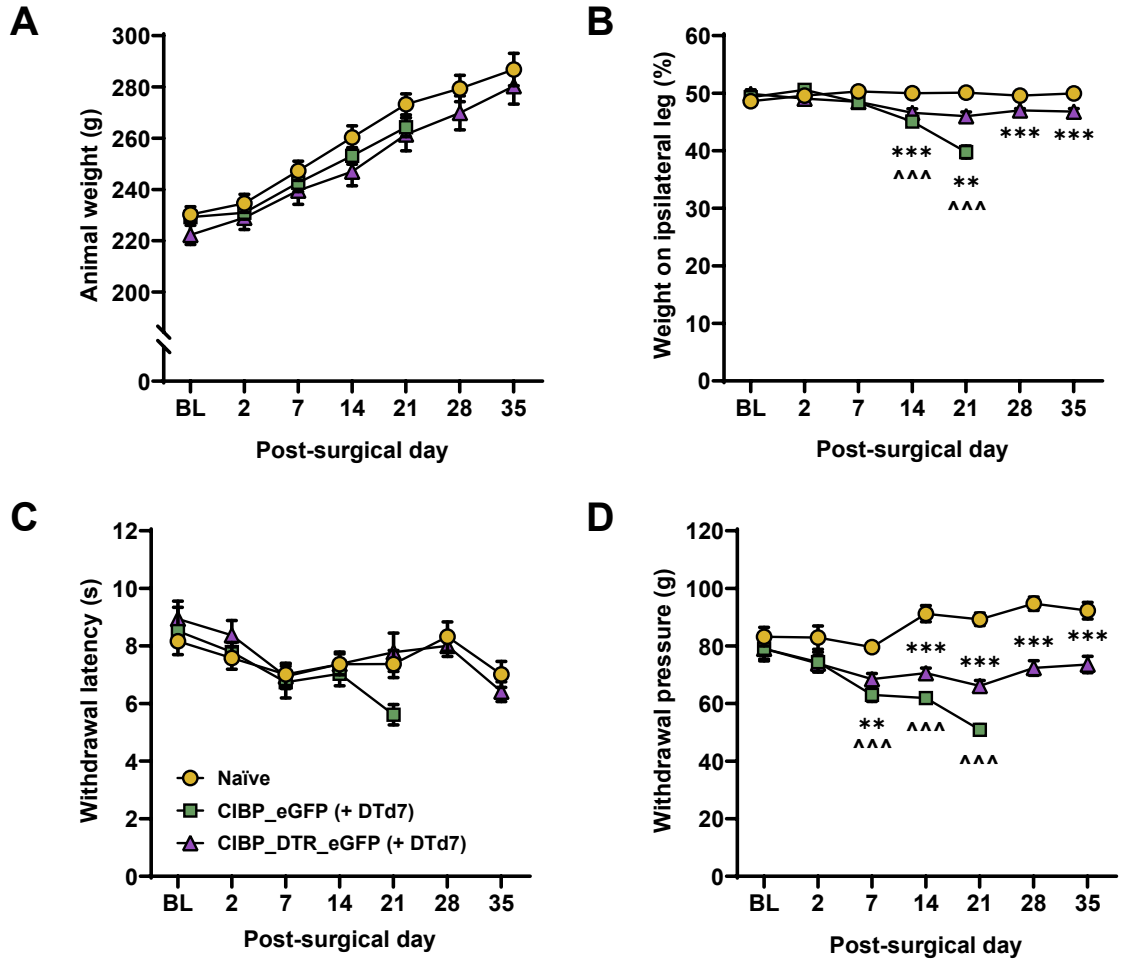

Figure 4.2. Cancer ablation on week one does not resolve mechanical hypersensitivity in CIBP female rats. ***(A)*** *Animal weight gain following surgery and DT treatment on week 1.* ***(B)*** *Weight percentage born on the ipsilateral leg (expressed as % of total rear-bearing weight) (static weight-bearing test).* ***(C)*** *Paw withdrawal latency in response to ipsilateral heat stimulation (plantar test).* ***(D)*** *Paw withdrawal threshold in response to gradual mechanical ipsilateral pressure (paw pressure test). Differences between control CIBP_eGFP (+ DTd7) and naïve rats (^) and between CIBP_DTR_eGFP (+ DTd7) and naïve rats (*) are included. **P < 0.01; ***P < 0.001. Data represent mean ± SEM. Each line represents the same group of naïve (n = 10), CIBP_eGFP (+ DTd7) (n = 10), or CIBP_DTR_eGFP (+ DTd7) (n = 10) female rats across time. The figure key presented in (C) is valid for the entire figure. CIBP: cancer-induced bone pain; DTR: diphtheria toxin receptor; DT: diphtheria toxin.*

Additional comparisons between the pain-like phenotype elicited by the unmodified MRMT-1 cell line (results presented in the previous chapter) and the control CIBP_eGFP (+ DTd7) showed no differences at any given timepoint for the static weight-bearing test (2-way mixed ANOVA: $F_{(2.857, 51.430)} = 0.498$, $p > 0.05$), the plantar test (2-way mixed ANOVA: $F_{(2.297, 41.338)} = 0.892$, $p > 0.05$), nor the paw pressure test (2-way mixed ANOVA: $F_{(4, 72)} = 1.012$, $p > 0.05$).

Summarising, cancer cell transduction did not affect the behavioural pain-like phenotype (neither in terms of its initiation nor progression) when compared to the unmodified cancer cell line. However, following cancer cell ablation on week 1, CIBP_DTR_eGFP rats did not develop a progressive and degenerative pain-like phenotype although they retained (to a lesser extent) mechanical hypersensitivity, indicating a long-lasting modification that still manifests as a pathophysiological phenotype even after cancer elimination.

4.4.3. Cancer ablation on week one prevents bone degeneration in CIBP female rats

Evaluation of bone integrity in naïve, CIBP_eGFP, and CIBP_DTR_eGFP female Sprague Dawley rats was carried out using high-resolution micro-computed tomography (μCT) following collection of tibiae (with the corresponding fibula and patella) from CIBP_eGFP (+ DTd7) week 2 (n = 5), CIBP_eGFP (+ DTd7) week 3 (n = 5), CIBP_DTR_eGFP (+ DTd7) week 2 (n = 5), and CIBP_DTR_eGFP (+ DTd7) week 3 (n = 5) rats and daily DT injections on post-surgical days 7-10 (+ DTd7), where a naïve group provided the reference control for all comparisons (n = 5).

CIBP_eGFP (+ DTd7) groups (week 2 and week 3): Total tibial length showed no differences between any of the groups (1-way ANOVA: $F_{(2, 12)} = 0.092$, $p > 0.05$) despite clear progressive macroscopic bone damage (see **Figure 4.3A**). When compared to naïve rats, trabecular bone properties showed progressive degradation (see **Table 4.1** for a result overview). Interestingly, trabecular tissue mineral density (degree of mineralization within the bone volume of interest) showed no differences between groups (1-way ANOVA: $F_{(2, 12)} = 2.361$, $p > 0.05$) (see **Figure 4.3B**). Cortical bone morphometric characteristics followed a similar degradation pattern (see **Table 4.1** for a result overview), with cortical tissue mineral density (surprisingly but following the trabecular results) showing no differences between groups (1-way ANOVA: $F_{(2, 12)} = 1.235$, $p > 0.05$) (see **Figure 4.3B**).

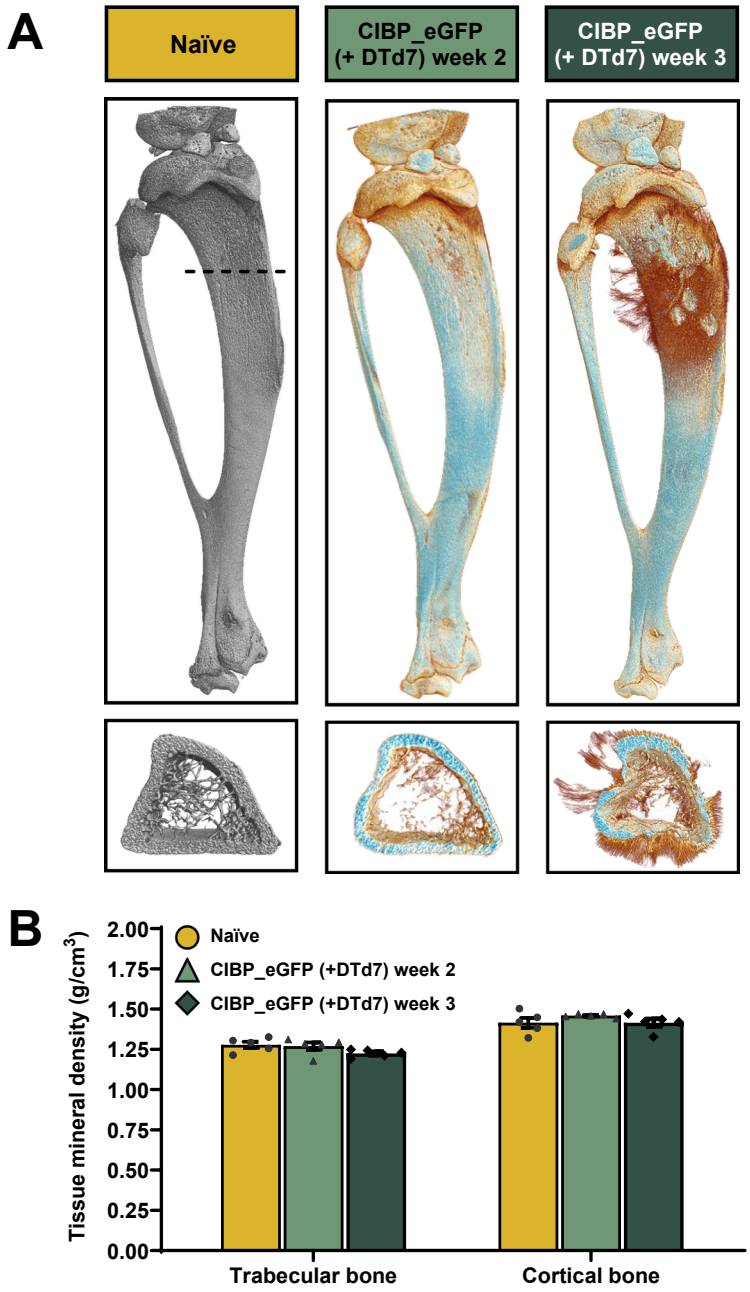

Figure 4.3. DT treatment on week one does not affect bone degeneration in CIBP female rats. (A) *Representative scanned tibial samples (micro-computed tomography) showcasing the macroscopic changes following CIBP surgery and DT treatment on week 1.* ***(B)*** *Trabecular and cortical tissue mineral density (degree of mineralization within the bone volume of interest) comparisons. Data represent mean ± SEM. Each dot corresponds to individual tibial samples from naïve (n = 5), CIBP_eGFP (+ DTd7) week 2 (n = 5), or CIBP_eGFP (+ DTd7) week 3 (n = 5) female rats. CIBP: cancer-induced bone pain; DT: diphtheria toxin.*

Table 4.1. Impact of week-one DT treatment on rat bone microarchitecture. *Summary of representative parameters obtained from the trabecular and cortical micro-computed tomography tibial analysis. Data represent the mean ± SEM from naïve (n = 5), CIBP_eGFP (+ DTd7) week 2 (n = 5), and CIBP_eGFP (+ DTd7) week 3 (n = 5) female rats. One-way ANOVA with Bonferroni post-hoc test: *p < 0.05, **p < 0.01, ***p < 0.001 (comparisons against naïve rats). Whenever homoscedasticity was not met, Welch's one-way ANOVA with Games-Howell post-hoc test was performed (or Kruskal-Wallis test with Dunn-Bonferroni post hoc test if data were additionally not normally distributed). CIBP: cancer-induced bone pain; DT: diphtheria toxin.*

		Naïve	CIBP_ eGFP (+DTd7) week 2	CIBP_ eGFP (+DTd7) week 3
Trabecular total surface	mm^2	79.20 ± 3.54	80.28 ± 1.80	81.38 ± 0.99
Trabecular bone surface	mm^2	212.95 ± 42.05	156.25 ± 19.70	68.75 ± 12.15
Trabecular bone surface fraction	%	70.92 ± 3.36	64.87 ± 3.88	**44.22 ± 4.66***
Trabecular total volume	mm^3	28.61 ± 2.98	29.59 ± 1.63	32.73 ± 0.64
Trabecular bone volume	mm^3	4.42 ± 0.98	2.91 ± 0.46	1.06 ± 0.21
Trabecular bone volume fraction	%	15.16 ± 2.54	10.18 ± 1.83	**3.23 ± 0.61***
Trabecular number	mm^{-1}	2.01 ± 0.30	1.48 ± 0.53	**0.51 ± 0.09****
Trabecular pattern factor	mm^{-1}	14.07 ± 1.22	17.66 ± 1.93	**26.58 ± 1.14*****
Trabecular separation	mm	0.42 ± 0.10	0.50 ± 0.07	**0.77 ± 0.07***
Trabecular thickness ($x10^{-2}$)	mm	7.44 ± 0.16	6.75 ± 0.22	**6.30 ± 0.23****
Trabecular tissue mineral density	g/cm^3	1.28 ± 0.02	1.27 ± 0.02	1.22 ± 0.01
Connectivity density ($x10^{-5}$)	mm^{-3}	3.86 ± 0.71	2.60 ± 0.40	**0.80 ± 0.20***
Degree of anisotropy	N/A	0.66 ± 0.01	0.60 ± 0.03	**0.54 ± 0.02****
Fractal dimension	N/A	2.40 ± 0.04	2.30 ± 0.06	**2.03 ± 0.06****

		Naïve	CIBP_ eGFP (+DTd7) week 2	CIBP_ eGFP (+DTd7) week 3
Cortical total area (mean)	mm^2	9.04 ± 0.51	9.58 ± 0.36	**13.69 ± 0.67*****
Cortical bone area (mean)	mm^2	4.33 ± 0.16	4.15 ± 0.05	4.12 ± 0.15
Cortical bone area fraction	%	48.23 ± 2.14	43.58 ± 1.73	**30.25 ± 1.28****
Cortical total surface (mean)	mm^2	134.92 ± 4.04	137.63 ± 3.54	253.95 ± 36.64
Cortical bone surface (mean)	mm^2	326.30 ± 21.93	331.62 ± 11.28	**709.57 ± 89.77***
Cortical bone surface fraction	%	70.56 ± 0.87	70.48 ± 0.63	73.76 ± 1.75
Cortical thickness	mm	0.25 ± 0.01	0.24 ± 0.01	**0.12 ± 0.01*****
Cortical tissue mineral density	g/cm^3	1.41 ± 0.03	1.46 ± 0.01	1.41 ± 0.02
Cortical porosity	%	51.86 ± 2.14	56.23 ± 1.73	**69.93 ± 1.30****
Connectivity density	mm^{-3}	1.00 ± 0.00	1.00 ± 0.00	**7.60 ± 1.50****
Eccentricity	N/A	0.61 ± 0.03	0.62 ± 0.02	0.56 ± 0.02

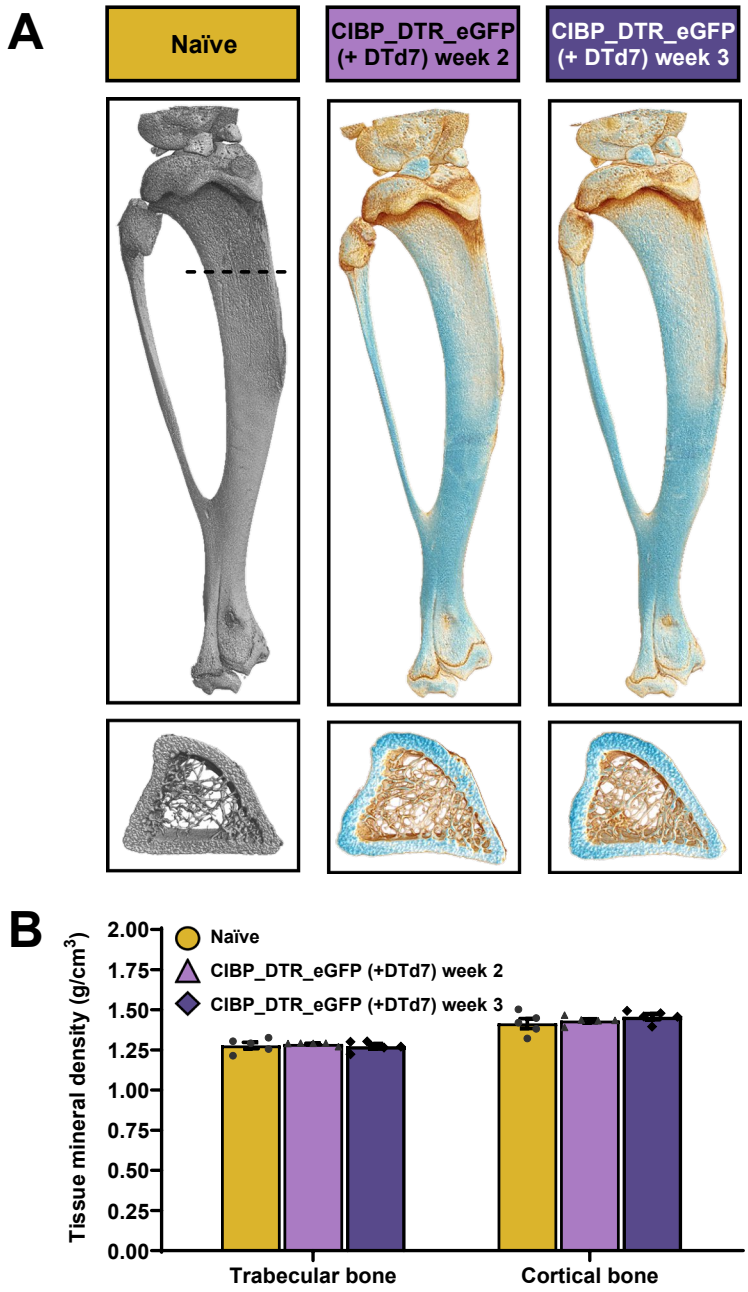

Figure 4.4. Cancer ablation on week one prevents bone degeneration in CIBP female rats. (A) *Representative scanned tibial samples (micro-computed tomography) showcasing the lack of macroscopic changes following CIBP surgery and cancer cell ablation on week 1.* ***(B)*** *Trabecular and cortical tissue mineral density (degree of mineralization within the bone volume of interest) comparisons. Data represent mean ± SEM. Each dot corresponds to individual tibial samples from naïve (n = 5), CIBP_DTR_eGFP (+ DTd7) week 2 (n = 5), or CIBP_DTR_eGFP (+ DTd7) week 3 (n = 5) female rats. CIBP: cancer-induced bone pain; DTR: diphtheria toxin receptor; DT: diphtheria toxin.*

Table 4.2. Impact of week-one cancer cell ablation on rat bone microarchitecture. *Summary of representative parameters obtained from the trabecular and cortical micro-computed tomography tibial analysis. Data represent the mean ± SEM from naïve (n = 5), CIBP_DTR_eGFP (+ DTd7) week 2 (n = 5), and CIBP_DTR_eGFP (+ DTd7) week 3 (n = 5) female rats. One-way ANOVA with Bonferroni post-hoc test: **p < 0.01 (comparisons against naïve rats). Whenever homoscedasticity was not met, Welch's one-way ANOVA with Games-Howell post-hoc test was performed (or Kruskal-Wallis test with Dunn-Bonferroni post hoc test if data were additionally not normally distributed). CIBP: cancer-induced bone pain; DTR: diphtheria toxin receptor; DT: diphtheria toxin.*

		Naïve	CIBP_DTR_eGFP (+DTd7) week 2	CIBP_DTR_eGFP (+DTd7) week 3
Trabecular total surface	mm^2	79.20 ± 3.54	78.11 ± 2.15	73.49 ± 3.57
Trabecular bone surface	mm^2	212.95 ± 42.05	202.81 ± 14.66	151.83 ± 14.60
Trabecular bone surface fraction	%	70.92 ± 3.36	71.93 ± 1.40	67.01 ± 1.22
Trabecular total volume	mm^3	28.61 ± 2.98	26.82 ± 1.27	26.44 ± 2.24
Trabecular bone volume	mm^3	4.42 ± 0.98	3.97 ± 0.31	2.85 ± 0.28
Trabecular bone volume fraction	%	15.16 ± 2.54	14.87 ± 1.19	10.74 ± 0.34
Trabecular number	mm^{-1}	2.01 ± 0.30	2.11 ± 0.15	1.53 ± 0.05
Trabecular pattern factor	mm^{-1}	14.07 ± 1.22	13.78 ± 0.62	16.83 ± 0.12
Trabecular separation	mm	0.42 ± 0.10	0.39 ± 0.02	0.41 ± 0.02
Trabecular thickness ($x10^{-2}$)	mm	7.44 ± 0.16	7.05 ± 0.12	7.03 ± 0.09
Trabecular tissue mineral density	g/cm^3	1.28 ± 0.02	1.29 ± 0.01	1.27 ± 0.01
Connectivity density ($x10^{-5}$)	mm^{-3}	3.86 ± 0.71	4.40 ± 0.51	2.60 ± 0.25
Degree of anisotropy	N/A	0.66 ± 0.01	0.65 ± 0.01	**0.59 ± 0.01****
Fractal dimension	N/A	2.40 ± 0.04	2.40 ± 0.02	2.33 ± 0.02

		Naïve	CIBP_DTR_eGFP (+DTd7) week 2	CIBP_DTR_eGFP (+DTd7) week 3
Cortical total area (mean)	mm^2	9.04 ± 0.51	9.27 ± 0.19	9.31 ± 0.37
Cortical bone area (mean)	mm^2	4.33 ± 0.16	4.48 ± 0.09	4.43 ± 0.06
Cortical bone area fraction	%	48.23 ± 2.14	48.41 ± 1.51	47.86 ± 2.11
Cortical total surface (mean)	mm^2	134.92 ± 4.04	141.41 ± 2.30	130.77 ± 3.32
Cortical bone surface (mean)	mm^2	326.30 ± 21.93	386.67 ± 20.96	309.13 ± 17.88
Cortical bone surface fraction	%	70.56 ± 0.87	73.09 ± 0.75	70.13 ± 0.79
Cortical thickness	mm	0.25 ± 0.01	0.22 ± 0.01	0.27 ± 0.02
Cortical tissue mineral density	g/cm^3	1.41 ± 0.03	1.43 ± 0.01	1.46 ± 0.02
Cortical porosity	%	51.86 ± 2.14	51.70 ± 1.52	52.23 ± 2.11
Connectivity density ($x10^{-5}$)	mm^{-3}	1.00 ± 0.00	1.52 ± 0.21	0.80 ± 0.11
Eccentricity	N/A	0.61 ± 0.03	0.62 ± 0.02	0.57 ± 0.01

CIBP_DTR_eGFP (+ DTd7) groups (week 2 and week 3): Total tibial length showed no differences between any of the groups (1-way ANOVA: $F_{(2, 12)} = 3.941$, $p > 0.05$) nor signs of macroscopic bone damage (see **Figure 4.4A**). When compared to naïve rats, trabecular bone properties were stable with no notable significant differences (see **Table 4.2** for a result overview). Of special interest, the trabecular tissue mineral density (degree of mineralization within the bone volume of interest) remained stable (1-way ANOVA: $F_{(2, 12)} = 0.265$, $p > 0.05$) (see **Figure 4.4B**). Cortical bone morphometric characteristics followed a similar pattern (see **Table 4.2** for a result overview), with cortical tissue mineral density showing no differences at any given timepoint (1-way ANOVA: $F_{(2, 12)} = 0.968$, $p > 0.05$) (see **Figure 4.4B**).

These results showcase how disease progression affects trabecular and cortical bone properties in control CIBP_eGFP (+ DTd7) rats similarly to the original unmodified cancer cell line, although tissue mineral density did not tightly reflect visually evident bone lesions. More importantly, cancer ablation on week 1 prevented trabecular and cortical bone alterations on posterior weeks in CIBP_DTR_eGFP (+ DTd7) rats, showing no evidence of macro or microarchitectural changes.

4.4.4. Cancer ablation on week one prevents DNIC recovery in CIBP female rats

Spinal WDR responses to natural stimuli as well as DNIC expression were studied in CIBP_eGFP and CIBP_DTR_eGFP female Sprague Dawley rats under isoflurane anaesthesia in a gaseous N_2O/O_2 mix. CIBP_eGFP and CIBP_DTR_eGFP rats underwent surgical tibial cancer cell implantation 2 or 3 weeks prior to the electrophysiological recordings followed by subsequent daily DT injections performed on post-surgical days 7-10 (+ DTd7). A minimum of one and maximum of two neurons were recorded per CIBP_eGFP (+ DTd7) week 2 (n = 10, N = 8), CIBP_eGFP (+ DTd7) week 3 (n = 10, N = 6), CIBP_DTR_eGFP (+ DTd7) week 2 (n = 10, N = 8), and CIBP_DTR_eGFP (+ DTd7) week 3 (n = 10, N = 6) rat, where a naïve group provided the reference control for all comparisons (n = 10; N = 9).

CIBP_eGFP (+ DTd7) groups (week 2 and week 3): Neuronal WDR responses to dynamic brush (1-way ANOVA: $F_{(2, 26)} = 0.302$, $p > 0.05$) and punctate von Frey stimulation (2-way mixed ANOVA: $F_{(2.227, 30.064)} = 0.843$, $p > 0.05$) showed no significant differences between any of the groups (see **Figure 4.5A** and **Figure 4.5B**, respectively). Upon application of a noxious ear clamp (conditioning stimulus), WDR baseline neuronal activity was significantly reduced for all von Frey filaments tested in CIBP_eGFP (+ DTd7) week 2 (2-way RM-ANOVA: $F_{(2, 18)} = 41.499$, $p < 0.001$; Bonferroni post hoc: $p < 0.001$ for all tests)

and CIBP_eGFP (+ DTd7) week 3 rats (2-way RM-ANOVA: $F_{(1.274, 11.470)} = 97.339$, $p < 0.001$; Bonferroni post hoc: $p < 0.001$ for all tests) (see **Figure 4.5C** for 60 g von Frey). The inhibitory effect of DNIC (% reduction of cell activity with respect to baseline upon ear clamp application) was comparable throughout groups for 8 g von Frey (Kruskal-Wallis test: $H_{(2)} = 2.449$, $p > 0.05$), 26 g von Frey (Kruskal-Wallis test: $H_{(2)} = 2.550$, $p > 0.05$), and 60 g von Frey (Kruskal-Wallis test: $H_{(2)} = 3.169$, $p > 0.05$) bending forces (see **Figure 4.5D**).

CIBP_DTR_eGFP (+ DTd7) groups (week 2 and week 3): Neuronal WDR responses to dynamic brush (1-way ANOVA: $F_{(2, 26)} = 2.668$, $p > 0.05$) and punctate von Frey stimulation (2-way mixed ANOVA: $F_{(2.347, 31.680)} = 0.819$, $p > 0.05$) showed no significant differences between any of the groups (see **Figure 4.6A** and **Figure 4.6B**, respectively). However, upon application of a noxious ear clamp (conditioning stimulus), WDR baseline neuronal activity showed no significant reduction for any von Frey filaments tested in CIBP_DTR_eGFP (+ DTd7) week 2 (2-way RM-ANOVA: $F_{(2, 18)} = 0.042$, $p > 0.05$) and CIBP_DTR_eGFP (+ DTd7) week 3 rats (2-way RM-ANOVA: $F_{(2, 18)} = 2.655$, $p > 0.05$) (see **Figure 4.6C** for 60 g von Frey). Thus, the inhibitory effect of DNIC (% reduction of cell activity with respect to baseline upon ear clamp application) showed significant differences between groups for 8 g von Frey (Kruskal-Wallis test: $H_{(2)} = 24.351$, $p < 0.001$), 26 g von Frey (Kruskal-Wallis test: $H_{(2)} = 20.191$, $p < 0.001$), and 60 g von Frey (Kruskal-Wallis test: $H_{(2)} = 19.667$, $p < 0.001$) bending forces. These differences were observed in both CIBP_DTR_eGFP (+ DTd7) week 1 and week 2 rats for all von Frey forces when compared to naïve rats (Dunn-Bonferroni post hoc: $p < 0.01$ for all tests) (see **Figure 4.6D**).

Additional comparisons between the unmodified MRMT-1 cell line (CIBP week 2 and week 3 rats) (results shown in previous chapter) and the control CIBP_eGFP (+ DTd7) week 2 and week 3 rats, showed no differences between neuronal WDR responses to dynamic brush (1-way ANOVA: $F_{(3, 46)} = 0.277$, $p > 0.05$) nor punctate von Frey stimulation (2-way mixed ANOVA: $F_{(3.912, 59.990)} = 1.316$, $p > 0.05$).

In sum, cancer cell ablation on week 1, a timepoint at which DNIC expression is known to be dysfunctional following cancer cell implantation (see previous chapter), prevents DNIC recovery in CIBP_DTR_eGFP rats (see **Figure 4.7**).

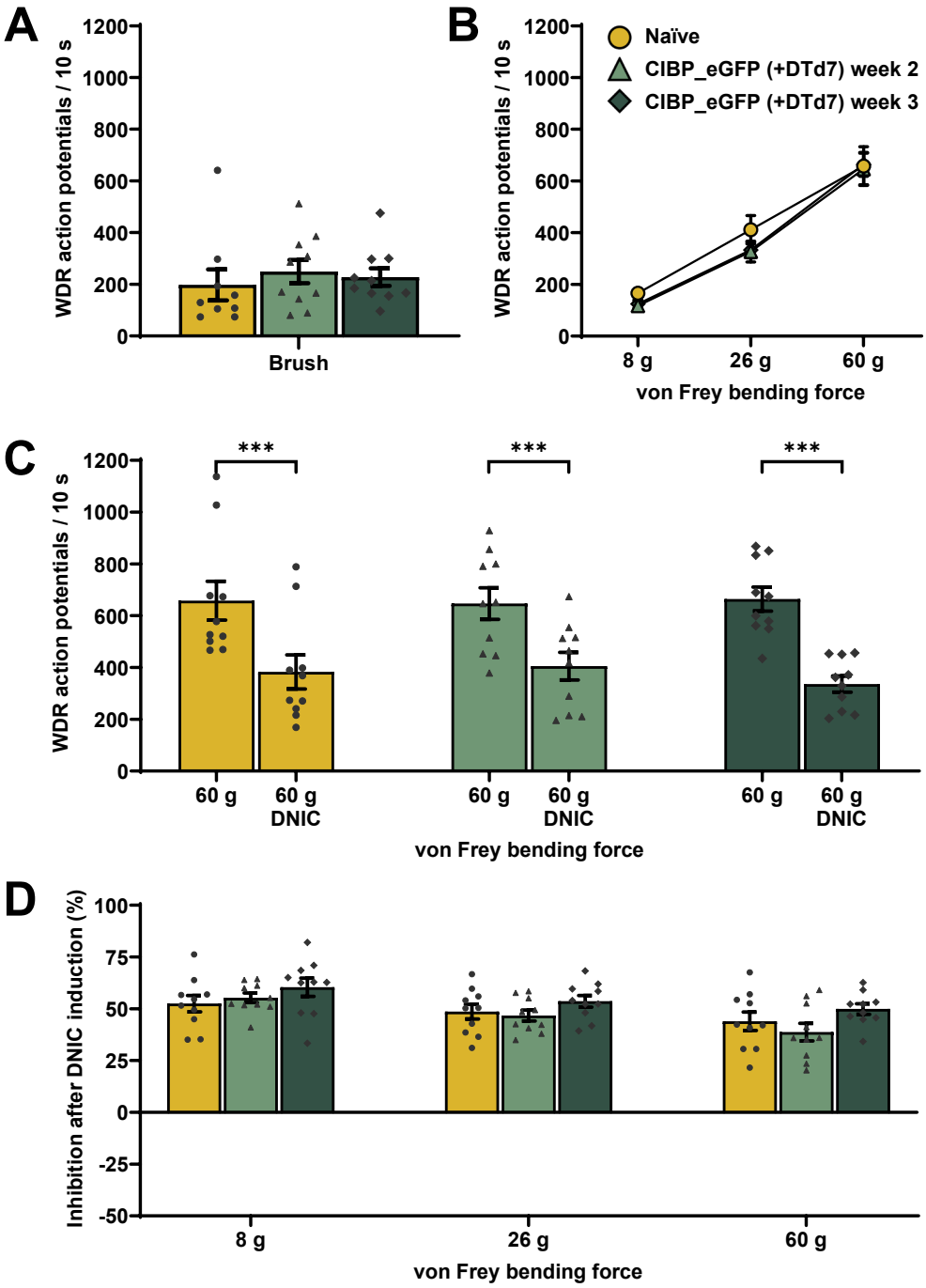

Figure 4.5. DT treatment on week one does not affect DNIC recovery in CIBP female rats. (A) *WDR neuronal responses to dynamic mechanical stimulation (brush).* ***(B)*** *WDR neuronal responses to increasing punctate mechanical forces (von Frey).* ***(C)*** *DNIC effect on WDR baseline activity upon simultaneous noxious ear clamp (60 g von Frey).* ***(D)*** *DNIC effect comparison (% reduction in cell activity with respect to baseline) attending to different von Frey bending forces. ***P < 0.001. Data represent mean ± SEM. Each dot corresponds to an individual cell from naïve (n = 10; N = 9), CIBP_eGFP (+ DTd7) week 2 (n = 10, N = 8), or CIBP_eGFP (+ DTd7) week 3 (n = 10, N = 6) female rats. The figure key presented in (B) is valid for the entire figure. WDR: wide-dynamic range; CIBP: cancer-induced bone pain; DT: diphtheria toxin; DNIC: diffuse noxious inhibitory controls.*

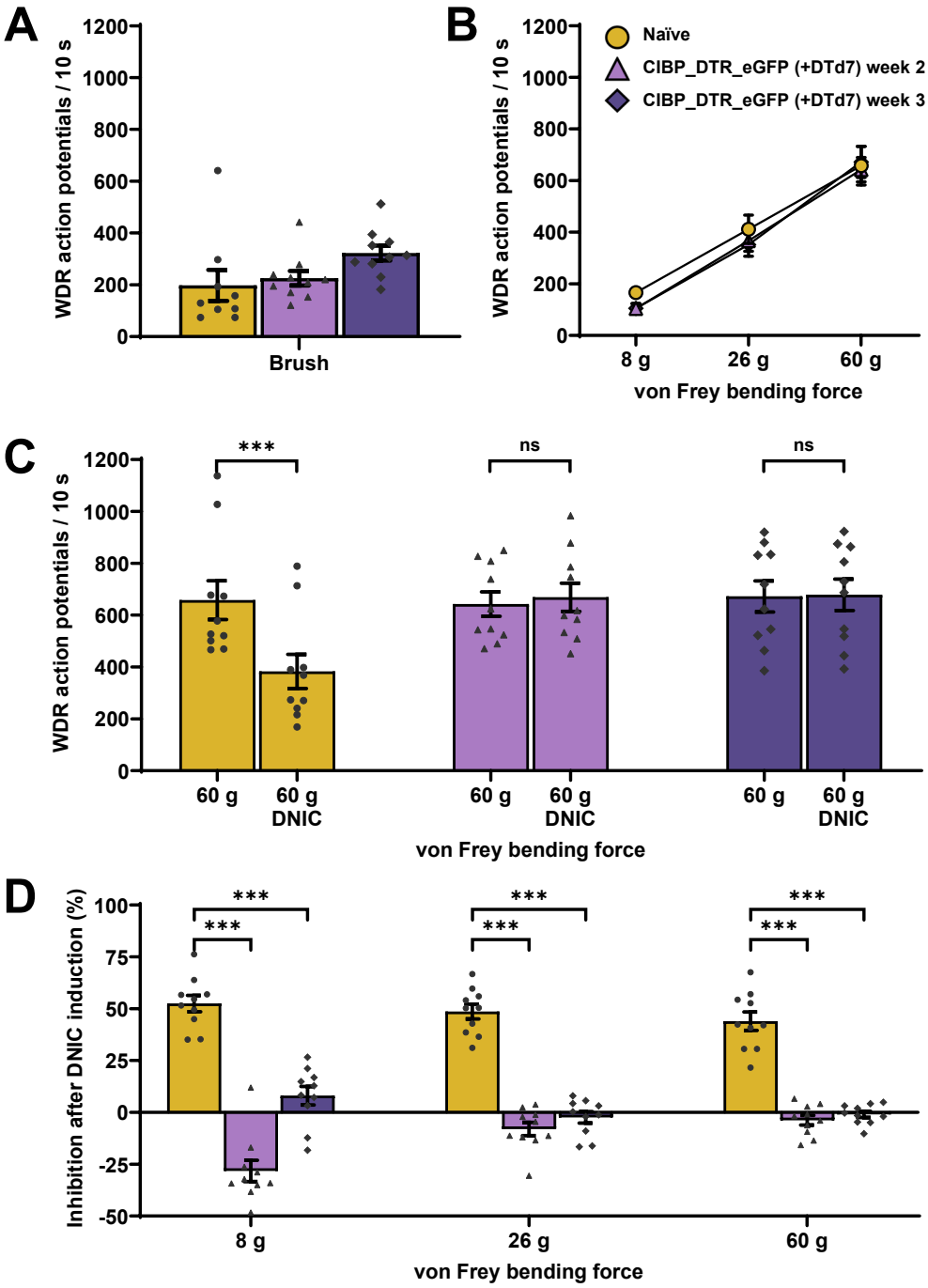

Figure 4.6. Cancer ablation on week one prevents DNIC recovery in CIBP female rats. (A) *WDR neuronal responses to dynamic mechanical stimulation (brush).* ***(B)*** *WDR neuronal responses to increasing punctate mechanical forces (von Frey).* ***(C)*** *DNIC effects on WDR baseline activity upon simultaneous noxious ear clamp (60 g von Frey).* ***(D)*** *DNIC effect comparison (% reduction in cell activity with respect to baseline) attending to different von Frey bending forces. ***P < 0.001. Data represent mean ± SEM. Each dot corresponds to an individual cell from naïve (n = 10; N = 9), CIBP_DTR_eGFP (+ DTd7) week 2 (n = 10, N = 8), or CIBP_DTR_eGFP (+ DTd7) week 3 (n = 10, N = 6) female rats. The figure key presented in (B) is valid for the entire figure. WDR: wide-dynamic range; CIBP: cancer-induced bone pain; DTR: diphtheria toxin receptor; DT: diphtheria toxin; DNIC: diffuse noxious inhibitory controls.*

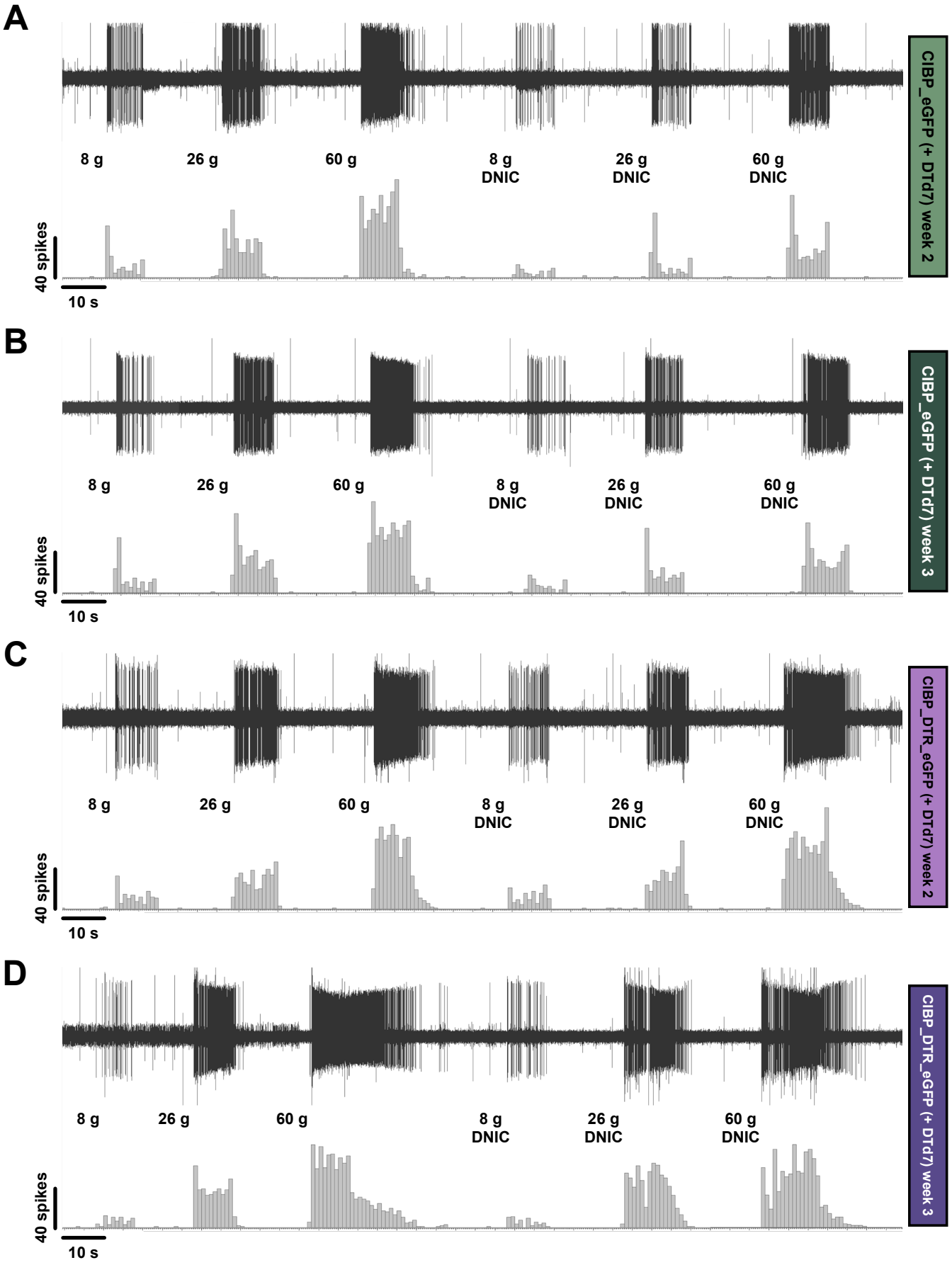
A
8 g
26 g
60 g
8 g DNIC
26 g DNIC
60 g DNIC
40 spikes
10 s
CIBP_eGFP (+ DTd7) week 2
B
8 g
26 g
60 g
8 g DNIC
26 g DNIC
60 g DNIC
40 spikes
10 s
CIBP_eGFP (+ DTd7) week 3
C
8 g
26 g
60 g
8 g DNIC
26 g DNIC
60 g DNIC
40 spikes
10 s
CIBP_DTR_eGFP (+ DTd7) week 2
D
8 g
26 g
60 g
8 g DNIC
26 g DNIC
60 g DNIC
40 spikes
10 s
CIBP_DTR_eGFP (+ DTd7) week 3

Figure 4.7. Cancer ablation on week one prevents DNIC recovery (neuronal traces). *Representative examples of spinal WDR neuronal traces and action potential quantification in* ***(A)*** *CIBP_eGFP (+ DTd7) week 2,* ***(B)*** *CIBP_eGFP (+ DTd7) week 3,* ***(C)*** *CIBP_DTR_eGFP (+ DTd7) week 2, and* ***(D)*** *CIBP_DTR_eGFP (+ DTd7) week 3 female rats before and upon simultaneous noxious ear clamp application (DNIC). Each example corresponds to the same cell during the same stimulation trial. Some non-stimulation periods (resting time between each stimulus) may have been cropped out for illustrative purposes. CIBP: cancer-induced bone pain; DTR: diphtheria toxin receptor; DT: diphtheria toxin; DNIC: diffuse noxious inhibitory controls.*

4.4.5. Spinal α2-adrenoceptor blockade inhibits WDR activity in CIBP female rats following cancer ablation on week one

Following spinal WDR and DNIC characterisation, an investigation of the pharmacological control of DNIC was carried out in CIBP_DTR_eGFP female Sprague Dawley rats 2 weeks post-cancer cell implantation followed by subsequent daily DT injections performed on post-surgical days 7-10 (+ DTd7). Following topical spinal cord atipamezole (a selective α2-adrenoceptor antagonist), WDR activity and DNIC expression were recorded at 10-, 20-, 30-, 40-, and 60-minutes post-drug application. One neuron was recorded per CIBP_DTR_eGFP (+ DTd7) rat (n = 7; N = 7), where a naïve group provided the reference control for all comparisons (n = 7; N = 7).

CIBP_DTR_eGFP (+ DTd7) group (week 2): Topical spinal atipamezole application showed an inhibitory effect on evoked WDR neuronal activity (2-way RM-ANOVA: $F_{(1.603, 9.617)} = 7.633$, $p < 0.001$; Bonferroni post hoc: $p < 0.05$) (see **Figure 4.8A** for 60 g von Frey), with this effect being differentially affected according to the von Frey bending force ($F_{(10, 60)} = 9.610$, $p < 0.001$). Upon application of a noxious ear clamp (conditioning stimulus), atipamezole did not impact DNIC expression for any of the von Frey filaments tested (3-way RM-ANOVA: $F_{(10, 60)} = 0.496$, $p > 0.05$) (see **Figure 4.8C** and **Figure 4.8D** for 60 g von Frey) (see **Figure 4.9** for individual von Frey forces). The inhibitory effect of DNIC (% reduction of cell activity with respect to baseline upon ear clamp application) for 8 g von Frey (2-way mixed ANOVA: $F_{(5, 60)} = 4.383$, $p < 0.01$), 26 g von Frey (2-way mixed ANOVA: $F_{(5, 60)} = 5.072$, $p < 0.001$), and 60 g von Frey (2-way mixed ANOVA: $F_{(5, 60)} = 5.372$, $p < 0.001$) bending forces showed significant differences along time when compared to naïve rats. These differences were shown exclusively at baseline and 60 minutes post drug application (Bonferroni post hoc: $p < 0.05$) but not for any other timepoint (Bonferroni post hoc: $p > 0.05$) (see **Figure 4.8B** for 60 g von Frey).

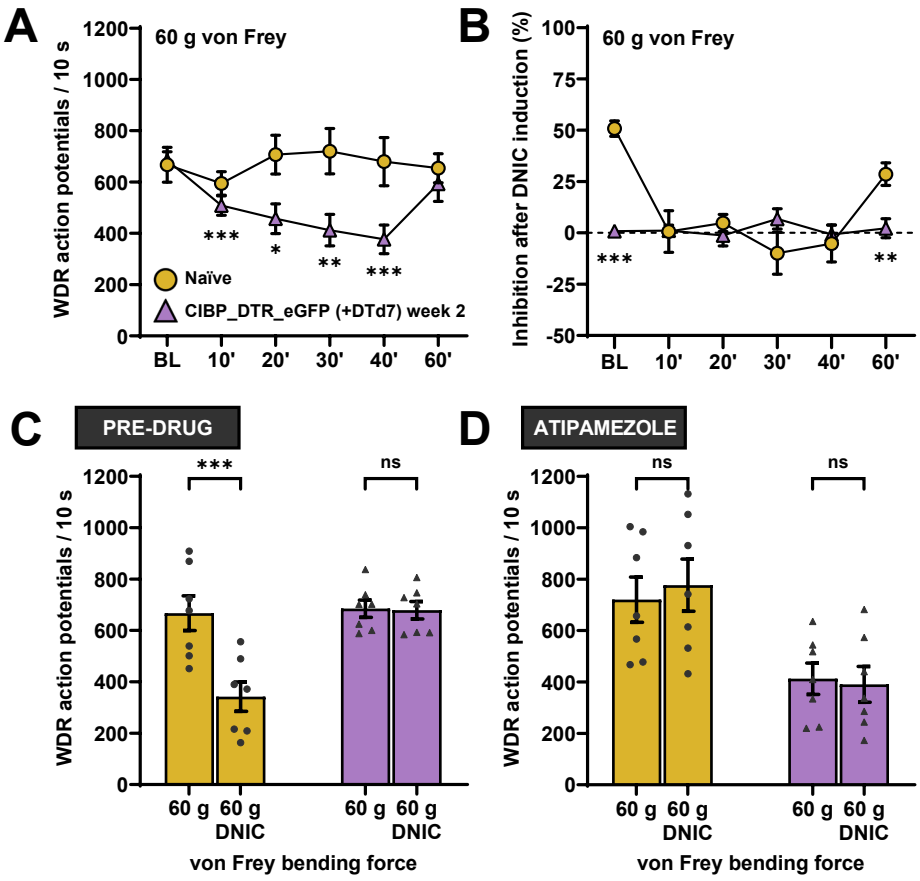

Figure 4.8. Spinal α2-adrenergic receptors mediate WDR activity following cancer ablation on week one. ***(A)*** *Atipamezole effect on evoked WDR neuronal responses (60 g von Frey).* ***(B)*** *Atipamezole effect on DNIC (% reduction in cell activity with respect to baseline) (60 g von Frey).* ***(C)*** *and* ***(D)*** *DNIC effect on WDR baseline activity upon simultaneous noxious ear clamp before (pre-drug) and 30 minutes after atipamezole application, respectively (60 g von Frey). *P < 0.05; **P < 0.01; ***P < 0.001. Data represent mean ± SEM. Each line represents the same group of cells across time and each dot corresponds to an individual cell from naïve (n = 7, N = 7) or CIBP_DTR_eGFP (+ DTd7) week 2 (n = 7, N = 7) female rats. The figure key presented in (A) is valid for the entire figure. WDR: wide-dynamic range; CIBP: cancer-induced bone pain; DTR: diphtheria toxin receptor; DT: diphtheria toxin; DNIC: diffuse noxious inhibitory controls.*

4.4.6. Cancer ablation on week zero prevents DNIC loss in CIBP female rats

CIBP_eGFP and CIBP_DTR_eGFP Sprague Dawley female rats underwent surgical tibial cancer cell implantation 1 week prior to *in vivo* electrophysiological recordings followed by subsequent daily DT injections performed on post-surgical days 3-6 (+ DTd3). A minimum of one and maximum of two neurons were recorded per CIBP_eGFP (+ DTd3) week 1 (n = 10, N = 6) and CIBP_DTR_eGFP (+ DTd3) week 1 (n = 10, N = 6) rat under isoflurane anaesthesia in a gaseous N_2O/O_2 mix, where a naïve group provided the reference control for all comparisons (n = 10; N = 9).

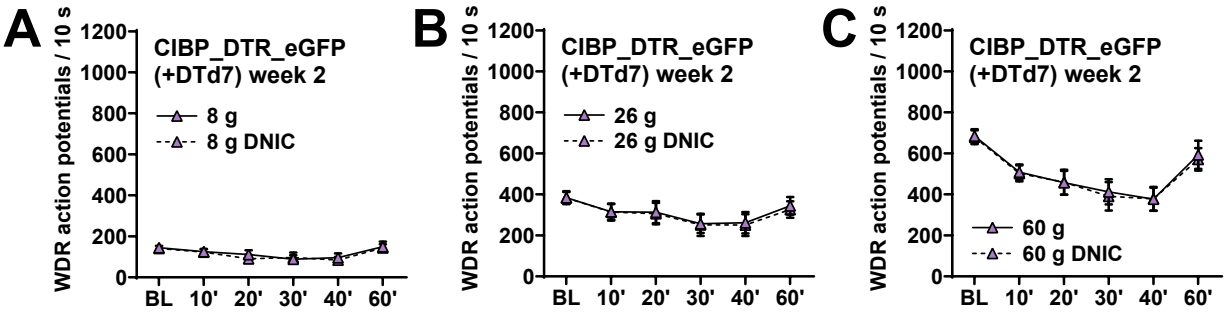

Figure 4.9. Spinal α2-adrenergic receptors mediate WDR activity following cancer ablation on week one (continued). *Effect of atipamezole across time on evoked WDR neuronal responses to* ***(A)*** *8 g,* ***(B)*** *26 g, or* ***(C)*** *60 g von Frey stimulation alone or upon simultaneous ear clamp application (DNIC). Data represent mean ± SEM. Each line represents the same group of cells across time from CIBP_DTR_eGFP (+ DTd7) week 2 female rats (n = 7, N = 7). WDR: wide-dynamic range; CIBP: cancer-induced bone pain; DTR: diphtheria toxin receptor; DT: diphtheria toxin; DNIC: diffuse noxious inhibitory controls.*

CIBP_eGFP (+ DTd3) group (week 1): Neuronal WDR responses to dynamic brush (Independent T-Test: $t_{(17)} = -1.042$, $p > 0.05$) and punctate von Frey stimulation (2-way mixed ANOVA: $F_{(1.210, 21.780)} = 0.945$, $p > 0.05$) showed no significant differences between groups (see **Figure 4.10A** and **Figure 4.10B**, respectively). Upon application of a noxious ear clamp (conditioning stimulus), WDR baseline neuronal activity showed no significant effect for any von Frey filaments tested in CIBP_eGFP (+ DTd3) week 1 rats (2-way RM-ANOVA: $F_{(2, 18)} = 0.980$, $p > 0.05$) (see **Figure 4.10C** for 60 g von Frey). Thus, the inhibitory effect of DNIC (% reduction of cell activity with respect to baseline upon ear clamp application) showed significant differences compared to naïve rats for 8 g von Frey (Mann-Whitney test: $U = 0.000$, $p < 0.001$), 26 g von Frey (Mann-Whitney test: $U = 0.000$, $p < 0.001$), and 60 g von Frey (Mann-Whitney test: $U = 0.000$, $p < 0.001$) bending forces (see **Figure 4.10D**).

CIBP_DTR_eGFP (+ DTd3) group (week 1): Neuronal WDR responses to dynamic brush (Independent T-Test: $t_{(17)} = -1.320$, $p > 0.05$) and punctate von Frey stimulation (2-way mixed ANOVA: $F_{(1.274, 22.930)} = 1.165$, $p > 0.05$) showed no significant differences between groups (see **Figure 4.11A** and **Figure 4.11B**, respectively). Upon application of a noxious ear clamp (conditioning stimulus), WDR baseline neuronal activity was significantly reduced for all von Frey filaments tested in CIBP_DTR_eGFP (+ DTd3) week 1 rats (2-way RM-ANOVA: $F_{(2, 18)} = 56.947$, $p < 0.001$; Bonferroni post hoc: $p < 0.01$ for all tests) (see **Figure 4.11C** for 60 g von Frey). The inhibitory effect of DNIC (% reduction of cell activity with respect to baseline upon ear clamp application) was comparable to naïve rats for 8 g von Frey (Mann-Whitney test: $U = 36.000$, $p > 0.05$), 26 g von Frey (Mann-Whitney test: $U = 39.000$, $p > 0.05$), and 60 g von Frey (Mann-Whitney test: $U = 45.000$, $p > 0.05$) bending forces (see **Figure 4.11D**).

Additional comparisons between the unmodified MRMT-1 cell line (CIBP week 1 rats) (results shown in previous chapter) and the control CIBP_eGFP (+ DTd3) week 1 rats, showed no differences between neuronal WDR responses to dynamic brush (Independent T-Test: $t_{(20)} = 1.198$, $p > 0.05$) nor punctate von Frey stimulation (2-way mixed ANOVA: $F_{(1.553, 35.728)} = 0.932$, $p > 0.05$).

In sum, cancer cell ablation on week 0 following cancer cell implantation, a timepoint at which DNIC expression is not yet dysfunctional, prevents DNIC loss in CIBP_DTR_eGFP rats (see **Figure 4.12**) highlighting a role for active tumour growth on modulatory mechanisms in the CIBP rat model.

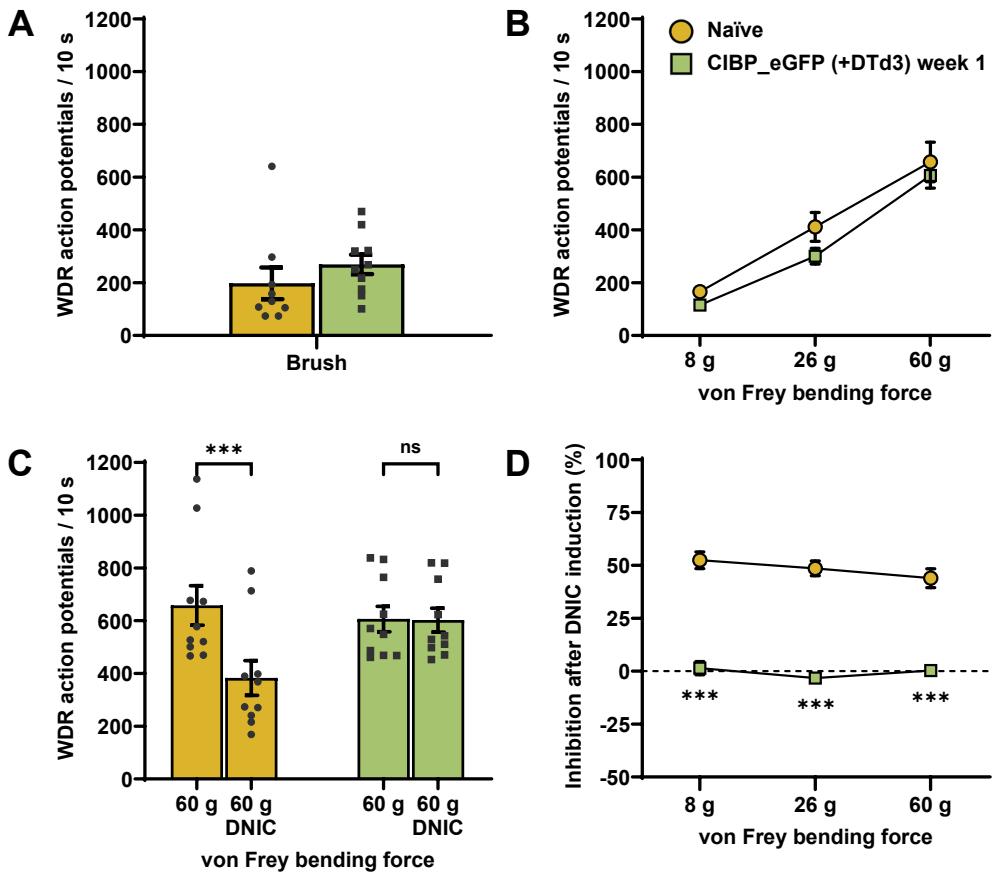

Figure 4.10. DT treatment on week zero does not affect DNIC loss in CIBP female rats. (A) *WDR neuronal responses to dynamic mechanical stimulation (brush).* ***(B)*** *WDR neuronal responses to increasing punctate mechanical forces (von Frey).* ***(C)*** *DNIC effects on WDR baseline activity upon simultaneous noxious ear clamp (60 g von Frey).* ***(D)*** *DNIC effect comparison (% reduction in cell activity with respect to baseline) attending to different von Frey bending forces. ***P < 0.001. Data represent mean ± SEM. Each dot corresponds to an individual cell from naïve (n = 10; N = 9) or CIBP_eGFP (+ DTd3) week 1 (n = 10, N = 6) female rats. The figure key presented in (B) is valid for the entire figure. WDR: wide-dynamic range; CIBP: cancer-induced bone pain; DT: diphtheria toxin; DNIC: diffuse noxious inhibitory controls.*

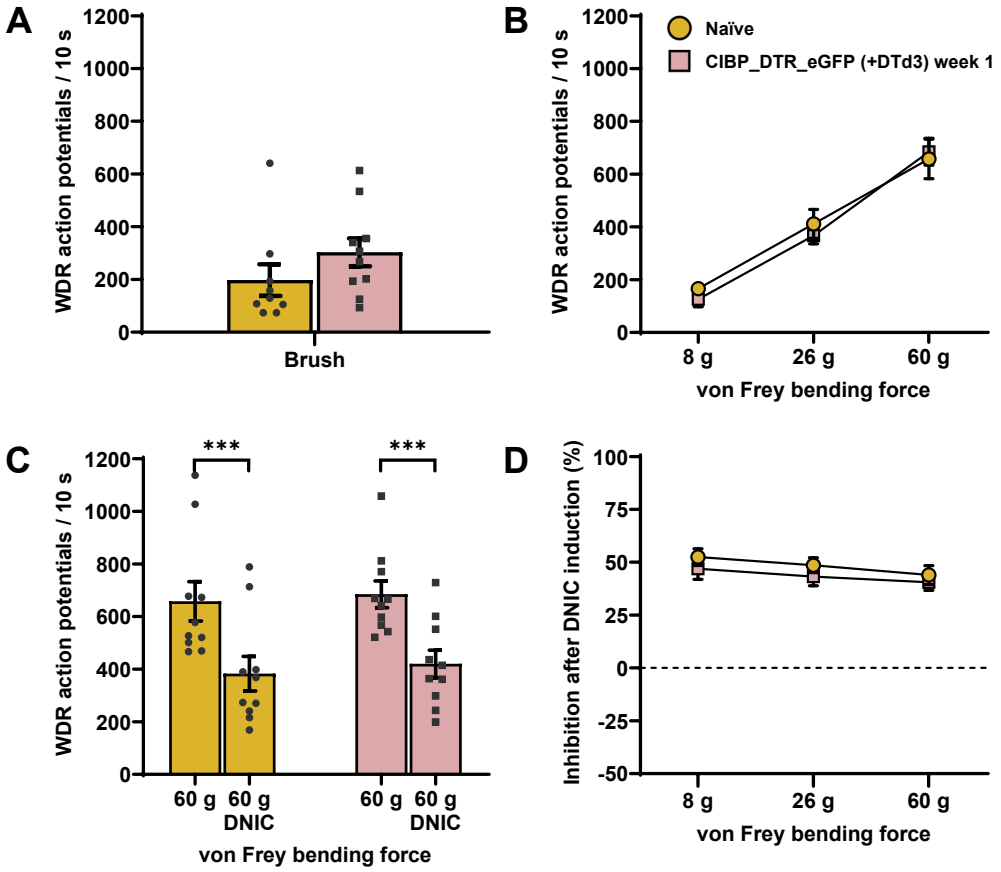

Figure 4.11. Cancer ablation on week zero prevents DNIC loss in CIBP female rats. (A) *WDR neuronal responses to dynamic mechanical stimulation (brush).* ***(B)*** *WDR neuronal responses to increasing punctate mechanical forces (von Frey).* ***(C)*** *DNIC effects on WDR baseline activity upon simultaneous noxious ear clamp (60 g von Frey).* ***(D)*** *DNIC effect comparison (% reduction in cell activity with respect to baseline) attending to different von Frey bending forces. ***P < 0.001. Data represent mean ± SEM. Each dot corresponds to an individual cell from naïve (n = 10; N = 9) or CIBP_DTR_eGFP (+ DTd3) week 1 (n = 10, N = 6) female rats. The figure key presented in (B) is valid for the entire figure. WDR: wide-dynamic range; CIBP: cancer-induced bone pain; DTR: diphtheria toxin receptor; DT: diphtheria toxin; DNIC: diffuse noxious inhibitory controls.*

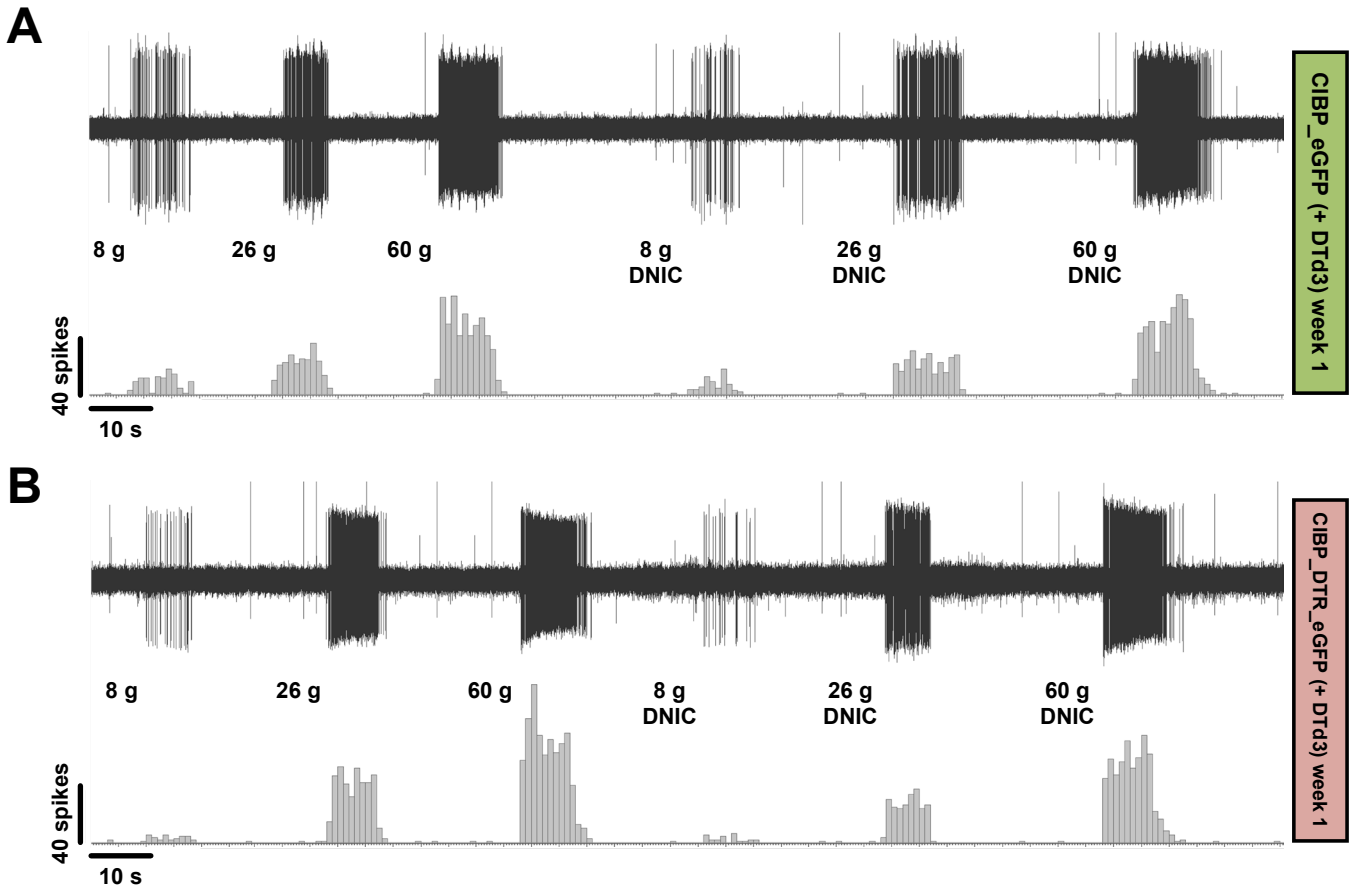

Figure 4.12. Cancer ablation on week zero prevents DNIC loss (neuronal traces). *Representative examples of spinal WDR neuronal traces and action potential quantification in* ***(A)*** *CIBP_eGFP (+ DTd3) week 1 and* ***(B)*** *CIBP_DTR_eGFP (+ DTd3) week 1 female rats before and upon simultaneous noxious ear clamp application (DNIC). Each example corresponds to the same cell during the same stimulation trial. Some non-stimulation periods (resting time between each stimulus) may have been cropped out for illustrative purposes. CIBP: cancer-induced bone pain; DTR: diphtheria toxin receptor; DT: diphtheria toxin; DNIC: diffuse noxious inhibitory controls.*

4.4.7. Cancer ablation on week two does not affect DNIC recovery in CIBP female rats

Control CIBP_eGFP and experimental CIBP_DTR_eGFP rats underwent surgical tibial cancer cell implantation 3 weeks prior to the electrophysiological recordings followed by subsequent daily DT injections performed on post-surgical days 14-17 (+ DTd14). One or two neurons were recorded per rat in CIBP_eGFP (+ DTd14) week 3 (n = 10, N = 6) and CIBP_DTR_eGFP (+ DTd14) week 3 (n = 10, N = 6) groups, with naïve rats being used as the reference control for all comparisons (n = 10; N = 9).

CIBP_eGFP (+ DTd14) group (week 3): Neuronal WDR responses to dynamic brush (Independent T-Test: $t_{(17)} = -1.439$, $p > 0.05$) and punctate von Frey stimulation (2-way mixed ANOVA: $F_{(1.174, 21.141)} = 0.851$, $p > 0.05$) showed no significant differences between groups (see **Figure 4.13A** and **Figure 4.13B**, respectively). Upon application of a noxious ear clamp (conditioning stimulus), WDR baseline neuronal activity was significantly reduced for all von Frey filaments tested in CIBP_DTR_eGFP (+ DTd14) week 3 rats (2-way RM-ANOVA: $F_{(2, 18)} = 63.196$, $p < 0.001$; Bonferroni post hoc: $p < 0.001$ for all tests) (see **Figure 4.13C** for 60 g von Frey). The inhibitory effect of DNIC (% reduction of cell activity with respect to baseline upon ear clamp application) was comparable to naïve rats 8 g von Frey (Mann-Whitney test: $U = 61.000$, $p > 0.05$), 26 g von Frey (Mann-Whitney test: $U = 51.000$, $p > 0.05$), and 60 g von Frey (Mann-Whitney test: $U = 52.000$, $p > 0.05$) bending forces (see **Figure 4.13D**).

CIBP_DTR_eGFP (+ DTd14) group (week 3): Neuronal WDR responses to dynamic brush (Independent T-Test: $t_{(17)} = -0.742$, $p > 0.05$) and punctate von Frey stimulation (2-way mixed ANOVA: $F_{(1.282, 23.070)} = 0.598$, $p > 0.05$) showed no significant differences between groups (see **Figure 4.14A** and **Figure 4.14B**, respectively). Upon application of a noxious ear clamp (conditioning stimulus), WDR baseline neuronal activity was significantly reduced for all von Frey filaments tested in CIBP_DTR_eGFP (+ DTd14) week 3 rats (2-way RM-ANOVA: $F_{(2, 18)} = 27.607$, $p < 0.001$; Bonferroni post hoc: $p < 0.001$ for all tests) (see **Figure 4.14C** for 60 g von Frey). The inhibitory effect of DNIC (% reduction of cell activity with respect to baseline upon ear clamp application) was comparable to naïve rats 8 g von Frey (Mann-Whitney test: $U = 61.000$, $p > 0.05$), 26 g von Frey (Mann-Whitney test: $U = 63.000$, $p > 0.05$), and 60 g von Frey (Mann-Whitney test: $U = 53.000$, $p > 0.05$) bending forces (see **Figure 4.14D**).

Additional comparisons between the unmodified MRMT-1 cell line (CIBP week 3 rats) (results shown in previous chapter) and the control CIBP_eGFP (+ DTd14) week 3 rats, showed no differences between neuronal WDR responses to dynamic brush (Independent T-Test: $t_{(23)} = -0.342$, $p > 0.05$) nor punctate von Frey stimulation (2-way mixed ANOVA: $F_{(1.354, 31.143)} = 0.349$, $p > 0.05$).

These results demonstrate that while cancer cell ablation on week 1 (coinciding with the absence of DNIC expression) has long lasting effects on a descending pain modulatory mechanism, cancer ablation on week 2 (a timepoint where DNIC expression is recovered) does not impact DNIC (see **Figure 4.15**).

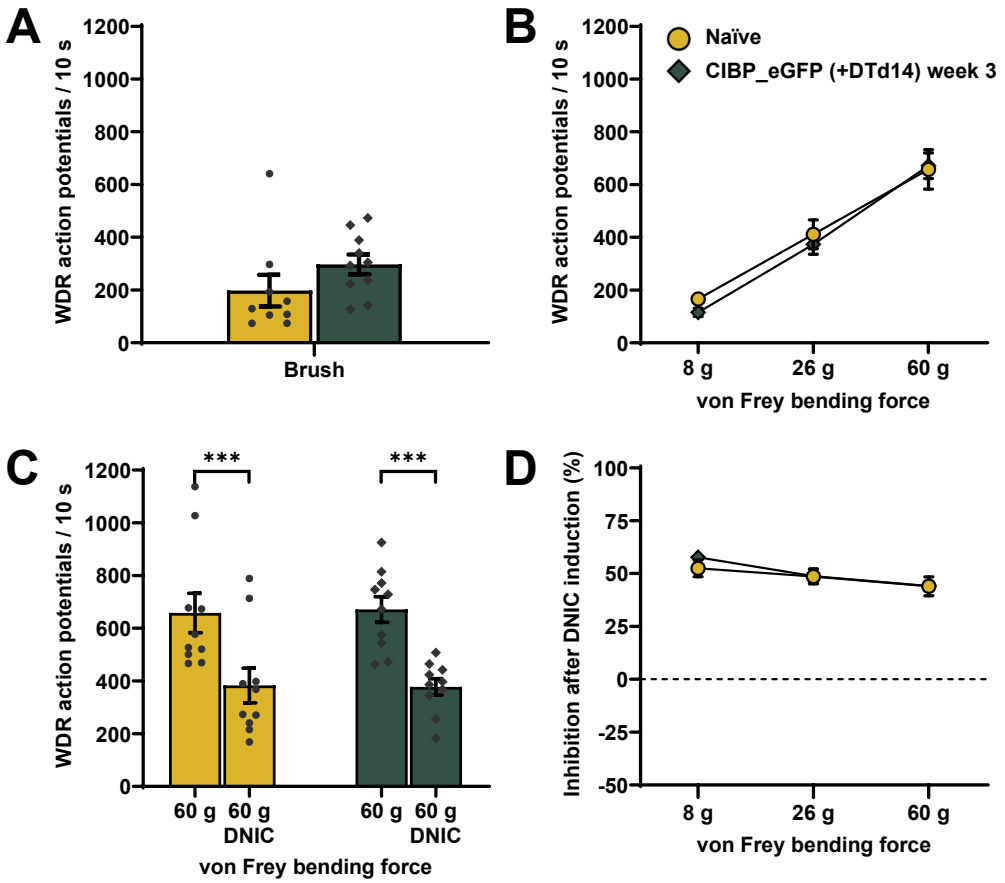

Figure 4.13. DT treatment on week two does not affect DNIC recovery in CIBP female rats. (A) *WDR neuronal responses to dynamic mechanical stimulation (brush).* ***(B)*** *WDR neuronal responses to increasing punctate mechanical forces (von Frey).* ***(C)*** *DNIC effects on WDR baseline activity upon simultaneous noxious ear clamp (60 g von Frey).* ***(D)*** *DNIC effect comparison (% reduction in cell activity with respect to baseline) attending to different von Frey bending forces. ***P < 0.001. Data represent mean ± SEM. Each dot corresponds to an individual cell from naïve (n = 10; N = 9) or CIBP_eGFP (+ DTd14) week 3 (n = 10, N = 6) female rats. The figure key presented in (B) is valid for the entire figure. WDR: wide-dynamic range; CIBP: cancer-induced bone pain; DT: diphtheria toxin; DNIC: diffuse noxious inhibitory controls.*

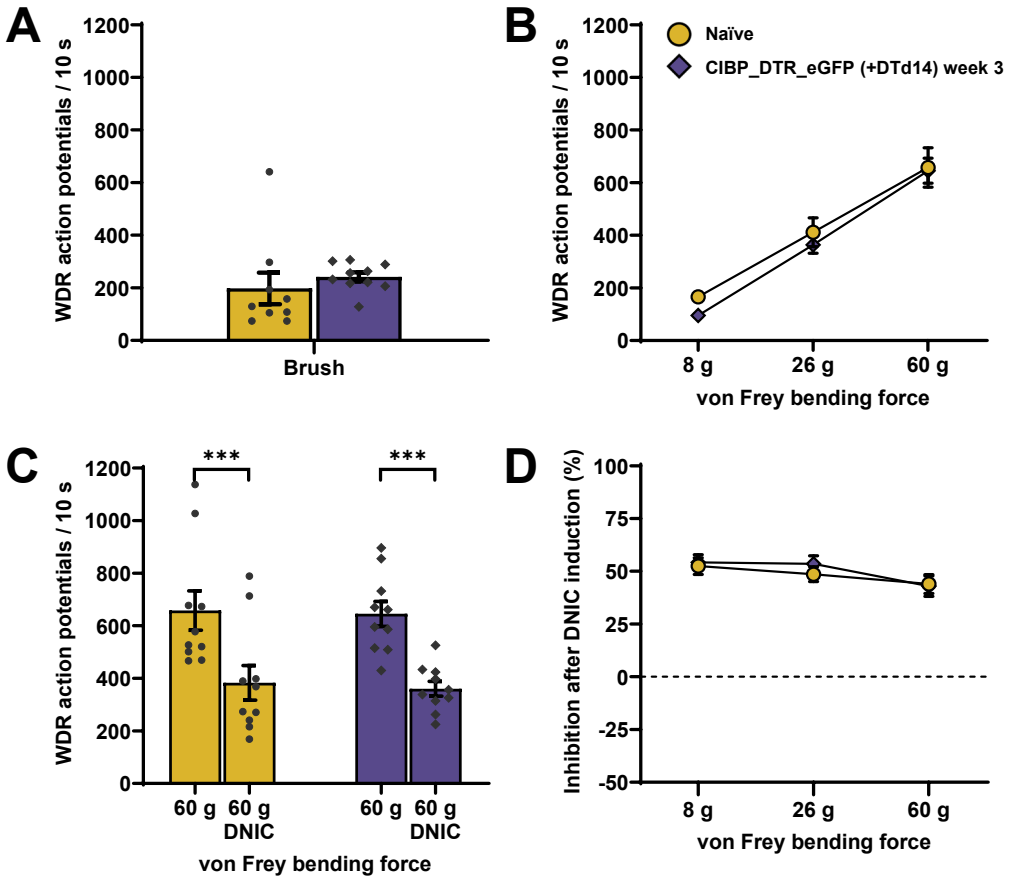

Figure 4.14. Cancer ablation on week two does not affect DNIC recovery in CIBP female rats. (A) *WDR neuronal responses to dynamic mechanical stimulation (brush).* ***(B)*** *WDR neuronal responses to increasing punctate mechanical forces (von Frey).* ***(C)*** *DNIC effects on WDR baseline activity upon simultaneous noxious ear clamp (60 g von Frey).* ***(D)*** *DNIC effect comparison (% reduction in cell activity with respect to baseline) attending to different von Frey bending forces. ***P < 0.001. Data represent mean ± SEM. Each dot corresponds to an individual cell from naïve (n = 10; N = 9) or CIBP_DTR_eGFP (+ DTd14) week 3 (n = 10, N = 6) female rats. The figure key presented in (B) is valid for the entire figure. WDR: wide-dynamic range; CIBP: cancer-induced bone pain; DTR: diphtheria toxin receptor; DT: diphtheria toxin; DNIC: diffuse noxious inhibitory controls.*

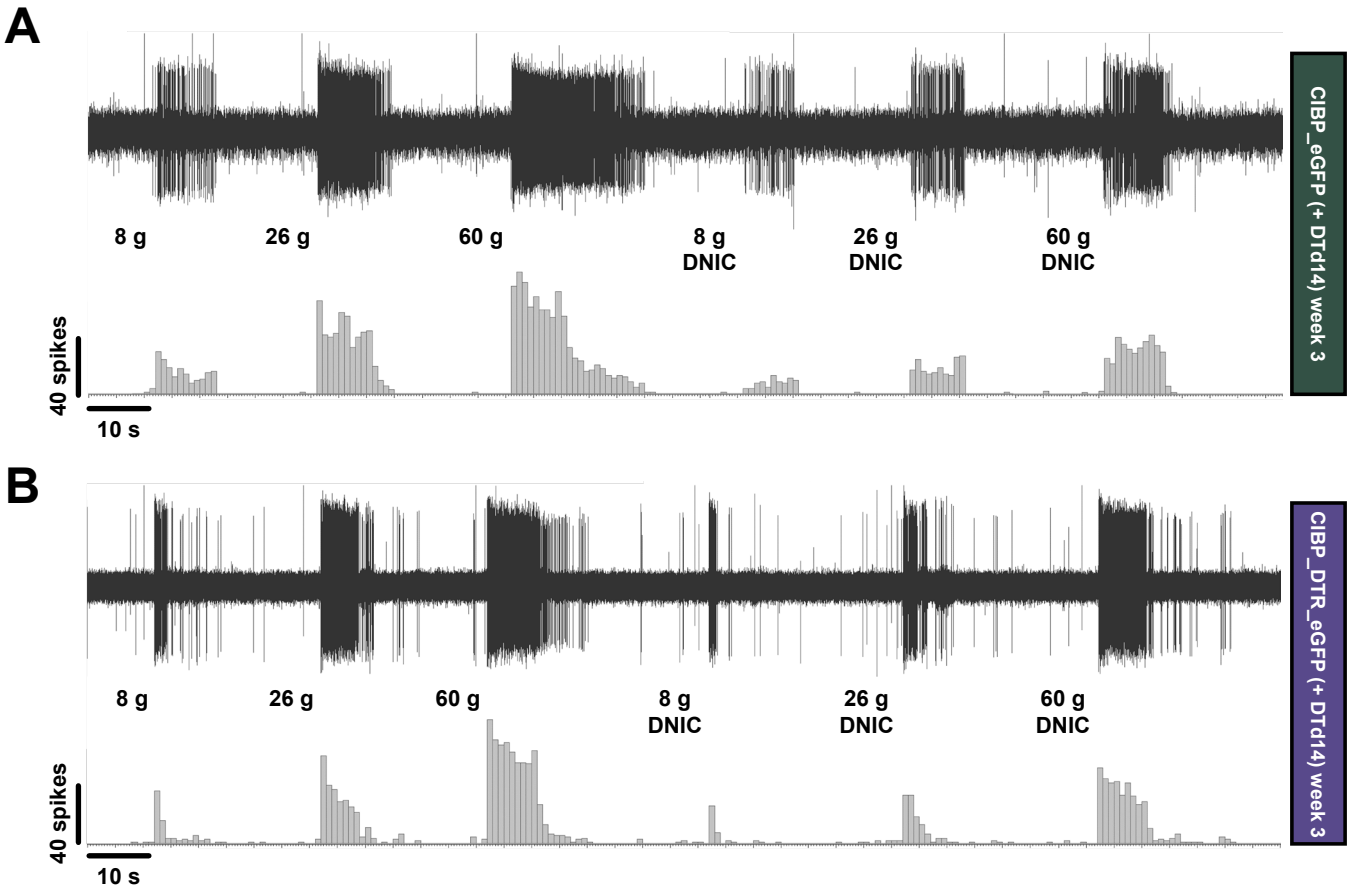

Figure 4.15. Cancer ablation on week two does not affect DNIC recovery (neuronal traces). *Representative examples of spinal WDR neuronal traces and action potential quantification in* ***(A)*** *CIBP_eGFP (+ DTd14) week 3 and* ***(B)*** *CIBP_DTR_eGFP (+ DTd14) week 3 female rats before and upon simultaneous noxious ear clamp application (DNIC). Each example corresponds to the same cell during the same stimulation trial. Some non-stimulation periods (resting time between each stimulus) may have been cropped out for illustrative purposes. CIBP: cancer-induced bone pain; DTR: diphtheria toxin receptor; DT: diphtheria toxin; DNIC: diffuse noxious inhibitory controls.*

4.5. Discussion

4.5.1. Tumour progression in CIBP female rats following cancer cell ablation

For the data described in this chapter, I created a cell line by transducing cancerous MRMT-1 cells with the simian DTR to confer DT sensitivity (CIBP_DTR_eGFP), as well as a control cell line without the gene of interest (CIBP_eGFP), allowing for targeted cancer cell ablation at specific timepoints during the disease. These new cell lines showed *in vitro* dynamics comparable to the unmodified MRMT-1 cells and demonstrated a strong and long-lasting construct expression after numerous cell divisions. *In vivo*, I assessed how cancer cell ablation on week 1 (coinciding with DNIC expression loss) would affect behavioural outcomes. Localised tibial transduced cancer cell implantation in CIBP_eGFP rats (i.e., insensitive to DT) faithfully replicated the progressive pain-like phenotype of CIBP rats implanted with the unmodified cell line previously presented in this thesis. More importantly, localised tibial transduced cancer cell implantation in CIBP_DTR_eGFP rats (i.e., sensitive to DT) also recreated this pain-like phenotype. However, following cancer cell ablation on week 1, stabilisation of this phenotype occurred, with no signs of progressive degeneration, despite still retaining (albeit to a lesser extent) mechanical hypersensitivity.

Collectively, these results support that pain-like behavioural outcomes in the CIBP rat model can be reliably replicated using transduced cancer cells without affecting the initiation nor the evolution of the progressive pain-like phenotype, in accordance with previous CIBP studies using modified MRMT-1 cell lines (Appel et al., 2017; Falk, Al-Dihaissy, et al., 2015; Zhu et al., 2017). Once the early pain-like phenotype was established, cancer cell ablation prevented this hypersensitivity from advancing, although it was not completely resolved. Theoretically, this long-lasting hypersensitivity following cancer ablation could be mechanistically underpinned by primary afferent sprouting on the tumour area; i*n vitro* exposure of primary afferents to the MRMT-1 secretome (conditioned medium exposed to MRMT-1 cells and containing secreted factors) led to neuronal sprouting increasing the number of neurites (20-25% neurite increase after 5 days) in a previous study (Jerard et al., 2023). Moreover, DT induces cell death via apoptosis (Chang et al., 1989), which can release proinflammatory components into the microenvironment if not quickly phagocytosed, stimulating a host response (Faouzi et al., 2001). This inflammation would lead to hyperaemia (increase of blood flow to the affected tissue), leak of plasma proteins, and recruitment of leukocytes to deal with any cell remnants affecting the previously

mentioned recruitment of silent nociceptors (Kucharczyk, Chisholm et al., 2020), prolonging their 'un-silencing' and increasing the peripheral drive even further. Thus, the retained 'residual' hypersensitivity following cancer cell ablation could be affected by an abnormal peripheral neuronal sprouting and/or the recruitment of silent nociceptors that persist in time, altering primary afferent responses even after successful cancer cell ablation.

Additionally, and similarly to results presented in the previous chapter, gradual pain-related behaviours correlate with progressive trabecular and cortical bone destruction regardless of the transduced cell used. The data presented here follow the same timeframe of disease progression, evidencing once again, differential tumour growth between CIBP female and male rats (Kucharczyk, Chisholm et al., 2020). Radiolucent tibial trabecular lesions and trabecular bone loss were evident in control CIBP_eGFP rats from week 2 onwards, with cortical bone loss and severely compromised bone integrity appearing on week 3 (despite DT treatment on week 1). Interestingly, notwithstanding clear progressive bone deterioration and osteolytic lesions, tissue mineral density did not show significant alterations. Differential interactions between cancer cells and bone tissue leading to disparate bone damage, higher mineralization and density of the newly created bone, different age of the animals (Fukuda and Iida, 2004), and/or possible previous parturitions (McAlpine et al., 2021; Zeni et al., 1999) could explain this situation. Conversely, high-resolution morphometric analysis showed comparable parameters between CIBP_DTR_eGFP and naïve rats following cancer cell ablation on week 1, demonstrating efficient targeted ablation preventing any bone loss and/or radiolucent lesions.

4.5.2. WDR activity in CIBP female rats following cancer cell ablation

Increased peripheral input in CIBP rats driven by augmented primary afferent sensitivity (Zhu et al., 2016), an increased number of recruited primary afferents (e.g., silent nociceptors) (Kucharczyk, Chisholm et al., 2020), and/or abnormal primary afferent sprouting (Jimenez-Andrade et al., 2010) can be linked to the behavioural hypersensitivity observed in this model. Interestingly, in the previous chapter I demonstrated that any previously evidenced enhanced peripheral input/painful phenotype did not translate into spinal deep dorsal horn WDR hyperactivity in the CIBP model, in line with previous studies (Falk, Schwab et al., 2015; Kucharczyk, Derrien et al., 2020). Here, I demonstrate an identical finding in the case of control CIBP_eGFP and experimental CIBP_DTR_eGFP rats (where no differences

in WDR basal evoked responses, regardless of the post-operative week and/or the toxin treatment received, were observed).

As already mentioned in the previous chapter, primary afferents project differentially to superficial and deep dorsal horn laminae. The fact that some fibres (e.g., C-fibres) project indirectly (i.e., polysynaptically) to the deep dorsal horn offers a spatial local anatomical window for modulation favouring a reduction of any enhanced peripheral nociceptive input (e.g., by inhibitory interneuron activation). Spinal modulation of peripheral input is an important consideration; compared to the diversity of primary afferent skin-innervating fibres, bone innervation has a more limited repertoire, with Aδ- and C-fibres comprising most bone-innervating primary afferents (where Aβ-fibre counts are marginal) (Ivanusic, 2009; Mahns et al., 2006). These bone-innervating Aδ- and C-fibres were demonstrated to be responsive to noxious chemical and/or mechanical stimulation, contributing to nociception and modulating CIBP (Ishida et al., 2016; Morgan et al., 2019; Nencini and Ivanusic, 2017; Nencini et al., 2017). Moreover, even though every bone compartment has sensory innervation, fibre density is significantly variable, with the periosteum being the most innervated area, followed by the trabecular and cortical areas, respectively (Steverink et al., 2021; see also Mantyh, 2013). As such, understanding spinal innervation of bone-originating afferent fibres is an important part of identifying the molecular mechanisms that contribute to pain states borne from bone disease. It is noteworthy that the electrophysiological recordings presented in this thesis are performed on WDR neurons that receive their peripheral input from the glabrous surface of the hind paw of the animal. Thus, recording from WDR cells that receive direct bone tibial peripheral input would likely return different results in evoked baseline WDR activity to the ones obtained here.

Compensatory central nervous system activity promoting descending inhibitory mechanisms will also impact the spinal response to peripheral input. For example, activity in the brainstem modulates deep dorsal horn WDR neuronal activity via α1-adrenoceptors even in health (Kucharczyk et al., 2022). The α1-adrenoceptor couples with G-proteins exerting a facilitatory action (Wada et al., 1997; see also Millan, 2002), which makes its inhibitory effect on WDR activity likely to be indirectly mediated (e.g., via activation of inhibitory interneurons) (Gassner et al., 2009; Sonohata et al., 2004). Altogether, modulation of enhanced peripheral input in CIBP conditions (either by individual or combined compensatory mechanisms) seems likely, maintaining a homeostatic balance that aims to reduce spinal

WDR activity. New studies focused on understanding these plastic modulatory changes in CIBP conditions may reveal novel insights requiring many complimentary anatomical and pharmacological angles.

4.5.3. DNIC expression in CIBP female rats following cancer cell ablation

Having outlined that, like male rats, female Sprague Dawley rats show a transient DNIC expression loss on week 1 following cancer cell implantation, I wanted to investigate whether cancer cell ablation at key timepoints would impact DNIC expression with the aim of understanding the impact of dividing cancer cells on DNIC dynamism. In finding that targeted cancer cell ablation on week 1 prolonged the malfunctioning DNIC state, I revealed that it is likely that a compensatory central nervous system mechanism normally leads to DNIC expression recovery in the CIBP model, perhaps driven by peripheral plasticity. Moreover, cancer ablation prior to DNIC functionality loss on week 1 prevented this loss, while cancer ablation following DNIC expression recovery on week 2 had no effect on this functionality.

As previously mentioned, optoactivation of ventrally located noradrenergic neurons in the locus coeruleus abolishes DNIC expression (Kucharczyk et al., 2022). This could translate into a coerulean hyperactivity driving DNIC dysfunctionality in the CIBP model, where plastic changes could revert or compensate this effect on posterior weeks, restoring DNIC expression. Thus, cancer ablation on week 1 could impair or restrict the plastic changes necessary for DNIC recovery, hampering any compensatory actions aimed to reverse these maladaptive communications. Altogether, these results evidence the importance of actively dividing cancer cells in the initiation of DNIC malfunction as well as its recovery, altering the peripheral microenvironment that will, ultimately, lead to and/or impact plastic central changes.

Additionally, I have demonstrated how topical spinal atipamezole application (a selective α2-adrenoceptor antagonist) inhibited WDR evoked responses in CIBP_DTR_eGFP rats (week 2) following cancer cell ablation (week 1). These results are in line with the findings I provided in the previous chapter where atipamezole also exerted a slight inhibitory effect on WDR evoked activity in CIBP female rats (week 2). This outcome was unexpected, as one could infer that the transient atipamezole inhibition observed in the CIBP model was driven by cancer progression and therefore would not be observed following cancer cell ablation. However, some studies have also shown that blockade of inhibitory α2-

adrenoceptors can counterintuitively lead to inhibitory potentiation (Hickey et al., 2014; Kucharczyk et al., 2022).

In health, stimulation of spinally projecting noradrenergic neurons in the locus coeruleus inhibits spinal WDR activity via activation of inhibitory interneurons, with spinal atipamezole potentiating this effect (Kucharczyk et al., 2022). α2-adrenoceptors, functionally enhanced in animal models of inflammatory pain (Pereira-Silva et al., 2020), are located in both pre- and postsynaptic terminals, with the former location serving as a negative auto-regulatory noradrenergic feedback loop (Sonohata et al., 2004; Stone et al., 1998; see also Fairbanks et al., 2009). Thus, and following the speculated coerulean involvement in the CIBP model during cancer progression and after cancer cell ablation, blockade of these functionally enhanced auto-regulatory α2-adrenoceptors on the spinal coerulean presynaptic terminals could drive a higher noradrenaline release upon the inhibitory interneuron, leading to a potentiated WDR inhibition. Collectively, despite DNIC expression loss and recovery being seemingly dependant on the presence of active disease, changes affecting the noradrenergic spinal tone may occur even in its absence.

4.6. Summary

To summarise, the data provided evidence how targeted and efficient cancer cell ablation can be reached in the CIBP model. If this cancer cell ablation occurs at crucial timepoints when DNIC expression is compromised by disease progression, the transient descending modulatory dysregulation endures over time. Studies focusing on elucidating the complex mechanisms driving this such state are crucial for understanding sensorimotor modulation in active disease as well as remission, allowing to reach individualised and effective clinical treatments.

CHAPTER

RESULTS III: DNIC EXPRESSION IS DYNAMIC IN A CIBP MOUSE MODEL OF DISEASE PROGRESSION

5.1. Introduction

Animal models of cancer-induced bone pain (CIBP) (see **section 1.6**) faithfully replicate pain-like phenotypes that likely correspond to the pain experienced by cancer patients with bone metastases originating from common cancers (face validity), while sharing the underlying mechanisms driving such painful clinical states (construct validity) (Havelin et al., 2017; Tang et al., 2016; see also Sliepen, 2021). In addition, CIBP models show good results when predicting and/or replicating clinically observed treatment outcomes (predictive validity) (Mouedden and Meert, 2007; Wu et al., 2021). The combination of distinct animal models using different species has allowed us to build our understanding of pain mechanisms in this disease state. CIBP mouse and rat models have many parallels, including similar pain-like phenotypes (Medhurst et al., 2002; Ji et al., 2022), bone remodelling (Doré-Savard et al., 2013; Jimenez-Andrad et al., 2023), immune responses (Diaz-delCastillo et al., 2020; Wang et al., 2021), mediator release (Halvorson et al., 2005; Wang et al., 2012), primary afferent sensitivity (Cain et al., 2001; Zhu et al., 2016), and spinal alterations (Schwei et al., 1999; Yang et al., 2023). Nonetheless, nuances in the development of the model itself and the ease with which different techniques can be applied between species means that carrying out studies in both mouse and rat models has the potential to reveal greater insight regarding disease.

Previously, studies that have used CIBP models to understand alterations in descending pain modulatory pathways, have typically used rats (Donovan-Rodriguez et al., 2006; Falk, Schwab et al., 2015; Kucharczyk, Derrien et al., 2020). Central nervous system dysfunction is likely to affect peripheral tumour characteristics as descending modulation is exerted at the level of the spinal cord by both direct synaptic connections and indirect volume transmission (non-synaptic diffusion of transmitters in the extracellular matrix) (Marlier et al., 1991; Rajaofetra et al., 1992; Ridet et al., 1993), with the latter being able to induce persistent and widespread effects on distant targets, including the central terminals of primary afferents (Travagli and Williams, 1996; Zhang et al., 2015). This can lead to action potentials that initiate in the central terminal and propagate retrogradely (antidromically) back to the periphery (Barron and Matthews, 1935; Lin et al., 2000; Toennies, 1938; Weng and Dougherty, 2005). These action potentials (named dorsal root reflexes) promote transmitter release in peripheral tissue (e.g., glutamate, substance P, CGRP) (de Groot et al., 2000; Sauer et al., 2001; White and Helme, 1985) and contribute to neurogenic inflammation (Lobanov and Peng, 2011; Lucas-Romero et al., 2022; see also

Sorkin et al., 2018), promoting all stages of tumorigenesis (Mitsou et al., 2023; see also Greten and Grivennikov, 2019; Reavis et al., 2020). Thus, inter-species replication and/or the usage of different animal models together with an exploration of peripheral and central processes and their impact on one another (crosstalk and overlap) is necessary for novel molecular mechanism underlying this disease phenotype to be revealed. This is vital if mechanistically targeted analgesia and effective clinical pain relief is to be achieved.

5.2. Rationale and aims

While CIBP rat models are mostly induced in the tibia of the animal, CIBP mouse models frequently use the femur as the inoculation site due to its relatively easy access (Fan et al., 2022; Haroun et al., 2023; Ji et al., 2022; Yang et al., 2018; Zhang et al., 2020). The reported tibial CIBP mouse models are mostly induced by cancer cell implantation through tibial plateau injection (or in extremely close proximity to it) (Wakabayashi et al., 2018; Zhou, Cui et al., 2022), which can lead to articular damage and may not allow for sealing of the injection site, risking cell leaking (Heo et al., 2017; Menéndez et al., 2003; Zinonos et al., 2014). This differential inter-species characterisation also extends to research focusing on descending pain modulatory pathways, where the descending control of nociception (DCN) has been studied using mouse pain models (Kopruszinski et al., 2021; Sahbaie et al., 2022; Yuan et al., 2018), although its anaesthetised animal counterpart, diffuse noxious inhibitory controls (DNIC) (see **section 1.5.4**), has not been widely characterised or indeed described in mice (neither in health nor CIBP conditions). Furthermore, despite previous work studying *in vivo* primary afferent activity in CIBP models (de Clauser et al., 2020; Kucharczyk, Chisholm et al., 2020), the influence of DNIC activation on primary afferent neuronal activity (e.g., effect on spinal ganglion activity) remains unexplored in both health and disease.

This study aims to recreate a CIBP mouse model following the same tibial induction methodology used in rats (as already presented in this thesis). This chapter also characterises DNIC expression in both naïve and CIBP female and male mice with an additional assessment of rodent pain-like phenotypes using evoked and non-evoked paradigms. Moreover, *in vivo* calcium imaging was performed in naïve mice to explore whether the activation of DNIC impacts primary afferent fibre responses.

5.3. Materials and methods

Naïve, sham, and CIBP female and male C57BL/6 wildtype mice (see **section 2.1**) underwent *in vivo* spinal cord electrophysiology for single-unit wide-dynamic range (WDR) characterisation under isoflurane anaesthesia where CIBP and sham mice underwent tibial cancer cell implantation surgery (or sham surgery) 1-2 or 3-4 weeks prior to the spinal cord recordings according to the timeline of the experiment (see **section 2.2** and **section 2.3**). Evoked WDR firing rates to natural stimuli (dynamic mechanical brush, punctate mechanical von Frey, and thermal heat waterjet) were recorded before and during simultaneous ipsilateral application of a noxious conditioning stimulus (tail clamp, 125 g) to evoke DNIC (see **section 2.4**)[*]. Recordings were followed by euthanasia and bone collection for analysis (see **section 2.5**). Evoked and non-evoked behavioural testing was also carried out in naïve, sham, and CIBP mice (see **section 2.7**).

Finally, *in vivo* dorsal root ganglion (DRG) calcium imaging was performed in naïve female and male C57BL/6 wildtype mice under urethane and isoflurane anaesthesia. Evoked primary afferent responses to different stimuli (dynamic mechanical brush, tonic mechanical pressure, and electrical volley) were recorded at DRG level L3 before and during simultaneous ipsilateral application of a noxious conditioning stimulus (ear clamp) to evoke DNIC (see **section 2.6**)[**]. For the statistical analysis, a value of $p < 0.05$ was considered significant for all comparisons (see **section 2.8**).

5.4. Results

5.4.1. CIBP mice present with progressive mechanical hyperalgesia

Pain-like behaviours were studied in naïve (n = 10), sham (n = 10), and CIBP (n = 10) female (n = 5 per group) and male (n = 5 per group) C57BL/6 wildtype mice on pre-surgical day 2 (baseline) and post-operative days 2, 7, 14, 21, and 28. Following baseline data collection, CIBP and sham mice underwent surgical tibial cancer cell implantation (or sham surgery) (day 0). Animal weight prior to behavioural testing (baseline weight) showed no differences between any of the groups (Kruskal-Wallis test: $H_{(2)} = 0.712$, $p > 0.05$). Analysis of animal weight over time between groups (2-way mixed ANOVA) revealed weight gain across time ($F_{(5, 135)} = 43.301$, $p < 0.001$; Bonferroni post hoc), with this weight gain

[*] *Electrophysiological mouse recordings were performed in parallel with Dr Ryan Patel, who recorded 18 out of 50 cells.*

[**] *Calcium imaging mouse recordings were surgically set up and assisted by Dr Mateusz Kucharczyk.*

being consistent across all groups ($F_{(10, 135)}$ = 1.883, p > 0.05) (see **Figure 5.1A**). Weight gain was also consistent between females (2-way mixed ANOVA: $F_{(10, 60)}$ = 1.195, p > 0.05) and males (2-way mixed ANOVA: $F_{(10, 60)}$ = 1.191, p > 0.05) across groups and time.

Static weight-bearing: The non-evoked paradigm revealed significant differences in the rear-leg body weight distribution between groups across time (2-way mixed ANOVA: $F_{(7.262, 98.034)}$ = 18.099, p < 0.001). When compared to naïve mice, sham mice showed no differences in weight distribution at any given timepoint (Bonferroni post hoc: p > 0.05 for all tests). In contrast, CIBP mice showed gradual impairment of weight distribution on the ipsilateral (cancer-bearing) leg from day 21 onwards (Bonferroni post hoc: p < 0.01) but not before (Bonferroni post hoc: p > 0.05) (see **Figure 5.1B**). There were no observed sex differences in naïve (2-way mixed ANOVA: $F_{(5, 40)}$ = 1.863, p > 0.05), sham (2-way mixed ANOVA: $F_{(5, 40)}$ = 1.628, p > 0.05), nor CIBP mice (2-way mixed ANOVA: $F_{(5, 40)}$ = 2.424, p > 0.05) at any given timepoint.

Paw pressure test: Mechanical ipsilateral paw stimulation revealed significant differences between groups across time (2-way mixed ANOVA: $F_{(10, 135)}$ = 30.594, p < 0.001). When compared to naïve mice, sham animals showed mechanical hypersensitivity on post-surgical days 2 and 7 (Bonferroni post hoc: p < 0.01) with no differences at any other timepoints (Bonferroni post hoc: p > 0.05). In contrast, CIBP mice showed mechanical hypersensitivity on the ipsilateral (cancer-bearing) leg from day 2 onwards (Bonferroni post hoc: p < 0.01) (see **Figure 5.1C**). There were no observed sex differences in naïve (2-way mixed ANOVA: $F_{(5, 40)}$ = 0.449, p > 0.05), sham (2-way mixed ANOVA: $F_{(5, 40)}$ = 0.735, p > 0.05), nor CIBP mice (2-way mixed ANOVA: $F_{(5, 40)}$ = 0.722, p > 0.05) at any given timepoint. As a control measure, mechanical contralateral paw stimulation showed no distinctions between groups across time (2-way mixed ANOVA: $F_{(10, 135)}$ = 1.222, p > 0.05) (see **Figure 5.1D**), nor between sexes in naïve (2-way mixed ANOVA: $F_{(5, 40)}$ = 0.353, p > 0.05), sham (2-way mixed ANOVA: $F_{(5, 40)}$ = 0.633, p > 0.05), nor CIBP mice (2-way mixed ANOVA: $F_{(5, 40)}$ = 0.482, p > 0.05) at any given timepoint.

Summarising, the behavioural data clearly demonstrate that tumour growth in CIBP female and male mice produces ipsilateral mechanical hypersensitivity, leading to changes in body weight distribution with mice favouring the non-tumour bearing side.

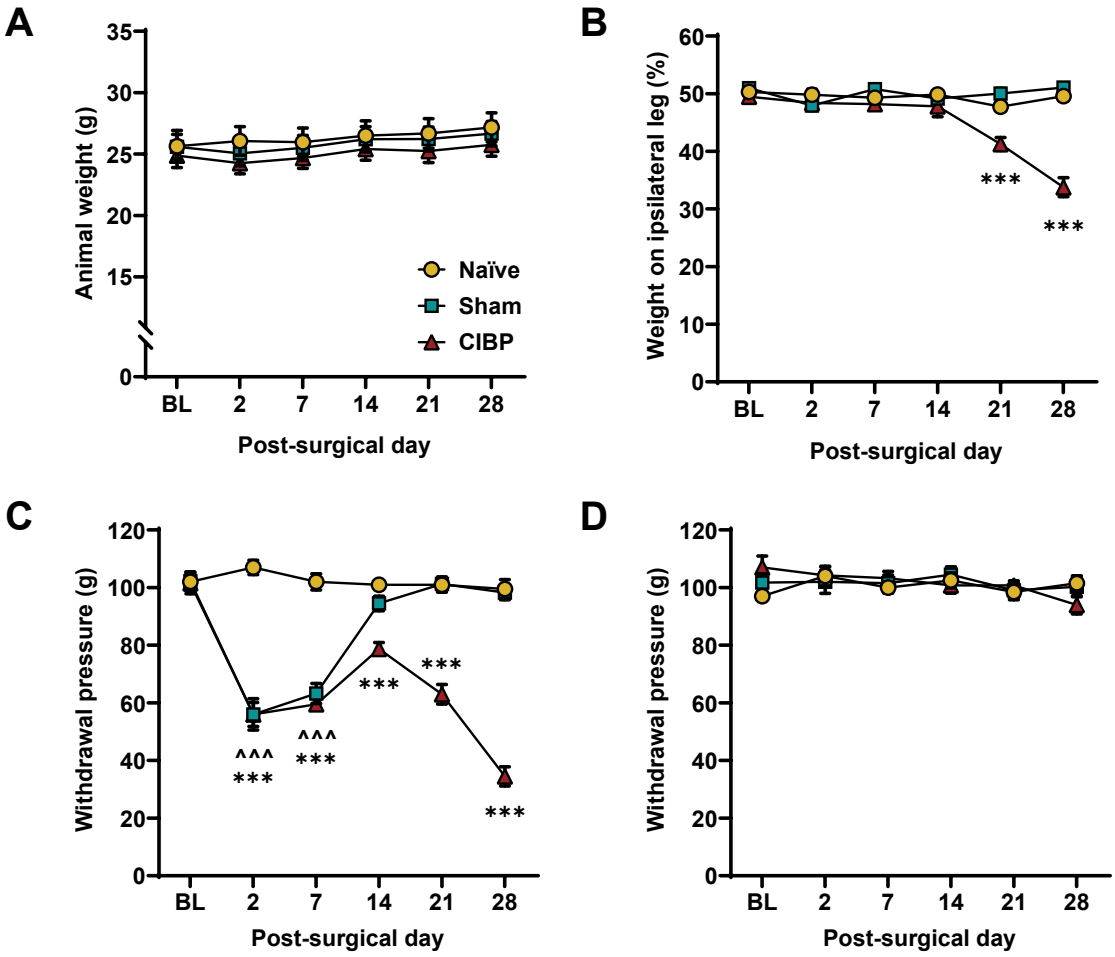

Figure 5.1. Cancer progression leads to mechanical hypersensitivity in CIBP mice. (A) *Animal weight gain following surgery.* ***(B)*** *Weight percentage born on the ipsilateral leg (expressed as % of total rear-bearing weight) (static weight-bearing test).* ***(C)*** *Paw withdrawal threshold in response to gradual mechanical ipsilateral pressure (paw-pressure test).* ***(D)*** *Paw withdrawal threshold in response to gradual mechanical contralateral pressure (paw-pressure test). Differences between control sham and naïve mice (^) and between CIBP and naïve mice (*) are included. ***P < 0.001. Data represent mean ± SEM. Each line represents the same group of naïve (n = 10), sham (n = 10), or CIBP (n = 10) female (n = 5 per group) and male (n = 5 per group) mice across time. The figure key presented in (A) is valid for the entire figure. CIBP: cancer-induced bone pain.*

5.4.2. CIBP mice show compromised bone macro and microstructure

Evaluation of bone integrity in naïve, sham, and CIBP female and male C57BL/6 wildtype mice was carried out using high-resolution micro-computed tomography (µCT) following collection of tibiae (with the corresponding fibula and patella) from sham week 1-2 (n = 10), sham week 3-4 (n = 10), CIBP week 1-2 (n = 10), and CIBP week 3-4 (n = 10) female (n = 5 per group) and male (n = 5 per group) mice, where a naïve group provided the reference control for all comparisons (n = 10).

Sham groups (week 1-2 and week 3-4): Total tibial length showed differences between groups (Welch's 1-way ANOVA: $F_{(2,\ 16.231)} = 10.125$, $p < 0.01$; Games-Howell post hoc) with no signs of macroscopic bone damage (see **Figure 5.2A**) nor macroscopic sex differences. When compared to naïve mice, trabecular bone properties were stable with no notable significant differences (see **Table 5.1** for a result overview). Of special interest, the trabecular bone mineral density (degree of mineralization within the tissue volume of interest) remained stable (1-way ANOVA: $F_{(2, 27)} = 0.095$, $p > 0.05$) (see **Figure 5.2B**). Cortical bone morphometric characteristics followed a similar pattern (see **Table 5.2** for a result overview), with cortical tissue mineral density (degree of mineralization within the bone volume of interest) showing differences on week 1-2 (1-way ANOVA: $F_{(2, 27)} = 4.997$, $p < 0.05$; Bonferroni post hoc: $p < 0.05$) but not after (Bonferroni post hoc: $p > 0.05$) (see **Figure 5.2C**).

CIBP groups (week 1-2 and week 3-4): Total tibial length showed no differences between any of the groups (1-way ANOVA: $F_{(2, 27)} = 2.391$, $p > 0.05$) despite clear progressive macroscopic bone damage (see **Figure 5.3A**). When compared to naïve mice, trabecular bone properties showed progressive degradation (see **Table 5.2** for a result overview). Of special interest, trabecular bone mineral density (degree of mineralization within the tissue volume of interest) showed differences on week 3-4 (1-way ANOVA: $F_{(2, 27)} = 11.348$, $p < 0.001$; Bonferroni post hoc: $p < 0.001$), but not before (Bonferroni post hoc: $p > 0.05$) (see **Figure 5.3B**). Cortical bone morphometric characteristics followed a similar degradation pattern (see **Table 5.4** for a result overview), with cortical tissue mineral density (degree of mineralization within the bone volume of interest) surprisingly showing no differences between groups (Kruskal-Wallis test: $H_{(2)} = 4.862$, $p > 0.05$) (see **Figure 5.3C**).

These results showcase how disease progression affects trabecular and cortical bone properties in CIBP mice, with trabecular bone being compromised from week 1-2, while cortical bone was additionally impaired from week 3-4.

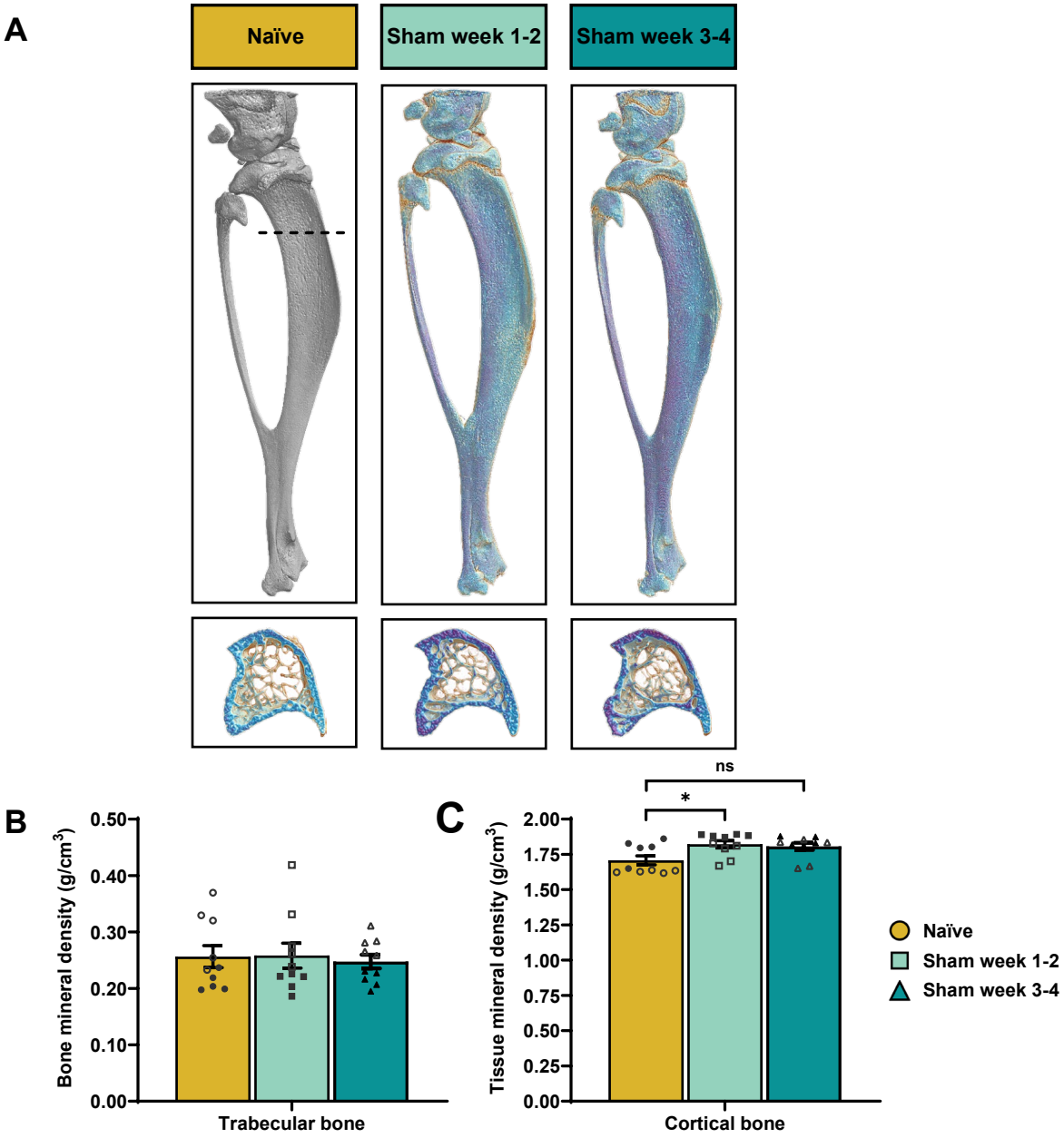

Figure 5.2. Bone macro and microarchitecture remain stable in sham mice. (A) *Representative scanned tibial male samples (micro-computed tomography) showcasing the lack of macroscopic changes following sham surgery.* ***(B)*** *Trabecular bone mineral density (degree of mineralization within the tissue volume of interest) and cortical tissue mineral density (degree of mineralization within the bone volume of interest) comparisons. *P < 0.05. Data represent mean ± SEM. Each dot corresponds to individual tibial samples from naïve (n = 10), sham week 1-2 (n = 10), or sham week 3-4 (n = 10) female (n = 5 per group; solid symbols) and male (n = 5 per group; open symbols) mice.*

Table 5.1. Impact of sham surgery on mouse bone microarchitecture. *Summary of representative parameters obtained from the trabecular and cortical micro-computed tomography tibial analysis. Data represent the mean ± SEM from naïve (n = 10), sham week 1-2 (n = 10), and sham week 3-4 (n = 10) female (n = 5 per group) and male (n = 5 per group) mice. One-way ANOVA with Bonferroni post-hoc test: *p < 0.05, **p < 0.01 (comparisons against naïve mice). Whenever homoscedasticity was not met, Welch's one-way ANOVA with Games-Howell post-hoc test was performed (or Kruskal-Wallis test with Dunn-Bonferroni post hoc test if data were additionally not normally distributed).*

		Naïve	Sham week 1-2	Sham week 3-4
Trabecular total surface	mm^2	17.17 ± 0.77	17.48 ± 0.76	17.35 ± 0.45
Trabecular bone surface	mm^2	19.29 ± 3.46	16.87 ± 3.30	16.04 ± 2.16
Trabecular bone surface fraction	%	48.98 ± 3.91	44.86 ± 4.10	46.04 ± 2.88
Trabecular total volume	mm^3	2.65 ± 0.19	2.66 ± 0.18	2.63 ± 0.10
Trabecular bone volume	mm^3	0.23 ± 0.05	0.20 ± 0.04	0.17 ± 0.03
Trabecular bone volume fraction	%	7.82 ± 1.33	6.93 ± 1.24	6.21 ± 0.80
Trabecular number	mm^{-1}	1.77 ± 0.26	1.52 ± 0.25	1.52 ± 0.17
Trabecular pattern factor	mm^{-1}	32.01 ± 3.18	31.46 ± 2.13	35.04 ± 2.48
Trabecular separation	mm	0.27 ± 0.01	0.31 ± 0.02	0.29 ± 0.01
Trabecular thickness ($x10^{-2}$)	mm	4.29 ± 0.14	4.58 ± 0.17	4.01 ± 0.09
Trabecular bone mineral density	g/cm^3	0.26 ± 0.02	0.26 ± 0.02	0.25 ± 0.01
Connectivity density ($x10^{-5}$)	mm^{-3}	1.38 ± 0.21	1.14 ± 0.22	1.12 ± 0.16
Degree of anisotropy	N/A	0.64 ± 0.02	0.62 ± 0.02	0.63 ± 0.01
Fractal dimension	N/A	2.08 ± 0.05	2.03 ± 0.05	2.05 ± 0.04

		Naïve	Sham week 1-2	Sham week 3-4
Cortical total area (mean)	mm^2	2.01 ± 0.10	1.97 ± 0.09	1.99 ± 0.04
Cortical bone area (mean)	mm^2	0.90 ± 0.04	0.90 ± 0.04	0.89 ± 0.02
Cortical bone area fraction	%	45.19 ± 1.22	46.03 ± 0.79	44.67 ± 0.73
Cortical total surface (mean)	mm^2	35.31 ± 1.01	36.45 ± 1.23	36.61 ± 0.65
Cortical bone surface (mean)	mm^2	69.16 ± 2.99	64.39 ± 2.63	70.35 ± 2.19
Cortical bone surface fraction	%	66.09 ± 0.42	**63.80 ± 0.22****	65.69 ± 0.52
Cortical thickness	mm	0.12 ± 0.01	**0.13 ± 0.01***	0.12 ± 0.01
Cortical tissue mineral density	g/cm^3	1.71 ± 0.03	**1.82 ± 0.03***	1.81 ± 0.03
Cortical porosity	%	54.93 ± 1.22	54.08 ± 0.79	55.45 ± 0.73
Connectivity density ($x10^{-5}$)	mm^{-3}	0.78 ± 0.06	**0.46 ± 0.04****	0.81 ± 0.13
Eccentricity	N/A	0.60 ± 0.01	0.62 ± 0.02	**0.64 ± 0.01***

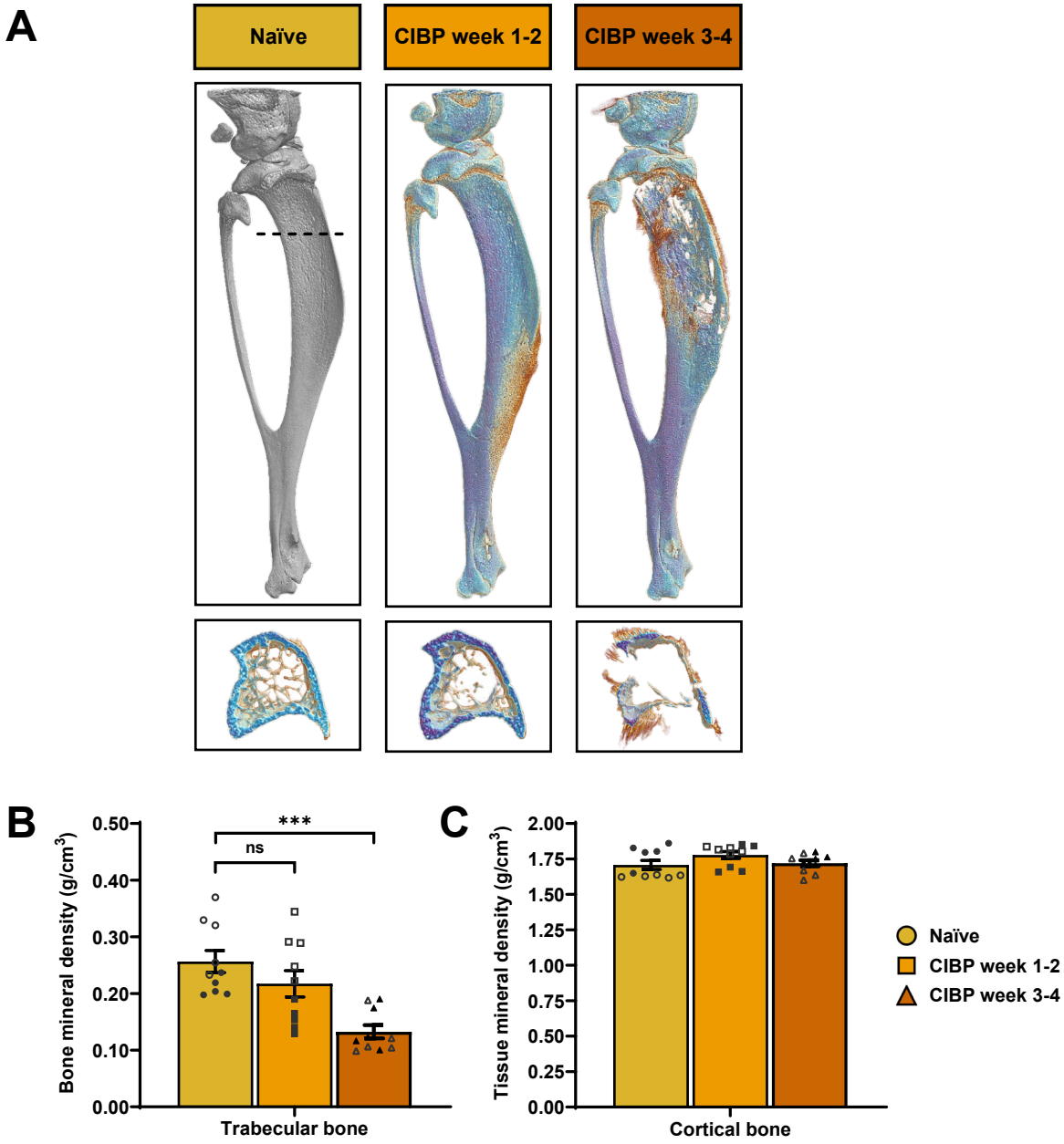

Figure 5.3. Bone macro and microarchitecture progressively degenerate in CIBP mice. (A) *Representative scanned tibial male samples (micro-computed tomography) showcasing the macroscopic changes following CIBP surgery.* ***(B)*** *Trabecular bone mineral density (degree of mineralization within the tissue volume of interest) and cortical tissue mineral density (degree of mineralization within the bone volume of interest) comparisons. ***P < 0.001. Data represent mean ± SEM. Each dot corresponds to individual tibial samples from naïve (n = 10), CIBP week 1-2 (n = 10), or CIBP week 3-4 (n = 10) female (n = 5 per group; solid symbols) and male (n = 5 per group; open symbols) mice. CIBP: cancer-induced bone pain.*

Table 5.2. Impact of cancer cell implantation on mouse bone microarchitecture. *Summary of representative parameters obtained from the trabecular and cortical micro-computed tomography tibial analysis. Data represent the mean ± SEM from naïve (n = 10), sham week 1-2 (n = 10), and sham week 3-4 (n = 10) female (n = 5 per group) and male (n = 5 per group) mice. One-way ANOVA with Bonferroni post-hoc test: *p < 0.05, **p < 0.01, ***p < 0.001 (comparisons against naïve mice). Whenever homoscedasticity was not met, Welch's one-way ANOVA with Games-Howell post-hoc test was performed (or Kruskal-Wallis test with Dunn-Bonferroni post hoc test if data were additionally not normally distributed). CIBP: cancer-induced bone pain.*

		Naïve	CIBP week 1-2	CIBP week 3-4
Trabecular total surface	mm^2	17.17 ± 0.77	17.23 ± 0.67	18.82 ± 0.63
Trabecular bone surface	mm^2	19.29 ± 3.46	13.34 ± 2.99	**2.88 ± 1.34****
Trabecular bone surface fraction	%	48.98 ± 3.91	37.78 ± 5.76	**10.60 ± 4.22*****
Trabecular total volume	mm^3	2.65 ± 0.19	2.61 ± 0.15	3.22 ± 0.18
Trabecular bone volume	mm^3	0.23 ± 0.05	0.15 ± 0.04	**0.03 ± 0.01****
Trabecular bone volume fraction	%	7.82 ± 1.33	5.25 ± 1.21	**0.89 ± 0.41*****
Trabecular number	mm^{-1}	1.77 ± 0.26	1.23 ± 0.27	**0.21 ± 0.10*****
Trabecular pattern factor	mm^{-1}	32.01 ± 3.18	35.45 ± 2.53	40.90 ± 3.14
Trabecular separation	mm	0.27 ± 0.01	0.37 ± 0.04	**0.65 ± 0.05*****
Trabecular thickness ($x10^{-2}$)	mm	4.29 ± 0.14	4.10 ± 0.12	4.24 ± 0.32
Trabecular bone mineral density	g/cm^3	0.26 ± 0.02	0.22 ± 0.07	**0.13 ± 0.01*****
Connectivity density ($x10^{-5}$)	mm^{-3}	1.38 ± 0.21	0.91 ± 0.23	**0.12 ± 0.06*****
Degree of anisotropy	N/A	0.64 ± 0.02	0.66 ± 0.03	0.60 ± 0.03
Fractal dimension	N/A	2.08 ± 0.05	1.89 ± 0.10	**1.45 ± 0.10*****

		Naïve	CIBP week 1-2	CIBP week 3-4
Cortical total area (mean)	mm^2	2.01 ± 0.10	1.93 ± 0.07	**2.54 ± 0.16***
Cortical bone area (mean)	mm^2	0.90 ± 0.04	0.85 ± 0.03	**0.74 ± 0.04***
Cortical bone area fraction	%	45.19 ± 1.22	43.87 ± 0.66	**30.37 ± 2.20*****
Cortical total surface (mean)	mm^2	35.31 ± 1.01	36.08 ± 1.08	**47.55 ± 2.00*****
Cortical bone surface (mean)	mm^2	69.16 ± 2.99	64.51 ± 2.12	78.10 ± 3.46
Cortical bone surface fraction	%	66.09 ± 0.42	64.11 ± 0.24	**62.10 ± 0.94****
Cortical thickness	mm	0.12 ± 0.01	0.12 ± 0.01	**0.09 ± 0.01*****
Cortical tissue mineral density	g/cm^3	1.71 ± 0.03	1.78 ± 0.02	1.72 ± 0.02
Cortical porosity	%	54.93 ± 1.22	56.25 ± 0.66	**69.77 ± 1.50*****
Connectivity density ($x10^{-5}$)	mm^{-3}	0.78 ± 0.06	**0.48 ± 0.05****	**1.60 ± 0.17****
Eccentricity	N/A	0.60 ± 0.01	0.60 ± 0.01	**0.66 ± 0.02***

5.4.3. DNIC are expressed in naïve female and male mice

Spinal WDR responses to natural stimuli as well as DNIC expression were studied in naïve female and male C57BL/6 wildtype mice under isoflurane anaesthesia in a gaseous N_2O/O_2 mix (see **Figure 5.4A**). A minimum of one and maximum of two neurons were recorded per mouse (n = 10; N = 7). Each WDR neuron responded to dynamic brush and punctate von Frey stimulation with intensity coding to 1 g, 4 g, 8 g, and 15 g bending forces (1-way RM-ANOVA: $F_{(3, 27)} = 108.050$, $p < 0.001$; Bonferroni post hoc: $p < 0.01$ for all tests) (see **Figure 5.4B** and **Figure 5.4C**) as well as thermal 42°C, 45°C, and 48°C waterjet (Friedman test: $\chi^2_{(2)} = 20.000$, $p < 0.001$; Wilcoxon post hoc: $p < 0.01$ for all tests) (see **Figure 5.4D**). Neuronal WDR responses to dynamic brush (independent samples T-test: $t_{(8)} = 0.483$, $p > 0.05$), punctate von Frey stimulation (2-way mixed ANOVA: $F_{(3, 24)} = 1.216$, $p > 0.05$), and thermal waterjet (2-way mixed ANOVA: $F_{(1.009, 8.069)} = 0.707$, $p > 0.05$) showed no significant differences between female (n = 5; N = 3) and male (n = 5; N = 4) mice. Upon application of a noxious tail clamp (conditioning stimulus), WDR baseline neuronal activity was significantly reduced for 15 g von Frey (paired samples T-test: $t_{(9)} = 11.209$, $p < 0.001$) (see **Figure 5.4E**). Moreover, the inhibitory effect of DNIC (% reduction of cell activity with respect to baseline) upon tail clamp application was comparable between naïve female and male mice (Mann-Whitney U test: U = 11.000, $p > 0.05$) (see **Figure 5.4F**).

These results evidence a functional DNIC system expressed upon noxious conditioning stimulation in naïve female and male C57BL/6 wildtype mice, with WDR neuronal responses to mechanical and thermal stimuli, as well as DNIC expression and inhibitory intensity, not being affected by sex.

5.4.4. DNIC expression is dynamic in the CIBP mouse model

CIBP and sham female and male C57BL/6 wildtype mice underwent surgical tibial cancer cell implantation (or sham surgery) 1-2 or 3-4 weeks prior to the electrophysiological recordings. A minimum of one and maximum of two neurons were recorded per sham week 1-2 (n = 10, N = 8), sham week 3-4 (n = 10, N = 8), CIBP week 1-2 (n = 10, N = 7), and CIBP week 3-4 (n = 10, N = 8) mouse under isoflurane anaesthesia in a gaseous N_2O/O_2 mix, where a naïve group provided the reference control for all comparisons (n = 10; N = 7). Each group included female (n = 5) and male (n = 5) WDR recordings.

Sham groups (week 1-2 and week 3-4): Neuronal WDR responses to dynamic brush (1-way ANOVA: $F_{(2, 27)} = 0.135$, $p > 0.05$) (see **Figure 5.5A**), punctate von Frey stimulation (2-way mixed ANOVA: $F_{(2.772, 37.425)} = 2.699$, $p > 0.05$), and thermal waterjet (2-way mixed ANOVA: $F_{(2.378, 32.105)} = 0.719$, $p > 0.05$) showed no significant differences between any of the groups (see **Figure 5.5B** and **Figure 5.5C**, respectively). Upon application of a noxious tail clamp (conditioning stimulus), WDR baseline neuronal activity was significantly reduced in sham week 1-2 (paired samples T-test: $t_{(9)} = 20.953$, $p < 0.001$) and sham week 3-4 mice (Wilcoxon signed rank test: $Z = 0.000$, $p < 0.01$) (see **Figure 5.5E**). The inhibitory effect of DNIC (% reduction of cell activity with respect to baseline upon tail clamp application) was comparable throughout groups for 15 g von Frey bending force (Kruskal-Wallis test: $H_{(2)} = 3.827$, $p > 0.05$) (see **Figure 5.5D**). This DNIC effect was comparable between sham week 1-2 female ($n = 5$, $N = 5$) and male ($n = 5$, $N = 3$) mice (Mann-Whitney U test: $U = 10.000$, $p > 0.05$), and between sham week 3-4 female ($n = 5$, $N = 4$) and male ($n = 5$, $N = 4$) mice (Mann-Whitney U test: $U = 14.000$, $p > 0.05$).

CIBP groups (week 1-2 and week 3-4): Neuronal WDR responses to dynamic brush (1-way ANOVA: $F_{(2, 27)} = 0.534$, $p > 0.05$) (see **Figure 5.6A**), punctate von Frey stimulation (2-way mixed ANOVA: $F_{(2.569, 34.680)} = 1.323$, $p > 0.05$), and thermal waterjet (2-way mixed ANOVA: $F_{(2.235, 30.172)} = 1.249$, $p > 0.05$) showed no significant differences between any of the groups (see **Figure 5.6B** and **Figure 5.6C**, respectively). Upon application of a noxious tail clamp (conditioning stimulus), WDR baseline neuronal activity was significantly reduced in CIBP week 3-4 mice (paired samples T-test: $t_{(9)} = 5.318$, $p < 0.001$), but not in CIBP week 1-2 mice (Wilcoxon signed rank test: $Z = 16.000$, $p > 0.05$) (see **Figure 5.6E**). Thus, the inhibitory effect of DNIC (% reduction of cell activity with respect to baseline upon tail clamp application) showed significant differences between groups for 15 g von Frey (Kruskal-Wallis test: $H_{(2)} = 14.895$, $p < 0.001$). These differences were observed in CIBP week 1-2 (Dunn-Bonferroni post hoc: $p < 0.01$), but not in CIBP week 3-4 when compared to naïve mice (Dunn-Bonferroni post hoc: $p > 0.05$) (see **Figure 5.6D**). This DNIC effect (or lack thereof) was comparable between CIBP week 1-2 female ($n = 5$, $N = 4$) and male ($n = 5$, $N = 3$) mice (Mann-Whitney U test: $U = 15.000$, $p > 0.05$), and between CIBP week 3-4 female ($n = 5$, $N = 4$) and male ($n = 5$, $N = 4$) mice (Mann-Whitney U test: $U = 17.000$, $p > 0.05$).

These results showcase how cancer progression does not affect WDR neuronal responses to mechanical nor thermal stimulation in CIBP female and male mice. However, disease progression

correlates with dynamic DNIC expression in CIBP mice, whereby DNIC is abolished on post-surgical week 1-2, but once again recovered on post-surgical week 3-4 (see **Figure 5.7**).

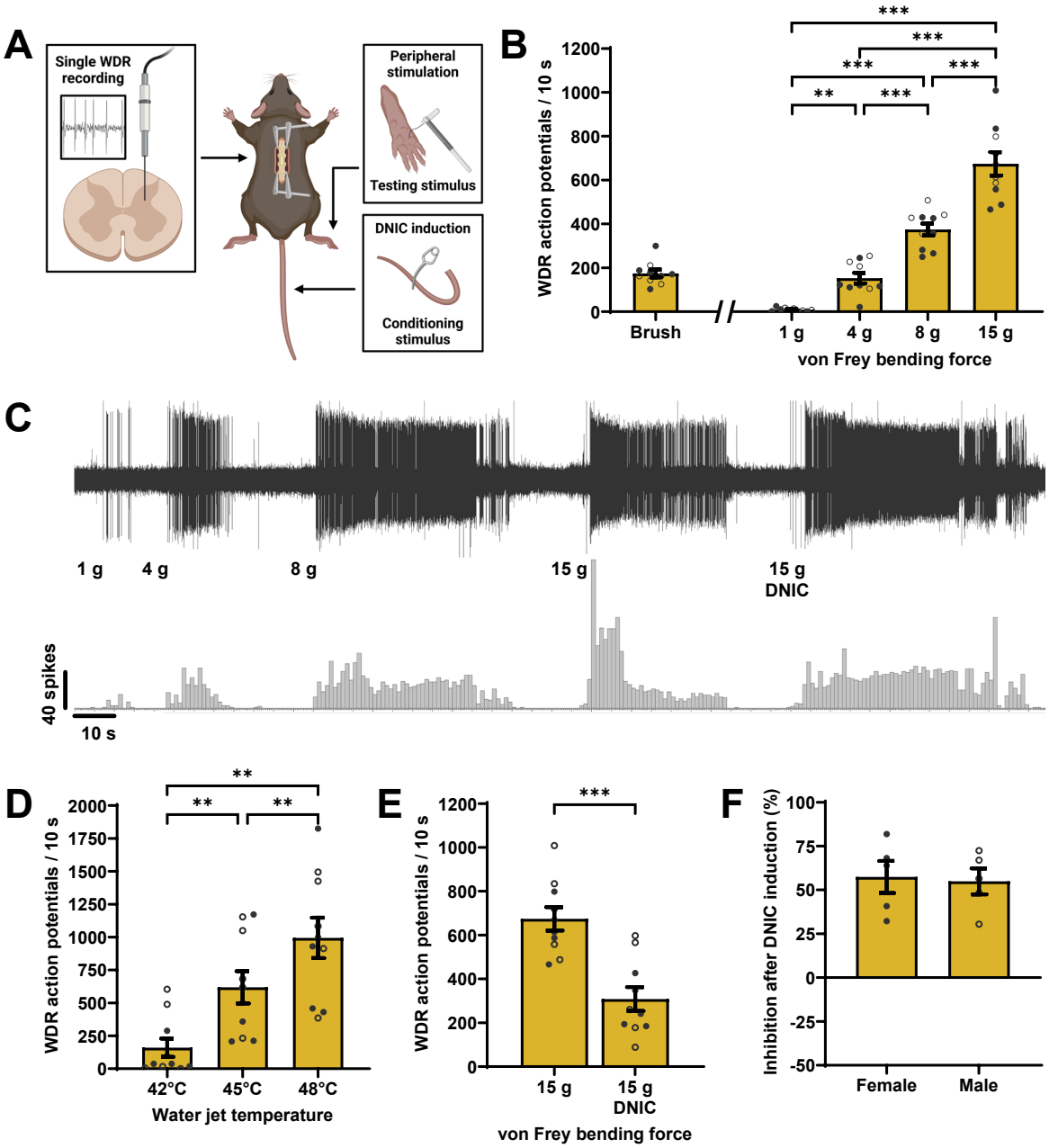

Figure 5.4. DNIC are expressed in naïve female and male mice. (A) *Schematic representation of the experimental paradigm.* ***(B)*** *WDR neuronal responses to dynamic mechanical stimulation (brush) and increasing punctate mechanical forces (von Frey).* ***(C)*** *Representative example of spinal WDR neuronal traces and action potential quantification before and upon simultaneous noxious tail clamp application (DNIC) (male mouse).* ***(D)*** *WDR neuronal responses to increasing thermal heat stimulation (waterjet).* ***(E)*** *DNIC effects on WDR baseline activity (15 g von Frey).* ***(F)*** *DNIC effect comparison (% reduction in cell activity with respect to baseline) between sexes. **P < 0.01; ***P < 0.001. Data represent mean ± SEM. Each dot corresponds to an individual cell from naïve (n = 10; N = 7) female (n = 5 per group; solid symbols) and male (n = 5 per group; open symbols) mice. WDR: wide-dynamic range; DNIC: diffuse noxious inhibitory controls.*

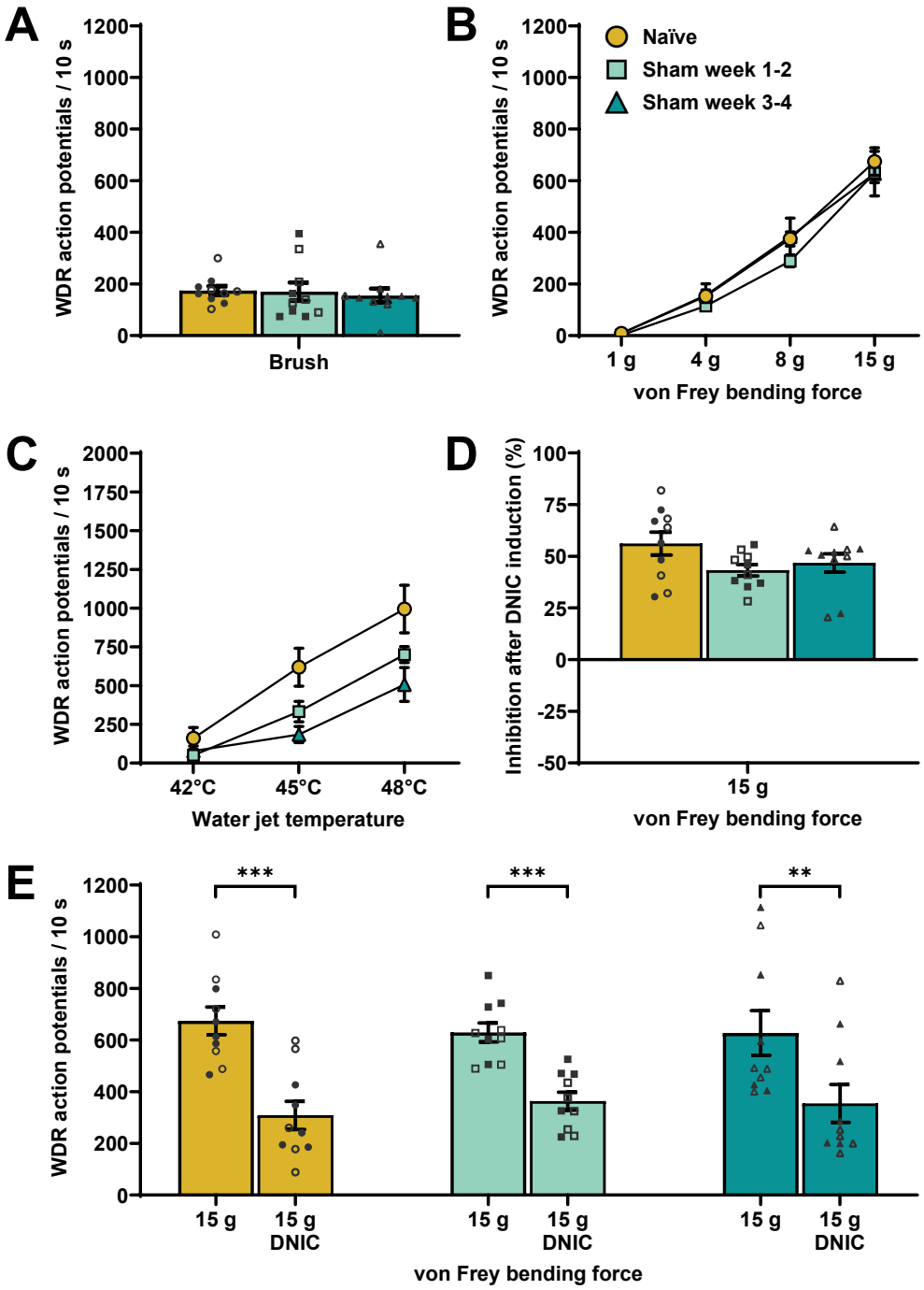

Figure 5.5. DNIC are expressed in sham mice. (A) *WDR neuronal responses to dynamic mechanical stimulation (brush).* ***(B)*** *WDR neuronal responses to increasing punctate mechanical forces (von Frey).* ***(C)*** *WDR neuronal responses to increasing thermal heat temperature (waterjet).* ***(D)*** *DNIC effect comparison (% reduction in cell activity with respect to baseline).* ***(E)*** *DNIC effects on WDR baseline activity upon simultaneous noxious tail clamp (15 g von Frey). **P < 0.01; ***P < 0.001. Data represent mean ± SEM. Each dot corresponds to an individual cell from naïve (n = 10; N = 7), sham week 1-2 (n = 10; N = 8), and sham week 3-4 (n = 10; N = 8) female (n = 5 per group; solid symbols) and male (n = 5 per group; open symbols) mice. The figure key presented in (B) is valid for the entire figure. WDR: wide-dynamic range; DNIC: diffuse noxious inhibitory controls.*

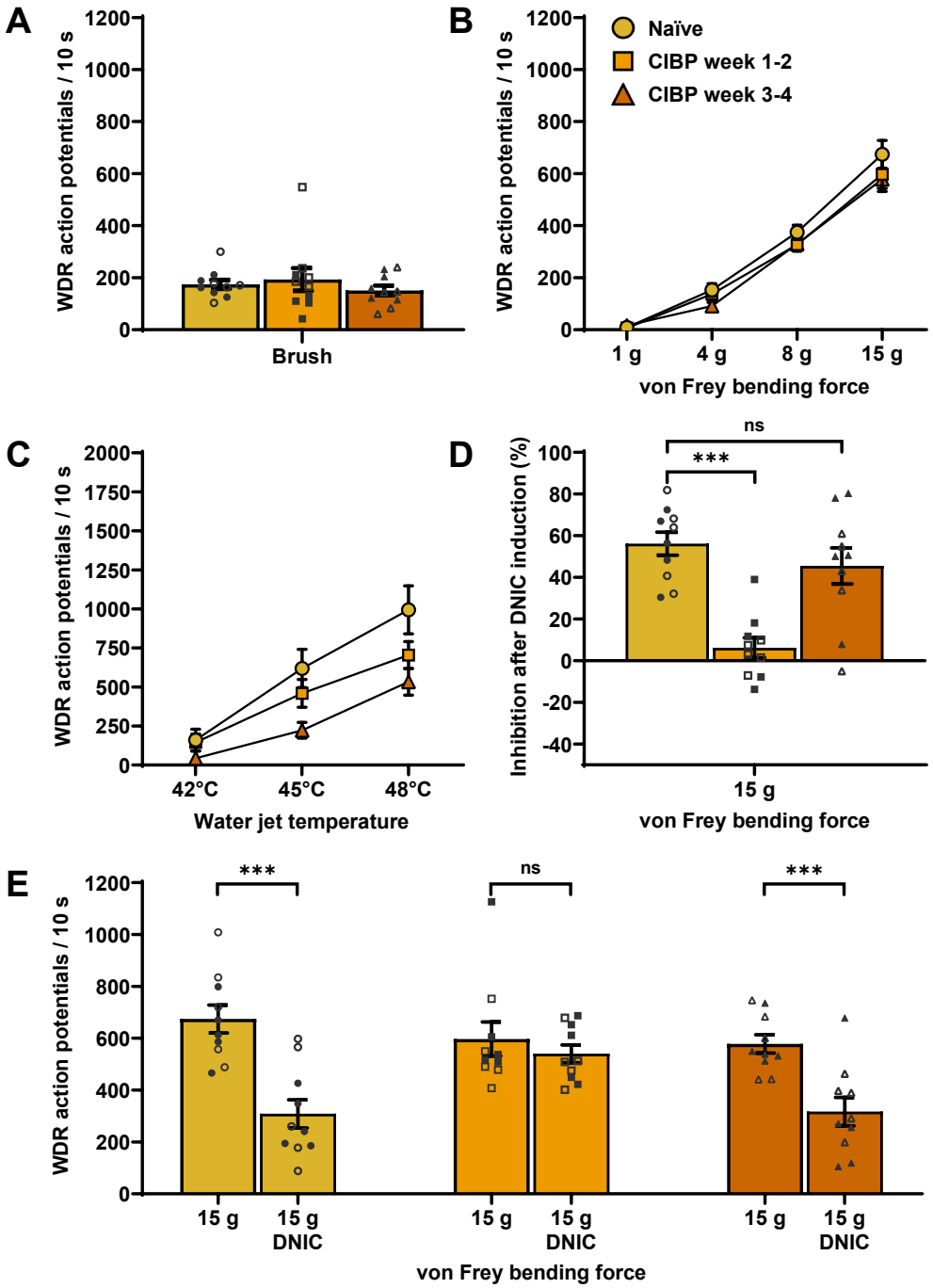

Figure 5.6. DNIC are dynamically expressed in CIBP mice. (A) *WDR neuronal responses to dynamic mechanical stimulation (brush).* ***(B)*** *WDR neuronal responses to increasing punctate mechanical forces (von Frey).* ***(C)*** *WDR neuronal responses to increasing thermal heat temperature (waterjet).* ***(D)*** *DNIC effect comparison (% reduction in cell activity with respect to baseline).* ***(E)*** *DNIC effects on WDR baseline activity upon simultaneous noxious tail clamp (15 g von Frey). ***P < 0.001. Data represent mean ± SEM. Each dot corresponds to an individual cell from naïve (n = 10; N = 7), CIBP week 1-2 (n = 10, N = 7), and CIBP week 3-4 (n = 10, N = 8) female (n = 5 per group; solid symbols) and male (n = 5 per group; open symbols) mice. The figure key presented in (B) is valid for the entire figure. WDR: wide-dynamic range; CIBP: cancer-induced bone pain; DNIC: diffuse noxious inhibitory controls.*

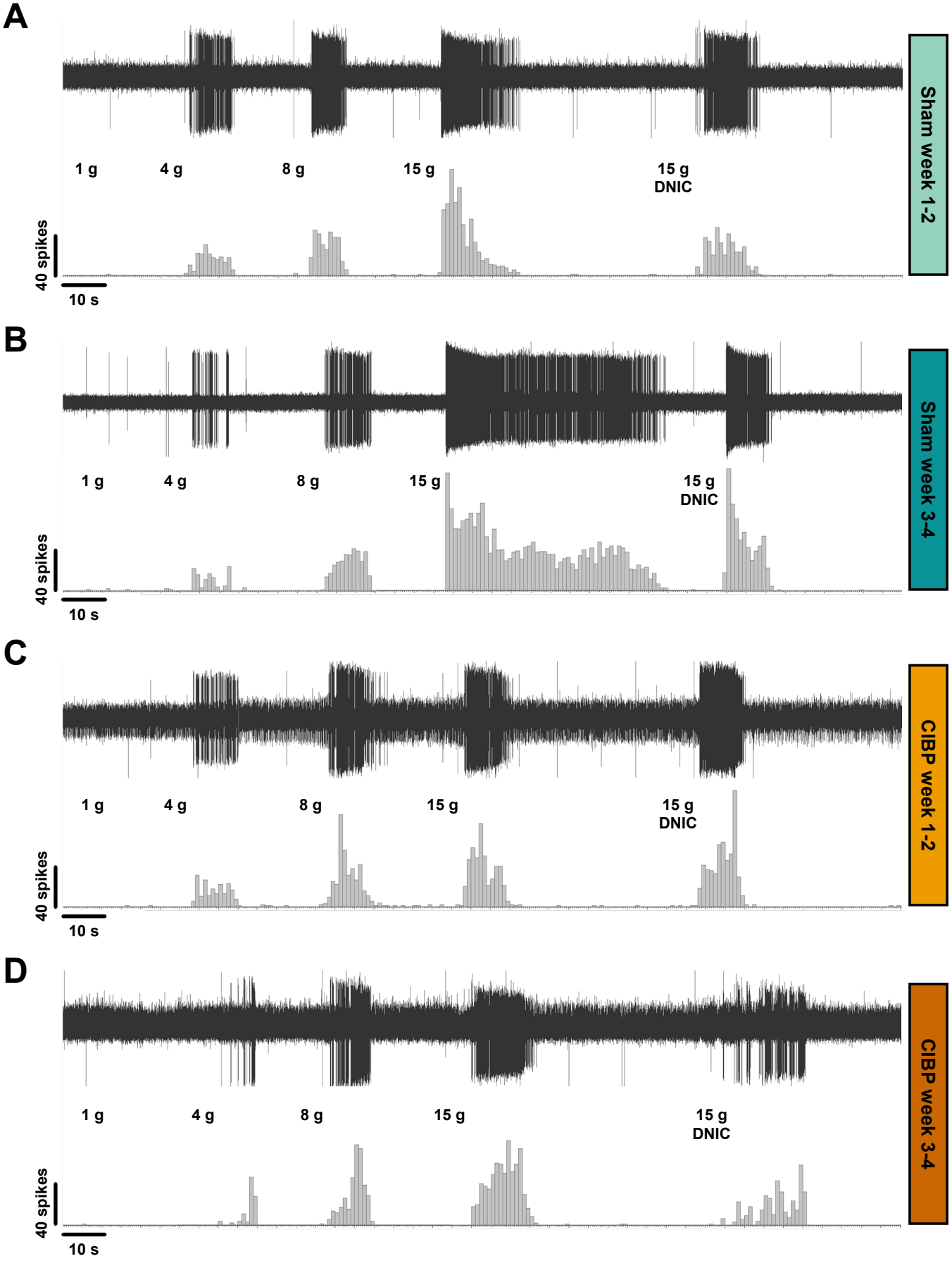
A
1 g
4 g
8 g
15 g
15 g DNIC
40 spikes
10 s
Sham week 1-2
B
1 g
4 g
8 g
15 g
15 g DNIC
40 spikes
10 s
Sham week 3-4
C
1 g
4 g
8 g
15 g
15 g DNIC
40 spikes
10 s
CIBP week 1-2
D
1 g
4 g
8 g
15 g
15 g DNIC
40 spikes
10 s
CIBP week 3-4

Figure 5.7. DNIC are dynamically expressed in CIBP mice (neuronal traces). *Representative examples of spinal WDR neuronal traces and action potential quantification in* ***(A)*** *sham week 1-2,* ***(B)*** *sham week 3-4,* ***(C)*** *CIBP week 1-2, and* ***(D)*** *CIBP week 3-4 male mice before and upon simultaneous noxious tail clamp application (DNIC). Each example corresponds to the same cell during the same stimulation trial. Some non-stimulation periods (resting time between each stimulus) may have been cropped out for illustrative purposes. CIBP: cancer-induced bone pain; DNIC: diffuse noxious inhibitory controls.*

5.4.5. Primary afferent somas are not affected at the group level by DNIC in naïve mice

Calcium responses of primary afferents to natural and electrical stimuli were studied in naïve female and male C57BL/6 wildtype mice (n = 9; n = 6 for electrical stimulation) at the DRG level (L3) under a mix of urethane and isoflurane anaesthesia (see **Figure 5.8A**). All comparisons were made at group level (i.e., responses according to primary afferent fibre diameter were not made; all sensory neurons were grouped). Responses to dynamic brush, tonic pressure (100 g, 300 g, 500 g, and 700 g) (Friedman test: $\chi^2_{(3)} = 17.284$, $p < 0.001$; Dunn-Bonferroni post hoc), and electrical volley were evidenced at the recorded DRG by an increase in the number of responding cells (see **Figure 5.8B**). Within these responsive afferents, dynamic brush (Wilcoxon signed rank test: $Z = 45.000$, $p < 0.01$), tonic pressure (Friedman test: $\chi^2_{(4)} = 33.156$, $p < 0.001$; Dunn-Bonferroni post hoc), and electrical volley (paired samples T-test: $t_{(5)} = -2.942$, $p < 0.05$) elicited responses that correlated with an increase in fluorescence intensity when compared to baseline values (see **Figure 5.8C**). Upon application of a noxious ear clamp (conditioning stimulus), neuronal DRG calcium activity was not affected for any of the modalities tested, including tonic pressure (300 g and 700 g) (2-way RM-ANOVA: $F_{(1, 8)} = 1.547$, $p > 0.05$) and electrical volley (paired samples T-test: $t_{(5)} = 2.202$, $p > 0.05$) (see **Figure 5.8D**).

The number of recruited primary afferents during dynamic brush (Mann-Whitney U test: $U = 5.000$, $p > 0.05$), tonic pressure (2-way mixed ANOVA: $F_{(1.028, 7.199)} = 1.875$, $p > 0.05$), and electrical volley (Mann-Whitney U test: $U = 3.000$, $p > 0.05$) showed no significant differences between naïve female (n = 5; n = 2 for electrical stimulation) and male (n = 4) mice. Within the responsive cells, the intensity of the fluorescence elicited by dynamic brush (Mann-Whitney U test: $U = 4.000$, $p > 0.05$), tonic pressure (2-way mixed ANOVA: $F_{(1.317, 9.216)} = 0.113$, $p > 0.05$), and electrical volley (Mann-Whitney U test: $U = 1.000$, $p > 0.05$) showed no significant differences between sexes.

Summarising, these preliminary data suggest that, at the group level, activation of the DNIC circuit does not impact calcium flux in the DRG of healthy mice. While it is not possible to draw definitive conclusions from this experiment due to its pilot nature, it lays the foundation for the research that will follow, for example, regarding the influence of DNIC activation on individual sensory neuron types.

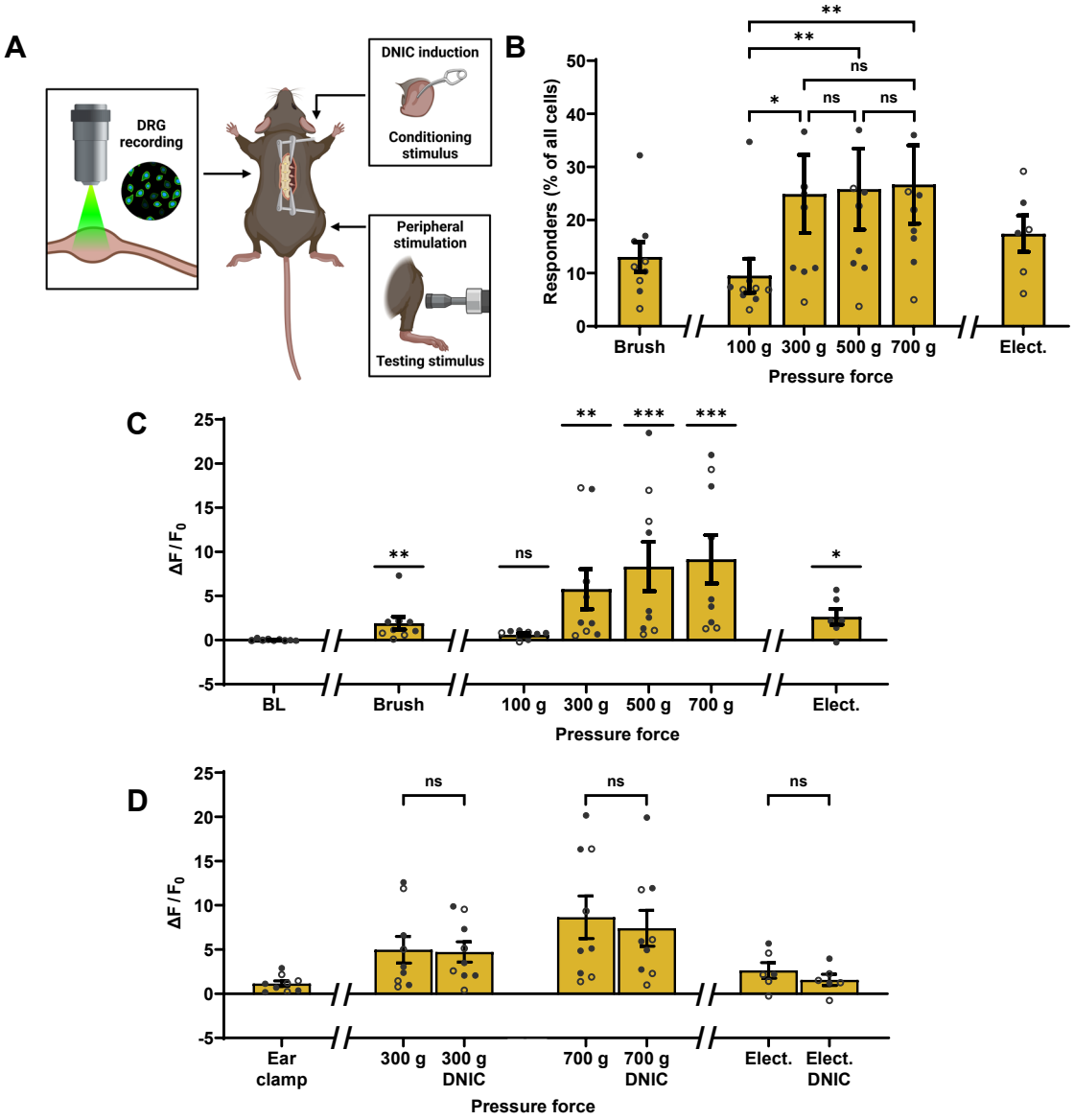

Figure 5.8. Primary afferent somas are not affected at the group level by DNIC in naïve mice. (A) *Schematic representation of the experimental paradigm.* ***(B)*** *Percentage of responding cells out of the total neuronal cell bodies analysed during dynamic mechanical (brush), tonic mechanical (pressure), and electrical (volley) stimulation.* ***(C)*** *Normalised fluorescence intensities of all responding neuronal cell bodies to the different stimuli (comparisons against baseline values).* ***(D)*** *DNIC effects on normalised fluorescence intensities of all responding neuronal cell bodies upon simultaneous noxious ear clamp (300 g, 700 g, and electrical stimulation). *P < 0.05; **P < 0.01; ***P < 0.001. Data represent mean ± SEM. Each dot represents averaged animal data from naïve (n = 9; n = 6 for electrical stimulation) female (n = 5; n = 2 for electrical stimulation; solid symbols) and male (n = 4; open symbols) mice. DRG: dorsal root ganglion; F: fluorescence; DNIC: diffuse noxious inhibitory controls.*

5.5. Discussion

5.5.1. Tumour progression in CIBP mice

Cancer patients often suffer from pain that incorporates skeletal-related phenotypes and mechanical detection anomalies (Lipton et al., 1991; Martland et al., 2020; Scott et al., 2012). Mechanical hypersensitivity, motor impairments, and loading pain have previously been recapitulated in femoral CIBP male mice (where CIBP was induced using the LLC cell line) utilising a variety of behavioural paradigms (Fan et al., 2022; Geppert et al., 2021; Maeda et al., 2016; Yang et al., 2018; Zhou, Cui et al., 2022). Here I used localised LLC cancer cell implantation into the tibia to produce a mouse model of CIBP, resulting in the progressive development of mechanical ipsilateral hypersensitivity. No differences in behavioural outcomes were observed when comparing female and male mouse data. Interestingly, a previous study using a femoral CIBP mouse model evidenced an earlier onset of the pain-like phenotype in female mice when compared to males, although these sex differences quickly disappeared with model progression (Falk et al., 2013). The earlier female onset could still exist in the tibial CIBP model presented herein, as the chosen post-surgical timepoints differed from those used in the aforementioned study, possibly impacting the observation of transient differences.

Progressive trabecular and cortical bone destruction was tightly linked with the onset of pain-related behaviours. The data presented in this chapter revealed how small radiolucent tibial trabecular lesions were present on week 1-2, while full cortical bone loss and severely compromised bone integrity was seen on week 3-4 following cancer cell implantation surgery. These osteolytic lesions (i.e., creation of cavities, holes, and weakened bone areas) on week 3-4 were accompanied by signs of potential fracture, with no evident sex differences. These results are in line with previous femoral CIBP studies that used the LLC cell line and pooled the data from both sexes together with no reported sex differences (de Clauser et al., 2020: Haroun et al., 2023). Femoral CIBP studies that used different cancer cell lines also showed no sex differences in bone degradation (Falk et al., 2013).

5.5.2. WDR activity and DNIC expression in naïve mice

In the present body of work, I characterised WDR neuronal responses in naïve female and male mice, demonstrating that sex did not impact evoked responses to mechanical nor thermal stimulation. Indeed, these evoked responses were comparable to those reported in previous electrophysiological

experiments that included both female and male wildtype mice (Peck et al., 2021; Trendafilova et al., 2022). Additionally, I described how, following the concomitant application of a noxious conditioning stimulus (tail clamp), WDR activity was consistently inhibited in naïve mice. The inhibitory effect (40-60% inhibition) was comparable between sexes and similar to those reported in rats (see **Chapter 3**). These results reveal that DNIC are functional in naïve mice and support the fact that inclusion of female animals in electrophysiological studies characterising WDR activity and DNIC expression is not equivalent to larger sample sizes.

A clear definition of the neurotransmitter subserving DNIC in mice cannot be achieved at this point due to pharmacological manipulations being extremely challenging and restricted by the nature of the set-up and the species utilised. However, previous studies have revealed how brainstem noradrenergic and serotonergic neurons are rapidly activated by nociceptive stimuli in mice (Moriya et al., 2019) and how the inhibition produced by the application of a noxious conditioning stimulus in wakeful mice (DCN) can be blocked by atipamezole (Nemoto et al., 2023). This is consistent with a role in DNIC and matches previous pharmacological knowledge from rats (Bannister et al., 2015; Bannister et al., 2017; see also Kucharczyk et al., 2021).

5.5.3. WDR activity and DNIC expression in CIBP mice

Previous studies have linked the progressive pain-like phenotype observed in CIBP mice to primary afferent hyperexcitability (de Clauser et al., 2020) and/or an increase in peripheral neurotrophic factors (e.g., NGF) that sensitise primary afferents, promote abnormal neuronal sprouting, and recruit silent nociceptors (Hannila and Kawaja, 2005; Kawaja et al., 2011; Prato et al., 2017; Tanaka et al., 2023; Sevcik et al., 2005). While one could speculate that such peripheral effects may be suggestive of hyperexcitability in the spinal cord, the results described herein demonstrate that cancer progression does not affect the evoked responses of WDR neurons to mechanical and thermal innocuous and noxious stimulation in both CIBP female and male mice.

Previous electrophysiological characterisation of evoked WDR baseline activity in mouse models of chronic pain have showed heterogeneous results. Studies using nerve constriction models declared potentiated WDR responses to innocuous stimuli, while responses to noxious stimuli were reduced (Medrano et al., 2016). On the other hand, mouse ligation models (Omori et al., 2009) as well as femoral

mouse models of CIBP (Khasabov et al., 2007) revealed increased WDR neuronal responses to both innocuous and noxious stimulation. As already mentioned, these differences could be partly explained by a possible divergence in responsiveness between superficial and deep dorsal horn WDR neurons, as some of these studies included deep dorsal horn WDR recordings exclusively (Omori et al., 2009), whilst others grouped both superficial and deep dorsal horn WDR recordings, treating them as a whole homogeneous group and potentially introducing a confounding element in the interpretation of the results (Khasabov et al., 2007; Medrano et al., 2016). This highlights how treating the neurons that reside in each of the laminae as separate functional populations is crucial not least since each neuronal type comprises a distinct element of separable circuits that govern pain processing.

Akin to the rat CIBP model (Kucharczyk, Derrien et al., 2020; see **Chapter 3**), the mouse model of CIBP incorporates DNIC dysfunctionality shortly after cancer cell implantation (week 1-2), where DNIC expression is recovered further in the course of the disease (week 3-4). Despite the lack of studies characterising DNIC in mice, mouse models of chronic pain have revealed descending modulatory affections, evidenced by DCN alterations in wakeful mouse models of osteoarthritis (Yuan et al., 2018) and traumatic brain injury (Kopruszinski et al., 2021; Sahbaie et al., 2022), consistent with previous rat knowledge (Irvine et al., 2020; Yoneda et al., 2020).

Previously, chemogenetic activation of direct spinally-projecting noradrenergic neurons located in the locus coeruleus was shown to abolish WDR spinal responses to both innocuous and noxious stimulation in healthy mice (Li et al., 2022). This is in direct correlation with the results observed in healthy rats, where optoactivation of this same set of neurons in a ventrally located area of the locus coeruleus also inhibited deep dorsal horn WDR neuronal activity as well as DNIC expression (Kucharczyk et al., 2022). However, despite both inhibitory spinal coerulean effects postulated as driven by noradrenergic mechanisms, α2-adrenoceptors were reported as the underpinning effectors in mice (revealed by the α2-adrenoceptor antagonist yohimbine) (Li et al., 2022), whilst α1-adrenoceptors were the main effectors in rats (revealed by the α1-adrenoceptor antagonist prazosin) (Kucharczyk et al., 2022), indicative of a possible differential mechanism of action upon WDR activity according to the species. These findings could imply a shared but not necessarily identical inter-species mechanism whereby hyperactivity in the locus coeruleus could drive the loss of DNIC expression in CIBP mice via maladaptive communications with the DNIC circuitry. Sex differences could also add a further layer of

complexity as previous studies have evidenced that coerulean neurons in female mice present fewer noradrenergic cells with larger dendritic volumes (Mariscal et al., 2023). In summary, a large body of research remains to be conducted before central nervous system manifestations of CIBP, in pharmacological, anatomical, and functional terms, are fully revealed.

5.5.4. DRG calcium activity in naïve mice

In part, our understanding of central nervous system manifestations of CIBP must include an exploration of what is happening in the peripheral nervous system. Primary afferent fibres conduct action potentials generated in the periphery, conveying this 'pain message' to the dorsal horn of the spinal cord. The 'law of dynamic polarization of the neuron' states that even though their axons can conduct in both directions, the propagation of action potentials is unidirectional, showing a preferred direction for transmission from dendrites to axons (van Gehuchten, 1891; see also Berlucchi, 1999). However, this preference can be reversed in situations where action potentials originate in the central terminals of primary afferents, travelling retrogradely to the periphery (dorsal root reflex). Activation of supraspinal areas involved in descending pain modulation has the potential to generate and/or modulate dorsal root reflexes (Martin et al., 1979; Peng et al., 2001; Peng et al., 2003; see also Sorkin et al., 2018). Interestingly, noradrenaline plays a role in this type of modulation, leading to a depression of antidromic action potentials (García-Ramírez et al., 2014; Mena-Avila et al., 2020). Thus, taking these previous findings and current knowledge of the circuitry (Kucharczyk et al., 2023) into account, I crudely investigated whether activation of DNIC had an effect on primary afferent activity at the level of the DRG. Under the conditions of my study, activation of DNIC had no effect on primary afferent calcium flux at the soma level in healthy mice. Of course, these results do not imply a lack of DNIC 'modulation' of the primary afferent fibres, but they do serve as a foundation for future studies that will delve into this question more specifically. For example, in the future it would be necessary to investigate whether there is a differential effect according to the type of fibre (i.e., Aβ-, Aδ-, and C-fibres), which could be masked when analysing group level activity in the DRG as opposed to per specific fibre type.

It could also be possible that any effect of DNIC on primary afferent fibres is not as strong as to elicit a dorsal root reflex, evidencing no effects at the DRG level. Dorsal root reflexes are only elicited once the summation of primary afferent depolarizations (PADs) reach a threshold potential.

Interestingly, PADs act as a modulatory mechanism of peripheral signals, offering a window for DNIC to modulate primary afferent sensitivity even in the absence of dorsal root reflexes. Despite cell depolarizations being associated with neuronal excitation, PADs lead to a counterintuitive inhibition of transmitter release on the primary afferent terminal. The proposed mechanisms driving this phenomenon may include impairing the propagation of action potentials from the periphery (via inhibition of voltage-gated sodium channels), attenuating the amplitude of peripheral action potentials with a subsequent reduction in spinal neurotransmitter release (through shunting inhibition), and/or reducing presynaptic calcium influx and transmitter release (via inactivation of voltage-gated calcium channels) (Graham and Redman, 1994; Willis, 2006; see also Bardoni et al., 2013; Guo and Hu, 2014). Thus, DNIC could still act upon the presynaptic terminals, even if this effect is not strong enough to produce a dorsal root reflex, and one could postulate that this is via a noradrenergic mechanism given what we know about the subserving pharmacology.

Finally, with dorsal root reflexes reported to be increased in animal inflammation models (Lin et al., 2000; Lucas-Romero et al., 2022; Sluka et al., 1995; Vicente-Baz et al., 2022) and with presynaptic spinal inhibition revealed to be decreased in neuropathic models (Chen et al., 2014; Wei et al., 2013), characterising these mechanisms in models of CIBP would prove extremely valuable (not further pursued in this thesis due to time constraints). Thus, any possible DNIC effects on primary afferent responsiveness remain to be further explored, with the results presented here serving as a first step in a battery of experiments focusing on unveiling the underpinning mechanisms of pain processing not only in health but also in disease.

5.6. Summary

To recapitulate, the data evidence the expression of a functional DNIC circuit in both female and male mice. The output of this circuit is compromised in a mouse model of CIBP and its activation has no effect on whole level primary afferent neuronal activity at a somatic level. These results demonstrate shared inter-species mechanisms with previously characterised rat models, improving our understanding of sensorimotor modulation in health and disease and allowing for potential therapeutic targets to be ultimately revealed.

CHAPTER

GENERAL DISCUSSION

6.1. Clinical value of CIBP models

This thesis largely focused on characterising spinal nociceptive processing in both health and disease using rodent models of cancer-induced bone pain (CIBP) at different stages of tumour growth. Considering sexual dimorphism and circulating hormones as crucial biological variables, I began by investigating the functionality of a modulatory pathway, diffuse noxious inhibitory controls (DNIC), in healthy naïve female rats (previously characterised in healthy male rats) (Bannister et al., 2015; Kucharczyk et al., 2023). A lack of impact of the oestrous cycle on DNIC expression correlated with studies from the human literature where a paradigm proposed to elicit a proxy measure of DNIC, so called conditioned pain modulation (CPM), also shows no difference in terms of expression patterns along the menstrual cycle in the majority (Bartley and Rhudy, 2012; Palit et al., 2016; Rezaii and Ernberg, 2010; Teepker et al., 2014; Vollert et al., 2022; Wilson et al., 2013), but not all (Rezaii et al., 2012; Tousignant-Laflamme and Marchand, 2009) studies.

Previous data demonstrated that the descending control of nociception (DCN), a measure of a behavioural response to a conditioning stimulus in wakeful animals, is weaker in females compared to males (Da Silva et al., 2018; Da Silva et al., 2020), with human studies also showing a slight tendency for CPM to be stronger in the male population (Popescu et al., 2010; Staud et al., 2003; see also Hermans et al., 2016). Interestingly, I observed no difference in DNIC expression between healthy naïve female and male mice, and so while the circulating hormonal and/or sex effects observed in wakeful animals (DCN) and humans (CPM) may not rely on a cellular spinal mechanism, it may be associated with sex-inferred cognitive-influenced differences in the processing of nociceptive information (Martin et al., 2019; see also Mogil, 2020) when a conditioning stimulus is applied. Further research is required for this to be addressed properly.

Having characterised DNIC expression patterns in healthy naïve rats (female) and mice (male and female), I investigated its function in CIBP animals. Expanding the previous results reported in CIBP male rats (Kucharczyk, Derrien et al., 2020), I evidenced dynamic DNIC expression in CIBP female rats following mammary gland adenocarcinoma cell implantation, characterised by a progressive bone degeneration and pain-like behavioural phenotype. Moreover, using an epidermoid lung carcinoma cell line (i.e., not sex-restricted), I observed the same pattern of DNIC expression in CIBP female and male mice, with corresponding progressive bone degeneration and behavioural hypersensitivity. Having

defined the function of a modulatory circuit in healthy animals as well as in rat (female) and mouse (female and male) models of CIBP at different stages of disease, I next investigated the effect of cancer cell ablation on DNIC expression patterns in female rats. My tumour cell targeting strategy resulted in cessation of advancing bone degeneration and pain-like behavioural phenotypes in the animals tested, and also highlighted how the peripheral nervous system, as per its output from the tumour dwelling bone to the central nervous system, impacts central modulatory circuits, evidenced by the extended abolishment of DNIC expression.

The precise molecular mechanisms that underpin the transient loss of DNIC observed in the CIBP model are yet to be determined. Since we know that, in health, reciprocity between the locus coeruleus and A5 nucleus permits functional DNIC (Kucharczyk et al., 2022; Kucharczyk et al., 2023), this transient loss may involve plastic changes that lead to maladaptive coerulean-A5 communication. This plasticity would correlate with clinical functional magnetic resonance imaging (fMRI) studies in which cancer patients suffering from CIBP showed altered functional activity and connectivity in different brain areas including the prefrontal cortex and the thalamus (Liu, Zhou et al., 2022; Zhou, Tan et al., 2022), which are connected to and affected by the coerulean system (Kaushal et al., 2016; Voisin et al., 2005). Upon tumour growth ablation, the extended time for which DNIC is dysfunctional could be linked to peripheral and central nervous system communication, which drives maladaptivity in a bottom-up fashion. Both are entirely discrete mechanisms that must be explored, bringing the importance of timing when it comes to targeted cancer therapy to the fore (Cone et al., 2020; Gonçalves et al., 2023; van Maaren et al., 2017).

The next set of experiments that I performed laid the foundation for future research investigating the role of peripheral and central nervous system communication in terms of pain development in CIBP, where tumour growth, neurogenic inflammation, and primary afferent responsiveness are all likely to be involved. I characterised the effect of DNIC on primary afferent activity in naïve female and male mice, demonstrating that application of a conditioning stimulus did not impact whole level dorsal root ganglion (DRG) neuronal activity. Many experiments should follow this preliminary effort such that the impact of DNIC on, for example, primary afferent spinal relays, in the progression of CIBP can be understood.

In sum, improving our understanding of the mechanisms underpinning CIBP is important since it remains poorly controlled in nearly half of all sufferers (Breivik et al., 2009; Deandrea et al., 2008), presenting itself as a combination of background pain (ongoing pain that can be successfully controlled with traditional analgesics) and/or breakthrough pain (exacerbation of pain that 'breaks through' the analgesic regimen) (Davies et al., 2013; Deandrea et al., 2014; Gonella et al., 2019). Commonly, prescribed drugs for ongoing cancer pain follow the 3-step system proposed by the World Health Organization (WHO), which heavily rely on opioids (e.g., morphine, oxycodone) making them the mainstay of treatment for numerous patients (Maltoni et al., 2005; Sulistio et al., 2021; see also Fielding et al., 2013). This situation, together with maximising symptom relief and a wide availability of analgesic drugs, has created a more relaxed prescription pattern driving, ultimately, to a scenario whereby opioids became synonymous with pain management, playing an obvious role in the opioid epidemic (see Vadivelu et al., 2018). However, opioid pain relief does not mechanistically target the cause of the pain, presenting numerous adverse effects and high addictive potential (Doyle et al., 2023; Kallupi et al., 2020), evidencing the need for mechanistically targeted analgesics and cancer treatments to be revealed, which would improve immensely cancer patients' quality of life.

6.2. Experimental limitations

6.2.1. Behavioural testing

Behavioural tests offer highly informative cognitive-influenced outputs in relevant animal models. Due to their partially subjective nature and susceptibility to environmental influences, multi-dimensional precautions while measuring manifestations of pain with behavioural paradigms should include group housing (to avoid isolation) (Han et al., 2016; Tuboly et al., 2009), minimal noise (Bulduk and Canbeyli, 2004; Voipio et al., 2006) and odours (Aloisi et al., 2002; de Almeida et al., 2004; Nakashima et al., 2004), researcher/equipment familiarity (Bigelow et al., 2023; Segelcke et al., 2023), and correct researcher manipulation technique (Gouveia and Hurst, 2019; Kylie et al., 2023). I ensured that each of these aspects were carefully attended to as well as employing a grouping strategy whereby each cage exclusively housed animals from the same experimental group to prevent 'pain' transfer between animals from different experimental conditions (empathy-like mechanism) (Andraka et al., 2021; Li et al., 2014; Lu et al., 2018).

6.2.2. Micro-computed tomography

Micro-computed tomography (μCT) is a very useful X-ray-based three-dimensional non-destructive imaging method that provides valuable internal and external morphometric information from biological samples. If longitudinal, the radiation received by animals undergoing this imaging process should be carefully considered during *in vivo* studies, especially in oncological ones, where the high amounts of radiation could interfere with tumour progression (Cowey et al., 2007; Johnson et al., 2011). To avoid this, the experiments presented in this thesis used fixed *ex vivo* tibial samples collected from animals following *in vivo* spinal cord electrophysiology. However, animal weight should be taken into consideration as it was dictated by electrophysiological requirements, which could mask or evidence small differences between samples due to slightly different animal ages (Beaucage et al., 2016; Fukuda and Iida, 2004; Jast and Jasiuk, 2013; Shim et al., 2022).

6.2.3. *In vivo* spinal cord electrophysiology

In vivo spinal cord electrophysiology is a powerful technique that allows for an objective assessment of spinal neuronal responses where convergent deep dorsal horn wide-dynamic range (WDR) neurons exhibit great sensitivity to small differences in stimulus intensity, showing many analogies with human pain score results (Cummins et al., 2020; Patel et al., 2024; Sikandar et al., 2013). However, it is important to acknowledge that WDR neurons are not representative of the whole spinal neuronal population and that neurons exhibiting elevated spontaneous firing and/or extreme evoked responses were often discarded, as these typically fail to stabilise and, in most cases, depolarise or burst. Additionally, despite isoflurane anaesthesia showing minimal effects on evoked WDR responses at low concentrations (Barter et al., 2009; Jinks, Antognini, and Carstens, 2003; Kim, Yao et al., 2007), it can significantly reduce spinal neuronal excitability (Cuellar et al., 2005; Kim, Atherley et al., 2007) and DNIC expression (Jinks, Martin et al., 2003) at medium-high concentrations. Thus, isoflurane was individually tailored to the minimum concentration needed to achieve areflexia in each animal and was additionally mixed with nitrous oxide, reducing the need for isoflurane even further (Santos et al., 2005; Stevens et al., 1975).

6.2.4. *In vivo* dorsal root ganglion calcium imaging

In vivo calcium imaging is a valuable technique that has significantly improved large cell populational studies, enabling the investigation of collective firing patterns in neuronal matrices even in freely moving animals (Wirtshafter and Disterhoft, 2022; Zong et al., 2022). However, calcium indicators offer a lower temporal resolution when compared to electrophysiological recordings as they are an indirect measurement of electrical activity, creating a potential window for information loss (Rahmati et al., 2016; Wei et al., 2020). Generally, any attempt to improve the temporal resolution of calcium indicators has translated into lower calcium affinities, although some new studies are trying to bridge these gaps (Zhang, Rózsa et al., 2023). Additionally, anaesthesia can affect cell properties during *in vivo* calcium imaging, with isoflurane reducing primary afferent excitability (Kameyama et al., 1999; Nakahiro et al., 1989). Thus, throughout all calcium recordings, isoflurane was reduced to the minimum concentration needed to achieve areflexia in each animal and was additionally mixed with urethane to achieve a more stable anaesthesia, limiting isoflurane levels (Bauquier and Golder, 2010).

6.3. Future directions

Differential coding properties between the deep WDR neurons characterised in this thesis and their superficial laminae counterparts is likely in the CIBP model (Donovan-Rodriguez et al., 2004; Donovan-Rodriguez et al., 2005). Thus, in healthy rats and mice, recordings that characterise superficial WDR activity upon DNIC circuit activation would be highly informative, allowing for direct comparisons between deep and superficial WDR responses and modulatory actions. These inter-laminar comparisons in health could be expanded with a deep characterisation of WDR evoked responses and DNIC expression in CIBP animals during both disease progression and regression (with characterisation of CIBP mice following cancer cell ablation still lacking). These studies could pose some technical difficulties since, when compared to deeper laminae residing WDR neurons, superficial WDR neurons are reduced in number, show smaller evoked responses, and offer a more challenging stabilization (Seagrove et al., 2004), complicating long term pharmacological studies.

In addition to the inter-laminar electrophysiological comparisons, identifying the mechanisms driving DNIC dysfunctionality in the CIBP model during cancer progression and following cancer ablation are critical for clinically relevant targets to be uncovered. Importantly, the recently revealed crosstalk

between the locus coeruleus and the DNIC circuitry (e.g., A5 nucleus) and an overriding coerulean effect upon DNIC expression (Kucharczyk et al., 2023) improves our understanding of pain processing in health (crucial before focussing on processing in disease) and offers a base on which to build our knowledge of brainstem mechanisms in CIBP. Thus, studies including optogenetic coerulean manipulation at timepoints at which DNIC expression is known to be dysfunctional could evidence mechanisms that underpin the pain phenotype.

With ongoing and breakthrough pain being clinically relevant CIBP symptoms (Laird et al., 2011; Scarpi et al., 2014), behavioural studies are focusing on finding better indicators of overall animal welfare that could be used as markers of ongoing and/or breakthrough pain. For such markers to be revealed in the CIBP animal model, home-cage monitoring systems could prove highly informative as they support long-term tracking and data analysis on group-housed animals, which could evidence alterations in diverse parameters during disease progression and/or regression, including locomotor activity, isolation, mobility, burrowing, and rearing (Hasriadi et al., 2021; Urban et al., 2011; Yip et al., 2019). Moreover, to achieve a deeper understanding of the mechanisms driving the 'residual' pain-like phenotype after successful cancer cell ablation, peripheral alterations affecting primary afferent responses should be studied. Thus, investigating primary afferent sprouting by selectively marking bone marrow- and periosteum-innervating primary afferents would be a great addition to further characterise the model (Thai et al., 2020).

In vivo DRG calcium imaging could be performed in CIBP animals allowing for the exploration of augmented primary afferent sensitivity (Zhu et al., 2016) and/or the recruitment of silent nociceptors (Kucharczyk, Chisholm et al., 2020) during disease progression and regression. Any differential DNIC effects upon primary afferent responsiveness and peripheral barrage should be studied attending to the fibre type in the cancer model. If the impact of DNIC activation is only to alter the primary afferent spinal relay with no impact on the sensory neuron soma, calcium imaging at the entrance level of the dorsal root in the spinal cord would allow calcium flux in primary afferent axons to be measured and could be used as a proxy measure of presynaptic activity allowing for this modulation to be revealed (Broussard et al., 2018; Warwick et al., 2022). Complementary experiments to assess whether DNIC impacts primary afferent activity could include individual teased primary afferent electrophysiological characterisations (Goodwin et al., 2020; Satkeviciute et al., 2018) during opto-manipulation of the DNIC circuitry (e.g., A5

nucleus) or the locus coeruleus, studying the electrical properties of different fibre types and dorsal root reflexes during health and disease progression/regression.

Finally, characterising how clinically relevant therapies affect the CIBP model would prove extremely valuable. Radiotherapy stands as one of the most effective treatments in patients suffering from CIBP, showing pain relief even after one unique session (Chow et al., 2017; Chow et al., 2019; Sze et al., 2003). Thus, the addition of a radiotherapy group in which CIBP animals undergo radiating sessions could show whether radiotherapy also leads to the expanded DNIC dysfunctionality observed after cancer cell ablation, linking these results to any changes in pain-like phenotypes and allowing for direct inter-group comparisons.

6.4. Closing remarks

Cancer incidence is rapidly growing, with new cases estimated to reach nearly 30 million during 2040 (Sung et al., 2021). While these numbers reflect the growth of the aging global population, cancer deaths are themselves declining, with more patients achieving complete curative treatment. This scenario is intrinsically linked to an increase in pain prevalence, one of the most common symptoms in cancer patients during both disease progression and remission. The studies outlined here support the importance of revealing the underpinning processes that drive descending pain modulation dysfunctionality during cancer progression and regression. Identifying novel markers and mechanisms would allow for mechanistically targeted analgesics to be revealed and tailored pain relief to be achieved.

CHAPTER

REFERENCES

Abdulla, A., Adams, N., Bone, M., Elliott, A.M., Gaffin, J., Jones, D., Knaggs, R., Martin, D., Sampson, L., Schofield, P., & British Geriatric Society (2013). Guidance on the management of pain in older people. *Age and Ageing*, *42*, i1-i57.

Abrahamsen, B., Zhao, J., Asante, C.O., Cendan, C.M., Marsh, S., Martinez-Barbera, J.P., Nassar, M.A., Dickenson, A.H., & Wood, J.N. (2008). The cell and molecular basis of mechanical, cold, and inflammatory pain. *Science*, *321*, 702-705.

Aicher, S.A., Hermes, S.M., Whittier, K.L., & Hegarty, D.M. (2012). Descending projections from the rostral ventromedial medulla (RVM) to trigeminal and spinal dorsal horns are morphologically and neurochemically distinct. *Journal of Chemical Neuroanatomy*, *43*, 103-111.

Aimone, L.D., & Gebhart, G.F. (1986). Stimulation-produced spinal inhibition from the midbrain in the rat is mediated by an excitatory amino acid neurotransmitter in the medial medulla. *The Journal of Neuroscience*, *6*, 1803-1813.

Albisetti, G.W., Ganley, R.P., Pietrafesa, F., Werynska, K., Magalhaes de Sousa, M., Sipione, R., Scheurer, L., Bösl, M.R., Pelczar, P., Wildner, H., & Zeilhofer, H.U. (2023). Inhibitory Kcnip2 neurons of the spinal dorsal horn control behavioral sensitivity to environmental cold. *Neuron*, *111*, 92-105.e5.

Albu, S., Gómez-Soriano, J., Avila-Martin, G., & Taylor, J. (2015). Deficient conditioned pain modulation after spinal cord injury correlates with clinical spontaneous pain measures. *Pain*, *156*, 260-272.

Alessio, N., Belardo, C., Trotta, M.C., Paino, S., Boccella, S., Gargano, F., Pieretti, G., Ricciardi, F., Marabese, I., Luongo, L., Galderisi, U., D'Amico, M., Maione, S., & Guida, F. (2021). Vitamin D deficiency induces chronic pain and microglial phenotypic changes in mice. *International Journal of Molecular Sciences*, *22*, 3604.

Al-Khater, K.M., & Todd, A.J. (2009). Collateral projections of neurons in laminae I, III, and IV of rat spinal cord to thalamus, periaqueductal gray matter, and lateral parabrachial area. *The Journal of Comparative Neurology*, *515*, 629-646.

Alles, S.R.A., & Smith, P.A. (2018). Etiology and pharmacology of neuropathic pain. *Pharmacological Reviews*, *70*, 315-347.

Almeida, T.F., Roizenblatt, S., & Tufik, S. (2004). Afferent pain pathways: a neuroanatomical review. *Brain Research*, *1000*, 40-56.

Aloisi, A.M., Ceccarelli, I., Masi, F., & Scaramuzzino, A. (2002). Effects of the essential oil from citrus lemon in male and female rats exposed to a persistent painful stimulation. *Behavioural Brain Research*, *136*, 127-135.

An, X., Bandler, R., Ongür, D., & Price, J.L. (1998). Prefrontal cortical projections to longitudinal columns in the midbrain periaqueductal gray in macaque monkeys. *The Journal of Comparative Neurology*, *401*, 455-479.

Andraka, K., Kondrakiewicz, K., Rojek-Sito, K., Ziegart-Sadowska, K., Meyza, K., Nikolaev, T., Hamed, A., Kursa, M., Wójcik, M., Danielewski, K., Wiatrowska, M., Kublik, E., Bekisz, M., Lebitko, T., Duque, D., Jaworski, T., Madej, H., Konopka, W., Boguszewski, P.M., & Knapska, E. (2021). Distinct circuits in rat central amygdala for defensive behaviors evoked by socially signaled imminent versus remote danger. *Current Biology*, *31*, 2347-2358.

Apkarian, A.V., Bushnell, M.C., Treede, R.D., & Zubieta, J.K. (2005). Human brain mechanisms of pain perception and regulation in health and disease. *European Journal of Pain*, *9*, 463-484.

Apkarian, A.V., & Hodge, C.J. (1989). Primate spinothalamic pathways: II. The cells of origin of the dorsolateral and ventral spinothalamic pathways. *The Journal of Comparative Neurology*, *288*, 474-492.

Appel, C.K., Gallego-Pedersen, S., Andersen, L., Blancheflor Kristensen, S., Ding, M., Falk, S., Sayilekshmy, M., Gabel-Jensen, C., & Heegaard, A.M. (2017). The Src family kinase inhibitor dasatinib delays pain-related behaviour and conserves bone in a rat model of cancer-induced bone pain. *Scientific Reports*, *7*, 4792.

Arora, V., Morado-Urbina, C.E., Gwak, Y.S., Parker, R.A., Kittel, C.A., Munoz-Islas, E., Miguel Jimenez-Andrade, J., Romero-Sandoval, E.A., Eisenach, J.C., & Peters, C.M. (2021). Systemic administration of a β2-adrenergic receptor agonist reduces mechanical allodynia and suppresses the immune response to surgery in a rat model of persistent post-incisional hypersensitivity. *Molecular Pain*, *17*, 1744806921997206.

Asano, T., Dohi, S., Ohta, S., Shimonaka, H., & Iida, H. (2000). Antinociception by epidural and systemic alpha(2)-adrenoceptor agonists and their binding affinity in rat spinal cord and brain. *Anesthesia and Analgesia*, *90*, 400-407.

Bahney, J., & von Bartheld, C.S. (2018). The cellular composition and glia-neuron ratio in the spinal cord of a human and a nonhuman primate: comparison with other species and brain regions. *Anatomical Record*, *301*, 697-710.

Bajic, D., & Proudfit, H.K. (1999). Projections of neurons in the periaqueductal gray to pontine and medullary catecholamine cell groups involved in the modulation of nociception. *The Journal of Comparative Neurology*, *405*, 359-379.

Balood, M., Ahmadi, M., Eichwald, T., Ahmadi, A., Majdoubi, A., Roversi, K., Roversi, K., Lucido, C.T., Restaino, A.C., Huang, S., Ji, L., Huang, K.C., Semerena, E., Thomas, S.C., Trevino, A.E., Merrison, H., Parrin, A., Doyle, B., Vermeer, D.W., Spanos, W.C., … Talbot, S. (2022). Nociceptor neurons affect cancer immunosurveillance. *Nature*, *611*, 405-412.

Bannister, K. (2019). Descending pain modulation: influence and impact. *Current Opinion in Physiology*, *11*, 62-66.

Bannister, K., & Hughes, S. (2023). One size does not fit all: towards optimising the therapeutic potential of endogenous pain modulatory systems. *Pain*, *164*, e5-e9.

Bannister, K., Kucharczyk, M.W., Graven-Nielsen, T., & Porreca, F. (2021). Introducing descending control of nociception: a measure of diffuse noxious inhibitory controls in conscious animals. *Pain*, *162*, 1957-1959.

Bannister, K., Lockwood, S., Goncalves, L., Patel, R., & Dickenson, A.H. (2017). An investigation into the inhibitory function of serotonin in diffuse noxious inhibitory controls in the neuropathic rat. *European Journal of Pain*, *21*, 750-760.

Bannister, K., Patel, R., Goncalves, L., Townson, L., & Dickenson, A.H. (2015). Diffuse noxious inhibitory controls and nerve injury: restoring an imbalance between descending monoamine inhibitions and facilitations. *Pain*, *156*, 1803-1811.

Bardoni, R., Takazawa, T., Tong, C.K., Choudhury, P., Scherrer, G., & Macdermott, A.B. (2013). Pre- and postsynaptic inhibitory control in the spinal cord dorsal horn. *Annals of the New York Academy of Sciences*, *1279*, 90-96.

Barrett, A.C., Smith, E.S., & Picker, M.J. (2002). Sex-related differences in mechanical nociception and antinociception produced by mu- and kappa-opioid receptor agonists in rats. *European Journal of Pharmacology*, *452*, 163-173.

Barrière, D.A., Midavaine, É., Doré-Savard, L., Kirby, K., Tremblay, L., Beaudoin, J.F., Beaudet, N., Longpré, J.M., Lecomte, R., Lepage, M., & Sarret, P. (2019). Dichotomic effects of clinically used drugs on tumor growth, bone remodeling and pain management. *Scientific Reports*, *9*, 20155.

Barron, D.H., & Matthews, B.H. (1935). Intermittent conduction in the spinal cord. *The Journal of Physiology*, *85*, 73-103.

Barter, L.S., Carstens, E.E., Jinks, S.L., & Antognini, J.F. (2009). Rat dorsal horn nociceptive-specific neurons are more sensitive than wide dynamic range neurons to depression by immobilizing doses of volatile anesthetics: an effect partially reversed by the opioid receptor antagonist naloxone. *Anesthesia and Analgesia*, *109*, 641-647.

Bartley, E.J., & Rhudy, J.L. (2012). Endogenous inhibition of the nociceptive flexion reflex (NFR) and pain ratings during the menstrual cycle in healthy women. *Annals of Behavioral Medicine*, *43*, 343-351.

Basbaum, A.I., Bautista, D.M., Scherrer, G., & Julius, D. (2009). Cellular and molecular mechanisms of pain. *Cell*, *139*, 267-284.

Bauquier, S.H., & Golder, F.J. (2010). The effects of urethane on the isoflurane minimum alveolar concentration in rats. *Laboratory Animals*, *44*, 323-328.

Bayne, T., Brainard, D., Byrne, R.W., Chittka, L., Clayton, N., Heyes, C., Mather, J., Ölveczky, B., Shadlen, M., Suddendorf, T., & Webb, B. (2019). What is cognition?. *Current Biology*, *29*, R608-R615.

Beaucage, K.L., Pollmann, S.I., Sims, S.M., Dixon, S.J., & Holdsworth, D.W. (2016). Quantitative *in vivo* micro-computed tomography for assessment of age-dependent changes in murine whole-body composition. *Bone Reports*, *5*, 70-80.

Becker, J.B., Prendergast, B.J., & Liang, J.W. (2016). Female rats are not more variable than male rats: a meta-analysis of neuroscience studies. *Biology of Sex Differences*, *7*, 34.

Beery, A.K. (2018). Inclusion of females does not increase variability in rodent research studies. *Current Opinion in Behavioral Sciences*, *23*, 143-149.

Behbehani, M.M., Park, M.R., & Clement, M.E. (1988). Interactions between the lateral hypothalamus and the periaqueductal gray. *The Journal of Neuroscience*, *8*, 2780-2787.

Benarroch, E.E. (2012). Periaqueductal gray: an interface for behavioral control. *Neurology*, *78*, 210-217.

Benarroch, E.E. (2015). Ion channels in nociceptors: recent developments. *Neurology*, *84*, 1153-1164.

Bennett, D.L., Clark, A.J., Huang, J., Waxman, S.G., & Dib-Hajj, S.D. (2019). The role of voltage-gated sodium channels in pain signaling. *Physiological Reviews*, *99*, 1079-1151.

Bennett, M.J., & Eisenberg, D. (1994). Refined structure of monomeric diphtheria toxin at 2.3 A resolution. *Protein Science*, *3*, 1464-1475.

Berlucchi, G. (1999). Some aspects of the history of the law of dynamic polarization of the neuron. From William James to Sherrington, from Cajal and van Gehuchten to Golgi. *Journal of the History of the Neurosciences*, *8*, 191-201.

Biermann, J.S., Adkins, D.R., Agulnik, M., Benjamin, R.S., Brigman, B., Butrynski, J.E., Cheong, D., Chow, W., Curry, W.T., Frassica, D.A., Frassica, F.J., Hande, K.R., Hornicek, F.J., Jones, R.L., Mayerson, J., McGarry, S.V., McGrath, B., Morris, C.D., O'Donnell, R.J., Randall, R.L., … National comprehensive cancer network (2013). Bone cancer. *Journal of the National Comprehensive Cancer Network*, *11*, 688-723.

Bigelow, L.J., Pope, E.K., MacDonald, D.S., Rock, J.E., & Bernard, P.B. (2023). Getting a handle on rat familiarization: The impact of handling protocols on classic tests of stress in *Rattus norvegicus*. *Laboratory Animals*, *57*, 259-269.

Blanca, M.J., Alarcón, R., Arnau, J., Bono, R., & Bendayan, R. (2017). Non-normal data: is ANOVA still a valid option?. *Psicothema*, *29*, 552-557.

Blanca, M.J., Arnau, J., García-Castro, F.J., Alarcón, R., & Bono, R. (2023). Non-normal data in repeated measures ANOVA: impact on type I error and power. *Psicothema*, *35*, 21-29.

Blyth, F.M., March, L.M., Nicholas, M.K., & Cousins, M.J. (2005). Self-management of chronic pain: a population-based study. *Pain*, *113*, 285-292.

Boureau, F., Doubrère, J.F., & Luu, M. (1990). Study of verbal description in neuropathic pain. *Pain*, *42*, 145-152.

Bowker, R.M., Westlund, K.N., & Coulter, J.D. (1981). Origins of serotonergic projections to the spinal cord in rat: an immunocytochemical-retrograde transport study. *Brain Research*, *226*, 187-199.

Bowker, R.M., Westlund, K.N., & Coulter, J.D. (1982). Origins of serotonergic projections to the lumbar spinal cord in the monkey using a combined retrograde transport and immunocytochemical technique. *Brain Research Bulletin*, *9*, 271-278.

Boyer, N., Signoret-Genest, J., Artola, A., Dallel, R., & Monconduit, L. (2017). Propranolol treatment prevents chronic central sensitization induced by repeated dural stimulation. *Pain*, *158*, 2025-2034.

Brain, K., Burrows, T.L., Rollo, M.E., Chai, L.K., Clarke, E.D., Hayes, C., Hodson, F.J., & Collins, C.E. (2019). A systematic review and meta-analysis of nutrition interventions for chronic noncancer pain. *Journal of Human Nutrition and Dietetics*, *32*, 198-225.

Breivik, H., Cherny, N., Collett, B., de Conno, F., Filbet, M., Foubert, A.J., Cohen, R., & Dow, L. (2009). Cancer-related pain: a pan-European survey of prevalence, treatment, and patient attitudes. *Annals of oncology*, *20*, 1420-1433.

Brescia, F.J., Portenoy, R.K., Ryan, M., Krasnoff, L., & Gray, G. (1992). Pain, opioid use, and survival in hospitalized patients with advanced cancer. *Journal of Clinical Oncology*, *10*, 149-155.

Brignell, J.L., Chapman, V., & Kendall, D.A. (2008). Comparison of icilin- and cold-evoked responses of spinal neurones, and their modulation of mechanical activity, in a model of neuropathic pain. *Brain Research*, *1215*, 87-96.

Broussard, G.J., Liang, Y., Fridman, M., Unger, E.K., Meng, G., Xiao, X., Ji, N., Petreanu, L., & Tian, L. (2018). *In vivo* measurement of afferent activity with axon-specific calcium imaging. *Nature Neuroscience*, *21*, 1272-1280.

Brown, M., & Farquhar-Smith, P. (2017). Pain in cancer survivors; filling in the gaps. *British journal of anaesthesia*, *119*, 723-736.

Bruinstroop, E., Cano, G., Vanderhorst, V.G., Cavalcante, J.C., Wirth, J., Sena-Esteves, M., & Saper, C.B. (2012). Spinal projections of the A5, A6 (locus coeruleus), and A7 noradrenergic cell groups in rats. *The Journal of Comparative Neurology*, *520*, 1985-2001.

Bruno, G., De Logu, F., Souza Monteiro de Araujo, D., Subbiani, A., Lunardi, F., Rettori, S., Nassini, R., Favre, C., & Calvani, M. (2021). β2-and β3-adrenergic receptors contribute to cancer-evoked pain in a mouse model of osteosarcoma via modulation of neural macrophages. *Frontiers in Pharmacology*, *12*, 697912.

Bryan, R.N., Coulter, J.D., & Willis, W.D. (1974). Cells of origin of the spinocervical tract in the monkey. *Experimental Neurology*, *42*, 574-586.

Buch, T., Heppner, F.L., Tertilt, C., Heinen, T.J., Kremer, M., Wunderlich, F.T., Jung, S., & Waisman, A. (2005). A Cre-inducible diphtheria toxin receptor mediates cell lineage ablation after toxin administration. *Nature Methods*, *2*, 419-426.

Buhle, J.T., Kober, H., Ochsner, K.N., Mende-Siedlecki, P., Weber, J., Hughes, B.L., Kross, E., Atlas, L.Y., McRae, K., & Wager, T.D. (2013). Common representation of pain and negative emotion in the midbrain periaqueductal gray. *Social Cognitive and Affective Neuroscience*, *8*, 609-616.

Bulduk, S., & Canbeyli, R. (2004). Effect of inescapable tones on behavioral despair in Wistar rats. *Progress in Neuro-psychopharmacology & Biological Psychiatry*, *28*, 471-475.

Burma, N.E., Leduc-Pessah, H., Fan, C.Y., & Trang, T. (2017). Animal models of chronic pain: advances and challenges for clinical translation. *Journal of Neuroscience Research*, *95*, 1242-1256.

Burnett, A., & Gebhart, G.F. (1991). Characterization of descending modulation of nociception from the A5 cell group. *Brain Research*, *546*, 271-281.

Burstein, R., Cliffer, K.D., & Giesler, G.J. (1987). Direct somatosensory projections from the spinal cord to the hypothalamus and telencephalon. *The Journal of Neuroscience*, *7*, 4159-4164.

Burstein, R., Cliffer, K.D., & Giesler, G.J. (1990). Cells of origin of the spinohypothalamic tract in the rat. *The Journal of Comparative Neurology*, *291*, 329-344.

Burstein, R., Dado, R.J., Cliffer, K.D., & Giesler, G.J. (1991). Physiological characterization of spinohypothalamic tract neurons in the lumbar enlargement of rats. *Journal of Neurophysiology*, *66*, 261-284.

Byrum, C.E., & Guyenet, P.G. (1987). Afferent and efferent connections of the A5 noradrenergic cell group in the rat. *The Journal of Comparative Neurology*, *261*, 529-542.

Cabañero, D., Villalba-Riquelme, E., Fernández-Ballester, G., Fernández-Carvajal, A., & Ferrer-Montiel, A. (2022). ThermoTRP channels in pain sexual dimorphism: new insights for drug intervention. *Pharmacology & Therapeutics*, *240*, 108297.

Cadden, S.W. (1993). The ability of inhibitory controls to 'switch-off' activity in dorsal horn convergent neurones in the rat. *Brain Research*, *628*, 65-71.

Cain, D.M., Wacnik, P.W., Turner, M., Wendelschafer-Crabb, G., Kennedy, W.R., Wilcox, G.L., & Simone, D.A. (2001). Functional interactions between tumor and peripheral nerve: changes in excitability and morphology of primary afferent fibers in a murine model of cancer pain. *The Journal of Neuroscience*, *21*, 9367-9376.

Caraceni, A., & Shkodra, M. (2019). Cancer pain assessment and classification. *Cancers*, *11*, 510.

Castañeda-Corral, G., Jimenez-Andrade, J.M., Bloom, A.P., Taylor, R.N., Mantyh, W.G., Kaczmarska, M.J., Ghilardi, J.R., & Mantyh, P.W. (2011). The majority of myelinated and unmyelinated sensory nerve fibers that innervate bone express the tropomyosin receptor kinase A. *Neuroscience*, *178*, 196-207.

Cathcart, S., Winefield, A.H., Lushington, K., & Rolan, P. (2010). Noxious inhibition of temporal summation is impaired in chronic tension-type headache. *Headache*, *50*, 403-412.

Cavaletti, G., Alberti, P., Frigeni, B., Piatti, M., & Susani, E. (2011). Chemotherapy-induced neuropathy. *Current Treatment Options in Neurology*, *13*, 180-190.

Cechetto, D.F., Standaert, D.G., & Saper, C.B. (1985). Spinal and trigeminal dorsal horn projections to the parabrachial nucleus in the rat. *The Journal of Comparative Neurology*, *240*, 153-160.

Cedarbaum, J.M., & Aghajanian, G.K. (1978). Afferent projections to the rat locus coeruleus as determined by a retrograde tracing technique. *The Journal of Comparative Neurology*, *178*, 1-16.

Cervero, F., Iggo, A., & Molony, V. (1977). Responses of spinocervical tract neurones to noxious stimulation of the skin. *The Journal of Physiology*, *267*, 537-558.

Cha, J.H., Brooke, J.S., & Eidels, L. (1999). Hamster diphtheria toxin receptor: a naturally occurring chimera of monkey and mouse HB-EGF precursors. *Biochemical and biophysical research communications*, *254*, 325-329.

Chandar, K., & Freeman, B.K. (2014). Spinal cord anatomy. In M.J. Aminoff & B.D. Robert (Eds.), *Encyclopedia of the Neurological Sciences* (pp.254-263). Academic Press.

Chandler, D.J., Gao, W.J., & Waterhouse, B.D. (2014). Heterogeneous organization of the locus coeruleus projections to prefrontal and motor cortices. *Proceedings of the National Academy of Sciences of the United States of America*, *111*, 6816-6821.

Chang, M.P., Bramhall, J., Graves, S., Bonavida, B., & Wisnieski, B.J. (1989). Internucleosomal DNA cleavage precedes diphtheria toxin-induced cytolysis. Evidence that cell lysis is not a simple consequence of translation inhibition. *The Journal of Biological Chemistry*, *264*, 15261-15267.

Chen, J.T., Guo, D., Campanelli, D., Frattini, F., Mayer, F., Zhou, L., Kuner, R., Heppenstall, P.A., Knipper, M., & Hu, J. (2014). Presynaptic GABAergic inhibition regulated by BDNF contributes to neuropathic pain induction. *Nature Communications*, *5*, 5331.

Chen, L., Li, Y., Zhu, L., Jin, H., Kang, X., & Feng, Z. (2023). Single-cell RNA sequencing in the context of neuropathic pain: progress, challenges, and prospects. *Translational Research*, *251*, 96-103.

Chen, Q., & Heinricher, M.M. (2022). Shifting the balance: how top-down and bottom-up input modulate pain *via* the rostral ventromedial medulla. *Frontiers in Pain Research*, *3*, 932476.

Chen, Q., Roeder, Z., Li, M.H., Zhang, Y., Ingram, S.L., & Heinricher, M.M. (2017). Optogenetic evidence for a direct circuit linking nociceptive transmission through the parabrachial complex with pain-modulating neurons of the rostral ventromedial medulla (RVM). *eNeuro*, *4*, ENEURO.0202-17.2017.

Chen, S.P., Sun, J., Zhou, Y.Q., Cao, F., Braun, C., Luo, F., Ye, D.W., & Tian, Y.K. (2018). Sinomenine attenuates cancer-induced bone pain via suppressing microglial JAK2/STAT3 and neuronal CAMKII/CREB cascades in rat models. *Molecular Pain*, *14*, 1744806918793232.

Cheng, L., Duan, B., Huang, T., Zhang, Y., Chen, Y., Britz, O., Garcia-Campmany, L., Ren, X., Vong, L., Lowell, B.B., Goulding, M., Wang, Y., & Ma, Q. (2017). Identification of spinal circuits involved in touch-evoked dynamic mechanical pain. *Nature Neuroscience*, *20*, 804-814.

Chisholm, K.I., Khovanov, N., Lopes, D.M., La Russa, F., & McMahon, S.B. (2018). Large scale *in vivo* recording of sensory neuron activity with GCaMP6. *eNeuro*, *5*, ENEURO.0417-17.2018.

Chistyakov, D.V., Azbukina, N.V., Astakhova, A.A., Goriainov, S.V., Chistyakov, V.V., & Sergeeva, M.G. (2018). Sex-mediated differences in LPS induced alterations of TNFα, IL-10 expression, and prostaglandin synthesis in primary astrocytes. *International Journal of Molecular Sciences*, *19*, 2793.

Choi, I., Lee, J.Y., & Lee, S.H. (2018). Bottom-up and top-down modulation of multisensory integration. *Current Opinion in Neurobiology*, *52*, 115-122.

Chow, R., Hoskin, P., Hollenberg, D., Lam, M., Dennis, K., Lutz, S., Lam, H., Mesci, A., DeAngelis, C., Chan, S., & Chow, E. (2017). Efficacy of single fraction conventional radiation therapy for painful uncomplicated bone metastases: a systematic review and meta-analysis. *Annals of Palliative Medicine*, *6*, 125-142.

Chow, R., Hoskin, P., Schild, S.E., Raman, S., Im, J., Zhang, D., Chan, S., Chiu, N., Chiu, L., Lam, H., Chow, E., & Lock, M. (2019). Single vs multiple fraction palliative radiation therapy for bone metastases: Cumulative meta-analysis. *Radiotherapy and Oncology*, *141*, 56-61.

Christensen, B.N., & Perl, E.R. (1970). Spinal neurons specifically excited by noxious or thermal stimuli: marginal zone of the dorsal horn. *Journal of Neurophysiology*, *33*, 293-307.

Clark, F.M., & Proudfit, H.K. (1991). The projection of noradrenergic neurons in the A7 catecholamine cell group to the spinal cord in the rat demonstrated by anterograde tracing combined with immunocytochemistry. *Brain Research*, *547*, 279-288.

Clark, F.M., & Proudfit, H.K. (1993). The projections of noradrenergic neurons in the A5 catecholamine cell group to the spinal cord in the rat: anatomical evidence that A5 neurons modulate nociception. *Brain Research*, *616*, 200-210.

Coghill, R.C., Mayer, D.J., & Price, D.D. (1993). Wide dynamic range but not nociceptive-specific neurons encode multidimensional features of prolonged repetitive heat pain. *Journal of Neurophysiology*, *69*, 703-716.

Condés-Lara, M., Omaña Zapata, I., León-Olea, M., & Sánchez-Alvarez, M. (1989). Dorsal raphe and nociceptive stimulations evoke convergent responses on the thalamic centralis lateralis and medial prefrontal cortex neurons. *Brain Research*, *499*, 145-152.

Cone, E.B., Marchese, M., Paciotti, M., Nguyen, D.D., Nabi, J., Cole, A.P., Molina, G., Molina, R.L., Minami, C.A., Mucci, L.A., Kibel, A.S., & Trinh, Q.D. (2020). Assessment of time-to-treatment initiation and survival in a cohort of patients with common cancers. *JAMA Network Open*, *3*, e2030072.

Cortes-Altamirano, J.L., Olmos-Hernandez, A., Jaime, H.B., Carrillo-Mora, P., Bandala, C., Reyes-Long, S., & Alfaro-Rodríguez, A. (2018). Review: 5-HT1, 5-HT2, 5-HT3 and 5-HT7 receptors and their role in the modulation of pain response in the central nervous system. *Current Neuropharmacology*, *16*, 210-221.

Cowey, S., Szafran, A.A., Kappes, J., Zinn, K.R., Siegal, G.P., Desmond, R.A., Kim, H., Evans, L., & Hardy, R.W. (2007). Breast cancer metastasis to bone: evaluation of bioluminescent imaging and microSPECT/CT for detecting bone metastasis in immunodeficient mice. *Clinical & Experimental Metastasis*, *24*, 389-401.

Cox-Martin, E., Anderson-Mellies, A., Borges, V., & Bradley, C. (2020). Chronic pain, health-related quality of life, and employment in working-age cancer survivors. *Journal of Cancer Survivorship*, *14*, 179-187.

Cregg, R., Momin, A., Rugiero, F., Wood, J.N., & Zhao, J. (2010). Pain channelopathies. *The Journal of Physiology*, *588*, 1897-1904.

Cuellar, J.M., Dutton, R.C., Antognini, J.F., & Carstens, E. (2005). Differential effects of halothane and isoflurane on lumbar dorsal horn neuronal windup and excitability. *British Journal of Anaesthesia*, *94*, 617-625.

Cui, M., Feng, Y., McAdoo, D.J., & Willis, W.D. (1999). Periaqueductal gray stimulation-induced inhibition of nociceptive dorsal horn neurons in rats is associated with the release of norepinephrine, serotonin, and amino acids. *The Journal of Pharmacology and Experimental Therapeutics*, *289*, 868-876.

Cummins, T.M., Kucharczyk, M.M., Graven-Nielsen, T., & Bannister, K. (2020). Activation of the descending pain modulatory system using cuff pressure algometry: Back translation from man to rat. *European Journal of Pain*, *24*, 1330-1338.

Da Silva, J.T., Tricou, C., Zhang, Y., Seminowicz, D.A., & Ro, J.Y. (2020). Brain networks and endogenous pain inhibition are modulated by age and sex in healthy rats. *Pain*, *161*, 1371-1380.

Da Silva, J.T., Zhang, Y., Asgar, J., Ro, J.Y., & Seminowicz, D.A. (2018). Diffuse noxious inhibitory controls and brain networks are modulated in a testosterone-dependent manner in Sprague Dawley rats. *Behavioural Brain Research*, *349*, 91-97.

Dams, L., Van der Gucht, E., Meeus, M., Devoogdt, N., Smeets, A., Penen, F., De Baerdemaecker, T., Haenen, V., Bernar, K., De Vrieze, T., & De Groef, A. (2021). Quantitative sensory testing in women after surgery for breast cancer: a systematic review and narrative synthesis. *The Clinical Journal of Pain*, *37*, 538-564.

Davies, A., Buchanan, A., Zeppetella, G., Porta-Sales, J., Likar, R., Weismayr, W., Slama, O., Korhonen, T., Filbet, M., Poulain, P., Mystakidou, K., Ardavanis, A., O'Brien, T., Wilkinson, P., Caraceni, A., Zucco, F., Zuurmond, W., Andersen, S., Damkier, A., Vejlgaard, T., … Stenberg, M. (2013). Breakthrough cancer pain: an observational study of 1000 European oncology patients. *Journal of Pain and Symptom Management*, *46*, 619-628.

de Almeida, R.N., Motta, S.C., de Brito Faturi, C., Catallani, B., & Leite, J.R. (2004). Anxiolytic-like effects of rose oil inhalation on the elevated plus-maze test in rats. *Pharmacology, Biochemistry, and Behavior*, *77*, 361-364.

de Clauser, L., Luiz, A.P., Santana-Varela, S., Wood, J.N., & Sikandar, S. (2020). Sensitization of cutaneous primary afferents in bone cancer revealed by *in vivo* calcium imaging. *Cancers*, *12*, 3491.

de Groot, J., Zhou, S., & Carlton, S.M. (2000). Peripheral glutamate release in the hindpaw following low and high intensity sciatic stimulation. *Neuroreport*, *11*, 497-502.

Deandrea, S., Corli, O., Consonni, D., Villani, W., Greco, M.T., & Apolone, G. (2014). Prevalence of breakthrough cancer pain: a systematic review and a pooled analysis of published literature. *Journal of Pain and Symptom Management*, *47*, 57-76.

Deandrea, S., Montanari, M., Moja, L., & Apolone, G. (2008). Prevalence of undertreatment in cancer pain. A review of published literature. *Annals of Oncology*, *19*, 1985-1991.

DeLeo, J.A., & Rutkowski, M.D. (2000). Gender differences in rat neuropathic pain sensitivity is dependent on strain. *Neuroscience letters*, *282*, 197-199.

Della Pietra, A., Mikhailov, N., & Giniatullin, R. (2020). The emerging role of mechanosensitive Piezo channels in migraine pain. *International Journal of Molecular Sciences*, *21*, 696.

Diaz-delCastillo, M., Hansen, R.B., Appel, C.K., Nielsen, L., Nielsen, S.N., Karyniotakis, K., Dahl, L.M., Andreasen, R.B., & Heegaard, A.M. (2020). Modulation of rat cancer-induced bone pain is independent of spinal microglia activity. *Cancers*, *12*, 2740.

Dinakar, P., & Stillman, A.M. (2016). Pathogenesis of pain. *Seminars in Pediatric Neurology*, *23*, 201-208.

D'Mello, R., & Dickenson, A.H. (2008). Spinal cord mechanisms of pain. *British Journal of Anaesthesia*, *101*, 8-16.

Domenichiello, A.F., & Ramsden, C.E. (2019). The silent epidemic of chronic pain in older adults. *Progress in Neuro-psychopharmacology & Biological Psychiatry*, *93*, 284-290.

Dominick, C.H., Blyth, F.M., & Nicholas, M.K. (2012). Unpacking the burden: understanding the relationships between chronic pain and comorbidity in the general population. *Pain*, *153*, 293-304.

Dong, W.K., Salonen, L.D., Kawakami, Y., Shiwaku, T., Kaukoranta, E.M., & Martin, R.F. (1989). Nociceptive responses of trigeminal neurons in SII-7b cortex of awake monkeys. *Brain Research*, *484*, 314-324.

Donovan-Rodriguez, T., Dickenson, A.H., & Urch, C.E. (2004). Superficial dorsal horn neuronal responses and the emergence of behavioural hyperalgesia in a rat model of cancer-induced bone pain. *Neuroscience Letters*, *360*, 29-32.

Donovan-Rodriguez, T., Dickenson, A.H., & Urch, C.E. (2005). Gabapentin normalizes spinal neuronal responses that correlate with behavior in a rat model of cancer-induced bone pain. *Anesthesiology*, *102*, 132-140.

Donovan-Rodriguez, T., Urch, C.E., & Dickenson, A.H. (2006). Evidence of a role for descending serotonergic facilitation in a rat model of cancer-induced bone pain. *Neuroscience Letters*, *393*, 237-242.

Doré-Savard, L., Beaudet, N., Tremblay, L., Xiao, Y., Lepage, M., & Sarret, P. (2013). A micro-imaging study linking bone cancer pain with tumor growth and bone resorption in a rat model. *Clinical & Experimental Metastasis*, *30*, 225-236.

Doré-Savard, L., Otis, V., Belleville, K., Lemire, M., Archambault, M., Tremblay, L., Beaudoin, J.F., Beaudet, N., Lecomte, R., Lepage, M., Gendron, L., & Sarret, P. (2010). Behavioral, medical imaging and histopathological features of a new rat model of bone cancer pain. *PloS One*, *5*, e13774.

Doyle, M.R., Martinez, A.R., Qiao, R., Dirik, S., Di Ottavio, F., Pascasio, G., Martin-Fardon, R., Benner, C., George, O., Telese, F., & de Guglielmo, G. (2023). Strain and sex-related behavioral variability of oxycodone dependence in rats. *Neuropharmacology*, *237*, 109635.

Drake, R.A., Steel, K.A., Apps, R., Lumb, B.M., & Pickering, A.E. (2021). Loss of cortical control over the descending pain modulatory system determines the development of the neuropathic pain state in rats. *eLife*, *10*, e65156.

Dropcho, E.J. (2010). Neurotoxicity of radiation therapy. *Neurologic clinics*, *28*, 217-234.

Dubin, A.E., & Patapoutian, A. (2010). Nociceptors: the sensors of the pain pathway. *The Journal of Clinical Investigation*, *120*, 3760-3772.

Dubner, R., Kenshalo, D.R., Maixner, W., Bushnell, M.C., & Oliveras, J.L. (1989). The correlation of monkey medullary dorsal horn neuronal activity and the perceived intensity of noxious heat stimuli. *Journal of Neurophysiology*, *62*, 450-457.

Dupont, M., & Vosshenrich, C.A.J. (2019). Conditional genetic ablation mouse models as a tool to study cancer immunosurveillance *in vivo*. *Methods in Molecular Biology*, *1884*, 161-176.

Egli, M., Koob, G.F., & Edwards, S. (2012). Alcohol dependence as a chronic pain disorder. *Neuroscience and Biobehavioral Reviews*, *36*, 2179-2192.

Eide, P.K., & Hole, K. (1993). The role of 5-hydroxytryptamine (5-HT) receptor subtypes and plasticity in the 5-HT systems in the regulation of nociceptive sensitivity. *Cephalalgia*, *13*, 75-85.

Eliasson, P., & Jönsson, J.I. (2010). The hematopoietic stem cell niche: low in oxygen but a nice place to be. *Journal of Cellular Physiology*, *222*, 17-22.

Elliott, A.M., Smith, B.H., Hannaford, P.C., Smith, W.C., & Chambers, W.A. (2002). The course of chronic pain in the community: results of a 4-year follow-up study. *Pain*, *99*, 299-307.

Elzahaf, R.A., Tashani, O.A., Unsworth, B.A., & Johnson, M.I. (2012). The prevalence of chronic pain with an analysis of countries with a human development index less than 0.9: a systematic review without meta-analysis. *Current Medical Research and Opinion*, *28*, 1221-1229.

Eskander, M.A., Ruparel, S., Green, D.P., Chen, P.B., Por, E.D., Jeske, N.A., Gao, X., Flores, E.R., & Hargreaves, K.M. (2015). Persistent Nociception Triggered by Nerve Growth Factor (NGF) Is Mediated by TRPV1 and Oxidative Mechanisms. *The Journal of Neuroscience*, *35*, 8593-8603.

Fairbanks, C.A., Stone, L. S., & Wilcox, G.L. (2009). Pharmacological profiles of alpha 2 adrenergic receptor agonists identified using genetically altered mice and isobolographic analysis. *Pharmacology & Therapeutics*, *123*, 224-238.

Falk, S., Al-Dihaissy, T., Mezzanotte, L., & Heegaard, A.M. (2015). Effect of sex in the MRMT-1 model of cancer-induced bone pain. *F1000Research*, *4*, 445.

Falk, S., & Dickenson, A.H. (2014). Pain and nociception: mechanisms of cancer-induced bone pain. *Journal of Clinical Oncology*, *32*, 1647-1654.

Falk, S., Ipsen, D.H., Appel, C.K., Ugarak, A., Durup, D., Dickenson, A.H., & Heegaard, A.M. (2015). Randall Selitto pressure algometry for assessment of bone-related pain in rats. *European Journal of Pain*, *19*, 305-312.

Falk, S., Schwab, S.D., Frøsig-Jørgensen, M., Clausen, R.P., Dickenson, A.H., & Heegaard, A.M. (2015). P2X7 receptor-mediated analgesia in cancer-induced bone pain. *Neuroscience*, *291*, 93-105.

Falk, S., Uldall, M., Appel, C., Ding, M., & Heegaard, A.M. (2013). Influence of sex differences on the progression of cancer-induced bone pain. *Anticancer Research*, *33*, 1963-1969.

Fan, L.J., Kan, H.M., Chen, X.T., Sun, Y.Y., Chen, L.P., & Shen, W. (2022). Vascular endothelial growth factor-A/vascular endothelial growth factor2 signaling in spinal neurons contributes to bone cancer pain. *Molecular Pain*, *18*, 17448069221075891.

Faouzi, S., Burckhardt, B.E., Hanson, J.C., Campe, C.B., Schrum, L.W., Rippe, R.A., & Maher, J.J. (2001). Anti-Fas induces hepatic chemokines and promotes inflammation by an NF-kappa B-independent, caspase-3-dependent pathway. *The Journal of Biological Chemistry*, *276*, 49077-49082.

Fielding, F., Sanford, T.M., & Davis, M.P. (2013). Achieving effective control in cancer pain: a review of current guidelines. *International Journal of Palliative Nursing*, *19*, 584-591.

Fields, H.L., Bry, J., Hentall, I., & Zorman, G. (1983). The activity of neurons in the rostral medulla of the rat during withdrawal from noxious heat. *The Journal of Neuroscience*, *3*, 2545-2552.

Fields, H.L., Malick, A., & Burstein, R. (1995). Dorsal horn projection targets of ON and OFF cells in the rostral ventromedial medulla. *Journal of Neurophysiology*, *74*, 1742-1759.

Forsythe, L.P., Alfano, C.M., George, S.M., McTiernan, A., Baumgartner, K.B., Bernstein, L., & Ballard-Barbash, R. (2013). Pain in long-term breast cancer survivors: the role of body mass index, physical activity, and sedentary behavior. *Breast Cancer Research and Treatment*, *137*, 617-630.

Francis-Malavé, A.M., Martínez González, S., Pichardo, C., Wilson, T.D., Rivera-García, L.G., Brinster, L.R., & Carrasquillo, Y. (2023). Sex differences in pain-related behaviors and clinical progression of disease in mouse models of colonic pain. *Pain*, *164*, 197-215.

Frezel, N., Ranucci, M., Foster, E., Wende, H., Pelczar, P., Mendes, R., Ganley, R.P., Werynska, K., d'Aquin, S., Beccarini, C., Birchmeier, C., Zeilhofer, H. U., & Wildner, H. (2023). c-Maf-positive spinal cord neurons are critical elements of a dorsal horn circuit for mechanical hypersensitivity in neuropathy. *Cell Reports*, *42*, 112295.

Fu, Q., Shi, D., Zhou, Y., Zheng, H., Xiang, H., Tian, X., Gao, F., Manyande, A., Cao, F., Tian, Y., & Ye, D. (2016). MHC-I promotes apoptosis of GABAergic interneurons in the spinal dorsal horn and contributes to cancer induced bone pain. *Experimental Neurology*, *286*, 12-20.

Fuchs, P.N., Peng, Y.B., Boyette-Davis, J.A., & Uhelski, M.L. (2014). The anterior cingulate cortex and pain processing. *Frontiers in Integrative Neuroscience*, *8*, 35.

Fukuda, S., & Iida, H. (2004). Age-related changes in bone mineral density, cross-sectional area and the strength of long bones in the hind limbs and first lumbar vertebra in female Wistar rats. *The Journal of Veterinary Medical Science*, *66*, 755-760.

Gan, T.J. (2017). Poorly controlled postoperative pain: prevalence, consequences, and prevention. *Journal of Pain Research*, *10*, 2287-2298.

García-Ramírez, D.L., Calvo, J.R., Hochman, S., & Quevedo, J.N. (2014). Serotonin, dopamine and noradrenaline adjust actions of myelinated afferents via modulation of presynaptic inhibition in the mouse spinal cord. *PloS One*, *9*, e89999.

Garland, E.L. (2012). Pain processing in the human nervous system: a selective review of nociceptive and biobehavioral pathways. *Primary Care*, *39*, 561-571.

Gassner, M., Ruscheweyh, R., & Sandkühler, J. (2009). Direct excitation of spinal GABAergic interneurons by noradrenaline. *Pain*, *145*, 204-210.

Gaumond, I., Arsenault, P., & Marchand, S. (2002). The role of sex hormones on formalin-induced nociceptive responses. *Brain Research*, *958*, 139-145.

Gauriau, C., & Bernard, J.F. (2002). Pain pathways and parabrachial circuits in the rat. *Experimental Physiology*, *87*, 251-258.

Geertsen, S.S., Willerslev-Olsen, M., Lorentzen, J., & Nielsen, J.B. (2017). Development and aging of human spinal cord circuitries. *Journal of Neurophysiology*, *118*, 1133-1140.

Geneen, L.J., Moore, R.A., Clarke, C., Martin, D., Colvin, L.A., & Smith, B.H. (2017). Physical activity and exercise for chronic pain in adults: an overview of Cochrane Reviews. *The Cochrane Database of Systematic Reviews*, *4*, CD011279.

Geppert, J., Walth, A.A., Terrón Expósito, R., Kaltenecker, D., Morigny, P., Machado, J., Becker, M., Simoes, E., Lima, J.D.C.C., Daniel, C., Berriel Diaz, M., Herzig, S., Seelaender, M., & Rohm, M. (2021). Aging aggravates cachexia in tumor-bearing mice. *Cancers*, *14*, 90.

Gerhart, K.D., Yezierski, R.P., Wilcox, T.K., & Willis, W.D. (1984). Inhibition of primate spinothalamic tract neurons by stimulation in periaqueductal gray or adjacent midbrain reticular formation. *Journal of Neurophysiology*, *51*, 450-466.

Gill, D.M. (1982). Bacterial toxins: a table of lethal amounts. *Microbiological Reviews*, *46*, 86-94.

Gingold, S.I., Greenspan, J.D., & Apkarian, A.V. (1991). Anatomic evidence of nociceptive inputs to primary somatosensory cortex: relationship between spinothalamic terminals and thalamocortical cells in squirrel monkeys. *The Journal of Comparative Neurology*, *308*, 467-490.

Gobina, I., Villberg, J., Välimaa, R., Tynjälä, J., Whitehead, R., Cosma, A., Brooks, F., Cavallo, F., Ng, K., de Matos, M.G., & Villerusa, A. (2019). Prevalence of self-reported chronic pain among adolescents: evidence from 42 countries and regions. *European Journal of Pain*, *23*, 316-326.

Godínez-Chaparro, B., Barragán-Iglesias, P., Castañeda-Corral, G., Rocha-González, H.I., & Granados-Soto, V. (2011). Role of peripheral 5-HT(4), 5-HT(6), and 5-HT(7) receptors in development and maintenance of secondary mechanical allodynia and hyperalgesia. *Pain*, *152*, 687-697.

Gokin, A.P., Fareed, M.U., Pan, H.L., Hans, G., Strichartz, G.R., & Davar, G. (2001). Local injection of endothelin-1 produces pain-like behavior and excitation of nociceptors in rats. *The Journal of Neuroscience, 21*, 5358-5366.

Gold, M.S., & Gebhart, G.F. (2010). Nociceptor sensitization in pain pathogenesis. *Nature Medicine*, *16*, 1248-1257.

Gonçalves, L., Gonçalves, D., Esteban-Casanelles, T., Barroso, T., Soares de Pinho, I., Lopes-Brás, R., Esperança-Martins, M., Patel, V., Torres, S., Teixeira de Sousa, R., Mansinho, A., & Costa, L. (2023). Immunotherapy around the clock: impact of infusion timing on stage iv melanoma outcomes. *Cells*, *12*, 2068.

Gonella, S., Sperlinga, R., Sciannameo, V., Dimonte, V., & Campagna, S. (2019). Characteristics of breakthrough pain and its impact on quality of life in terminally ill cancer patients. *Integrative Cancer Therapies*, *18*, 1534735419859095.

Goodwin, G., Bove, G.M., Dayment, B., & Dilley, A. (2020). Characterizing the mechanical properties of ectopic axonal receptive fields in inflamed nerves and following axonal transport disruption. *Neuroscience*, *429*, 10-22.

Goodwin, G., McMurray, S., Stevens, E.B., Denk, F., & McMahon, S.B. (2022). Examination of the contribution of Nav1.7 to axonal propagation in nociceptors. *Pain*, *163*, e869-e881.

Gouveia, K., & Hurst, J.L. (2019). Improving the practicality of using non-aversive handling methods to reduce background stress and anxiety in laboratory mice. *Scientific Reports*, *9*, 20305.

Graham, B., & Redman, S. (1994). A simulation of action potentials in synaptic boutons during presynaptic inhibition. *Journal of Neurophysiology*, *71*, 538-549.

Granados-Soto, V., Argüelles, C.F., Rocha-González, H.I., Godínez-Chaparro, B., Flores-Murrieta, F.J., & Villalón, C.M. (2010). The role of peripheral 5-HT1A, 5-HT1B, 5-HT1D, 5-HT1E and 5-HT1F serotonergic receptors in the reduction of nociception in rats. *Neuroscience*, *165*, 561-568.

Granit, R., & Kaada, B.R. (1952). Influence of stimulation of central nervous structures on muscle spindles in cat. *Acta Physiologica Scandinavica*, *27*, 130-160.

Green, C.R., Hart-Johnson, T., & Loeffler, D.R. (2011). Cancer-related chronic pain: examining quality of life in diverse cancer survivors. *Cancer*, *117*, 1994-2003.

Green, G.M., Lyons, L., & Dickenson, A.H. (1998). Alpha2-adrenoceptor antagonists enhance responses of dorsal horn neurones to formalin induced inflammation. *European Journal of Pharmacology*, *347*, 201-204.

Greenspan, J.D., Craft, R.M., LeResche, L., Arendt-Nielsen, L., Berkley, K.J., Fillingim, R.B., Gold, M.S., Holdcroft, A., Lautenbacher, S., Mayer, E.A., Mogil, J.S., Murphy, A.Z., Traub, R.J., & Consensus Working Group of the Sex, Gender, and Pain SIG of the IASP (2007). Studying sex and gender differences in pain and analgesia: a consensus report. *Pain*, *132*, S26-S45.

Greten, F.R., & Grivennikov, S.I. (2019). Inflammation and cancer: triggers, mechanisms, and consequences. *Immunity*, *51*, 27-41.

Gribkoff, V.K. (2006). The role of voltage-gated calcium channels in pain and nociception. *Seminars in Cell & Developmental Biology*, *17*, 555-564.

Grichnik, K.P., & Ferrante, F.M. (1991). The difference between acute and chronic pain. *The Mount Sinai Journal of Medicine*, *58*, 217-220.

Grond, S., Zech, D., Diefenbach, C., Radbruch, L., & Lehmann, K.A. (1996). Assessment of cancer pain: a prospective evaluation in 2266 cancer patients referred to a pain service. *Pain*, *64*, 107-114.

Gu, X., Gao, Z., Wang, X., Liu, X., Knight, R.T., Hof, P.R., & Fan, J. (2012). Anterior insular cortex is necessary for empathetic pain perception. *Brain*, *135*, 2726-2735.

Guise, T.A., Mohammad, K.S., Clines, G., Stebbins, E.G., Wong, D.H., Higgins, L.S., Vessella, R., Corey, E., Padalecki, S., Suva, L., & Chirgwin, J.M. (2006). Basic mechanisms responsible for osteolytic and osteoblastic bone metastases. *Clinical Cancer Research*, *12*, 6213s-6216s.

Guo, D., & Hu, J. (2014). Spinal presynaptic inhibition in pain control. *Neuroscience*, *283*, 95-106.

Gustin, S.M., Wilcox, S.L., Peck, C.C., Murray, G.M., & Henderson, L.A. (2011). Similarity of suffering: equivalence of psychological and psychosocial factors in neuropathic and non-neuropathic orofacial pain patients. *Pain*, *152*, 825-832.

Haber, L.H., Moore, B.D., & Willis, W.D. (1982). Electrophysiological response properties of spinoreticular neurons in the monkey. *The Journal of Comparative Neurology*, *207*, 75-84.

Haenen, V., Evenepoel, M., De Baerdemaecker, T., Meeus, M., Devoogdt, N., Morlion, B., Dams, L., Van Dijck, S., Van der Gucht, E., De Vrieze, T., Vyvere, T.V., & De Groef, A. (2022). Pain prevalence and characteristics in survivors of solid cancers: a systematic review and meta-analysis. *Supportive Care in Cancer*, *31*, 85.

Hagbarth, K.E., & Kerr, D.I. (1954). Central influences on spinal afferent conduction. *Journal of Neurophysiology*, *17*, 295-307.

Hagihira, S., Senba, E., Yoshida, S., Tohyama, M., & Yoshiya, I. (1990). Fine structure of noradrenergic terminals and their synapses in the rat spinal dorsal horn: an immunohistochemical study. *Brain Research*, *526*, 73-80.

Hald, A., Nedergaard, S., Hansen, R.R., Ding, M., & Heegaard, A.M. (2009). Differential activation of spinal cord glial cells in murine models of neuropathic and cancer pain. *European Journal of Pain*, *13*, 138-145.

Haley, J.E., Dickenson, A.H., & Schachter, M. (1989). Electrophysiological evidence for a role of bradykinin in chemical nociception in the rat. *Neuroscience Letters*, *97*, 198-202.

Halpern, M.T., de Moor, J.S., & Yabroff, K.R. (2022). Impact of pain on employment and financial outcomes among cancer survivors. *Journal of Clinical Oncology*, *40*, 24-31.

Halvorson, K.G., Kubota, K., Sevcik, M.A., Lindsay, T.H., Sotillo, J.E., Ghilardi, J.R., Rosol, T.J., Boustany, L., Shelton, D.L., & Mantyh, P.W. (2005). A blocking antibody to nerve growth factor attenuates skeletal pain induced by prostate tumor cells growing in bone. *Cancer Research*, *65*, 9426-9435.

Han, R.T., Lee, H., Lee, J., Lee, S.B., Kim, H.J., Back, S.K., & Na, H.S. (2016). Brief isolation changes nociceptive behaviors and compromises drug tests in mice. *Pain Practice*, *16*, 749-757.

Hanamori, T., Kunitake, T., Kato, K., & Kannan, H. (1998). Responses of neurons in the insular cortex to gustatory, visceral, and nociceptive stimuli in rats. *Journal of Neurophysiology*, *79*, 2535-2545.

Hankinson, S.E., & Eliassen, A.H. (2007). Endogenous estrogen, testosterone and progesterone levels in relation to breast cancer risk. *The Journal of Steroid Biochemistry and Molecular Biology*, *106*, 24-30.

Hannila, S.S., & Kawaja, M.D. (2005). Nerve growth factor-mediated collateral sprouting of central sensory axons into deafferentated regions of the dorsal horn is enhanced in the absence of the p75 neurotrophin receptor. *The Journal of Comparative Neurology*, *486*, 331-343.

Haroun, R., Gossage, S.J., Luiz, A.P., Arcangeletti, M., Sikandar, S., Zhao, J., Cox, J.J., & Wood, J.N. (2023). Chemogenetic silencing of $Na_V1.8$-positive sensory neurons reverses chronic neuropathic and bone cancer pain in FLEx $PSAM^4$-GlyR mice. *eNeuro*, *10*, ENEURO.0151-23.2023.

Harvie, D.S., Poolman, E.Y., Madden, V.J., Olthof, N.A., & Coppieters, M.W. (2022). Classically conditioned modulation of pain depends on stimulus intensity. *Experimental Brain Research*, *240*, 1151-1158.

Hasriadi, Dasuni Wasana, P.W., Vajragupta, O., Rojsitthisak, P., & Towiwat, P. (2021). Automated home-cage monitoring as a potential measure of sickness behaviors and pain-like behaviors in LPS-treated mice. *PloS One*, *16*, e0256706.

Havelin, J., Imbert, I., Sukhtankar, D., Remeniuk, B., Pelletier, I., Gentry, J., Okun, A., Tiutan, T., Porreca, F., & King, T.E. (2017). Mediation of movement-induced breakthrough cancer pain by IB4-binding nociceptors in rats. *The Journal of Neuroscience*, *37*, 5111-5122.

Heinricher, M.M., Barbaro, N.M., & Fields, H.L. (1989). Putative nociceptive modulating neurons in the rostral ventromedial medulla of the rat: firing of on- and off-cells is related to nociceptive responsiveness. *Somatosensory & Motor Research*, *6*, 427-439.

Heinricher, M.M., Morgan, M.M., Tortorici, V., & Fields, H.L. (1994). Disinhibition of off-cells and antinociception produced by an opioid action within the rostral ventromedial medulla. *Neuroscience*, *63*, 279-288.

Heo, M.H., Kim, J.Y., Hwang, I., Ha, E., & Park, K.U. (2017). Analgesic effect of quetiapine in a mouse model of cancer-induced bone pain. *The Korean Journal of Internal Medicine*, *32*, 1069-1074.

Hermans, L., Van Oosterwijck, J., Goubert, D., Goudman, L., Crombez, G., Calders, P., & Meeus, M. (2016). Inventory of personal factors influencing conditioned pain modulation in healthy people: a systematic literature review. *Pain Practice*, *16*, 758-769.

Hickey, L., Li, Y., Fyson, S.J., Watson, T.C., Perrins, R., Hewinson, J., Teschemacher, A.G., Furue, H., Lumb, B.M., & Pickering, A.E. (2014). Optoactivation of locus ceruleus neurons evokes bidirectional changes in thermal nociception in rats. *The Journal of Neuroscience*, *34*, 4148-4160.

Hitt, H.C., McMillen, R.C., Thornton-Neaves, T., Koch, K., & Cosby, A.G. (2007). Comorbidity of obesity and pain in a general population: results from the southern pain prevalence study. *The Journal of Pain*, *8*, 430-436.

Honore, P., Luger, N.M., Sabino, M.A., Schwei, M.J., Rogers, S.D., Mach, D.B., O'keefe, P.F., Ramnaraine, M.L., Clohisy, D.R., & Mantyh, P.W. (2000). Osteoprotegerin blocks bone cancer-induced skeletal destruction, skeletal pain and pain-related neurochemical reorganization of the spinal cord. *Nature Medicine*, *6*, 521-528.

Hoover, W.B., & Vertes, R.P. (2007). Anatomical analysis of afferent projections to the medial prefrontal cortex in the rat. *Brain Structure & Function*, *212*, 149-179.

Hosobuchi, Y., Adams, J.E., & Linchitz, R. (1977). Pain relief by electrical stimulation of the central gray matter in humans and its reversal by naloxone. *Science*, *197*, 183-186.

Howorth, P.W., Teschemacher, A.G., & Pickering, A.E. (2009). Retrograde adenoviral vector targeting of nociresponsive pontospinal noradrenergic neurons in the rat *in vivo*. *The Journal of Comparative Neurology*, *512*, 141-157.

Hsieh, C.L., Xie, Z., Liu, Z.Y., Green, J.E., Martin, W.D., Datta, M.W., Yeung, F., Pan, D., & Chung, L.W. (2005). A luciferase transgenic mouse model: visualization of prostate development and its androgen responsiveness in live animals. *Journal of Molecular Endocrinology*, *35*, 293-304.

Huang, Z.X., Lu, Z.J., Ma, W.Q., Wu, F.X., Zhang, Y.Q., Yu, W.F., & Zhao, Z.Q. (2014). Involvement of RVM-expressed P2X7 receptor in bone cancer pain: mechanism of descending facilitation. *Pain*, *155*, 783-791.

Huo, W., Liu, Y., Lei, Y., Zhang, Y., Huang, Y., Mao, Y., Wang, C., Sun, Y., Zhang, W., Ma, Z., & Gu, X. (2019). Imbalanced spinal infiltration of Th17/Treg cells contributes to bone cancer pain via promoting microglial activation. *Brain, Behavior, and Immunity*, *79*, 139-151.

Hutchison, W.D., Davis, K.D., Lozano, A.M., Tasker, R.R., & Dostrovsky, J.O. (1999). Pain-related neurons in the human cingulate cortex. *Nature Neuroscience*, *2*, 403-405.

Indo, Y., Tsuruta, M., Hayashida, Y., Karim, M.A., Ohta, K., Kawano, T., Mitsubuchi, H., Tonoki, H., Awaya, Y., & Matsuda, I. (1996). Mutations in the TRKA/NGF receptor gene in patients with congenital insensitivity to pain with anhidrosis. *Nature Genetics*, *13*, 485-488.

Ingram, S., Chisholm, K.I., Wang, F., De Koninck, Y., Denk, F., & Goodwin, G.L. (2023). Assessing spontaneous sensory neuron activity using *in vivo* calcium imaging. *Pain*, 10.1097/j.pain.0000000000003116. Advance online publication.

Inyang, K.E., Szabo-Pardi, T., Wentworth, E., McDougal, T.A., Dussor, G., Burton, M.D., & Price, T.J. (2019). The antidiabetic drug metformin prevents and reverses neuropathic pain and spinal cord microglial activation in male but not female mice. *Pharmacological Research*, *139*, 1-16.

Irvine, K.A., Sahbaie, P., Ferguson, A.R., & Clark, J.D. (2020). Loss of diffuse noxious inhibitory control after traumatic brain injury in rats: A chronic issue. *Experimental Neurology*, *333*, 113428.

Ishida, T., Tanaka, S., Sekiguchi, T., Sugiyama, D., & Kawamata, M. (2016). Spinal nociceptive transmission by mechanical stimulation of bone marrow. *Molecular Pain*, *12*, 1744806916628773.

Itoh, Y., & Arnold, A.P. (2015). Are females more variable than males in gene expression? Meta-analysis of microarray datasets. *Biology of Sex Differences*, *6*, 18.

Ivanusic, J.J. (2009). Size, neurochemistry, and segmental distribution of sensory neurons innervating the rat tibia. *The Journal of Comparative Neurology*, *517*, 276-283.

Janevic, M.R., McLaughlin, S.J., Heapy, A.A., Thacker, C., & Piette, J.D. (2017). Racial and socioeconomic disparities in disabling chronic pain: findings from the health and retirement study. *The Journal of Pain*, *18*, 1459-1467.

Jank, R., Gallee, A., Boeckle, M., Fiegl, S., & Pieh, C. (2017). Chronic pain and sleep disorders in primary care. *Pain Research and Treatment*, *2017*, 9081802.

Jasmin, L., Burkey, A.R., Granato, A., & Ohara, P.T. (2004). Rostral agranular insular cortex and pain areas of the central nervous system: a tract-tracing study in the rat. *The Journal of Comparative Neurology*, *468*, 425-440.

Jast, J., & Jasiuk, I. (2013). Age-related changes in the 3D hierarchical structure of rat tibia cortical bone characterized by high-resolution micro-CT. *Journal of Applied Physiology*, *114*, 923-933.

Jensen, M.P., Chang, H.Y., Lai, Y.H., Syrjala, K.L., Fann, J.R., & Gralow, J.R. (2010). Pain in long-term breast cancer survivors: frequency, severity, and impact. *Pain Medicine*, *11*, 1099-1106.

Jerard, C., Madhusudanan, P., Swamy, A., Ravikumar, K., & Shankarappa, S.A. (2023). Secretome mediated interactions between sensory neurons and breast cancer cells. *International Journal of Cancer*, *153*, 427-436.

Ji, H., Jin, X., Zhang, Q., Zhou, Y., Zhu, C., Yang, Y., Tang, Z., Yu, G., & Wang, C. (2022). A mouse model of cancer induced bone pain: from pain to movement. *Frontiers in Behavioral Neuroscience*, *16*, 873750.

Jiang, C., Wang, H., Wang, Q., Luo, Y., Sidlow, R., & Han, X. (2019). Prevalence of chronic pain and high-impact chronic pain in cancer survivors in the United States. *JAMA Oncology*, *5*, 1224-1226.

Jimenez-Andrade, J.M., Bloom, A.P., Stake, J.I., Mantyh, W.G., Taylor, R.N., Freeman, K.T., Ghilardi, J.R., Kuskowski, M.A., & Mantyh, P.W. (2010). Pathological sprouting of adult nociceptors in chronic prostate cancer-induced bone pain. *The Journal of Neuroscience*, *30*, 14649-14656.

Jimenez-Andrade, J.M., Ghilardi, J.R., Castañeda-Corral, G., Kuskowski, M.A., & Mantyh, P.W. (2011). Preventive or late administration of anti-NGF therapy attenuates tumor-induced nerve sprouting, neuroma formation, and cancer pain. *Pain*, *152*, 2564-2574.

Jimenez-Andrade, J.M., Ramírez-Rosas, M.B., Hee Park, S., Parker, R., Eber, M.R., Cain, R., Newland, M., Hsu, F.C., Kittel, C.A., Martin, T.J., Muñoz-Islas, E., Shiozawa, Y., & Peters, C.M. (2023). Evaluation of pain related behaviors and disease related outcomes in an immunocompetent mouse model of prostate cancer induced bone pain. *Journal of Bone Oncology*, *43*, 100510.

Jinks, S.L., Antognini, J.F., & Carstens, E. (2003). Isoflurane depresses diffuse noxious inhibitory controls in rats between 0.8 and 1.2 minimum alveolar anesthetic concentration. *Anesthesia and Analgesia*, *97*, 111-116.

Jinks, S.L., Martin, J.T., Carstens, E., Jung, S.W., & Antognini, J.F. (2003). Peri-MAC depression of a nociceptive withdrawal reflex is accompanied by reduced dorsal horn activity with halothane but not isoflurane. *Anesthesiology*, *98*, 1128-1138.

Johnson, L.C., Johnson, R.W., Munoz, S.A., Mundy, G.R., Peterson, T.E., & Sterling, J.A. (2011). Longitudinal live animal micro-CT allows for quantitative analysis of tumor-induced bone destruction. *Bone*, *48*, 141-151.

Julius, D., & Basbaum, A.I. (2001). Molecular mechanisms of nociception. *Nature*, *413*, 203-210.

Kallupi, M., Carrette, L.L.G., Kononoff, J., Solberg Woods, L.C., Palmer, A.A., Schweitzer, P., George, O., & de Guglielmo, G. (2020). Nociceptin attenuates the escalation of oxycodone self-administration by normalizing CeA-GABA transmission in highly addicted rats. *Proceedings of the National Academy of Sciences of the United States of America*, *117*, 2140-2148.

Kameyama, K., Aono, K., & Kitamura, K. (1999). Isoflurane inhibits neuronal Ca2+ channels through enhancement of current inactivation. *British Journal of Anaesthesia*, *82*, 402-411.

Kanda, M., Nagamine, T., Ikeda, A., Ohara, S., Kunieda, T., Fujiwara, N., Yazawa, S., Sawamoto, N., Matsumoto, R., Taki, W., & Shibasaki, H. (2000). Primary somatosensory cortex is actively involved in pain processing in human. *Brain Research*, *853*, 282-289.

Karlson, C.W., Alberts, N.M., Liu, W., Brinkman, T.M., Annett, R.D., Mulrooney, D.A., Schulte, F., Leisenring, W.M., Gibson, T.M., Howell, R.M., Srivastava, D., Oeffinger, K.C., Robison, L.L., Armstrong, G.T., Zeltzer, L.K., & Krull, K.R. (2020). Longitudinal pain and pain interference in long-term survivors of childhood cancer: a report from the childhood cancer survivor study. *Cancer*, *126*, 2915-2923.

Kaushal, R., Taylor, B.K., Jamal, A.B., Zhang, L., Ma, F., Donahue, R., & Westlund, K.N. (2016). GABA-A receptor activity in the noradrenergic locus coeruleus drives trigeminal neuropathic pain in the rat; contribution of NAα1 receptors in the medial prefrontal cortex. *Neuroscience*, *334*, 148-159.

Kawaja, M.D., Smithson, L.J., Elliott, J., Trinh, G., Crotty, A.M., Michalski, B., & Fahnestock, M. (2011). Nerve growth factor promoter activity revealed in mice expressing enhanced green fluorescent protein. *The Journal of Comparative Neurology*, *519*, 2522-2545.

Kayser, V., Elfassi, I.E., Aubel, B., Melfort, M., Julius, D., Gingrich, J.A., Hamon, M., & Bourgoin, S. (2007). Mechanical, thermal and formalin-induced nociception is differentially altered in 5-HT1A-/-, 5-HT1B-/-, 5-HT2A-/-, 5-HT3A-/- and 5-HTT-/- knock-out male mice. *Pain*, *130*, 235-248.

Kehlet, H., Jensen, T.S., & Woolf, C.J. (2006). Persistent postsurgical pain: risk factors and prevention. *Lancet*, *367*, 1618-1625.

Kenshalo, D.R., Iwata, K., Sholas, M., & Thomas, D.A. (2000). Response properties and organization of nociceptive neurons in area 1 of monkey primary somatosensory cortex. *Journal of Neurophysiology*, *84*, 719-729.

Khasabov, S.G., Hamamoto, D.T., Harding-Rose, C., & Simone, D.A. (2007). Tumor-evoked hyperalgesia and sensitization of nociceptive dorsal horn neurons in a murine model of cancer pain. *Brain Research*, *1180*, 7-19.

Kibaly, C., Loh, H.H., & Law, P.Y. (2016). A mechanistic approach to the development of gene therapy for chronic pain. *International Review of Cell and Molecular Biology*, *327*, 89-161.

Kilkenny, C., Browne, W.J., Cuthill, I.C., Emerson, M., & Altman, D.G. (2010). Improving bioscience research reporting: the ARRIVE guidelines for reporting animal research. *PLoS Biology*, *8*, e1000412.

Kim, J., Atherley, R., Werner, D.F., Homanics, G.E., Carstens, E., & Antognini, J.F. (2007). Isoflurane depression of spinal nociceptive processing and minimum alveolar anesthetic concentration are not attenuated in mice expressing isoflurane resistant gamma-aminobutyric acid type-A receptors. *Neuroscience Letters*, *420*, 209-212.

Kim, J., Yao, A., Atherley, R., Carstens, E., Jinks, S.L., & Antognini, J.F. (2007). Neurons in the ventral spinal cord are more depressed by isoflurane, halothane, and propofol than are neurons in the dorsal spinal cord. *Anesthesia and Analgesia*, *105*, 1020-contents.

King, C.D., Wong, F., Currie, T., Mauderli, A.P., Fillingim, R.B., & Riley, J.L. (2009). Deficiency in endogenous modulation of prolonged heat pain in patients with irritable bowel syndrome and temporomandibular disorder. *Pain*, *143*, 172-178.

King, S., Chambers, C.T., Huguet, A., MacNevin, R.C., McGrath, P.J., Parker, L., & MacDonald, A.J. (2011). The epidemiology of chronic pain in children and adolescents revisited: a systematic review. *Pain*, *152*, 2729-2738.

Koga, K., Furue, H., Rashid, M.H., Takaki, A., Katafuchi, T., & Yoshimura, M. (2005). Selective activation of primary afferent fibers evaluated by sine-wave electrical stimulation. *Molecular Pain*, *1*, 13.

Kopruszinski, C.M., Turnes, J.M., Swiokla, J., Weinstein, T.J., Schwedt, T.J., Dodick, D.W., Anderson, T., Navratilova, E., & Porreca, F. (2021). CGRP monoclonal antibody prevents the loss of diffuse noxious inhibitory controls (DNIC) in a mouse model of post-traumatic headache. *Cephalalgia*, *41*, 749-759.

Kosek, E., Cohen, M., Baron, R., Gebhart, G.F., Mico, J.A., Rice, A.S.C., Rief, W., & Sluka, A.K. (2016). Do we need a third mechanistic descriptor for chronic pain states?. *Pain*, *157*, 1382-1386.

Kosek, E., & Ordeberg, G. (2000). Lack of pressure pain modulation by heterotopic noxious conditioning stimulation in patients with painful osteoarthritis before, but not following, surgical pain relief. *Pain*, *88*, 69-78.

Kress, M., Koltzenburg, M., Reeh, P.W., & Handwerker, H.O. (1992). Responsiveness and functional attributes of electrically localized terminals of cutaneous C-fibers *in vivo* and *in vitro*. *Journal of Neurophysiology*, *68*, 581-595.

Kristianto, J., Johnson, M.G., Afzal, R., & Blank, R.D. (2017). Endothelin signaling in bone. *Endocrinology and Metabolism Clinics of North America*, *46*, 51-62.

Kröner-Herwig, B., Gaßmann, J., Tromsdorf, M., & Zahrend, E. (2012). The effects of sex and gender role on responses to pressure pain. *Psycho-Social Medicine*, *9*, Doc01.

Krout, K.E., Jansen, A.S., & Loewy, A.D. (1998). Periaqueductal gray matter projection to the parabrachial nucleus in rat. *The Journal of Comparative Neurology*, *401*, 437-454.

Kucharczyk, M.W., Chisholm, K.I., Denk, F., Dickenson, A.H., Bannister, K., & McMahon, S.B. (2020). The impact of bone cancer on the peripheral encoding of mechanical pressure stimuli. *Pain*, *161*, 1894-1905.

Kucharczyk, M.W., Derrien, D., Dickenson, A.H., & Bannister, K. (2020). The stage-specific plasticity of descending modulatory controls in a rodent model of cancer-induced bone pain. *Cancers*, *12*, 3286.

Kucharczyk, M.W., Di Domenico, F., & Bannister, K. (2022). Distinct brainstem to spinal cord noradrenergic pathways inversely regulate spinal neuronal activity. *Brain*, *145*, 2293-2300.

Kucharczyk, M.W., Di Domenico, F., & Bannister, K. (2023). A critical brainstem relay for mediation of diffuse noxious inhibitory controls. *Brain*, *146*, 2259-2267.

Kucharczyk, M.W., Valiente, D., & Bannister, K. (2021). Developments in understanding diffuse noxious inhibitory controls: pharmacological evidence from pre-clinical research. *Journal of Pain Research*, *14*, 1083-1095.

Kwiat, G.C., & Basbaum, A.I. (1992). The origin of brainstem noradrenergic and serotonergic projections to the spinal cord dorsal horn in the rat. *Somatosensory & Motor Research*, *9*, 157-173.

Kylie, J., Cooper, D.M., Kurpinski, J.K., Chase, F.T., Muzyka, M.D., & Plachta, T.C. (2023). Evaluation of potential low-stress handling methods in Crl:CDSD rats (*Rattus norvegicus*). *Journal of the American Association for Laboratory Animal Science*, *63*, 10-19.

Labrakakis, C. (2023). The role of the insular cortex in pain. *International Journal of Molecular Sciences*, *24*, 5736.

LaGraize, S.C., Labuda, C.J., Rutledge, M.A., Jackson, R.L., & Fuchs, P.N. (2004). Differential effect of anterior cingulate cortex lesion on mechanical hypersensitivity and escape/avoidance behavior in an animal model of neuropathic pain. *Experimental Neurology*, *188*, 139-148.

Laird, B.J., Walley, J., Murray, G.D., Clausen, E., Colvin, L.A., & Fallon, M.T. (2011). Characterization of cancer-induced bone pain: an exploratory study. *Supportive Care in Cancer*, *19*, 1393-1401.

Lakos, S., & Basbaum, A.I. (1988). An ultrastructural study of the projections from the midbrain periaqueductal gray to spinally projecting, serotonin-immunoreactive neurons of the medullary nucleus raphe magnus in the rat. *Brain Research*, *443*, 383-388.

Lapirot, O., Melin, C., Modolo, A., Nicolas, C., Messaoudi, Y., Monconduit, L., Artola, A., Luccarini, P., & Dallel, R. (2011). Tonic and phasic descending dopaminergic controls of nociceptive transmission in the medullary dorsal horn. *Pain*, *152*, 1821-1831.

Le Bars, D., Dickenson, A.H., & Besson, J.M. (1979a). Diffuse noxious inhibitory controls (DNIC). I. Effects on dorsal horn convergent neurones in the rat. *Pain*, *6*, 283-304.

Le Bars, D., Dickenson, A.H., & Besson, J.M. (1979b). Diffuse noxious inhibitory controls (DNIC). II. Lack of effect on non-convergent neurones, supraspinal involvement and theoretical implications. *Pain*, *6*, 305-327.

Leadley, R.M., Armstrong, N., Lee, Y.C., Allen, A., & Kleijnen, J. (2012). Chronic diseases in the European Union: the prevalence and health cost implications of chronic pain. *Journal of Pain & Palliative Care Pharmacotherapy*, *26*, 310-325.

Lee, G.I., & Neumeister, M.W. (2020). Pain: pathways and physiology. *Clinics in Plastic Surgery*, *47*, 173-180.

Lee, H.J., Choi, E.J., Nahm, F.S., Yoon, I.Y., & Lee, P.B. (2018). Prevalence of unrecognized depression in patients with chronic pain without a history of psychiatric diseases. *The Korean Journal of Pain*, *31*, 116-124.

Lee, J.Y., You, T., Lee, C.H., Im, G.H., Seo, H., Woo, C.W., & Kim, S.G. (2022). Role of anterior cingulate cortex inputs to periaqueductal gray for pain avoidance. *Current Biology*, *32*, 2834-2847.e5.

Leith, J.L., Koutsikou, S., Lumb, B.M., & Apps, R. (2010). Spinal processing of noxious and innocuous cold information: differential modulation by the periaqueductal gray. *The Journal of Neuroscience*, *30*, 4933-4942.

Levine, R., Morgan, M.M., Cannon, J.T., & Liebeskind, J.C. (1991). Stimulation of the periaqueductal gray matter of the rat produces a preferential ipsilateral antinociception. *Brain Research*, *567*, 140-144.

Lewis, G.N., Rice, D.A., & McNair, P.J. (2012). Conditioned pain modulation in populations with chronic pain: a systematic review and meta-analysis. *The Journal of Pain*, *13*, 936-944.

Li, C., Wang, S., Chen, Y., & Zhang, X. (2018). Somatosensory neuron typing with high-coverage single-cell RNA sequencing and functional analysis. *Neuroscience Bulletin*, *34*, 200-207.

Li, H.S., Monhemius, R., Simpson, B.A., & Roberts, M.H. (1998). Supraspinal inhibition of nociceptive dorsal horn neurones in the anaesthetized rat: tonic or dynamic?. *The Journal of Physiology*, *506*, 459-469.

Li, J., Wei, Y., Zhou, J., Zou, H., Ma, L., Liu, C., Xiao, Z., Liu, X., Tan, X., Yu, T., & Cao, S. (2022). Activation of locus coeruleus-spinal cord noradrenergic neurons alleviates neuropathic pain in mice via reducing neuroinflammation from astrocytes and microglia in spinal dorsal horn. *Journal of Neuroinflammation*, *19*, 123.

Li, Y., Liu, X., Fu, Q., Fan, W., Shao, X., Fang, J., Liu, J. G., & Xu, C. (2023). Electroacupuncture ameliorates depression-like behaviors comorbid to chronic neuropathic pain via Tet1-mediated restoration of adult neurogenesis. *Stem Cells*, *41*, 384-399.

Li, Z., Lu, Y. F., Li, C.L., Wang, Y., Sun, W., He, T., Chen, X.F., Wang, X.L., & Chen, J. (2014). Social interaction with a cagemate in pain facilitates subsequent spinal nociception via activation of the medial prefrontal cortex in rats. *Pain*, *155*, 1253-1261.

Light, A.R., Kavookjian, A.M., & Petrusz, P. (1983). The ultrastructure and synaptic connections of serotonin-immunoreactive terminals in spinal laminae I and II. *Somatosensory Research*, *1*, 33-50.

Lima, D. (1990). A spinomedullary projection terminating in the dorsal reticular nucleus of the rat. *Neuroscience*, *34*, 577-589.

Lin, Q., Zou, X., & Willis, W.D. (2000). Adelta and C primary afferents convey dorsal root reflexes after intradermal injection of capsaicin in rats. *Journal of Neurophysiology*, *84*, 2695-2698.

Lipton, R.B., Galer, B.S., Dutcher, J.P., Portenoy, R.K., Pahmer, V., Meller, F., Arezzo, J.C., & Wiernik, P.H. (1991). Large and small fibre type sensory dysfunction in patients with cancer. *Journal of Neurology, Neurosurgery, and Psychiatry*, *54*, 706-709.

Liu, D., Zhou, X., Tan, Y., Yu, H., Cao, Y., Tian, L., Yang, L., Wang, S., Liu, S., Chen, J., Liu, J., Wang, C., Yu, H., & Zhang, J. (2022). Altered brain functional activity and connectivity in bone metastasis pain of lung cancer patients: A preliminary resting-state fMRI study. *Frontiers in Neurology*, *13*, 936012.

Liu, Q., Feng, L., Han, X., Zhang, W., Zhang, H., & Xu, L. (2021). The TRPA1 channel mediates mechanical allodynia and thermal hyperalgesia in a rat bone cancer pain model. *Frontiers in Pain Research*, *2*, 638620.

Liu, X., Bu, H., Liu, C., Gao, F., Yang, H., Tian, X., Xu, A., Chen, Z., Cao, F., & Tian, Y. (2012). Inhibition of glial activation in rostral ventromedial medulla attenuates mechanical allodynia in a rat model of cancer-induced bone pain. *Journal of Huazhong University of Science and Technology*, *32*, 291-298.

Liu, X., Liu, B.L., Yang, Q., Zhou, X., & Tang, S.J. (2022). Microglial ablation does not affect opioid-induced hyperalgesia in rodents. *Pain*, *163*, 508-517.

Liu, Y., Broman, J., Zhang, M., & Edvinsson, L. (2009). Brainstem and thalamic projections from a craniovascular sensory nervous centre in the rostral cervical spinal dorsal horn of rats. *Cephalalgia*, *29*, 935-948.

Lobanov, O.V., & Peng, Y.B. (2011). Differential contribution of electrically evoked dorsal root reflexes to peripheral vasodilatation and plasma extravasation. *Journal of Neuroinflammation*, *8*, 20.

Lockwood, S.M., Bannister, K., & Dickenson, A.H. (2019). An investigation into the noradrenergic and serotonergic contributions of diffuse noxious inhibitory controls in a monoiodoacetate model of osteoarthritis. *Journal of Neurophysiology*, *121*, 96-104.

Lockwood, S.M., & Dickenson, A.H. (2019). A combination pharmacotherapy of tapentadol and pregabalin to tackle centrally driven osteoarthritis pain. *European Journal of Pain*, *23*, 1185-1195.

Lopes, D.M., Denk, F., Chisholm, K.I., Suddason, T., Durrieux, C., Thakur, M., Gentry, C., & McMahon, S.B. (2017). Peripheral inflammatory pain sensitisation is independent of mast cell activation in male mice. *Pain*, *158*, 1314-1322.

Lorenz, J., Minoshima, S., & Casey, K.L. (2003). Keeping pain out of mind: the role of the dorsolateral prefrontal cortex in pain modulation. *Brain*, *126*, 1079-1091.

Lu, Q., Krull, K.R., Leisenring, W., Owen, J.E., Kawashima, T., Tsao, J.C.I., Zebrack, B., Mertens, A., Armstrong, G.T., Stovall, M., Robison, L.L., & Zeltzer, L.K. (2011). Pain in long-term adult survivors of childhood cancers and their siblings: a report from the childhood cancer survivor study. *Pain*, *152*, 2616-2624.

Lu, Y.F., Ren, B., Ling, B.F., Zhang, J., Xu, C., & Li, Z. (2018). Social interaction with a cagemate in pain increases allogrooming and induces pain hypersensitivity in the observer rats. *Neuroscience Letters*, *662*, 385-388.

Lucas-Romero, J., Rivera-Arconada, I., & Lopez-Garcia, J.A. (2022). Synchronous firing of dorsal horn neurons at the origin of dorsal root reflexes in naïve and paw-inflamed mice. *Frontiers in Cellular Neuroscience*, *16*, 1004956.

Mach, D.B., Rogers, S.D., Sabino, M.C., Luger, N.M., Schwei, M.J., Pomonis, J.D., Keyser, C.P., Clohisy, D.R., Adams, D.J., O'Leary, P., & Mantyh, P.W. (2002). Origins of skeletal pain: sensory and sympathetic innervation of the mouse femur. *Neuroscience*, *113*, 155-166.

Maeda, T., Yamada, D., & Kawahara, K. (2016). Cancer pain relief achieved by disrupting tumor-driven semaphorin 3A signaling in mice. *Neuroscience Letters*, *632*, 147-151.

Mahns, D.A., Ivanusic, J.J., Sahai, V., & Rowe, M.J. (2006). An intact peripheral nerve preparation for monitoring the activity of single, periosteal afferent nerve fibres. *Journal of Neuroscience Methods*, *156*, 140-144.

Maihöfner, C., Herzner, B., & Otto Handwerker, H. (2006). Secondary somatosensory cortex is important for the sensory-discriminative dimension of pain: a functional MRI study. *The European Journal of Neuroscience*, *23*, 1377-1383.

Maltoni, M., Scarpi, E., Modonesi, C., Passardi, A., Calpona, S., Turriziani, A., Speranza, R., Tassinari, D., Magnani, P., Saccani, D., Montanari, L., Roudnas, B., Amadori, D., Fabbri, L., Nanni, O., Raulli, P., Poggi, B., Fochessati, F., Giannunzio, D., Barbagallo, M.L., … Ferrario, S. (2005). A validation study of the WHO analgesic ladder: a two-step vs three-step strategy. *Supportive Care in Cancer*, *13*, 888-894.

Manivannan, M., & Suresh, P.K. (2012). On the somatosensation of vision. *Annals of Neurosciences*, *19*, 31-39.

Mantyh, P. (2013). Bone cancer pain: causes, consequences, and therapeutic opportunities. *Pain*, *154*, S54-S62.

Mantyh, P.W., Catton, M.D., Boehmer, C.G., Welton, M.L., Passaro, E.P., Maggio, J.E., & Vigna, S.R. (1989). Receptors for sensory neuropeptides in human inflammatory diseases: implications for the effector role of sensory neurons. *Peptides*, *10*, 627-645.

Mantyh, P.W., & Peschanski, M. (1982). Spinal projections from the periaqueductal grey and dorsal raphe in the rat, cat and monkey. *Neuroscience*, *7*, 2769-2776.

Mantyh, W.G., Jimenez-Andrade, J.M., Stake, J.I., Bloom, A.P., Kaczmarska, M.J., Taylor, R.N., Freeman, K.T., Ghilardi, J.R., Kuskowski, M.A., & Mantyh, P.W. (2010). Blockade of nerve sprouting and neuroma formation markedly attenuates the development of late stage cancer pain. *Neuroscience*, *171*, 588-598.

Mardelle, U., Bretaud, N., Daher, C., & Feuillet, V. (2024). From pain to tumor immunity: influence of peripheral sensory neurons in cancer. *Frontiers in Immunology*, *15*, 1335387.

Margalit, D., & Segal, M. (1979). A pharmacologic study of analgesia produced by stimulation of the nucleus locus coeruleus. *Psychopharmacology*, *62*, 169-173.

Mariscal, P., Bravo, L., Llorca-Torralba, M., Razquin, J., Miguelez, C., Suárez-Pereira, I., & Berrocoso, E. (2023). Sexual differences in locus coeruleus neurons and related behavior in C57BL/6J mice. *Biology of Sex Differences*, *14*, 64.

Marlier, L., Sandillon, F., Poulat, P., Rajaofetra, N., Geffard, M., & Privat, A. (1991). Serotonergic innervation of the dorsal horn of rat spinal cord: light and electron microscopic immunocytochemical study. *Journal of Neurocytology*, *20*, 310-322.

Marques-Lopes, J., Pinho, D., Albino-Teixeira, A., & Tavares, I. (2010). The hyperalgesic effects induced by the injection of angiotensin II into the caudal ventrolateral medulla are mediated by the pontine A5 noradrenergic cell group. *Brain Research*, *1325*, 41-52.

Martin, G.F., Vertes, R.P., & Waltzer, R. (1985). Spinal projections of the gigantocellular reticular formation in the rat. Evidence for projections from different areas to laminae I and II and lamina IX. *Experimental Brain Research*, *58*, 154-162.

Martin, L.J., Acland, E.L., Cho, C., Gandhi, W., Chen, D., Corley, E., Kadoura, B., Levy, T., Mirali, S., Tohyama, S., Khan, S., MacIntyre, L.C., Carlson, E.N., Schweinhardt, P., & Mogil, J.S. (2019). Male-specific conditioned pain hypersensitivity in mice and humans. *Current Biology*, *29*, 192-201.

Martin, R.F., Haber, L.H., & Willis, W.D. (1979). Primary afferent depolarization of identified cutaneous fibers following stimulation in medial brain stem. *Journal of Neurophysiology*, *42*, 779-790.

Martin, R.J., Apkarian, A.V., & Hodge, C.J. (1990). Ventrolateral and dorsolateral ascending spinal cord pathway influence on thalamic nociception in cat. *Journal of Neurophysiology*, *64*, 1400-1412.

Martin, W.J., Gupta, N.K., Loo, C.M., Rohde, D.S., & Basbaum, A.I. (1999). Differential effects of neurotoxic destruction of descending noradrenergic pathways on acute and persistent nociceptive processing. *Pain*, *80*, 57-65.

Martland, M.E., Rashidi, A.S., Bennett, M.I., Fallon, M., Jones, C., Rolke, R., & Mulvey, M.R. (2020). The use of quantitative sensory testing in cancer pain assessment: A systematic review. *European Journal of Pain*, *24*, 669-684.

Mauguière, F. (2004). The role of secondary somatosensory cortex and insula in pain. *Supplements to Clinical Neurophysiology*, *57*, 62-71.

Mayer, D.J., Wolfle, T.L., Akil, H., Carder, B., & Liebeskind, J.C. (1971). Analgesia from electrical stimulation in the brainstem of the rat. *Science*, *174*, 1351-1354.

McAlpine, M.D., Yumol, J.L., & Ward, W.E. (2021). Pregnancy and lactation in sprague-dawley rats result in permanent reductions of tibia trabecular bone mineral density and structure but consumption of red rooibos herbal tea supports the partial recovery. *Frontiers in Nutrition*, *8*, 798936.

McGaraughty, S., & Heinricher, M.M. (2002). Microinjection of morphine into various amygdaloid nuclei differentially affects nociceptive responsiveness and RVM neuronal activity. *Pain*, *96*, 153-162.

McIlvried, L.A., Atherton, M.A., Horan, N.L., Goch, T.N., & Scheff, N.N. (2022). Sensory neurotransmitter calcitonin gene-related peptide modulates tumor growth and lymphocyte infiltration in oral squamous cell carcinoma. *Advanced Biology*, *6*, e2200019.

McMahon, S.B., & Wall, P.D. (1988). Descending excitation and inhibition of spinal cord lamina I projection neurons. *Journal of Neurophysiology*, *59*, 1204-1219.

Medhurst, S.J., Walker, K., Bowes, M., Kidd, B.L., Glatt, M., Muller, M., Hattenberger, M., Vaxelaire, J., O'Reilly, T., Wotherspoon, G., Winter, J., Green, J., & Urban, L. (2002). A rat model of bone cancer pain. *Pain*, *96*, 129-140.

Medrano, M.C., Dhanasobhon, D., Yalcin, I., Schlichter, R., & Cordero-Erausquin, M. (2016). Loss of inhibitory tone on spinal cord dorsal horn spontaneously and nonspontaneously active neurons in a mouse model of neuropathic pain. *Pain*, *157*, 1432-1442.

Melzack, R. (1999). From the gate to the neuromatrix. *Pain*, *Suppl 6*, S121-S126.

Mena-Avila, E., Milla-Cruz, J.J., Calvo, J.R., Hochman, S., Villalón, C.M., Arias-Montaño, J.A., & Quevedo, J.N. (2020). Activation of α-adrenoceptors depresses synaptic transmission of myelinated afferents and inhibits pathways mediating primary afferent depolarization (PAD) in the *in vitro* mouse spinal cord. *Experimental Brain Research*, *238*, 1293-1303.

Menéndez, L., Lastra, A., Fresno, M.F., Llames, S., Meana, A., Hidalgo, A., & Baamonde, A. (2003). Initial thermal heat hypoalgesia and delayed hyperalgesia in a murine model of bone cancer pain. *Brain Research*, *969*, 102-109.

Menétrey, D., Chaouch, A., Binder, D., & Besson, J.M. (1982). The origin of the spinomesencephalic tract in the rat: an anatomical study using the retrograde transport of horseradish peroxidase. *The Journal of Comparative Neurology*, *206*, 193-207.

Mercadante, S. (1997). Malignant bone pain: pathophysiology and treatment. *Pain*, *69*, 1-18.

Michaelides, A., & Zis, P. (2019). Depression, anxiety and acute pain: links and management challenges. *Postgraduate Medicine*, *131*, 438-444.

Middleton, S.J., Barry, A.M., Comini, M., Li, Y., Ray, P.R., Shiers, S., Themistocleous, A.C., Uhelski, M.L., Yang, X., Dougherty, P.M., Price, T.J., & Bennett, D.L. (2021). Studying human nociceptors: from fundamentals to clinic. *Brain*, *144*, 1312-1335.

Middleton, S.J., Perez-Sanchez, J., & Dawes, J.M. (2022). The structure of sensory afferent compartments in health and disease. *Journal of Anatomy*, *241*, 1186-1210.

Millan, M.J. (2002). Descending control of pain. *Progress in Neurobiology*, *66*, 355-474.

Mitamura, T., Higashiyama, S., Taniguchi, N., Klagsbrun, M., & Mekada, E. (1995). Diphtheria toxin binds to the epidermal growth factor (EGF)-like domain of human heparin-binding EGF-like growth factor/diphtheria toxin receptor and inhibits specifically its mitogenic activity. *The Journal of Biological Chemistry*, *270*, 1015-1019.

Mitsou, J.D., Tseveleki, V., Dimitrakopoulos, F.I., Konstantinidis, K., & Kalofonos, H. (2023). Radical tumor denervation activates potent local and global cancer treatment. *Cancers*, *15*, 3758.

Mogil, J.S. (2012). Sex differences in pain and pain inhibition: multiple explanations of a controversial phenomenon. *Nature Reviews. Neuroscience*, *13*, 859-866.

Mogil, J.S. (2020). Qualitative sex differences in pain processing: emerging evidence of a biased literature. *Nature Reviews. Neuroscience*, *21*, 353-365.

Molander, C., Xu, Q., & Grant, G. (1984). The cytoarchitectonic organization of the spinal cord in the rat. I. The lower thoracic and lumbosacral cord. *The Journal of Comparative Neurology*, *230*, 133-141.

Morgan, M., Nencini, S., Thai, J., & Ivanusic, J.J. (2019). TRPV1 activation alters the function of Aδ and C fiber sensory neurons that innervate bone. *Bone*, *123*, 168-175.

Moriya, S., Yamashita, A., Nishi, R., Ikoma, Y., Yamanaka, A., & Kuwaki, T. (2019). Acute nociceptive stimuli rapidly induce the activity of serotonin and noradrenalin neurons in the brain stem of awake mice. *IBRO Reports*, *7*, 1-9.

Mouedden, M.E., & Meert, T.F. (2007). Pharmacological evaluation of opioid and non-opioid analgesics in a murine bone cancer model of pain. *Pharmacology, Biochemistry, and Behavior*, *86*, 458-467.

Mouton, L.J., & Holstege, G. (1994). The periaqueductal gray in the cat projects to lamina VIII and the medial part of lamina VII throughout the length of the spinal cord. *Experimental Brain Research*, *101*, 253-264.

Mukhopadhyay, K.D., Liu, Z., Bandyopadhyay, A., Kirma, N.B., Tekmal, R.R., Wang, S., & Sun, L.Z. (2015). Aromatase expression increases the survival and malignancy of estrogen receptor positive breast cancer cells. *PloS One*, *10*, e0121136.

Nagae, M., Hiraga, T., & Yoneda, T. (2007). Acidic microenvironment created by osteoclasts causes bone pain associated with tumor colonization. *Journal of Bone and Mineral Metabolism*, *25*, 99-104.

Nagasako, E.M., Oaklander, A.L., & Dworkin, R.H. (2003). Congenital insensitivity to pain: an update. *Pain*, *101*, 213-219.

Nakahiro, M., Yeh, J.Z., Brunner, E., & Narahashi, T. (1989). General anesthetics modulate GABA receptor channel complex in rat dorsal root ganglion neurons. *FASEB Journal*, *3*, 1850-1854.

Nakashima, T., Akamatsu, M., Hatanaka, A., & Kiyohara, T. (2004). Attenuation of stress-induced elevations in plasma ACTH level and body temperature in rats by green odor. *Physiology & Behavior*, *80*, 481-488.

Navratilova, E., Nation, K., Remeniuk, B., Neugebauer, V., Bannister, K., Dickenson, A.H., & Porreca, F. (2020). Selective modulation of tonic aversive qualities of neuropathic pain by morphine in the central nucleus of the amygdala requires endogenous opioid signaling in the anterior cingulate cortex. *Pain*, *161*, 609-618.

Nelson, S., Simons, L.E., & Logan, D. (2018). The incidence of adverse childhood experiences (ACEs) and their association with pain-related and psychosocial impairment in youth with chronic pain. *The Clinical Journal of Pain*, *34*, 402-408.

Nemoto, W., Kozak, D., Sotocinal, S.G., Tansley, S., Bannister, K., & Mogil, J.S. (2023). Monoaminergic mediation of hyperalgesic and analgesic descending control of nociception in mice. *Pain*, *164*, 1096-1105.

Nencini, S., & Ivanusic, J. (2017). Mechanically sensitive Aδ nociceptors that innervate bone marrow respond to changes in intra-osseous pressure. *The Journal of Physiology*, *595*, 4399-4415.

Nencini, S., Ringuet, M., Kim, D.H., Chen, Y.J., Greenhill, C., & Ivanusic, J.J. (2017). Mechanisms of nerve growth factor signaling in bone nociceptors and in an animal model of inflammatory bone pain. *Molecular Pain*, *13*, 1744806917697011.

Neubert, M.J., Kincaid, W., & Heinricher, M.M. (2004). Nociceptive facilitating neurons in the rostral ventromedial medulla. *Pain*, *110*, 158-165.

Neziri, A.Y., Scaramozzino, P., Andersen, O.K., Dickenson, A.H., Arendt-Nielsen, L., & Curatolo, M. (2011). Reference values of mechanical and thermal pain tests in a pain-free population. *European Journal of Pain*, *15*, 376-383.

Ni, H.D., Xu, L.S., Wang, Y., Li, H., An, K., Liu, M., Liu, Q., Deng, H., He, Q., Huang, B., Fang, J., & Yao, M. (2019). Astrocyte activation in the periaqueductal gray promotes descending facilitation to cancer-induced bone pain through the JNK MAPK signaling pathway. *Molecular Pain*, *15*, 1744806919831909.

Nicotra, L., Tuke, J., Grace, P.M., Rolan, P.E., & Hutchinson, M.R. (2014). Sex differences in mechanical allodynia: how can it be preclinically quantified and analyzed?. *Frontiers in Behavioral Neuroscience*, *8*, 40.

Nitzschke, R., Fischer, M., & Funcke, S. (2022). Nociception level: what's in a name?. *British Journal of Anaesthesia*, *128*, e49-e50.

Normand, E., Potvin, S., Gaumond, I., Cloutier, G., Corbin, J.F., & Marchand, S. (2011). Pain inhibition is deficient in chronic widespread pain but normal in major depressive disorder. *The Journal of Clinical Psychiatry*, *72*, 219-224.

Nuseir, K., & Proudfit, H.K. (2000). Bidirectional modulation of nociception by GABA neurons in the dorsolateral pontine tegmentum that tonically inhibit spinally projecting noradrenergic A7 neurons. *Neuroscience*, *96*, 773-783.

Odeh, F., & Antal, M. (2001). The projections of the midbrain periaqueductal grey to the pons and medulla oblongata in rats. *The European Journal of Neuroscience*, *14*, 1275-1286.

Oefelein, M.G., Ricchiuti, V., Conrad, W., & Resnick, M.I. (2002). Skeletal fractures negatively correlate with overall survival in men with prostate cancer. *The Journal of Urology*, *168*, 1005-1007.

Oehler, B., Périer, C., Martin, V., Fisher, A., Lezmi, S., Kalinichev, M., & McMahon, S.B. (2022). Evaluation of recombinant botulinum neurotoxin type A1 efficacy in peripheral inflammatory pain in mice. *Frontiers in Molecular Neuroscience*, *15*, 909835.

Omori, Y., Kagaya, K., Enomoto, R., Sasaki, A., Andoh, T., Nojima, H., Takahata, H., & Kuraishi, Y. (2009). A mouse model of sural nerve injury-induced neuropathy: gabapentin inhibits pain-related behaviors and the hyperactivity of wide-dynamic range neurons in the dorsal horn. *Journal of Pharmacological Sciences*, *109*, 532-539.

O'Neill, J., Sikandar, S., McMahon, S.B., & Dickenson, A.H. (2015). Human psychophysics and rodent spinal neurones exhibit peripheral and central mechanisms of inflammatory pain in the UVB and UVB heat rekindling models. *The Journal of Physiology*, *593*, 4029-4042.

Ong, W.Y., Stohler, C.S., & Herr, D.R. (2019). Role of the prefrontal cortex in pain processing. *Molecular Neurobiology*, *56*, 1137-1166.

Oraki Kohshour, M., Mirzaie, S., Zeinali, M., Amin, M., Said Hakhamaneshi, M., Jalili, A., Mosaveri, N., & Jamalan, M. (2014). Ablation of breast cancer cells using trastuzumab-functionalized multi-walled carbon nanotubes and trastuzumab-diphtheria toxin conjugate. *Chemical Biology & Drug Design*, *83*, 259-265.

Orhurhu, V.J., Pittelkow, T.P., & Hooten, W.M. (2015). Prevalence of smoking in adults with chronic pain. *Tobacco Induced Diseases*, *13*, 17.

Ostrowsky, K., Magnin, M., Ryvlin, P., Isnard, J., Guenot, M., & Mauguière, F. (2002). Representation of pain and somatic sensation in the human insula: a study of responses to direct electrical cortical stimulation. *Cerebral Cortex*, *12*, 376-385.

Pachitariu, M., Stringer, C., Schröder, S., Dipoppa, M., Rossi, L.F., Carandini, M., & Harris, K.D. (2016). Suite2p: beyond 10,000 neurons with standard two-photon microscopy. BioRxiv, 061507.

Palit, S., Bartley, E.J., Kuhn, B.L., Kerr, K.L., DelVentura, J.L., Terry, E.L., & Rhudy, J.L. (2016). Endogenous inhibition of pain and spinal nociception in women with premenstrual dysphoric disorder. *Journal of Pain Research*, *9*, 57-66.

Park, S.H., Eber, M.R., Widner, D.B., & Shiozawa, Y. (2018). Role of the bone microenvironment in the development of painful complications of skeletal metastases. *Cancers*, *10*, 141.

Patel, R., & Dickenson, A.H. (2020). A study of cortical and brainstem mechanisms of diffuse noxious inhibitory controls in anaesthetised normal and neuropathic rats. *The European Journal of Neuroscience*, *51*, 952-962.

Patel, R., Gonçalves, L., Leveridge, M., Mack, S.R., Hendrick, A., Brice, N.L., & Dickenson, A.H. (2014). Anti-hyperalgesic effects of a novel TRPM8 agonist in neuropathic rats: a comparison with topical menthol. *Pain*, *155*, 2097-2107.

Patel, R., Qu, C., Xie, J.Y., Porreca, F., & Dickenson, A.H. (2018). Selective deficiencies in descending inhibitory modulation in neuropathic rats: implications for enhancing noradrenergic tone. *Pain*, *159*, 1887-1899.

Patel, R., Taylor, J.L., Dickenson, A.H., McMahon, S.B., & Bannister, K. (2024). A back-translational study of descending interactions with the induction of hyperalgesia by high-frequency electrical stimulation in rat and human. *Pain*, 10.1097/j.pain.0000000000003166. Advance online publication.

Peck, L.J., Patel, R., Diaz, P., Wintle, Y.M., Dickenson, A.H., Todd, A.J., Calvo, M., & Bennett, D.L.H. (2021). Studying independent *Kcna6* knock-out mice reveals toxicity of exogenous lacZ to central nociceptor terminals and differential effects of Kv1.6 on acute and neuropathic pain sensation. *The Journal of Neuroscience*, *41*, 9141-9162.

Peng, Y.B., Kenshalo, D.R., & Gracely, R.H. (2003). Periaqueductal gray-evoked dorsal root reflex is frequency dependent. *Brain Research*, *976*, 217-226.

Peng, Y.B., Wu, J., Willis, W.D., & Kenshalo, D.R. (2001). GABA(A) and 5-HT(3) receptors are involved in dorsal root reflexes: possible role in periaqueductal gray descending inhibition. *Journal of Neurophysiology*, *86*, 49-58.

Pereira-Silva, R., Costa-Pereira, J.T., Alonso, R., Serrão, P., Martins, I., & Neto, F.L. (2020). Attenuation of the diffuse noxious inhibitory controls in chronic joint inflammatory pain is accompanied by anxiodepressive-like behaviors and impairment of the descending noradrenergic modulation. *International Journal of Molecular Sciences*, *21*, 2973.

Pertovaara, A. (2006). Noradrenergic pain modulation. *Progress in Neurobiology*, *80*, 53-83.

Phelan, K.D., & Falls, W.M. (1991). The spinotrigeminal pathway and its spatial relationship to the origin of trigeminospinal projections in the rat. *Neuroscience*, *40*, 477-496.

Phelps, C.E., Navratilova, E., Dickenson, A.H., Porreca, F., & Bannister, K. (2019). Kappa opioid signaling in the right central amygdala causes hind paw specific loss of diffuse noxious inhibitory controls in experimental neuropathic pain. *Pain*, *160*, 1614-1621.

Pogorzala, L.A., Mishra, S.K., & Hoon, M.A. (2013). The cellular code for mammalian thermosensation. *The Journal of Neuroscience*, *33*, 5533-5541.

Popescu, A., LeResche, L., Truelove, E.L., & Drangsholt, M.T. (2010). Gender differences in pain modulation by diffuse noxious inhibitory controls: a systematic review. *Pain*, *150*, 309-318.

Prato, V., Taberner, F.J., Hockley, J.R.F., Callejo, G., Arcourt, A., Tazir, B., Hammer, L., Schad, P., Heppenstall, P.A., Smith, E.S., & Lechner, S.G. (2017). Functional and molecular characterization of mechanoinsensitive "silent" nociceptors. *Cell Reports*, *21*, 3102-3115.

Price, T. J., & Flores, C. M. (2007). Critical evaluation of the colocalization between calcitonin gene-related peptide, substance P, transient receptor potential vanilloid subfamily type 1 immunoreactivities, and isolectin B4 binding in primary afferent neurons of the rat and mouse. *The Journal of Pain*, *8*, 263-272.

Putzke, J.D., Richards, J.S., Hicken, B.L., Ness, T.J., Kezar, L., & DeVivo, M. (2002). Pain classification following spinal cord injury: the utility of verbal descriptors. *Spinal Cord*, *40*, 118-127.

Rabchevsky, A.G. (2006). Segmental organization of spinal reflexes mediating autonomic dysreflexia after spinal cord injury. *Progress in Brain Research*, *152*, 265-274.

Rahmati, V., Kirmse, K., Marković, D., Holthoff, K., & Kiebel, S.J. (2016). Inferring neuronal dynamics from calcium imaging data using biophysical models and bayesian inference. *PLoS Computational Biology*, *12*, e1004736.

Raja, S.N., Carr, D.B., Cohen, M., Finnerup, N.B., Flor, H., Gibson, S., Keefe, F.J., Mogil, J.S., Ringkamp, M., Sluka, K.A., Song, X.J., Stevens, B., Sullivan, M.D., Tutelman, P.R., Ushida, T., & Vader, K. (2020). The revised International Association for the Study of Pain definition of pain: concepts, challenges, and compromises. *Pain*, *161*, 1976-1982.

Rajaofetra, N., Ridet, J.L., Poulat, P., Marlier, L., Sandillon, F., Geffard, M., & Privat, A. (1992). Immunocytochemical mapping of noradrenergic projections to the rat spinal cord with an antiserum against noradrenaline. *Journal of Neurocytology*, *21*, 481-494.

Raoof, R., Martin Gil, C., Lafeber, F.P.J.G., de Visser, H., Prado, J., Versteeg, S., Pascha, M.N., Heinemans, A.L.P., Adolfs, Y., Pasterkamp, J., Wood, J.N., Mastbergen, S.C., & Eijkelkamp, N. (2021). Dorsal root ganglia macrophages maintain osteoarthritis pain. *The Journal of Neuroscience*, *41*, 8249-8261.

Reavis, H.D., Chen, H.I., & Drapkin, R. (2020). Tumor innervation: cancer has some nerve. *Trends in Cancer*, *6*, 1059-1067.

Reid, E., Harvie, D., Miegel, R., Spence, C., & Moseley, G.L. (2015). Spatial summation of pain in humans investigated using transcutaneous electrical stimulation. *The Journal of Pain*, *16*, 11-18.

Rexed, B. (1954). A cytoarchitectonic atlas of the spinal cord in the cat. *The Journal of Comparative Neurology*, *100*, 297-379.

Reynolds, D.V. (1969). Surgery in the rat during electrical analgesia induced by focal brain stimulation. *Science*, *164*, 444-445.

Rezaii, T., & Ernberg, M. (2010). Influence of oral contraceptives on endogenous pain control in healthy women. *Experimental Brain Research*, *203*, 329-338.

Rezaii, T., Hirschberg, A.L., Carlström, K., & Ernberg, M. (2012). The influence of menstrual phases on pain modulation in healthy women. *The Journal of Pain*, *13*, 646-655.

Rice, A.S.C., Smith, B.H., & Blyth, F.M. (2016). Pain and the global burden of disease. *Pain*, *157*, 791-796.

Richter, F., Natura, G., Löser, S., Schmidt, K., Viisanen, H., & Schaible, H.G. (2010). Tumor necrosis factor causes persistent sensitization of joint nociceptors to mechanical stimuli in rats. *Arthritis and Rheumatism*, *62*, 3806-3814.

Ridet, J.L., Rajaofetra, N., Teilhac, J.R., Geffard, M., & Privat, A. (1993). Evidence for nonsynaptic serotonergic and noradrenergic innervation of the rat dorsal horn and possible involvement of neuron-glia interactions. *Neuroscience*, *52*, 143-157.

Riley, J.L., Robinson, M.E., Wise, E.A., Myers, C.D., & Fillingim, R.B. (1998). Sex differences in the perception of noxious experimental stimuli: a meta-analysis. *Pain*, *74*, 181-187.

Rizvi, T.A., Ennis, M., Behbehani, M.M., & Shipley, M.T. (1991). Connections between the central nucleus of the amygdala and the midbrain periaqueductal gray: topography and reciprocity. *The Journal of Comparative Neurology*, *303*, 121-131.

Roncati, L., Manenti, A., Pusiol, T., Piscioli, F., Barbolini, G., & Maiorana, A. (2016). Testosterone aromatization to estradiol in course of ovarian functioning Brenner tumor associated with endometrial carcinoma and endometriosis (Roncati-Manenti triad). *International Journal of Gynecological Cancer*, *26*, 1461-1464.

Ross, J.L., Queme, L.F., Lamb, J.E., Green, K.J., & Jankowski, M.P. (2018). Sex differences in primary muscle afferent sensitization following ischemia and reperfusion injury. *Biology of Sex Differences*, *9*, 2.

Rostock, C., Schrenk-Siemens, K., Pohle, J., & Siemens, J. (2018). Human vs. mouse nociceptors - similarities and differences. *Neuroscience*, *387*, 13-27.

Ryan, C., Stoltzfus, K.C., Horn, S., Chen, H., Louie, A.V., Lehrer, E.J., Trifiletti, D.M., Fox, E.J., Abraham, J.A., & Zaorsky, N.G. (2022). Epidemiology of bone metastases. *Bone*, *158*, 115783.

Sahbaie, P., Irvine, K.A., Shi, X.Y., & Clark, J.D. (2022). Monoamine control of descending pain modulation after mild traumatic brain injury. *Scientific Reports*, *12*, 16359.

Saito, M., Iwawaki, T., Taya, C., Yonekawa, H., Noda, M., Inui, Y., Mekada, E., Kimata, Y., Tsuru, A., & Kohno, K. (2001). Diphtheria toxin receptor-mediated conditional and targeted cell ablation in transgenic mice. *Nature Biotechnology*, *19*, 746-750.

Salamanna, F., Martini, L., Pagani, S., Parrilli, A., Giavaresi, G., Maltarello, M.C., & Fini, M. (2013). MRMT-1 rat breast carcinoma cells and models of bone metastases: improvement of an *in vitro* system to mimic the *in vivo* condition. *Acta Histochemica*, *115*, 76-85.

Samulowitz, A., Gremyr, I., Eriksson, E., & Hensing, G. (2018). "Brave men" and "Emotional women": a theory-guided literature review on gender bias in health care and gendered norms towards patients with chronic pain. *Pain Research & Management*, *2018*, 6358624.

Sandkühler, J., Eblen-Zajjur, A., Fu, Q.G., & Forster, C. (1995). Differential effects of spinalization on discharge patterns and discharge rates of simultaneously recorded nociceptive and non-nociceptive spinal dorsal horn neurons. *Pain*, *60*, 55-65.

Santana-Varela, S., Bogdanov, Y.D., Gossage, S.J., Okorokov, A.L., Li, S., de Clauser, L., Alves-Simoes, M., Sexton, J.E., Iseppon, F., Luiz, A.P., Zhao, J., Wood, J.N., & Cox, J.J. (2021). Tools for analysis and conditional deletion of subsets of sensory neurons. *Wellcome Open Research*, *6*, 250.

Santos, M., Kuncar, V., Martínez-Taboada, F., & Tendillo, F.J. (2005). Large concentrations of nitrous oxide decrease the isoflurane minimum alveolar concentration sparing effect of morphine in the rat. *Anesthesia and Analgesia*, *100*, 404-408.

Satkeviciute, I., Goodwin, G., Bove, G.M., & Dilley, A. (2018). Time course of ongoing activity during neuritis and following axonal transport disruption. *Journal of Neurophysiology*, *119*, 1993-2000.

Sauer, S.K., Reeh, P.W., & Bove, G.M. (2001). Noxious heat-induced CGRP release from rat sciatic nerve axons *in vitro*. *The European Journal of Neuroscience*, *14*, 1203-1208.

Scarpi, E., Calistri, D., Klepstad, P., Kaasa, S., Skorpen, F., Habberstad, R., Nanni, O., Amadori, D., & Maltoni, M. (2014). Clinical and genetic factors related to cancer-induced bone pain and bone pain relief. *The Oncologist*, *19*, 1276-1283.

Schindelin, J., Arganda-Carreras, I., Frise, E., Kaynig, V., Longair, M., Pietzsch, T., Preibisch, S., Rueden, C., Saalfeld, S., Schmid, B., Tinevez, J.Y., White, D.J., Hartenstein, V., Eliceiri, K., Tomancak, P., & Cardona, A. (2012). Fiji: an open-source platform for biological-image analysis. *Nature Methods*, *9*, 676-682.

Schliessbach, J., Lütolf, C., Streitberger, K., Scaramozzino, P., Arendt-Nielsen, L., & Curatolo, M. (2019). Reference values of conditioned pain modulation. *Scandinavian Journal of Pain*, *19*, 279-286.

Schmidt, R., Schmelz, M., Forster, C., Ringkamp, M., Torebjörk, E., & Handwerker, H. (1995). Novel classes of responsive and unresponsive C nociceptors in human skin. *The Journal of Neuroscience*, *15*, 333-341.

Schneider, C.A., Rasband, W.S., & Eliceiri, K.W. (2012). NIH Image to ImageJ: 25 years of image analysis. *Nature Methods*, *9*, 671-675.

Schnitzler, A., & Ploner, M. (2000). Neurophysiology and functional neuroanatomy of pain perception. *Journal of Clinical Neurophysiology*, *17*, 592-603.

Schreiber, K.L., Martel, M.O., Shnol, H., Shaffer, J.R., Greco, C., Viray, N., Taylor, L.N., McLaughlin, M., Brufsky, A., Ahrendt, G., Bovbjerg, D., Edwards, R.R., & Belfer, I. (2013). Persistent pain in postmastectomy patients: comparison of psychophysical, medical, surgical, and psychosocial characteristics between patients with and without pain. *Pain*, *154*, 660-668.

Schwei, M.J., Honore, P., Rogers, S.D., Salak-Johnson, J.L., Finke, M.P., Ramnaraine, M.L., Clohisy, D.R., & Mantyh, P.W. (1999). Neurochemical and cellular reorganization of the spinal cord in a murine model of bone cancer pain. *The Journal of Neuroscience*, *19*, 10886-10897.

Scott, A.C., McConnell, S., Laird, B., Colvin, L., & Fallon, M. (2012). Quantitative Sensory Testing to assess the sensory characteristics of cancer-induced bone pain after radiotherapy and potential clinical biomarkers of response. *European Journal of Pain*, *16*, 123-133.

Seagrove, L.C., Suzuki, R., & Dickenson, A.H. (2004). Electrophysiological characterisations of rat lamina I dorsal horn neurones and the involvement of excitatory amino acid receptors. *Pain*, *108*, 76-87.

Segelcke, D., Talbot, S.R., Palme, R., La Porta, C., Pogatzki-Zahn, E., Bleich, A., & Tappe-Theodor, A. (2023). Experimenter familiarization is a crucial prerequisite for assessing behavioral outcomes and reduces stress in mice not only under chronic pain conditions. *Scientific Reports*, *13*, 2289.

Sengul, G., Puchalski, R.B., & Watson, C. (2012). Cytoarchitecture of the spinal cord of the postnatal (P4) mouse. *Anatomical Record*, *295*, 837-845.

Seretny, M., Currie, G.L., Sena, E.S., Ramnarine, S., Grant, R., MacLeod, M.R., Colvin, L.A., & Fallon, M. (2014). Incidence, prevalence, and predictors of chemotherapy-induced peripheral neuropathy: A systematic review and meta-analysis. *Pain*, *155*, 2461-2470.

Serra, J., Campero, M., Bostock, H., & Ochoa, J. (2004). Two types of C nociceptors in human skin and their behavior in areas of capsaicin-induced secondary hyperalgesia. *Journal of Neurophysiology*, *91*, 2770-2781.

Sevcik, M.A., Ghilardi, J.R., Peters, C.M., Lindsay, T.H., Halvorson, K.G., Jonas, B.M., Kubota, K., Kuskowski, M.A., Boustany, L., Shelton, D.L., & Mantyh, P.W. (2005). Anti-NGF therapy profoundly reduces bone cancer pain and the accompanying increase in markers of peripheral and central sensitization. *Pain*, *115*, 128-141.

Shiers, S.I., Sankaranarayanan, I., Jeevakumar, V., Cervantes, A., Reese, J.C., & Price, T.J. (2021). Convergence of peptidergic and non-peptidergic protein markers in the human dorsal root ganglion and spinal dorsal horn. *The Journal of Comparative Neurology*, *529*, 2771-2788.

Shim, J., Iwaya, C., Ambrose, C.G., Suzuki, A., & Iwata, J. (2022). Micro-computed tomography assessment of bone structure in aging mice. *Scientific Reports*, *12*, 8117.

Siembida, E.J., Smith, A.W., Potosky, A.L., Graves, K.D., & Jensen, R.E. (2021). Examination of individual and multiple comorbid conditions and health-related quality of life in older cancer survivors. *Quality of Life*, *30*, 1119-1129.

Sikandar, S., Ronga, I., Iannetti, G.D., & Dickenson, A.H. (2013). Neural coding of nociceptive stimuli-from rat spinal neurones to human perception. *Pain*, *154*, 1263-1273.

Sikora, M.J., Cordero, K.E., Larios, J.M., Johnson, M.D., Lippman, M.E., & Rae, J.M. (2009). The androgen metabolite 5alpha-androstane-3beta,17beta-diol (3betaAdiol) induces breast cancer growth via estrogen receptor: implications for aromatase inhibitor resistance. *Breast Cancer Research and Treatment*, *115*, 289-296.

Skirboll, L., Hökfelt, T., Dockray, G., Rehfeld, J., Brownstein, M., & Cuello, A.C. (1983). Evidence for periaqueductal cholecystokinin-substance P neurons projecting to the spinal cord. *The Journal of Neuroscience*, *3*, 1151-1157.

Sliepen, SHJ. (2021). Bone cancer pain, mechanism and treatment. In H. Amarasekera (Ed.), *Recent Advances in Bone Tumours and Osteoarthritis*. InTechOpen.

Sluka, K.A., Rees, H., Westlund, K.N., & Willis, W.D. (1995). Fiber types contributing to dorsal root reflexes induced by joint inflammation in cats and monkeys. *Journal of Neurophysiology*, *74*, 981-989.

Sneddon, L.U. (2018). Comparative physiology of nociception and pain. *Physiology*, *33*, 63-73.

Sonne-Hansen, K., & Lykkesfeldt, A.E. (2005). Endogenous aromatization of testosterone results in growth stimulation of the human MCF-7 breast cancer cell line. *The Journal of Steroid Biochemistry and Molecular Biology*, *93*, 25-34.

Sonohata, M., Furue, H., Katafuchi, T., Yasaka, T., Doi, A., Kumamoto, E., & Yoshimura, M. (2004). Actions of noradrenaline on substantia gelatinosa neurones in the rat spinal cord revealed by *in vivo* patch recording. *The Journal of Physiology*, *555*, 515-526.

Sorge, R.E., LaCroix-Fralish, M.L., Tuttle, A.H., Sotocinal, S.G., Austin, J.S., Ritchie, J., Chanda, M.L., Graham, A.C., Topham, L., Beggs, S., Salter, M.W., & Mogil, J.S. (2011). Spinal cord Toll-like receptor 4 mediates inflammatory and neuropathic hypersensitivity in male but not female mice. *The Journal of Neuroscience*, *31*, 15450-15454.

Sorge, R.E., Mapplebeck, J.C., Rosen, S., Beggs, S., Taves, S., Alexander, J.K., Martin, L.J., Austin, J.S., Sotocinal, S.G., Chen, D., Yang, M., Shi, X.Q., Huang, H., Pillon, N.J., Bilan, P.J., Tu, Y., Klip, A., Ji, R.R., Zhang, J., Salter, M.W., … Mogil, J.S. (2015). Different immune cells mediate mechanical pain hypersensitivity in male and female mice. *Nature Neuroscience*, *18*, 1081-1083.

Sorkin, L.S., Eddinger, K.A., Woller, S.A., & Yaksh, T.L. (2018). Origins of antidromic activity in sensory afferent fibers and neurogenic inflammation. *Seminars in Immunopathology*, *40*, 237-247.

Spike, R.C., Puskár, Z., Andrew, D., & Todd, A.J. (2003). A quantitative and morphological study of projection neurons in lamina I of the rat lumbar spinal cord. *The European Journal of Neuroscience*, *18*, 2433-2448.

Staud, R., Robinson, M.E., Vierck, C.J., & Price, D.D. (2003). Diffuse noxious inhibitory controls (DNIC) attenuate temporal summation of second pain in normal males but not in normal females or fibromyalgia patients. *Pain*, *101*, 167-174.

Stephens, K.E., Zhou, W., Ji, Z., Chen, Z., He, S., Ji, H., Guan, Y., & Taverna, S.D. (2019). Sex differences in gene regulation in the dorsal root ganglion after nerve injury. *BMC Genomics*, *20*, 147.

Stevens, R.T., London, S.M., & Apkarian, A.V. (1993). Spinothalamocortical projections to the secondary somatosensory cortex (SII) in squirrel monkey. *Brain Research*, *631*, 241-246.

Stevens, W.C., Dolan, W.M., Gibbons, R.T., White, A., Eger, E.I., Miller, R.D., DeJong, R.H., & Elashoff, R.M. (1975). Minimum alveolar concentrations (MAC) of isoflurande with and without nitrous oxide in patients of various ages. *Anesthesiology*, *42*, 197-200.

Steverink, J.G., Oostinga, D., van Tol, F.R., van Rijen, M.H.P., Mackaaij, C., Verlinde-Schellekens, S.A.M.W., Oosterman, B.J., Van Wijck, A.J.M., Roeling, T.A.P., & Verlaan, J.J. (2021). Sensory innervation of human bone: an immunohistochemical study to further understand bone pain. *The Journal of Pain*, *22*, 1385-1395.

Stone, L.S., Broberger, C., Vulchanova, L., Wilcox, G. L., Hökfelt, T., Riedl, M.S., & Elde, R. (1998). Differential distribution of alpha2A and alpha2C adrenergic receptor immunoreactivity in the rat spinal cord. *The Journal of Neuroscience*, *18*, 5928-5937.

Straube, S., Andrew Moore, R., Derry, S., & McQuay, H.J. (2009). Vitamin D and chronic pain. *Pain*, *141*, 10-13.

Sulistio, M., Wojnar, R., Key, S., Kwok, J., Al-Rubaie, Z., & Michael, N. (2021). The role of methadone in cancer-induced bone pain: a retrospective cohort study. *Supportive Care in Cancer*, *29*, 1327-1335.

Sung, H., Ferlay, J., Siegel, R.L., Laversanne, M., Soerjomataram, I., Jemal, A., & Bray, F. (2021). Global cancer statistics 2020: GLOBOCAN estimates of incidence and mortality worldwide for 36 cancers in 185 countries. *CA: A Cancer Journal for Clinicians*, *71*, 209-249.

Swenson, R.S., & Castro, A.J. (1983). The afferent connections of the inferior olivary complex in rats: a study using the retrograde transport of horseradish peroxidase. *The American Journal of Anatomy*, *166*, 329-341.

Sze, W.M., Shelley, M.D., Held, I., Wilt, T.J., & Mason, M.D. (2003). Palliation of metastatic bone pain: single fraction versus multifraction radiotherapy--a systematic review of randomised trials. *Clinical Oncology*, *15*, 345-352.

Tan, S., Faull, R.L. M., & Curtis, M.A. (2023). The tracts, cytoarchitecture, and neurochemistry of the spinal cord. *Anatomical Record*, *306*, 777-819.

Tanaka, K., Kondo, T., Narita, M., Muta, T., Yoshida, S., Sato, D., Suda, Y., Hamada, Y., Shimizu, T., Kuzumaki, N., & Narita, M. (2023). Cancer aggravation due to persistent pain signals with the increased expression of pain-related mediators in sensory neurons of tumor-bearing mice. *Molecular Brain*, *16*, 19.

Tanaka, M., Matsumoto, Y., Murakami, T., Hisa, Y., & Ibata, Y. (1996). The origins of catecholaminergic innervation in the rostral ventromedial medulla oblongata of the rat. *Neuroscience Letters*, *207*, 53-56.

Tang, Y., Peng, H., Liao, Q., Gan, L., Zhang, R., Huang, L., Ding, Z., Yang, H., Yan, X., Gu, Y., Zang, X., Huang, D., & Cao, S. (2016). Study of breakthrough cancer pain in an animal model induced by endothelin-1. *Neuroscience Letters*, *617*, 108-115.

Taylor, B.K., & Westlund, K.N. (2017). The noradrenergic locus coeruleus as a chronic pain generator. *Journal of Neuroscience Research*, *95*, 1336-1346.

Taylor-Clark, T.E., Undem, B.J., Macglashan, D.W., Ghatta, S., Carr, M.J., & McAlexander, M.A. (2008). Prostaglandin-induced activation of nociceptive neurons via direct interaction with transient receptor potential A1 (TRPA1). *Molecular Pharmacology*, *73*, 274-281.

Teasell, R.W., & Bombardier, C. (2001). Employment-related factors in chronic pain and chronic pain disability. *The Clinical Journal of Pain*, *17*, S39-S45.

Teepker, M., Kunz, M., Peters, M., Kundermann, B., Schepelmann, K., & Lautenbacher, S. (2014). Endogenous pain inhibition during menstrual cycle in migraine. *European Journal of Pain*, *18*, 989-998.

Teijeira, A., Garasa, S., Luri-Rey, C., de Andrea, C., Gato, M., Molina, C., Kaisho, T., Cirella, A., Azpilikueta, A., Wculek, S.K., Egea, J., Olivera, I., Rodriguez, I., Rouzaut, A., Verkhusha, V., Valencia, K., Sancho, D., Berraondo, P., & Melero, I. (2022). Depletion of conventional type-1 dendritic cells in established tumors suppresses immunotherapy efficacy. *Cancer Research*, *82*, 4373-4385.

Terner, J.M., Barrett, A.C., Cook, C.D., & Picker, M.J. (2003). Sex differences in (-)-pentazocine antinociception: comparison to morphine and spiradoline in four rat strains using a thermal nociceptive assay. *Behavioural Pharmacology*, *14*, 77-85.

Terner, J.M., Lomas, L.M., Smith, E.S., Barrett, A.C., & Picker, M.J. (2003). Pharmacogenetic analysis of sex differences in opioid antinociception in rats. *Pain*, *106*, 381-391.

Tétreault, P., Dansereau, M.A., Doré-Savard, L., Beaudet, N., & Sarret, P. (2011). Weight bearing evaluation in inflammatory, neuropathic and cancer chronic pain in freely moving rats. *Physiology & Behavior*, *104*, 495-502.

Thai, J., Kyloh, M., Travis, L., Spencer, N.J., & Ivanusic, J.J. (2020). Identifying spinal afferent (sensory) nerve endings that innervate the marrow cavity and periosteum using anterograde tracing. *The Journal of Comparative Neurology*, *528*, 1903-1916.

Timmermann, L., Ploner, M., Haucke, K., Schmitz, F., Baltissen, R., & Schnitzler, A. (2001). Differential coding of pain intensity in the human primary and secondary somatosensory cortex. *Journal of Neurophysiology*, *86*, 1499-1503.

Todd, A.J. (2010). Neuronal circuitry for pain processing in the dorsal horn. *Nature Reviews*, *11*, 823-836.

Toennies, J.F. (1938). Reflex discharge from the spinal cord over the dorsal roots. *Journal of Neurophysiology*, *1*, 378-390.

Tousignant-Laflamme, Y., & Marchand, S. (2009). Excitatory and inhibitory pain mechanisms during the menstrual cycle in healthy women. *Pain*, *146*, 47-55.

Traub, R.J., Sengupta, J.N., & Gebhart, G.F. (1996). Differential c-fos expression in the nucleus of the solitary tract and spinal cord following noxious gastric distention in the rat. *Neuroscience*, *74*, 873-884.

Travagli, R.A., & Williams, J.T. (1996). Endogenous monoamines inhibit glutamate transmission in the spinal trigeminal nucleus of the guinea-pig. *The Journal of Physiology*, *491*, 177-185.

Treede, R.D., Meyer, R.A., & Campbell, J.N. (1998). Myelinated mechanically insensitive afferents from monkey hairy skin: heat-response properties. *Journal of Neurophysiology*, *80*, 1082-1093.

Treede, R.D., Rief, W., Barke, A., Aziz, Q., Bennett, M.I., Benoliel, R., Cohen, M., Evers, S., Finnerup, N.B., First, M.B., Giamberardino, M.A., Kaasa, S., Korwisi, B., Kosek, E., Lavand'homme, P., Nicholas, M., Perrot, S., Scholz, J., Schug, S., Smith, B.H., … Wang, S.J. (2019). Chronic pain as a symptom or a disease: the IASP classification of chronic pain for the international classification of diseases (ICD-11). *Pain*, *160*, 19-27.

Trendafilova, T., Adhikari, K., Schmid, A.B., Patel, R., Polgár, E., Chisholm, K.I., Middleton, S.J., Boyle, K., Dickie, A.C., Semizoglou, E., Perez-Sanchez, J., Bell, A.M., Ramirez-Aristeguieta, L.M., Khoury, S., Ivanov, A., Wildner, H., Ferris, E., Chacón-Duque, J.C., Sokolow, S., Saad Boghdady, M.A., … Bennett, D.L. (2022). Sodium-calcium exchanger-3 regulates pain "wind-up": from human psychophysics to spinal mechanisms. *Neuron*, *110*, 2571-2587.e13.

Trouvin, A.P., & Perrot, S. (2019). New concepts of pain. *Best Practice & Research Clinical Rheumatology*, *33*, 101415.

Tsantoulas, C., & McMahon, S.B. (2014). Opening paths to novel analgesics: the role of potassium channels in chronic pain. *Trends in Neurosciences*, *37*, 146-158.

Tuboly, G., Benedek, G., & Horvath, G. (2009). Selective disturbance of pain sensitivity after social isolation. *Physiology & Behavior*, *96*, 18-22.

Turan, V.K., Sanchez, R.I., Li, J.J., Li, S.A., Reuhl, K.R., Thomas, P.E., Conney, A.H., Gallo, M.A., Kauffman, F.C., & Mesia-Vela, S. (2004). The effects of steroidal estrogens in ACI rat mammary carcinogenesis: 17beta-estradiol, 2-hydroxyestradiol, 4-hydroxyestradiol, 16alpha-hydroxyestradiol, and 4-hydroxyestrone. *The Journal of Endocrinology*, *183*, 91-99.

Ungard, R.G., Zhu, Y.F., Yang, S., Nakhla, P., Parzei, N., Zhu, K.L., & Singh, G. (2020). Response to pregabalin and progesterone differs in male and female rat models of neuropathic and cancer pain. *Canadian Journal of Pain*, *4*, 39-58.

Urban, M.O., & Gebhart, G.F. (1997). Characterization of biphasic modulation of spinal nociceptive transmission by neurotensin in the rat rostral ventromedial medulla. *Journal of Neurophysiology*, *78*, 1550-1562.

Urban, R., Scherrer, G., Goulding, E.H., Tecott, L.H., & Basbaum, A.I. (2011). Behavioral indices of ongoing pain are largely unchanged in male mice with tissue or nerve injury-induced mechanical hypersensitivity. *Pain*, *152*, 990-1000.

Urch, E.C., Donovan-Rodriguez, T., & Dickenson, H.A. (2003). Alterations in dorsal horn neurones in a rat model of cancer-induced bone pain. *Pain*, *106*, 347-356.

Usoskin, D., Furlan, A., Islam, S., Abdo, H., Lönnerberg, P., Lou, D., Hjerling-Leffler, J., Haeggström, J., Kharchenko, O., Kharchenko, P.V., Linnarsson, S., & Ernfors, P. (2015). Unbiased classification of sensory neuron types by large-scale single-cell RNA sequencing. *Nature Neuroscience*, *18*, 145-153.

Vacca, V., Marinelli, S., Pieroni, L., Urbani, A., Luvisetto, S., & Pavone, F. (2016). 17beta-estradiol counteracts neuropathic pain: a behavioural, immunohistochemical, and proteomic investigation on sex-related differences in mice. *Scientific Reports*, *6*, 18980.

Vadivelu, N., Kai, A.M., Kodumudi, V., Sramcik, J., & Kaye, A.D. (2018). The opioid crisis: a comprehensive overview. *Current Pain and Headache Reports*, *22*, 16.

van den Beuken-van Everdingen, M.H., de Rijke, J.M., Kessels, A.G., Schouten, H.C., van Kleef, M., & Patijn, J. (2007). Prevalence of pain in patients with cancer: a systematic review of the past 40 years. *Annals of Oncology*, *18*, 1437-1449.

van den Beuken-van Everdingen, M.H., Hochstenbach, L.M., Joosten, E.A., Tjan-Heijnen, V.C., & Janssen, D.J. (2016). Update on prevalence of pain in patients with cancer: systematic review and meta-analysis. *Journal of Pain and Symptom Management*, *51*, 1070-1090.e9.

van Gehuchten, A. (1891). La structure de centre nerveux: la moelle épinière et le cervelet. *Cellule*, *7*, 79-122.

van Maaren, M.C., Bretveld, R.W., Jobsen, J.J., Veenstra, R.K., Groothuis-Oudshoorn, C.G., Struikmans, H., Maduro, J.H., Strobbe, L.J., Poortmans, P.M., & Siesling, S. (2017). The influence of timing of radiation therapy following breast-conserving surgery on 10-year disease-free survival. *British Journal of Cancer*, *117*, 179-188.

Vendruscolo, L.F., Pamplona, F.A., & Takahashi, R.N. (2004). Strain and sex differences in the expression of nociceptive behavior and stress-induced analgesia in rats. *Brain Research*, *1030*, 277-283.

Vicente-Baz, J., Lopez-Garcia, J.A., & Rivera-Arconada, I. (2022). Central sensitization of dorsal root potentials and dorsal root reflexes: An *in vitro* study in the mouse spinal cord. *European Journal of Pain*, *26*, 356-369.

Vierck, C.J., Whitsel, B.L., Favorov, O.V., Brown, A.W., & Tommerdahl, M. (2013). Role of primary somatosensory cortex in the coding of pain. *Pain*, *154*, 334-344.

Villanueva, L., Cadden, S.W., & Le Bars, D. (1984a). Evidence that diffuse noxious inhibitory controls (DNIC) are medicated by a final post-synaptic inhibitory mechanism. *Brain Research*, *298*, 67-74.

Villanueva, L., Cadden, S.W., & Le Bars, D. (1984b). Diffuse noxious inhibitory controls (DNIC): evidence for post-synaptic inhibition of trigeminal nucleus caudalis convergent neurones. *Brain Research*, *321*, 165-168.

Villanueva, L., & Le Bars, D. (1995). The activation of bulbo-spinal controls by peripheral nociceptive inputs: diffuse noxious inhibitory controls. *Biological Research*, *28*, 113-125.

Villanueva, L., Chitour, D., & Le Bars, D. (1986). Involvement of the dorsolateral funiculus in the descending spinal projections responsible for diffuse noxious inhibitory controls in the rat. *Journal of Neurophysiology*, *56*, 1185-1195.

Voipio, H.M., Nevalainen, T., Halonen, P., Hakumäki, M., & Björk, E. (2006). Role of cage material, working style and hearing sensitivity in perception of animal care noise. *Laboratory Animals*, *40*, 400-409.

Voisin, D.L., Guy, N., Chalus, M., & Dallel, R. (2005). Nociceptive stimulation activates locus coeruleus neurones projecting to the somatosensory thalamus in the rat. *The Journal of Physiology*, *566*, 929-937.

Vollert, J., Trewartha, N., Kemkowski, D., Cremer, A.F., Zahn, P.K., Segelcke, D., & Pogatzki-Zahn, E.M. (2022). Conditioned pain modulation and offset analgesia: Influence of sex, sex hormone levels and menstrual cycle on the magnitude and retest reliability in healthy participants. *European Journal of Pain*, *26*, 1938-1949.

Wada, T., Hasegawa, Y., & Ono, H. (1997). Characterization of alpha1-adrenoceptor subtypes in facilitation of rat spinal motoneuron activity. *European Journal of Pharmacology*, *340*, 45-52.

Wagner, K.M., Roeder, Z., Desrochers, K., Buhler, A.V., Heinricher, M.M., & Cleary, D.R. (2013). The dorsomedial hypothalamus mediates stress-induced hyperalgesia and is the source of the pronociceptive peptide cholecystokinin in the rostral ventromedial medulla. *Neuroscience*, *238*, 29-38.

Wakabayashi, H., Wakisaka, S., Hiraga, T., Hata, K., Nishimura, R., Tominaga, M., & Yoneda, T. (2018). Decreased sensory nerve excitation and bone pain associated with mouse Lewis lung cancer in TRPV1-deficient mice. *Journal of Bone and Mineral Metabolism*, *36*, 274-285.

Wang, K., Donnelly, C.R., Jiang, C., Liao, Y., Luo, X., Tao, X., Bang, S., McGinnis, A., Lee, M., Hilton, M.J., & Ji, R.R. (2021). STING suppresses bone cancer pain via immune and neuronal modulation. *Nature Communications*, *12*, 4558.

Wang, L. N., Yang, J. P., Ji, F. H., Zhan, Y., Jin, X. H., Xu, Q. N., Wang, X. Y., & Zuo, J. L. (2012). Brain-derived neurotrophic factor modulates N-methyl-D-aspartate receptor activation in a rat model of cancer-induced bone pain. *Journal of Neuroscience Research*, *90*, 1249-1260.

Warwick, C., Salsovic, J., Hachisuka, J., Smith, K.M., Sheahan, T.D., Chen, H., Ibinson, J., Koerber, H.R., & Ross, S.E. (2022). Cell type-specific calcium imaging of central sensitization in mouse dorsal horn. *Nature Communications*, *13*, 5199.

Waters, A.J., & Lumb, B.M. (1997). Inhibitory effects evoked from both the lateral and ventrolateral periaqueductal grey are selective for the nociceptive responses of rat dorsal horn neurones. *Brain Research*, *752*, 239-249.

Wei, B., Kumada, T., Furukawa, T., Inoue, K., Watanabe, M., Sato, K., & Fukuda, A. (2013). Pre- and post-synaptic switches of GABA actions associated with Cl- homeostatic changes are induced in the spinal nucleus of the trigeminal nerve in a rat model of trigeminal neuropathic pain. *Neuroscience*, *228*, 334-348.

Wei, H., & Pertovaara, A. (2006). Spinal and pontine alpha2-adrenoceptors have opposite effects on pain-related behavior in the neuropathic rat. *European Journal of Pharmacology*, *551*, 41-49.

Wei, Z., Lin, B.J., Chen, T.W., Daie, K., Svoboda, K., & Druckmann, S. (2020). A comparison of neuronal population dynamics measured with calcium imaging and electrophysiology. *PLoS Computational Biology*, *16*, e1008198.

Weng, H.R., & Dougherty, P.M. (2005). Response properties of dorsal root reflexes in cutaneous C fibers before and after intradermal capsaicin injection in rats. *Neuroscience*, *132*, 823-831.

Wercberger, R., & Basbaum, A.I. (2019). Spinal cord projection neurons: a superficial, and also deep, analysis. *Current Opinion in Physiology*, *11*, 109-115.

West, S.J., Bannister, K., Dickenson, A.H., & Bennett, D.L. (2015). Circuitry and plasticity of the dorsal horn - toward a better understanding of neuropathic pain. *Neuroscience*, *300*, 254-275.

Westlund, K.N., Bowker, R.M., Ziegler, M.G., & Coulter, J.D. (1983). Noradrenergic projections to the spinal cord of the rat. *Brain Research*, *263*, 15-31.

Westlund, K.N., Bowker, R.M., Ziegler, M.G., & Coulter, J.D. (1984). Origins and terminations of descending noradrenergic projections to the spinal cord of monkey. *Brain Research*, *292*, 1-16.

Wetzel, C., Hu, J., Riethmacher, D., Benckendorff, A., Harder, L., Eilers, A., Moshourab, R., Kozlenkov, A., Labuz, D., Caspani, O., Erdmann, B., Machelska, H., Heppenstall, P.A., & Lewin, G.R. (2007). A stomatin-domain protein essential for touch sensation in the mouse. *Nature*, *445*, 206-209.

White, D.M., & Helme, R.D. (1985). Release of substance P from peripheral nerve terminals following electrical stimulation of the sciatic nerve. *Brain Research*, *336*, 27-31.

Wiech, K., Ploner, M., & Tracey, I. (2008). Neurocognitive aspects of pain perception. *Trends in Cognitive Sciences*, *12*, 306-313.

Wilkie, D.J., Huang, H.Y., Reilly, N., & Cain, K.C. (2001). Nociceptive and neuropathic pain in patients with lung cancer: a comparison of pain quality descriptors. *Journal of Pain and Symptom Management*, *22*, 899-910.

Willis, W.D. (1999). Dorsal root potentials and dorsal root reflexes: a double-edged sword. *Experimental Brain Research*, *124*, 395-421.

Willis, W.D. (2006). John Eccles' studies of spinal cord presynaptic inhibition. *Progress in Neurobiology*, *78*, 189-214.

Wilson, H., Carvalho, B., Granot, M., & Landau, R. (2013). Temporal stability of conditioned pain modulation in healthy women over four menstrual cycles at the follicular and luteal phases. *Pain*, *154*, 2633-2638.

Wirtshafter, H.S., & Disterhoft, J.F. (2022). *In vivo* multi-day calcium imaging of CA1 hippocampus in freely moving rats reveals a high preponderance of place cells with consistent place fields. *The Journal of Neuroscience*, *42*, 4538-4554.

Wu, L.X., Dong, Y.P., Zhu, Q.M., Zhang, B., Ai, B.L., Yan, T., Zhang, G.H., & Sun, L. (2021). Effects of dezocine on morphine tolerance and opioid receptor expression in a rat model of bone cancer pain. *BMC Cancer*, *21*, 1128.

Wu, P., Zhou, G., Wu, X., Lv, R., Yao, J., & Wen, Q. (2022). P2X7 receptor induces microglia polarization to the M1 phenotype in cancer-induced bone pain rat models. *Molecular Pain*, *18*, 17448069211060962.

Xu, Q., Zhang, X.M., Duan, K.Z., Gu, X.Y., Han, M., Liu, B.L., Zhao, Z.Q., & Zhang, Y.Q. (2013). Peripheral TGF-β1 signaling is a critical event in bone cancer-induced hyperalgesia in rodents. *The Journal of Neuroscience*, *33*, 19099-19111.

Xue, M., Shi, W.T., Zhou, S.B., Li, Y.N., Wu, F.Y., Chen, Q.Y., Liu, R.H., Zhou, Z.X., Zhang, Y.X., Chen, Y.X., Xu, F., Bi, G.Q., Li, X.H., Lu, J.S., & Zhuo, M. (2022). Mapping thalamic-anterior cingulate monosynaptic inputs in adult mice. *Molecular Pain*, *18*, 17448069221087034.

Yager, J.D., & Davidson, N.E. (2006). Estrogen carcinogenesis in breast cancer. *The New England Journal of Medicine*, *354*, 270-282.

Yam, M.F., Loh, Y.C., Tan, C.S., Khadijah Adam, S., Abdul Manan, N., & Basir, R. (2018). General pathways of pain sensation and the major neurotransmitters involved in pain regulation. *International Journal of Molecular Sciences*, *19*, 2164.

Yamamura, H., Iwata, K., Tsuboi, Y., Toda, K., Kitajima, K., Shimizu, N., Nomura, H., Hibiya, J., Fujita, S., & Sumino, R. (1996). Morphological and electrophysiological properties of ACCx nociceptive neurons in rats. *Brain Research*, *735*, 83-92.

Yanagisawa, Y., Furue, H., Kawamata, T., Uta, D., Yamamoto, J., Furuse, S., Katafuchi, T., Imoto, K., Iwamoto, Y., & Yoshimura, M. (2010). Bone cancer induces a unique central sensitization through synaptic changes in a wide area of the spinal cord. *Molecular Pain*, *6*, 38.

Yang, H., Wu, J., Zhen, S., Hu, Y., Li, D., Xie, M., & Zhu, H. (2022). Proteomic analysis of spinal cord tissue in a rat model of cancer-induced bone pain. *Frontiers in Molecular Neuroscience*, *15*, 1009615.

Yang, H., Yan, H., Li, X., Liu, J., Cao, S., Huang, B., Huang, D., & Wu, L. (2018). Inhibition of connexin 43 and phosphorylated nr2b in spinal astrocytes attenuates bone cancer pain in mice. *Frontiers in Cellular Neuroscience*, *12*, 129.

Yang, L., Fu, Q., Yang, L., & Zhang, Y. (2023). HIF-1α/MMP-9 promotes spinal cord central sensitization in rats with bone cancer pain. *European Journal of Pharmacology*, *954*, 175858.

Yang, Y., Zhang, J., Gao, Q., Bo, J., & Ma, Z. (2017). Etanercept attenuates thermal and mechanical hyperalgesia induced by bone cancer. *Experimental and Therapeutic Medicine*, *13*, 2565-2569.

Yarnitsky, D., Arendt-Nielsen, L., Bouhassira, D., Edwards, R.R., Fillingim, R.B., Granot, M., Hansson, P., Lautenbacher, S., Marchand, S., & Wilder-Smith, O. (2010). Recommendations on terminology and practice of psychophysical DNIC testing. *European Journal of Pain*, *14*, 339.

Yeomans, D.C., Clark, F.M., Paice, J.A., & Proudfit, H.K. (1992). Antinociception induced by electrical stimulation of spinally projecting noradrenergic neurons in the A7 catecholamine cell group of the rat. *Pain*, *48*, 449-461.

Yezierski, R.P., & Schwartz, R.H. (1986). Response and receptive-field properties of spinomesencephalic tract cells in the cat. *Journal of Neurophysiology*, *55*, 76-96.

Yip, P.K., Chapman, G.E., Sillito, R.R., Ip, T.H.R., Akhigbe, G., Becker, S.C., Price, A.W., Michael-Titus, A.T., Armstrong, J.D., & Tremoleda, J.L. (2019). Studies on long term behavioural changes in group-housed rat models of brain and spinal cord injury using an automated home cage recording system. *Journal of Neuroscience Methods*, *321*, 49-63.

Yoneda, S., Kasai, E., Matsuo, M., Tamano, R., Sakurai, Y., Asaki, T., & Fujita, M. (2020). Duloxetine ameliorates the impairment of diffuse noxious inhibitory control in rat models of peripheral neuropathic pain and knee osteoarthritis pain. *Neuroscience Letters*, *729*, 134990.

Yoneda, T., Hiasa, M., Nagata, Y., Okui, T., & White, F.A. (2015). Acidic microenvironment and bone pain in cancer-colonized bone. *BoneKEy Reports*, *4*, 690.

Yuan, X.C., Zhu, B., Jing, X.H., Xiong, L.Z., Wu, C. H., Gao, F., Li, H.P., Xiang, H.C., Zhu, H., Zhou, B., He, W., Lin, C.Y., Pan, H.L., Wang, Q., & Li, M. (2018). Electroacupuncture potentiates cannabinoid receptor-mediated descending inhibitory control in a mouse model of knee osteoarthritis. *Frontiers in Molecular Neuroscience*, *11*, 112.

Yue, W., Wang, J.P., Li, Y., Fan, P., Liu, G., Zhang, N., Conaway, M., Wang, H., Korach, K.S., Bocchinfuso, W., & Santen, R. (2010). Effects of estrogen on breast cancer development: Role of estrogen receptor independent mechanisms. *International Journal of Cancer*, *127*, 1748-1757.

Zeni, S.N., Di Gregorio, S., & Mautalen, C. (1999). Bone mass changes during pregnancy and lactation in the rat. *Bone*, *25*, 681-685.

Zhang, R.X., Liu, B., Li, A., Wang, L., Ren, K., Qiao, J.T., Berman, B.M., & Lao, L. (2008). Interleukin 1beta facilitates bone cancer pain in rats by enhancing NMDA receptor NR-1 subunit phosphorylation. *Neuroscience*, *154*, 1533-1538.

Zhang, T., Dong, S., Zhai, Y., Naatz, L., Zhou, Z., & Chen, M. (2023). Diphtheria toxin-derived, anti-PD-1 immunotoxin, a potent and practical tool to selectively deplete PD-1^{+} cells. *Protein Science*, *32*, e4741.

Zhang, X., Li, X., Wang, W., Zhang, Y., Gong, Z., Peng, Y., Wu, J., & You, X. (2022). STING contributes to cancer-induced bone pain by promoting m1 polarization of microglia in the medial prefrontal cortex. *Cancers*, *14*, 5188.

Zhang, Y., Liang, J., Liu, P., Wang, Q., Liu, L., & Zhao, H. (2022). The RANK/RANKL/OPG system and tumor bone metastasis: potential mechanisms and therapeutic strategies. *Frontiers in Endocrinology*, *13*, 1063815.

Zhang, Y., Rózsa, M., Liang, Y., Bushey, D., Wei, Z., Zheng, J., Reep, D., Broussard, G. J., Tsang, A., Tsegaye, G., Narayan, S., Obara, C.J., Lim, J.X., Patel, R., Zhang, R., Ahrens, M.B., Turner, G.C., Wang, S.S., Korff, W.L., Schreiter, E.R., … Looger, L.L. (2023). Fast and sensitive GCaMP calcium indicators for imaging neural populations. *Nature*, *615*, 884-891.

Zhang, Y., Zhao, S., Rodriguez, E., Takatoh, J., Han, B.X., Zhou, X., & Wang, F. (2015). Identifying local and descending inputs for primary sensory neurons. *The Journal of Clinical Investigation*, *125*, 3782-3794.

Zhang, Z., Deng, M., Huang, J., Wu, J., Li, Z., Xing, M., Wang, J., Guo, Q., & Zou, W. (2020). Microglial annexin A3 downregulation alleviates bone cancer-induced pain through inhibiting the Hif-1α/vascular endothelial growth factor signaling pathway. *Pain*, *161*, 2750-2762.

Zhen, G., Fu, Y., Zhang, C., Ford, N.C., Wu, X., Wu, Q., Yan, D., Chen, X., Cao, X., & Guan, Y. (2022). Mechanisms of bone pain: progress in research from bench to bedside. *Bone Research*, *10*, 44.

Zhou, H., Martinez, E., Lin, H.H., Yang, R., Dale, J.A., Liu, K., Huang, D., & Wang, J. (2018). Inhibition of the prefrontal projection to the nucleus accumbens enhances pain sensitivity and affect. *Frontiers in Cellular Neuroscience*, *12*, 240.

Zhou, X., Tan, Y., Chen, J., Wang, C., Tang, Y., Liu, J., Lan, X., Yu, H., Lai, Y., Hu, Y., Zhang, J., Cao, Y., Liu, D., & Zhang, J. (2022). Altered functional connectivity in pain-related brain regions and its correlation with pain duration in bone metastasis with cancer pain. *Disease Markers*, *2022*, 3044186.

Zhou, Y.S., Cui, Y., Zheng, J.X., Quan, Y. Q., Wu, S.X., Xu, H., & Han, Y. (2022). Luteolin relieves lung cancer-induced bone pain by inhibiting NLRP3 inflammasomes and glial activation in the spinal dorsal horn in mice. *Phytomedicine*, *96*, 153910.

Zhu, H., Ding, J., Wu, J., Liu, T., Liang, J., Tang, Q., & Jiao, M. (2017). Resveratrol attenuates bone cancer pain through regulating the expression levels of ASIC3 and activating cell autophagy. *Acta Biochimica et Biophysica Sinica*, *49*, 1008-1014.

Zhu, Y.F., Ungard, R., Seidlitz, E., Zacal, N., Huizinga, J., Henry, J.L., & Singh, G. (2016). Differences in electrophysiological properties of functionally identified nociceptive sensory neurons in an animal model of cancer-induced bone pain. *Molecular Pain*, *12*, 1744806916628778.

Zhuo, M., & Gebhart, G.F. (1990). Characterization of descending inhibition and facilitation from the nuclei reticularis gigantocellularis and gigantocellularis pars alpha in the rat. *Pain*, *42*, 337-350.

Zhuo, M., & Gebhart, G.F. (1992). Characterization of descending facilitation and inhibition of spinal nociceptive transmission from the nuclei reticularis gigantocellularis and gigantocellularis pars alpha in the rat. *Journal of Neurophysiology*, *67*, 1599-1614.

Zimmer, Z., Fraser, K., Grol-Prokopczyk, H., & Zajacova, A. (2022). A global study of pain prevalence across 52 countries: examining the role of country-level contextual factors. *Pain*, *163*, 1740-1750.

Zimmermann, M. (1983). Ethical guidelines for investigations of experimental pain in conscious animals. *Pain*, *16*, 109-110.

Zinonos, I., Luo, K.W., Labrinidis, A., Liapis, V., Hay, S., Panagopoulos, V., Denichilo, M., Ko, C.H., Yue, G.G., Lau, C.B., Ingman, W., Ponomarev, V., Atkins, G.J., Findlay, D.M., Zannettino, A.C., & Evdokiou, A. (2014). Pharmacologic inhibition of bone resorption prevents cancer-induced osteolysis but enhances soft tissue metastasis in a mouse model of osteolytic breast cancer. *International Journal of Oncology*, *45*, 532-540.

Zong, W., Obenhaus, H.A., Skytøen, E.R., Eneqvist, H., de Jong, N.L., Vale, R., Jorge, M.R., Moser, M.B., & Moser, E.I. (2022). Large-scale two-photon calcium imaging in freely moving mice. *Cell*, *185*, 1240-1256.e30.

Zorina-Lichtenwalter, K., Meloto, C.B., Khoury, S., & Diatchenko, L. (2016). Genetic predictors of human chronic pain conditions. *Neuroscience*, *338*, 36-62.

Zorman, G., Hentall, I.D., Adams, J.E., & Fields, H.L. (1981). Naloxone-reversible analgesia produced by microstimulation in the rat medulla. *Brain Research*, *219*, 137-148.